Thermodynamic Modeling and Experimental Investigation of the Mg-Al-Ca-Sr System

Mohammad Aljarrah

A Thesis

In

The Department

of

Mechanical and Industrial Engineering

Presented in Partial Fulfillment of the Requirements
for the Degree of Doctor of Philosophy (Mechanical Engineering) at
Concordia University
Montreal, Quebec, Canada

April 2008

Your file Votre référence
ISBN: 978-0-494-37762-8
Our file Notre référence
ISBN: 978-0-494-37762-8

ABSTRACT

Thermodynamic Modeling and Experimental Investigation of the Mg-Al-Ca-Sr System

Mohammad Aljarrah, Ph.D.
Concordia University, 2008

In this work, a self-consistent thermodynamic database for the Mg-Al-Ca-Sr system using the modified quasichemical model has been constructed. The thermodynamic description of the quaternary system was established by combining the thermodynamic descriptions of the constituent binary and ternary sub-systems. The Mg-Al-Ca and Mg-Al-Sr systems were investigated by combining thermodynamic modeling and experimental investigation. The experimental investigation has been performed using DSC, XRD, SEM and EPMA. Also, isothermal sections at 300°C and 400°C were constructed for the Mg-Al-Ca and Mg-Al-Sr systems. In the Mg-Al-Sr system, six ternary solubilities of the binary compounds extended into the ternary system have been found and denoted as ($Mg_{17}Sr_2$), ($Mg_{23}Sr_6$), ($Mg_{38}Sr_9$), (Mg_2Sr), (Al_4Sr) and (Al_2Sr). The reported ternary compound in the literature ($Mg_{58}Al_{38}Sr_4$) has been observed in this work. In the Mg-Al-Ca system, three binary compounds were found to dissolve the third component in the ternary system and were denoted as (Al_2Ca), (Al_3Ca_8), and (Mg_2Ca). The ternary compound (C36) reported in the literature has been confirmed.

A comparison between the calculated liquidus projection of the Mg-Ca-Sr system using the modified quasichemical model and random solution model has been presented. It was found that while the random solution model agrees well with the experimental

phase diagram, the modified quasichemical model gives better agreement with the experimental thermodynamic data and the experimental phase diagram.

Liquidus projection of the Al-Ca-Sr system was calculated using the modified quasichemical model and combined with the other three ternaries in one database for the Mg-Al-Ca-Sr system.

DEDICATION

In the loving memory of my mother

For her pride I decided to earn this degree

ACKNOWLEDGEMENTS

First of all, I would like to express my deep gratitude and sincere appreciation to my supervisor, Dr. Mamoun Medraj, for his advice, encouragement, and constructive suggestions during my Ph.D study at Concordia University. It is a privilege and pleasure to work for him.

I would like to take the opportunity to thank Dr. Elhachmi Essadiqi and Dr. Jian Li from CANMET-MTL, Dr. Muntasar from the Chemistry Department, Concordia University and Dr. Mathieu Brochu from the Mining, Metals and Materials Department, Mcgill University for their help and cooperation.

I would also like to thank the members of Dr. Medraj's research group. In addition, I would like to acknowledge the financial assistance provided by the Natural Science and Engineering Research Council (NSERC) to keep the research work going.

Special thanks to my father, brothers and sisters for their love, support, understanding and constant encouragement. Last by not least, I would like to thank my wife, Alia for her love, invaluable support and help.

TABLE OF CONTENTS

LIST OF FIGURES

LIST OF TABLES

LIST OF ABBREVIATIONS

DSC	Differential Scanning Calorimetry
DTA	Differential Thermal Analysis
XRD	X-ray Diffraction
OM	Optical Microscopy
SEM	Scanning Electron Microscopy
EDS	Energy Dispersive Spectroscopy
EDX	Energy Dispersive X-ray Spectrometer
STEM	Scanning Transmission Electron Microscopy
OIM	Orientation Imaging Microscopy
AZ91	Mg-9 wt.% Al-1 wt.% Zn
AM60	Mg-6 wt.% Al-0.33 wt.% Mn
AE42	Mg-4 wt.% Al-2 wt.% mischmetal such as Ce, La,..etc

CHAPTER I

Introduction

1.1 Magnesium Alloys

Magnesium is the lightest of all metals used as the basis for structural alloys. This makes magnesium alloys attractive for transportation applications such as automobiles and airplanes for weight reduction and higher fuel efficiency. However, one of the significant challenges for a wider application of magnesium alloys is the low creep strength. Like pure magnesium, the commonly used Mg-Al based alloys also suffer from poor creep resistance. High temperature deformation of these alloys is considered to be controlled by dislocation motion in Mg grains at higher stress, and grain boundary sliding at lower stress [1,2]. Moreno *et al.* [3] pointed out that the grain boundary strengthening and stability as well as solid solution and precipitation strengthening in α-Mg grains are the important factors for optimization of the high temperature strength of fine-grained die cast alloys. A large amount of efforts have been made to increase the service temperature of Mg-Al alloys [4-15].

AZ91 and AM60 alloys have been used for interior automotive applications [10]. However, neither of them exhibited suitable mechanical properties at moderate temperatures. This is because the tensile strength of these alloys decreases rapidly at a temperature higher than 150°C [13]. On the other hand, AE42 alloy, developed by Basner *et al.* [14], has good mechanical properties even at higher temperature than 150°C. But since this alloy contains rare-earth metals it is more expensive than AZ91 alloy.

Therefore, the use of low price metals (or similar price metals to magnesium) instead of rare earth metals is more desirable.

The addition of alkaline earth elements into Mg-Al alloys has been found to be beneficial not only to keep the cost low but also to improve the mechanical properties, especially the creep resistance at elevated temperature [13-16]; the addition of Ca into Mg - (3-9) wt.% Al alloys increased the hardness at relatively high temperatures up to 350°C, this is remarkable when the mass ratio of Ca to Al is higher than 0.8 due to precipitation of Al_2Ca and/or Mg_2Ca phases [14]. The addition of 2.4 wt.% Sr into Mg-6 wt.% Al (AJ62) alloy, on the other hand, has shown superior creep performance and tensile strength at 175°C, while Mg-6Al with less than 2.1 wt.% Sr (AJ62Lx) has better ductility than other AJ-alloys [16]. Therefore, the main challenge in these alloy systems is to obtain optimum combinations of creep resistance, tensile yield strength and castability. Since, high temperature strength and creep resistance of Mg-Al alloys can be improved by alloying with Sr and Ca, these two elements are particularly appealing to the carmakers due to their low cost.

In order to define the processing conditions for making Mg-Al based alloys and subsequent treatments to obtain the optimum mechanical properties, knowledge of the phase diagram and thermodynamic properties of these alloys is essential. In addition, phase relations and phase stability under given conditions can be better understood through computational thermodynamic modeling. Precise description of the ternary sub-systems in the Mg-Al-Ca-Sr quaternary system provides an opportunity to approach the phase equilibria aspects of alloy development and track of individual alloys during heat treatment or solidification by calculating the phase distributions and compositions.

To date, very few studies have been reported on the phase relationships in the Mg-Al-Sr system. The few published experimental works on the phase equilibria of the Mg-Al-Sr system are self-contradictory. Hence a thorough investigation of this system is required. Moreover, further investigation of the Mg-Al-Ca ternary system is needed, especially in the region close to Mg-Al side because Wang [17] pointed out the possibility of the existence of a new phase. Also, the Mg-Ca-Sr and the Al-Ca-Sr systems will be thermodynamically modeled and combined with the other two ternaries in one database for the Mg-Al-Ca-Sr system using CALPHAD approach.

1.2 CALPHAD Approach

The CALPHAD (CALculation of PHAse Diagrams) method is based on the fact that a phase diagram is a representation of the thermodynamic properties of a system. Thus, if the thermodynamic properties are known, it would be possible to calculate the multi-component phase diagrams. The Gibbs free energy of a phase is described by a representative model that contains some experimental information such as melting, transformation temperatures, solubility, as well as thermodynamic properties.

Experimental investigation of the multi-component phase diagram such as Mg-Al-Ca-Sr system can be time-consuming, expensive, and difficult. Therefore, the CALPHAD method offers a reliable and versatile alternative to generate phase diagrams, and requires key experiments that are identified using preliminary calculations to validate the thermodynamic models and to check inconsistencies in the reported experimental data. This combined approach of thermodynamic modeling and the experimental investigation will provide consistent and quantitative description of the phase equilibria

in the Mg-Al-Ca-Sr system. A schematic diagram illustrating this approach is given in Figure 1.

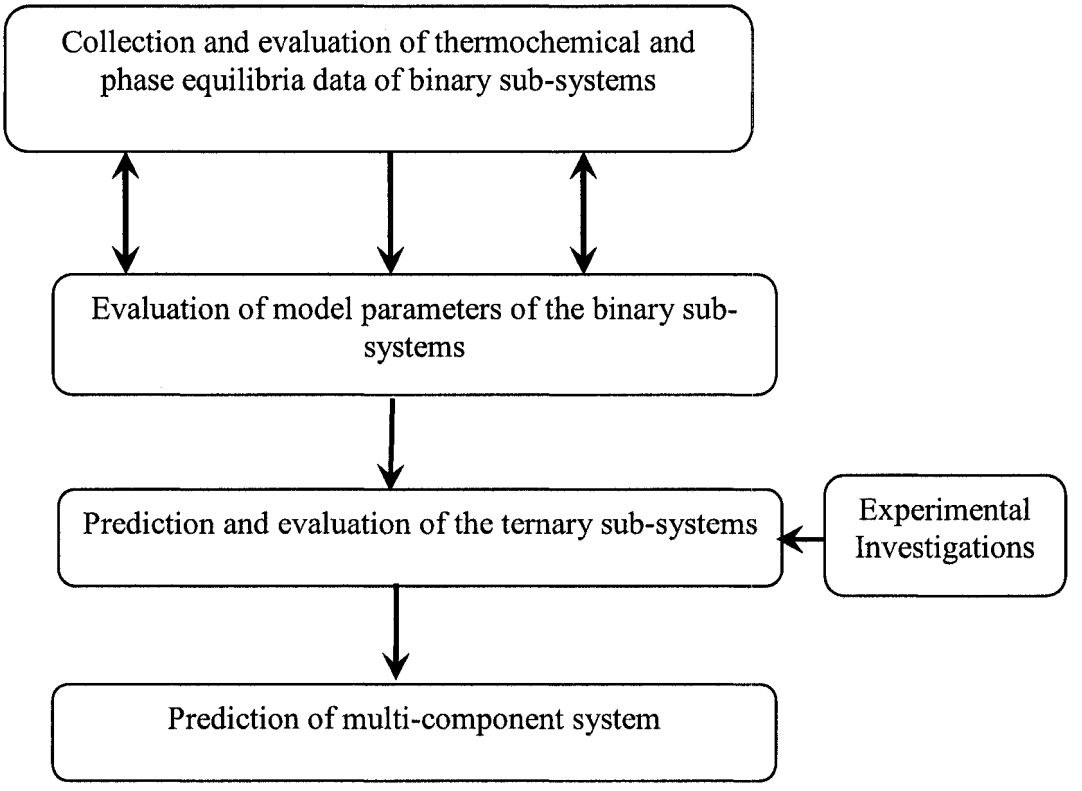

Figure 1.1: *A schematic diagram of the CALPHAD approach.*

Among the six binary sub-systems in the Mg-Al-Ca-Sr, three binary systems namely Al-Ca, Mg-Ca and Al-Sr, have short range ordering in the liquid. In order to develop the thermodynamic descriptions of these binaries, it is necessary to select the suitable model that can treat properly the short range ordering. Also, the choice of the model will affect how easily the descriptions of these binary systems can be combined with other binary systems for the calculations of higher order system. It has been found

that the description of the liquid using the modified quasichemical model developed by Chartrand and Pelton [21] and by Pelton *et al.* [22] comes close to observations in real systems.

1.3 Thesis Layout

The entire thesis is divided into eight chapters; the following describes the contents of the remaining chapters. Chapter 2 presents a review of all the experimental phase equilibria and thermodynamic descriptions of the six constituent binary systems; Al-Ca, Al-Sr, Mg-Al, Mg-Sr, Mg-Ca and Ca-Sr systems, and four ternary systems; Mg-Al-Sr, Mg-Al-Ca, Mg-Ca-Sr and Al-Ca-Sr are presented. Chapter 3 describes the principle behind the phase diagram calculations and discusses the reasons for using the modified quasichemical model to treat short range ordering. Chapter 4 presents a comparison between the random solution model and the modified quasichemical model for Mg-Ca and Mg-Sr systems, and provides thermodynamic modeling of the binary and ternary subsystems in the Mg-Al-Ca-Sr system. A brief description of the experimental methods used to construct the isothermal sections of the Mg-Al-Ca and Mg-Al-Sr systems and measure phase transformation temperatures is presented in Chapter 5. Next, Chapters 6 and 7 provide experimental results of the Mg-Al-Sr and Mg-Al-Ca system. Finally, Chapter 8 summarizes the contents of this thesis and suggests some possible directions for future research.

CHAPTER II

Literature Review

To create an accurate thermodynamic database of the Mg-Al-Ca-Sr quaternary system, it is necessary to obtain the thermodynamic descriptions of the constituent binary systems namely, Al-Sr, Mg-Sr, Ca-Sr, Mg-Al, Al-Ca and Mg-Ca. Therefore, a review of the work performed on these systems will be discussed in this chapter.

2.1 Al-Sr System

According to Burylev *et al.* [23], Vakhobov *et al.* [24] and Vakhobov *et al.* [25], the assessed phase diagram of the Al-Sr system consists of liquid, Sr-fcc and Sr-bcc, Al_4Sr, Al_2Sr, Al_7Sr_8 and terminal solid solution, Al-fcc, with a small solubility of 0.6 at.% Sr at 500°C after annealing for a period of 450 h [25]. Vakhobov *et al.* [25] reported that Sr dissolved 5.0 at.% Al at 600°C. Whereas Closset *et al.* [26] found a negligible solid solubility in this system. Furthermore, comparing the mutual solubilities between Al and Sr with similar system such as Al-Ca, the most reliable measurements show very small solubility of Ca in Al. Besides, in view of the relative atomic radii of Al and Sr atoms, the ratio of Al radius to that of Sr is 0.67 indicating the chance for small solid solubility. Therefore, the experimental solubilities of [25] are not considered reliable. In this work, it is assumed that the mutual solubility of the components in Al-Sr system is negligible.

In general, the thermodynamic data obtained from first-principle calculations are believed to be reliable when the corresponding experimental data are missing. The intermetallic compound Al_3Sr_8 was predicted using first-principle calculations by

Wolverton *et al.* [27] based on the existence of the Al_3Ca_8 compound in the Al-Ca system [28,29]. Thus, this compound will be included in the current optimization.

Over a complete composition range using differential thermal analysis (DTA), the Al-Sr system was investigated by Burylev *et al.* [23] and Vakhobov *et al.* [24,25]. Whereas, Bruzzone and Merlo [30] studied this system using thermal analysis, X-ray diffraction (XRD) and metallographic methods, using 99.8 wt.% Sr and 99.99 wt.% Al starting materials. They reported that Al_4Sr melts congruently at 1040°C. However, Burylev *et al.* [23] and Closset *et al.* [26] reported this melting point as 1000±20 and 1025°C, respectively. In addition, Al_2Sr melts congruently at 936°C according to Bruzzone and Merlo [30] compared to Closset's [26] result as 920°C. Furthermore, Bruzzone and Merlo [30] concluded that Al_7Sr_8 decomposes by peritectic reaction at 666°C.

Sato *et al.* [31] studied Al-rich region of the Al-Sr system using thermal analysis, XRD and optical microscopy. They reported that the invariant reaction in Al-rich region occurs at 0.85 at.% Sr and 654±1°C, compared to the results of Closset *et al.* [26] as 0.75 at.% Sr and 654°C. Whereas, Hanna and Hellawell's [32] values are 1.3 at.% Sr and 653°C. Closset *et al.* [26] and Burylev *et al.* [23] reported that the eutectic reaction in the Sr-rich region occurs at 73.5 at.% Sr at 580°C, and ~70 at.% Sr at 560°C, respectively. Closset *et al.* [26] mentioned that they had difficulties in detecting the thermal arrests in the alloys containing more than 60 at.% Sr. Therefore, the liquidus points at higher Sr concentrations seem to be less reliable than those from the work of Bruzzone and Merlo [30].

Alcock and Itkin [33] first reviewed and optimized the Al-Sr system. Subsequently, several efforts [26,34-37] have been made to calculate this system. The Al-Sr phase diagram presented by Chartrand and Pelton [34] is different from that published by Alcock and Itkin [33], especially in the Sr-rich part. The calculated phase diagram of [33] agrees reasonably with most of the experimental data except for the melting behavior of Al_2Sr. Calculations for the Al-Sr phase diagram [33,35,36] show that Al_2Sr melts incongruently because of symmetry in Al_4Sr liquidus. In contrast, the interpretations of the experimental data of Closset *et al.* [26], and Bruzzone and Merlo [30] showed asymmetry in Al_4Sr liquidus which is in agreement with Chartrand and Pelton's [34] assessment. In this work, therefore, melting of the intermetallic compound Al_2Sr is considered to be congruent.

Sommer *et al.* [37] and Esin *et al.* [38] measured the enthalpy of mixing of the Al-Sr liquid at 797, 852, 857, 900 and 902°C, using a high temperature mixing calorimeter. Burylev *et al.* [23] and Vakhobov *et al.* [24] measured the vapor pressure of Sr in the temperature range of 850-1100°C using Knudsen effusion method. Based on these data, they [23,24] derived the activities of Sr in Al-Sr liquid. Srikanth and Jacob [39] measured the activity of Sr in Al-Sr liquid at 1050°C in a composition range less than 17 at.% Sr and greater than 28 at.% Sr using Knudsen effusion-mass loss technique and pseudo isopiestic technique, respectively. These data are employed in the current work. Experimental data on the enthalpy of formations of the intermetallic compounds could not be found in the literature.

2.2 Al-Ca System

In 1908, Donski [40] carried out the first attempt to construct Al-Ca system using thermal analysis. This led Matsuyama [41] to investigate this system by thermal analysis, electrical resistance and microscopic examination. His samples were prepared from 99.4 wt.% Al and 98.34 wt.% Ca. He determined the liquidus curve, two eutectic reactions; one in the Al-rich region occurring at 5.2 at.% Ca and 616°C, compared to Donski's [40] results as 5.5 at.% Ca and 610°C. Whereas, Kevorkov and Schmid-Fetzer's [29] values were reported as 5.1 at.% Ca and 613°C. The other eutectic is in the Ca-rich side, and according to Matsuyama [41], occurs at 64.5 at.% Ca and 545°C, compared to Donski's [40] values of 66.9 at.% Ca and 550°C, and Kevorkov and Schmid-Fetzer's [29] results of 66.3 at.% Ca and 556°C. These results will be used for comparison with the current optimization.

In the Al-Ca system most of the experimental investigations mainly deal with Al-rich corner, which is technically interesting for aluminum alloys. Nevertheless, Kevorkov and Schmid-Fetzer [29] investigated the entire Al-Ca system using X-ray diffraction, SEM/EDX analysis, metallographic and diffusion couple techniques. They [29] reported four intermetallic compounds; Al_2Ca which melts congruently at 1086°C compared to Matsuyama's [41] value as 1079°C, Al_3Ca_8 which melts congruently at 579°C, Al_4Ca which decomposes at 700°C compared to Donski's [40] and Matsuyama [41] values as 690 and 700°C, and AlCa which melts incongruently at 633°C. However, Huang and Corbett [28] also reported the occurrence of $Al_{14}Ca_{13}$ compound with a monoclinic structure instead of AlCa. Nowotny *et al.* [42] determined the crystal structure of Al_4Ca and Al_2Ca as bct and fcc, respectively. Whereas Huang and Corbett [28] investigated the

crystal structures of $Al_{14}Ca_{13}$ and Al_3Ca_8 using X-ray analysis and mentioned that they have monoclinic and triclinic structures, respectively.

Several researchers [41,43-46] measured the solubility of Ca in Al. Among them Edwards and Taylor [45], and Jaquet and Warlimont [46] reported negligible solubility and their results agree fairly well. Therefore, the mutual solubility of the components in Al-Ca system is considered negligible in this work.

The enthalpy of formation of Al_2Ca and Al_4Ca compounds was measured by many researchers [47-52]. Notin *et al.* [47,48] determined the enthalpy of formation of these compounds at 680°C and 765°C precisely. They recorded calorimetric signals that corresponded to the enthalpy change during the addition of a solid Ca to Al melt. There is a reasonable agreement with the values of enthalpy of formation for Al_2Ca between [48] and [52]. According to Kevorkov *et al.* [52], the small difference between them may be due to the difference in heat capacity, ΔC_p, for the formation reaction between room temperature and 765°C. Experimental data on the enthalpy of formation of $Al_{14}Ca_{13}$ intermetallic compound could not be found in the literature and according to Kevorkov *et al.* [52] this is due to the sluggish formation kinetics of the phase and the difficulty of preparing an $Al_{14}Ca_{13}$-rich sample. The enthalpy of formation of Al_3Ca_8 phase was measured using drop solution calorimetry by Kevorkov *et al.* [52].

Notin *et al.* [48], Sommer *et al.* [37] and Kevorkov *et al.* [52] measured the heat of mixing of liquid Al-Ca alloys. Their experimental results are in good agreement. Jacob *et al.* [53] determined the activity of the components in the Al-Ca liquid using Knudsen effusion method for alloys in the composition range less than 38 at.% and greater than 44 at.% Ca at 1373K. Schürmann *et al.* [54] measured the activities of Ca in

the liquid alloys using boiling point determination technique. The activity measurements by Jacob *et al.* [53] and Schürmann *et al.* [54] agree fairly well.

Kevorkov and Schmid-Fetzer [29] calculated the phase diagram of the Al-Ca system using random solution model. In order to adjust the liquidus around Al_2Ca, their calculated enthalpy of mixing deviated from the experimental data. Whereas, fitting the enthalpy of mixing with the experimental data resulted in shifting the liquidus line of Al_2Ca to a higher temperature. When the random solution model is used for the liquid, higher order interaction parameters in the liquid are needed to reproduce the liquidus around Al_2Ca and it often results in a less satisfactory liquidus at other compositions. Ozturk *et al.* [55] used both random and associate models to re-optimize the Al-Ca system. They found that while the random solution model gives better agreement with the experimental phase diagram, the associate model agrees well with the experimental thermodynamic data. Using the modified quasichemical model to re-optimize the Al-Ca system provides not only better agreement with the experimental phase diagram but also with the experimental thermodynamic data and, therefore, it will be implemented in the current work.

2.3 Mg-Ca System

Baar [56] determined the liquidus curves for the Mg-Ca system. The starting materials in his work were of low purity. The melting point of the starting Ca was 808°C, and for Mg was 632.6°C, compared to 842°C and 650°C [57] for pure Ca and Mg, respectively. Further work on this system was carried out by Paris [58] while he was studying the Mg-Ca-Zn ternary system. He stated that his results differ slightly from those of Baar [56]. However, Paris [58] did not report the purity of the starting materials. Haughton *et al.*

[59] determined the liquidus temperatures in the Mg-rich region in the composition range of 0 to 26 at.% Ca. They found that the liquidus temperatures in this composition range are in fair agreement with Vosskühler [60], and Klemm and Dinkelacker [61] but differ slightly from those given by Baar [56]. Haughton *et al.* [59] reported that the invariant reaction in the Mg-rich region occurs at 10.5±0.5 at.% Ca and 517°C, compared to Baar's results as 12.46 at.% Ca and 514°C. Whereas, Klemm and Dinkelacker's [61] values are 10.5 at.% Ca and 516.5°C which are in good accord with Haughton *et al.* [59].

Nayeb-Hashemi and Clark [62] critically assessed this system based on the liquidus temperatures and the eutectic reactions of Vosskühler [60], and Klemm and Dinkelacker [61]. However, they [62] placed the melting point of Mg_2Ca at 715°C which is the average temperature measured by Baar [56] and Vosskühler [60]. Agarwal *et al.* [63] measured the enthalpy of mixing of liquid Mg-Ca alloy calorimetrically at 750°C and heat contents of Mg_2Ca between 477°C and 877°C. They used these values together with the experimental phase equilibria from [59-61] to calculate the phase diagram of the Mg-Ca system. The enthalpy of mixing measured by Sommer *et al.* [64] was not used since it contradicts with their measurement. According to Agarwal *et al.* [63], their experiments were performed in iron crucible and adding Ca to the melt reacted with the crucible and producing less reliable measurements. Hence, the enthalpy of mixing measured by Sommer *et al.* [64] seems to be more reliable than the one published by Agarwal *et al.* [63] and it will be used in the current work.

Several researchers [42,59-61,65,66] measured the solubility of Ca in Mg. Among them Burke [65] and Vosskühler [60] reported limited solubility and their results agree

fairly well, whereas other researchers reported larger solubility. Hence, the limited solubility will be adopted in the current work.

Many efforts had been made to measure the heat of formation of the compound Mg_2Ca [63,67-73]. The average heat of formation reported in [69-71,73] will be used during the optimization in this work because these results are more reliable. Mashovets and Puchkov [74], and Sommer [75] determined the activity of Mg and Ca in Mg-Ca liquid at 807°C, 927°C and 737°C using vapor pressure measurement. These data will be also used in this work.

2.4 Mg-Sr System

Nayeb-Hashemi and Clark [76] reviewed the Mg-Sr system and their article provides a comprehensive discussion of all the experimental results obtained by previous researchers [61,76-79]. Brown [78] used DTA and high temperature X-ray diffraction analysis to determine the (Sr) solidus and its allotropic transformations. Ray [79], also, determined the (Sr) solidus by thermal analysis. According to Nayeb-Hashemi and Clark [76], despite the possibility of hydrogen contamination of Brown's [78] samples, the solidus temperatures he obtained were more realistic than those of Ray [79]. Thermal analyses and metallographic examinations indicated a very small solid solubility of Sr in Mg, less than 0.5 at.% Sr [78]. This was considered negligible in the optimization of the Mg-Sr phase diagram by Chartrand and Pelton [34]. On the other hand, a significant solid solubility of Mg in Sr was detected by Ray [79] using thermal and metallographic analyses which does not agree with Brown [78] who reported limited solubility. In the current evaluation, the experimental data of Brown [78] are used because they are in better agreement with the limiting slope of the liquidus at $X_{Sr}=1$, equation 1, than those of

Ray [79]. If the solubility of Mg in Sr is negligible, the limiting slope is related to the enthalpy and temperature of fusion of Sr as shown by equation 2.1.

$$\left(\frac{dx_i}{dT}\right)^{l}_{X_i=1} - \left(\frac{dx_i}{dT}\right)^{s}_{X_i=1} = \frac{\Delta_{fus}H}{RT^2_{fus}} \qquad (2.1)$$

A tin solution calorimetry was used to measure the heat of formation of the congruently melting compound Mg_2Sr from solid Mg and Sr by King and Kleppa [73]. Sommer *et al.* [64] determined the enthalpy of mixing of the liquid alloys at 807°C, using high temperature calorimetry. The thermodynamic activities of liquid alloys at 781°C were determined by Sommer [80] using a modified Ruff boiling technique. These were the only thermodynamic data found for the system and they will be used in the current optimization.

2.5 Ca-Sr System

Schottmiller *et al.* [81] determined the liquidus as well as the solidus of the Ca-Sr phase over the entire range of composition using DTA. The melting point of the starting Ca was 843±1°C, and for Sr, it was 774±1°C, compared to 842°C and 776°C [57] for pure Ca and Sr, respectively. They [81] reported that the two-phase region, liquid and solid, is very narrow; never exceeds a range of 6°C and mentioned that there are three allotropies of Ca and Sr. Their proposed phase diagram was later redrawn by Elliott [82]. A more reliable report by Smith *et al.* [83] stated that there are only two allotropies occurring in both pure Ca and Sr. Schottmiller *et al.* [81] investigated the lattice parameter of fcc, hcp and bcc solid solutions using X-ray diffraction. They found a linear variation of lattice parameter with Sr content at room temperature for fcc solid solution obeying Vegard's law. Whereas, a positive deviation from Vegrad's law occurs in the Sr-rich region at 415°C for bcc and hcp solid solutions. It should be noted that the work of Peterson and

Fattore [85] for the Ca-H system indicated the non-existence of hcp allotropy of Ca. King [86] determined the lattice parameters at room temperature for six samples in the Ca-Sr system using XRD. He reported a linear variation of the unit cell volume with Sr content obeying Vegard's law. In addition, Klemm and Mika [84] reported only little deviation from Vegard's law. Such behaviour is expected considering the similar atomic size and crystal structure of Ca and Sr. Further, the results of Schottmiller *et al.* [81], King [85], and Klemm and Mika [84] were analyzed by Alcock *et al.* [87] who found that there is only little deviation from Vegard's law.

In this work, it is considered that Ca and Sr form a solid solution throughout the entire composition range. Both pure Ca and Sr have the same type of allotropic phase transformation from fcc to bcc at 443°C and 556°C [57], respectively. Predel *et al.* [88] determined the enthalpy of mixing for the liquid alloys at 870°C using high temperature calorimetry. The excess entropy of mixing of the Ca-Sr liquid is relatively small and it is assumed to be zero by Predel *et al.* [88]. Therefore, Ca and Sr atoms mix randomly in the liquid. But the modified quasichemical model still can be reduced to the random solution model and agrees with the experimental phase diagram and experimental thermodynamic data as can be noticed in Chapter 3.

2.6 Mg-Al System

Several researchers [90-100,167,168,172-173] studied the liquidus, solidus and solvus lines of the Mg-Al system. Murray [89] reviewed the Mg-Al system and his article provides a comprehensive discussion of the experimental results obtained by previous researchers. According to Murray [89] the assessed Mg-Al phase diagram consists of: liquid, β solid solution with hexagonal crystal structure, γ solid solution with the αMn

structure type, R phase with rhombohedral structure at 42 at.% Mg, (Al) solid solution with a maximum solubility of 18.9 at.% Mg at 450°C, and (Mg) solid solution with a maximum solubility of 11.8 at.% Al at 437°C. In view of the relative atomic radii of Al and Mg atoms, the ratio of the Al radius to that of Mg is 1.12 which suggests high mutual solid solubility. There is a good agreement between different authors regarding the solid solubility of Mg and Al, liquidus, solidus and solvus lines.

Several efforts [34,101-104] have been made to calculate the Mg-Al phase diagram. In addition, several researchers [105-110] measured the enthalpy of mixing of the Mg-Al liquid calorimetrically. Belton *et al.* [105] and Tiwari [109] obtained the enthalpy of mixing Mg-Al liquid from emf measurements at 800°C, while Bhatt *et al.* [107] and Juneja [108] derived the enthalpy of mixing from partial pressure measurements at 800°C. Agarwal *et al.* [110] measured enthalpy of mixing of Mg-Al liquid using three different calorimetric methods at 670, 674, 675 and 700°C. In 1998, Moser *et al.* [185] measured the enthalpy of mixing at 1023K using drop calorimetry. The experimental data of [185] are considered more reliable and will be used in the current optimization. The thermodynamic activities of liquid alloys at 800°C were determined by [105,107,109,111-114] using emf measurements. All reported results are scattered but show small negative deviation from ideal solution. These results will be used in the current optimization.

2.7 Mg-Al-Sr System

The interest in magnesium-based alloys is continuously increasing, especially because of their applications in the transportation industry for weight reduction and the consequent increased fuel efficiency [115,116]. However, magnesium alloys face a challenge at

higher temperature application because of their limited creep properties. In recent years, Mg-Al-Sr alloy system has emerged as a potential system for heat-resistant Mg-alloys [117]. Noranda developed alloys based on the Mg-Al-Sr system, which are being used by BMW for the manufacturing of die-cast engine blocks [118].

There are a huge number of possibilities of selecting alloy compositions within the ternary Mg-Al-Sr system. Wrought magnesium, particularly in the form of sheet, represents a tremendous growth opportunity in magnesium alloys applications. Significant improvement in creep resistance has been achieved. But the phase relations and phase stability under given conditions can be better understood through thermodynamic modeling and microstructural characterization. To date, little effort has been made to construct the phase relationships in the Mg-Al-Sr system. The published experimental works on the phase equilibria of the Mg-Al-Sr system are self-contradictory. Prince *et al.* [119] summarized the work done on the Mg-Al-Sr system. The experimental work on the phase equilibria of the Mg-Al-Sr system was primarily originated by Makhmudov and coworkers in early 1980's [120-123]. However, inconsistency was noticed between their works. Makhmudov *et al.* [121], also, reported a ternary compound with stoichiometry of $Al_{34}Mg_6Sr_{60}$ (Al_6MgSr_{10}), which is different from the earlier reported X compound by Makhmudov *et al.* [120]. Since the crystal structure of $Al_{34}Mg_6Sr_{60}$ has not been identified, it can also represent a ternary solubility of Mg in Al_2Sr_3. This binary compound, however, is not a stable phase in the Al-Sr system. The solubility limits for the binary compounds determined by Makhmudov *et al.* [122] do not agree with the 400°C isothermal section given by Makhmudov *et al.* [121] in 1981.

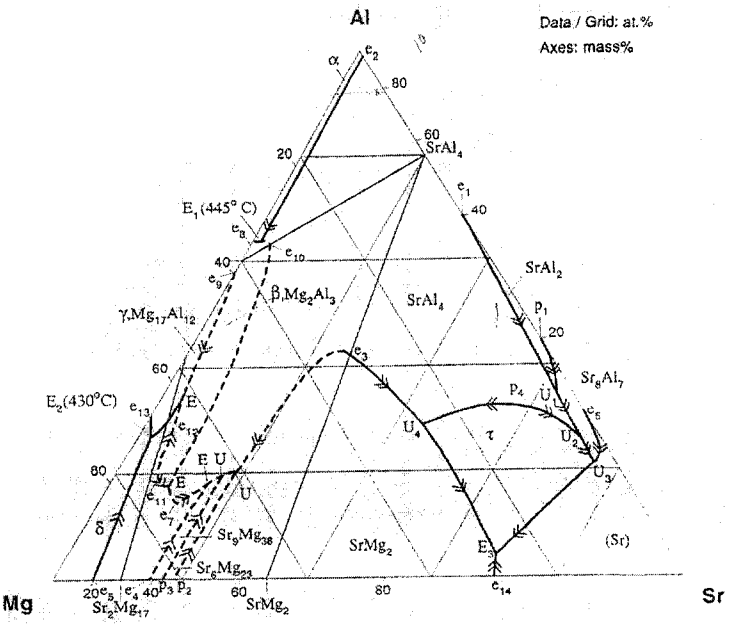

Figure 2.1: *Tentative liquidus surface of Mg-Al-Sr ternary phase diagram [119].*

Prince *et al.* [119] developed a tentative liquidus surface using the experimental results from references [120-123] with some disagreements in identifying the invariant points as shown in Figure 2.1.

Baril *et al.* [16] investigated four samples in the Mg-rich region of the Mg-Al-Sr system and tentatively designated a ternary phase as $Al_3Mg_{13}Sr$. In their work, the stoichiometry is not clearly identified and the chemical composition is not compatible with the ternary compound $Al_{34}Mg_6Sr_{60}$ reported by Makhmudov *et al.* [121]. Jing *et al.* [124] investigated the microstructure and tensile creep behavior of Mg-Al-Sr (AJ) based alloys and reported that a ternary interphase exists in the alloys containing 2-3 wt.% Sr at the grain boundaries. Czerwinski and Zielinska-Lipiec [125] investigated the microstructure evolution in the Mg-5Al-2Sr (wt.%) alloy and reported that the common feature of Sr-containing phases in the as-cast ingots is their location at grain or sub-grain boundaries. The presence of $Mg_{17}Al_{12}$ suggests an insufficient amount of Sr to bind all of

the Al. At the same time, however, Sr reacted exclusively with Mg forming $Mg_{17}Sr_2$. Hence, it is very likely that the local segregation of Al and Sr led to a variety of phases. Chartrand and Pelton [34] reviewed and calculated the Mg-Al-Sr ternary and the related binary sub-systems. No ternary terms were added to the thermodynamic model due to the uncertainties related to the existence, stability, homogeneity range and the melting and decomposition temperatures of the ternary compounds. The liquidus projection of the calculated Mg-Al-Sr system in weight percent is shown in Figure 2.2. Six ternary eutectics and four ternary peritectic invariant points are observed on the calculated liquidus surface.

In 2003, Koray *et al.* [126] calculated the liquidus projection of the ternary Mg-Al-Sr system that is very similar to Chartrand and Pelton's [34] calculation except for the narrower phase field of Mg_2Sr. The calculated phase diagram of [34,126] exhibited substantial disagreement with the experimental data. The extended solubilities between the solid phases were not considered in the thermodynamic assessment. Makhmudov *et al.* [121] reported an isothermal section at 400°C that shows triangulations involving (Mg), $Mg_{17}Sr_2$ and γ phase. This seems unlikely, as the thermodynamic stability of these compounds are lower than Al_4Sr and Al_2Sr at this temperature. Further, the thermodynamic optimization of Chartrand and Pelton [34] shows that these compounds are in triangulation with Al_2Sr. From these discrepancies, it is believed that these thermodynamic evaluations of the ternary system should be revised. Besides, in the experimental work of Makhmudov *et al.* [121], the binary compound $Mg_{38}Sr_9$ was not included in the Mg-Al-Sr phase diagram.

Parvez *et al.* [128-131] studied twenty-two alloys in the Mg-Al-Sr system using DSC, XRD and optical microscopy. They found four new phase fields which correspond to extended solubility of the binary compounds or new ternary compound(s). They observed that (Mg) and (Al_4Sr) were the dominating phases in the investigated samples. However, the ternary compounds claimed by Makhmudov *et al.* [121] and Baril *et al.* [16] were not observed, and the identified phases in as-cast condition are consistent with the post-DSC samples. Further experimental investigations of [130] samples have been studied by Aljarrah *et al.* [132] using EPMA, SEM/EDS and solidification curves deduced from DSC measurements. The discussions of these results will be presented in Chapter 6.

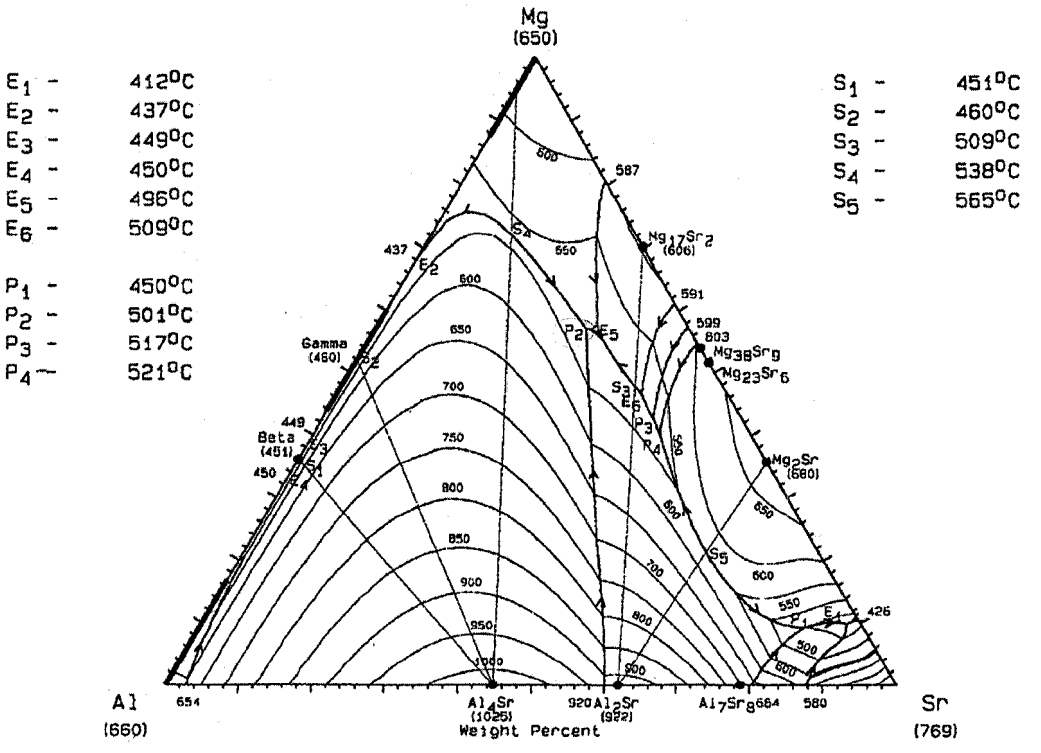

Figure 2.2: *Calculated liquidus surface of Mg-Al-Sr system in weight percent [34].*

In 2007, Janz *et al.* [127] investigated this system based on the experimental data obtained in the work of [128-132] together with seven new samples from their work. Their samples were synthesized in sealed Ta-capsules by electric arc welding under flowing argon at 1 bar. After the samples have been thermally analyzed using DSC, they were used to investigate the microstructure using SEM and EPMA. In their work, thermodynamic assessment of the Mg-Al-Sr system using random solution model was done taking into consideration the substitutional solid solubilities of Al and Mg in Mg-Sr and Al-Sr binary compounds. They included a new ternary compound in their analysis with Mg/Al ratio similar to that of $Mg_{17}Al_{12}$. The chemical composition is not compatible with the ternary compounds reported by [121,123]. Their [127] calculated liquidus projection of the Mg-Al-Sr system is shown in Figure 2.3.

Pan *et al.* [133] and Yan *et al.* [134] briefly reviewed the current research on the Mg-Al-based alloys focusing on alloy design, microstructure and mechanical properties.

A considerable discrepancy among the published results and few experimental data demands new investigation for this system. In addition, the chemistry of the phases and their microstructural details should be further studied. The purpose of the current thesis is to develop a comprehensive and consistent thermodynamic description of the phase equilibria based on the new experimental data obtained in this work together with the re-assessed experimental data from the literature.

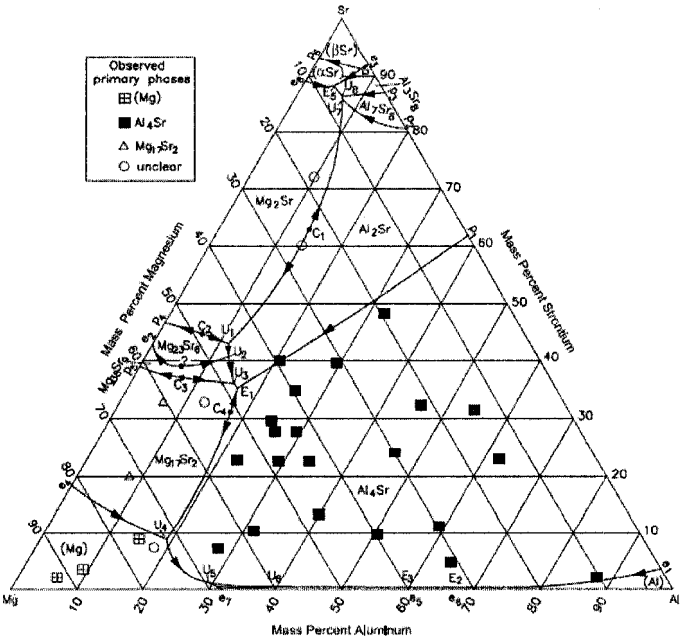

Figure 2.3: *Calculated liquidus surface of Mg-Al-Sr system in weight percent [127].*

2.8 Mg-Al-Ca System

A large amount of effort has been made to increase the service temperature of Mg alloys [4,8,11]. The addition of Ca element has been reported in recent years to replace the cost intensive rare earth metals. It is well known that the addition of Ca up to 0.3 wt.% increases ductility through grain size refinement [136]. The improvement of creep resistance is attributed to the thermal stability and the interface coherency of the Mg_2Ca and Al_2Ca precipitates with the Mg matrix. Calcium additions also protect the melt surface combined with less slag formation and additive loss. In addition, the resulting alloys show lower secondary creep rates and higher tensile strength than AZ91 coupled with comparable castability and good melt handling [4,9,10,135,137].

Pekguleryuz and Renaud [139] studied the creep resistance and mechanical properties of Mg-Al-Ca casting alloys with three calcium levels (0.6, 0.8, and 1 wt.% Ca). The maximum level of 1 wt.% Ca was selected to avoid hot cracking during casting

and 5 wt.% Al to compromise between strength and ductility. They compared the creep resistance of these alloys with AZ91D and AE42 and found that the percentage of creep resistance of AX alloys (tentative designation, where X denotes Ca) at 150°C, 35 MPa and 1200 hrs was 0.26-0.33% compared to a value of 2.5% for AZ91D and 0.33% for AE42. AX alloys also offer high temperature (150°C) tensile properties. The improved creep resistance is due to the existence of the thermally stable phase Al_2Ca at grain boundaries because Al_2Ca impedes grain boundary sliding and diffusion-related dislocation climb at high temperature.

Catterall *et al.* [140] studied the phase equilibria in the Mg-Al-Ca ternary system experimentally and reported a partial isothermal section of the Mg-rich corner. Ozturk *et al.* [104] carried out phase identification and microanalysis for two alloys in this system; Mg-4.5Al-1.9Ca wt.% (GM-B) and Mg-4.5Al-3.0Ca wt.% (GM-C). Three types of samples were prepared for each alloy: as-cast, heat-treated at 290°C and heat-treated at 370°C. The identified phases were compared with the calculated ternary phase diagram. It was found that both GM-B and GM-C have similar microstructural features. In addition, the primary α-Mg grains are surrounded by an interconnected network of grain boundaries. The grain boundary phases formed in the as-cast samples as a result of eutectic transformation as shown in Figure 2.4. After homogenization at 290°C for one week, the network is somehow less complete and the lamellae become spherical as shown in Figure 2.5. This effect is more pronounced when the heat treatment temperature was increased to 370°C.

In 2001, Ozturk *et al.* [141,143] investigated the thermodynamic properties of the Mg-Al-Ca ternary system. The calculated ternary system and Schiel simulation were used

to understand the effect of Ca content on the microstructure and phase relationships during solidification. They found that the calculated liquidus projection (Figure 2.6) and the experimental observations carried out in their work are in good agreement. In 2003, Ozturk *et al.* [126] reinvestigated the Mg-Al-Ca ternary phase diagram with a new understanding of the Al-Ca system; by including Al_3Ca_8 and $Al_{14}Ca_{13}$ as intermetallic compounds. Their new calculated liquidus projection is shown in Figure 2.7.

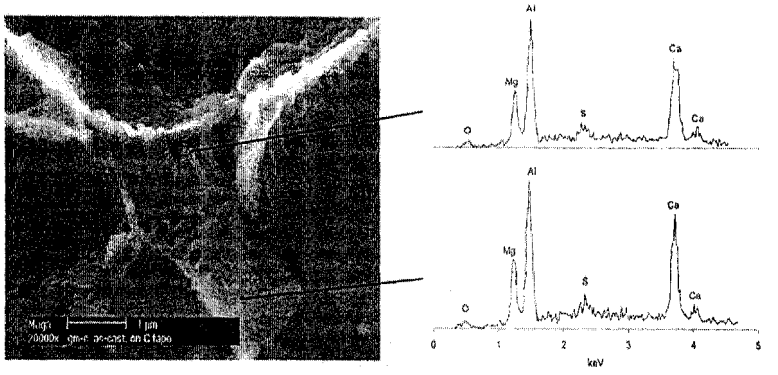

Figure 2.4: *SEM image and EDS analysis of the lamella-type grain boundary phase from a replica of GM-C sample on a carbon tape [104].*

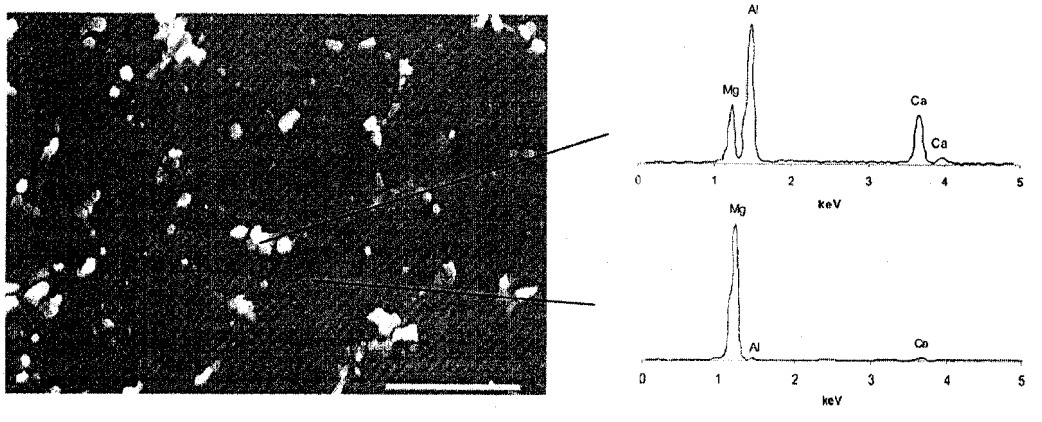

Figure 2.5: *SEM image and EDS analysis of both the particulate grain boundary phase and the matrix phase from a bulk GM-B sample after heat treatment at 370 °C for a week [104].*

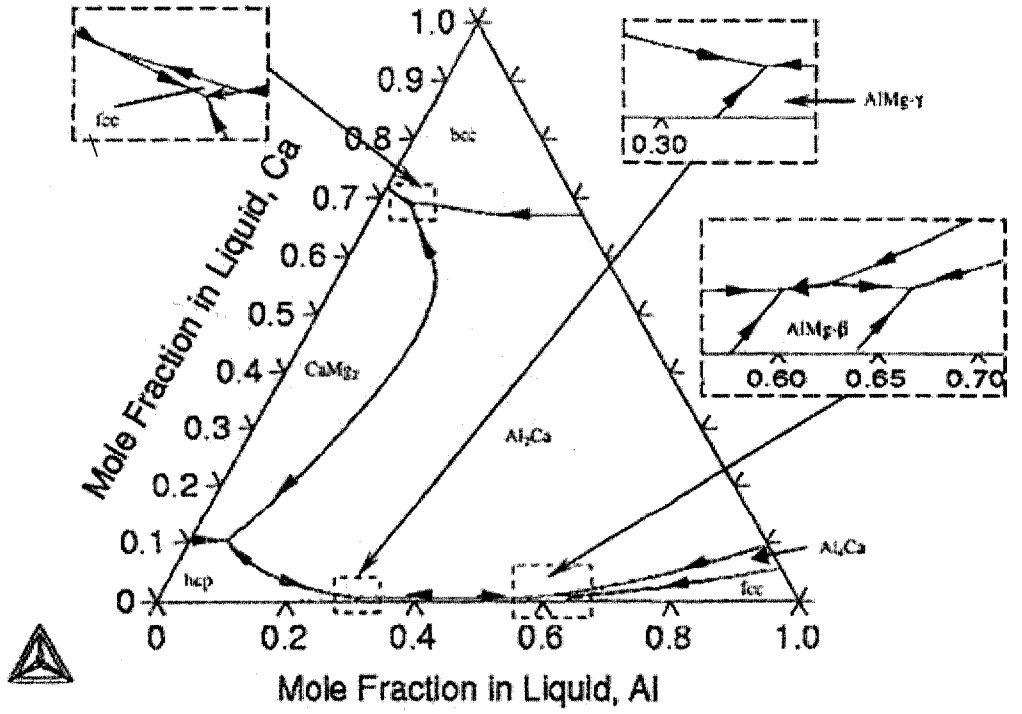

Figure 2.6: *The calculated liquidus projection of the Mg-Al-Ca ternary system [141].*

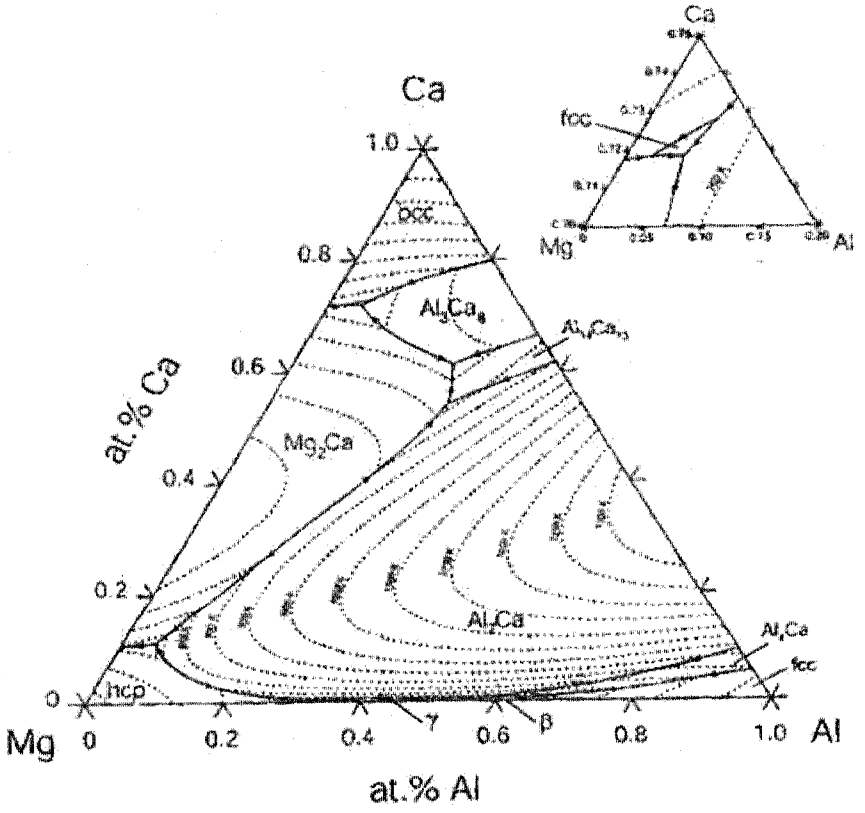

Figure 2.7: *Liquidus projection of the Mg-Al-Ca [126].*

Gröbner *et al.* [135] investigated twenty-five alloys in the Mg-Al-Ca system. The alloys were carefully arc melted under purified argon to avoid extensive evaporation of magnesium. They found that the ternary solid solubility does not vary substantially with temperature, which was confirmed by XRD analysis of lattice parameter variations in as-cast versus post-DTA samples. Figure 2.8 shows the microstructure of the alloys between Mg_2Ca and Al_2Ca; a strange rod-like phase with variable compositions can be seen. Based on the XRD results, SEM/EDX and thermal analysis using DTA, they [135] concluded that the rod-like crystals are an intergrowth between Mg_2Ca and Al_2Ca. By incorporating these experimental data, thermodynamic model was developed using random solution model and the Mg-Al-Ca phase diagram was calculated, as shown in Figure 2.8.

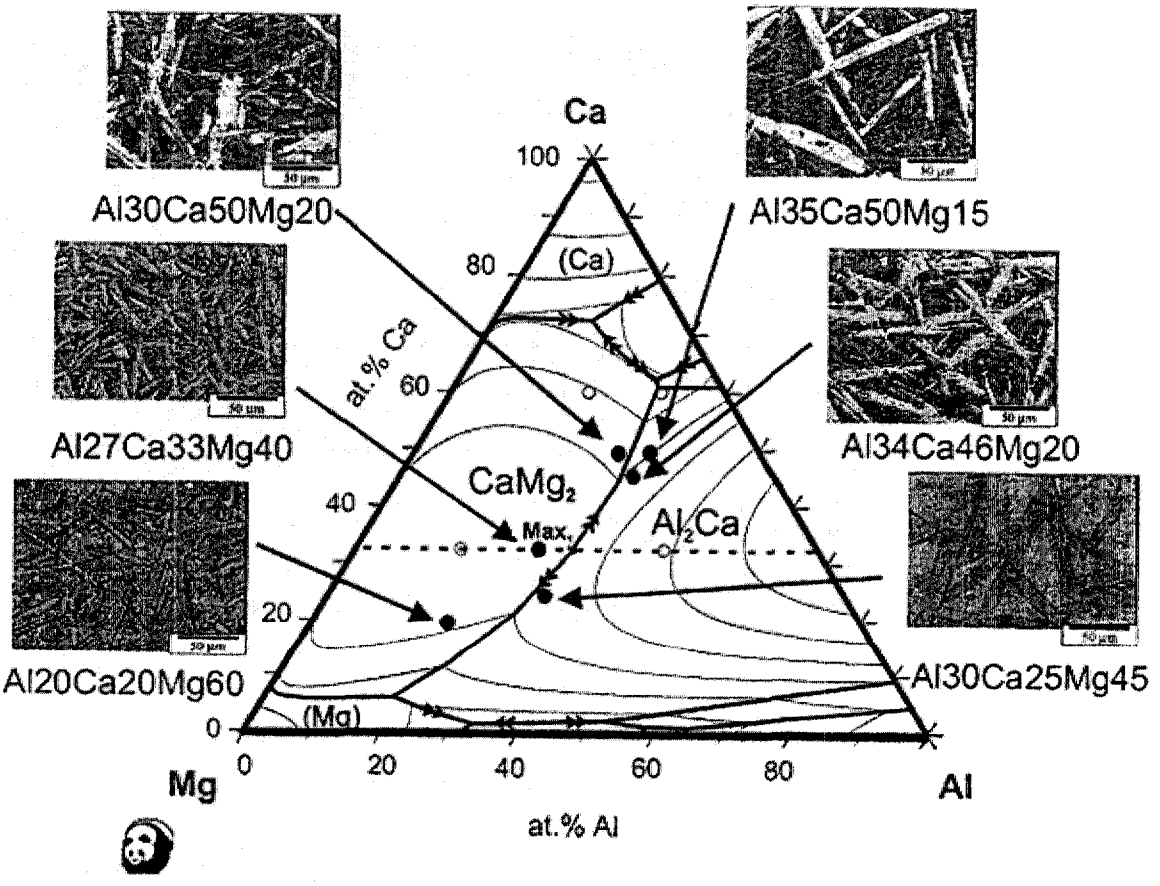

Figure 2.8: *Calculated liquidus surface with optical microscope image [135].*

At the same time Tkachenko *et al.* [142] published their experimental work on this system. They studied the phase equilibira in the composition range 50 to 100 wt.% Mg and reported an isothermal section at 150°C, the liquidus projection on Mg-rich corner and vertical section at 4.5, 8.5 and 16 wt.% Al. It was mentioned that additions of Al and Ca decrease the liquidus temperature of Mg alloys (from 650 to 438°C) and solubility of Al in Mg decreases with increasing Ca concentration in the alloys. In their work, to construct the liquidus projection, the eutectic temperature of the ternary eutectic ($L_E \rightarrow (Mg)+Mg_2Ca+Al_2Ca$) at composition 9 at.% Al, 79 at.% Mg and the quasibinary eutectic ($e_3 \leftrightarrow (Mg)+Al_2Ca$) were taken from the literature as 510°C and 535°C, respectively. Tkachenko *et al.* [142] determined another invariant point at P existing in the investigated range. This point corresponds to the peritectic transformation $L_p+Al_2Ca \leftrightarrow (Mg)+Mg_{17}Al_{12}$ that occurs at 470°C as shown in Figure 2.9.

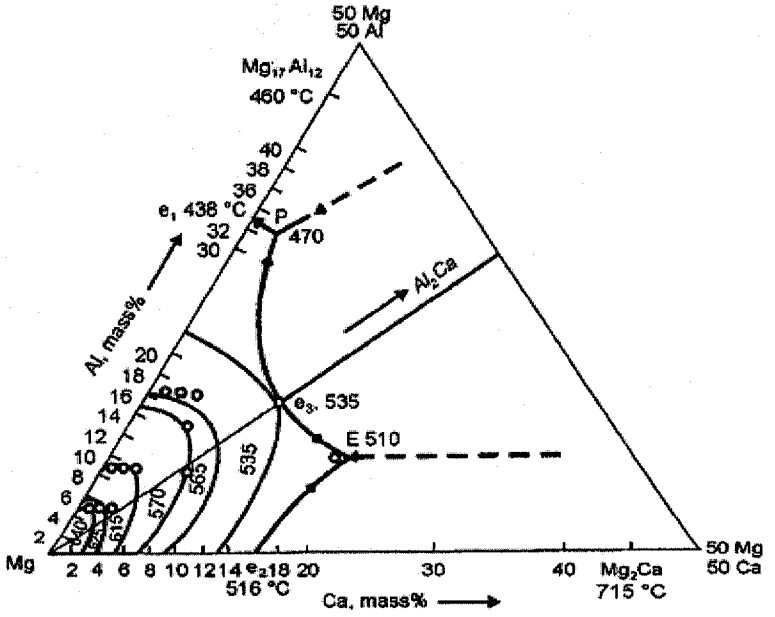

Figure 2.9: *Projection of the liquidus surface of the magnesium-rich region of Mg-Al-Ca system [142].*

Luo *et al.* [7] suggested the presence of a ternary solid solution phase $(Mg, Al)_2Ca$ which is responsible for the improved creep resistance of Mg-Al-Ca alloys up to 200°C due to its metallurgical stability and interfacial coherency with magnesium matrix [7].

Amerioun *et al.* [188] studied the crystal structure change of Laves phases from Al_2Ca to Mg_2Ca. They were the first to report the existence of C36 between Mg_2Ca and Al_2Ca in the composition range of $Mg_xAl_{(1-x)}Ca$ ($0.66<x<1.07$). In 2004, Suzuki *et al.* [144] studied the structure and transition of eutectic $(Mg, Al)_2Ca$ Laves phase in die-cast Mg-Al-Ca based alloys. They found that in the as-cast AXJ530, (Mg-5Al-3Ca-0.15 Sr, wt.%), the crystal structure of this compound is C36 which forms during an eutectic reaction. This compound could have transformed from the original Al_2Ca during cooling in the casting process or might be directly formed by the eutectic transformation. These uncertainties about the stability of the new ternary compound, C36, encouraged Suzuki *et al.* [157] to carry out further experimental investigations of the Mg-Al-Ca system in the Mg-rich region. They reported that C36, with a chemical composition of $Mg_{52}Al_{30}Ca_{18}$, exists at high temperature range between Mg_2Ca and Al_2Ca as a stable phase, but transforms to Mg and Al_2Ca at lower temperature. However, the chemical composition is different from the one reported later by Suzuki *et al.* [147] as $Mg_2Al_4Ca_3$. Also, they [147] found that C36 compound forms during the eutectic reaction $L \leftrightarrow Mg+C36+Mg_2Ca$ supporting their previous finding [144]. In addition, the similarity of the crystal structures of Mg_2Ca, Al_2Ca and C36 makes it difficult to distinguish these phases by X-ray diffraction. Since the existence of the ternary compound C36 was not taken into account, the reported isothermal section in the literature showed that Mg is in equilibrium with

Al_2Ca. Based on these findings and the experimental results in the current work, a new thermodynamic description for this system will be constructed.

In 2006, collaboration between Pennsylvania State University, University of Central California and EBSD Analytical [158] investigated the C36 Laves phase using SEM, EPMA, orientation imaging microscopy (OIM) and scanning transmission electron microscopy (STEM) combined with first-principle calculations. They found that C36 is a stable phase with lattice parameters: a=5.450Å and c=17.514 Å similar to that reported by Amerioun *et al.* [188]. This new ternary compound has been found in the present investigation in three samples and it will be incorporated in the current thermodynamic modeling. Recently, Cao *et al.* [158] studied the directional solidification of two samples in Mg-rich region. They found that there are two saddle points, S_1: L↔Mg+C14 and S_2: L↔Mg+C36. The first saddle point was reported by Gröbner *et al.* [135], Islam *et al.* [145] and Ozturk *et al.* [141,143]. Whereas, the argument of Cao *et al.* [158] about the existence of the saddle point (S_2: L↔Mg+C36) is not valid since this point is close to the binary eutectic in the Mg-Ca system at 516°C, whereas, the assumed saddle point occurs at 519°C. Besides, the composition of this saddle point was not reported in their work. Therefore, S_2: L↔Mg+C36 will not be considered in the current thermodynamic modeling.

Wang [17] investigated twenty-one alloys in this system using DSC, XRD and metallography. One of the invariant points predicted by thermodynamic modeling [145] was experimentally verified and found to occur at 512°C and the composition is close to Mg-9.7Al-10.8Ca, at.%. Moreover, the phases predicted from the thermodynamic modeling [145] agree with the XRD and metallographic results. Mg_2Ca was found to

exist as a solid solution and new phase was detected using XRD close to the Mg-Al side. Furthermore, Aljarrah *et al.* [146] re-assessed Wang's work and they found that three binary compounds, namely (Al_2Ca), (Mg_2Ca) and (Al_3Ca_8), have extended solubilities into the ternary system. This motivated further experimental study to determine the maximum solid solubility of the binary compounds and the existence of new ternary phases.

Further, Islam *et al.* [145] performed thermodynamic modeling of the Mg-Al-Ca system using random solution model and thermodynamic database was constructed with the optimized parameters of the three binary subsystems. No ternary terms were added to the thermodynamic model due to the uncertainties related to the existence, stability, homogeneity range and the melting and decomposition temperatures of the ternary compounds or solid solutions. The binary phase diagrams, their thermodynamic properties, ternary phase diagram (Figure 2.10) and the critical points were calculated from the database and compared with the experimental results from the literature.

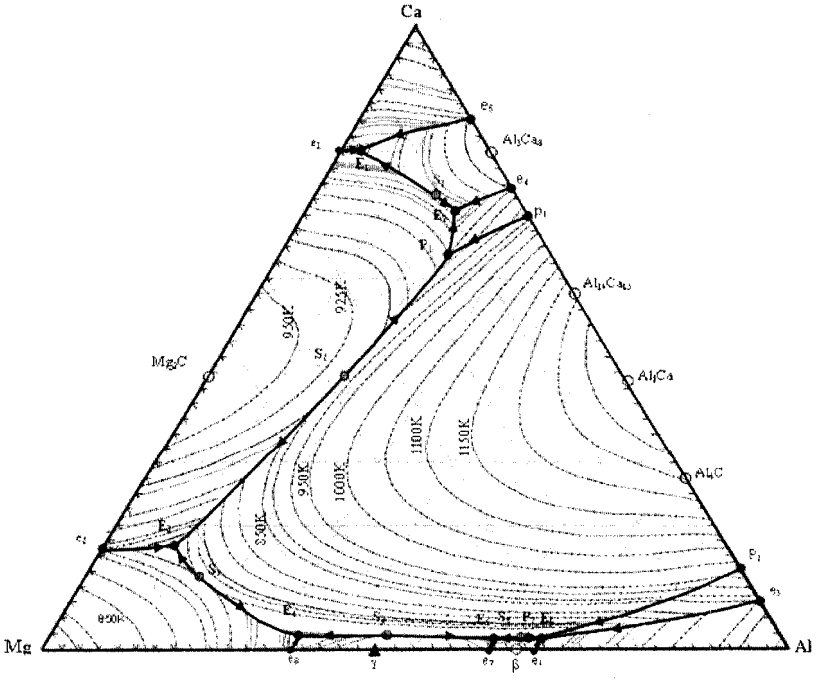

Figure 2.10: *Liquidus projection of the Mg-Al-Ca system based on mole fraction [145].*

To conclude, the rod-like crystals in the region between Al_2Ca and Mg_2Ca reported by Gröbner *et al.* [135] with different chemical composition belong most likely to the new ternary compound reported by Suzuki *et al.* [147] and which were also observed in current work.

2.9 Al-Ca-Sr System

No experimental thermodynamic or phase equilibrium data for the Al-Ca-Sr ternary system could be found in the literature. Thus, this work was initiated to critically evaluate the thermodynamic description of this system using the modified quasichemical model. The phase equilibria will be established for this system based on the optimized binary subsystems.

2.10 Mg-Ca-Sr System

No experimental thermodynamic data for the Mg-Ca-Sr ternary system could be found in the literature. Combining the computational thermodynamic with the first principle approach, Mg-Ca-Sr system was evaluated by Zhong *et al.* [148]. In their evaluation, even though there is no experimental data to verify the mutual solid solubility between Mg_2Sr and Mg_2Ca, a complete solid solution has been assumed based on the similarity with other systems that contain Laves phases and on the fact that Sr and Ca are very similar in terms of crystal structure and atomic size. Their model is based on random mixing, which cannot properly describe the short-range ordering. Thus, the current work was initiated to model this system using the modified quasichemical model. The phase equilibria will be established for this system based on the optimized binary subsystem.

2.11 Objectives

The objective of this study is to construct a self-consistent thermodynamic database for the Mg-Al-Ca-Sr system combined with experimental investigation. A systematic investigation, microstructural characterization and thermal analysis of the ternary Mg-Al-Sr and Mg-Al-Ca systems will be carried out using Differential Scanning Calorimetery (DSC), X-ray Diffraction (XRD), Optical microscopy, Scanning Electron Microscopy (SEM), and Electron Probe Micro-Analysis (EPMA). Specific objectives include:

- To measure phase transformation temperatures using DSC and identify the phases that form in the heat-treated samples in the Mg-Al-(Ca,Sr) systems using XRD.
- To identify the extended solid solubility of the binary compounds of the Al-Ca, Al-Sr, Mg-Ca, and Mg-Sr systems in the ternary systems experimentally and to compare the findings with thermodynamic modeling.
- To construct the isothermal sections at 400 and 300°C and the liquidus projections of the Mg-Al-Sr and Mg-Al-Ca by means of experimental investigation coupled with thermodynamic modeling.
- To thermodynamically model the Al-Ca-Sr and Mg-Ca-Sr ternary systems taking into consideration the short range ordering in the liquid phase.
- To establish the understanding of the equilbria in the Mg-Al-Ca-Sr system.

CHAPTER III

Thermodynamic Modeling

3.1 Introduction

A phase diagram is a graphical representation of the equilibrium relationships among phases. These relationships are governed by thermodynamic laws. The phase diagram shows how phases change as a function of temperature, pressure, composition, or combinations of these variables. Phase equilibrium calculations do not only determine the phases present and their compositions, but also give clear guidelines for alloy development and help to track the individual alloy during solidification and heat treatment. These are the basic inputs to understand and control process behavior of any alloy.

In recent years, a quantitative coupling of thermodynamics and phase diagram principles has become possible. With the use of computers, simultaneous optimization of thermodynamic and phase equilibrium data can be applied to critical evaluation of binary and ternary systems. This approach is used to generate enables good estimations of the thermodynamic properties and phase diagrams of multi-component systems. These estimates are based on structural models of solutions. Phase diagrams are always calculated by minimization of the Gibbs free energy.

3.2 *Unary Phases*

The principle behind phase diagram calculations is to present thermodynamic properties by a series expansion with sufficient adjustable parameters to adequately fit the experimental data. The specific heat capacities at constant pressure, C_P, for the pure

elements are represented by a polynomial [160] with a form which is known to describe the experimental data as shown in equation 3.1.

$$C_P = b_1 + b_2T + b_3T^2 + \frac{b_4}{T^2} + b_5T^6 + b_6\ln(T) + \frac{b_7}{T^{10}} \qquad (3.1)$$

Where b_i are empirical constants. The variation of enthalpy with temperature can then be calculated by the following integration: $\Delta H = \int_{298}^{T} C_P dT$, and the change in entropy can be calculated as: $\Delta S = \int_{0}^{T} \frac{C_P}{T} dT$, the Gibbs free energy of pure element is obtained by $\Delta G = \Delta H - T\Delta S$ as:

$$^{\circ}G_A^{\varphi}(T) = a + bT + cTlnT + dT^2 + eT^3 + fT^{-1} + gT^7 + hT^{-9} \qquad (3.2)$$

Where the parameters *a* through *h* are assigned from the SGTE database [160]. Allotropic transformations can be included if the transition temperatures, enthalpy of transformation and the heat capacities coefficients for all the phases are known.

3.3 *Stoichiometric phases*

In a system where there is strong chemical bonding between the atoms there is a tendency for the formation of intermetallic phases. These are distinct from solutions since they have a different crystal structure than the pure elements and may also be highly ordered.

The Gibbs energy function of the stoichiometric compounds is represented by equation 3.3:

$$G^{phase,\varphi} = x_i\,{}^{\circ}G_i^{\varphi} + x_j\,{}^{\circ}G_j^{\varphi} + \Delta G_f \qquad (3.3)$$

Where $^{\circ}G_i^{\varphi}$ and $^{\circ}G_j^{\varphi}$ denote Gibbs free energy of element *i* and *j* in their standard state and $\Delta G_f = a + bT$ represents the Gibbs energy of formation of the stoichiometric

compound. Where a and b are the model parameters to be optimized using experimental data.

3.4 *Disordered solution phase*

The Gibbs energy of a disordered solution phase is described by the following equation:

$$G = x_i {}^0G_i^{\phi} + x_j {}^0G_j^{\phi} + RT[x_i \ln x_i + x_j \ln x_j] + {}^{ex}G^{\phi} \tag{3.4}$$

where Φ denotes the phase in question and x_i, x_j denote the mole fraction of component i and j, respectively. The excess Gibbs energy is represented by random solution model using the Redlich-Kister equation:

$${}^{ex}G^{\phi} = x_i.x_j \sum_{n=0}^{n=m} {}^nL_{i,j}^{\phi}(x_i - x_j)^n \tag{3.5}$$

with $\quad {}^nL_{i,j}^{\phi} = a_n + b_n \times T \quad (\mathrm{n} = 0,\ldots.\mathrm{m})$

Where ${}^nL_{i,j}^{\phi}$ is the interaction parameters and a_n and b_n are model parameters to be optimized in terms of experimental phase diagram and thermodynamic data.

In this study, three terminal solid solution phases; the Mg-hcp phase in the Mg-Ca system, (Al) and (Mg) phases in Mg-Al system and two complete solid solutions, fcc and bcc, in the Ca-Sr system, were modeled using equation 3.5.

3.5 *Compound energy formalism*

The Gibbs energy for an ordered binary solution phase is described in equation 3.6.

$$\begin{aligned}
&\mathrm{G} = \mathrm{G}^{\mathrm{Ref}} + \mathrm{G}^{\mathrm{Ideal}} + \mathrm{G}^{\mathrm{Excess}} \text{ where} \\
&\mathrm{G}^{\mathrm{Ref}} = \sum y_p^i y_q^j \ldots\ldots y_s^l {}^0G_{(p:q:\ldots:s)} \\
&\mathrm{G}^{\mathrm{Ideal}} = RT \sum_{i=1}^{l} f_i \sum_{p=1}^{m} y_p^i \ln(y_p^i) \\
&\mathrm{G}^{\mathrm{Excess}} = \sum y_p^i y_q^i y_r^j \sum_{\gamma=0} {}^{\gamma}L_{(p,q):r}(y_p^i - y_q^j)^{\gamma}
\end{aligned} \tag{3.6}$$

Where,

- p, q, and r represent components or vacancy.
- $i, j \ldots l$ represent sublattices.
- y_p^i is the site fraction of component p on sublattice i.
- f_l is the fraction of the sublattice l with respect to the total lattice sites.
- $L_{(p,q):r}$ is the parameter describing the interaction within the sublattice.

In this work, one intermediate solid solution, the γ-Phase in Mg-Al system, was modeled using ordered solution model.

Based on the experimental findings in this work, there is a ternary solubility of Al in all the binary compounds of the Mg-Sr and Mg-Ca systems; similarly, some of the Al-Sr and Al-Ca binary compounds also dissolve Mg. These ternary solubilities are modeled with two sublattices with Sr atoms occupying the first lattice. In view of the fact that atomic size of Mg and Al are quite similar, these two elements replace each other and their mixing is allowed on the second sublattice, such as (**Mg**,Al)$_{17}$Sr$_2$, (**Mg**,Al)$_{38}$Sr$_9$, (**Mg**,Al)$_{23}$Sr$_6$, (**Mg**,Al)$_2$Sr, (Mg,**Al**)$_4$Sr, (Mg,**Al**)$_2$Sr and (**Al**,Mg)$_2$Ca, whereas for the Al$_3$Ca$_8$, Mg and Ca are assumed to replace each other (Mg,**Ca**)$_8$Al$_3$. The bold element denotes the majority species.

The Gibbs energy of (**Mg**,Al)$_{17}$Sr$_2$ is modeled using the compound energy formalism as shown in equation 3.7.

$$G^{(Mg,Al)_{17}Sr_2} = y_{Mg} G^{0,(Mg,Al)_{17}Sr_2}_{Mg:Sr} + y_{Al} G^{0,(Mg,Al)_{17}Sr_2}_{Al:Sr} + \frac{17}{19} RT(y_{Mg} \ln y_{Mg} + y_{Al} \ln y_{Al}) + y_{Mg} y_{Al} L^{0,(Mg,Al)_{17}Sr_2}_{Mg,Al:Sr} \quad (3.7)$$

where $G^{0,(Mg,Al)_{17}Sr_2}_{Mg:Sr}$ is the Gibbs energy of formation of Mg$_{17}$Sr$_2$ in the binary Mg-Sr system and $G^{0,(Mg,Al)_{17}Sr_2}_{Al:Sr}$ represents the metastable end member of the solid solution in the

binary Al-Sr phase diagram and it was given high positive value (10^5 J/mol). $L_{Mg,Al:Sr}^{0,(Mg,Al)_{17}Sr_2}$ describes the ternary interaction parameter within the sublattice, and this term is iteratively obtained based on the transformation temperatures obtained from DSC measurements.

3.6 *Liquid solution*

The mixing of two components can be made in two steps: (a) Bringing together X_A mole of pure A and X_B mole of pure B and this results in $\Delta G = X_A \Delta G_A + X_B \Delta G_B$ and (b) Allowing the A and B atoms to mix together to make a homogenous solution; $\Delta G_{mix} = \Delta H_{mix} - T\Delta S_{mix}$, where ΔH_{mix} is the enthalpy observed or evolved during mixing and where ΔS_{mix} is the difference in entropy between mixed and unmixed states [190], so that

$$\Delta G = X_A \Delta G_A + X_B \Delta G_B + \Delta H_{mix} - T\Delta S_{mix} \tag{3.8}$$

The following cases can be generated from equation 3.8:

(1) *Ideal solution*; $\Delta H_{mix}=0$ and the change in Gibbs free energy of mixing is due to change in entropy.

$$\Delta S_{ideal} = -R(X_A \ln(X_A) + X_B \ln(X_B)) \tag{3.9}$$

$$\Delta G_{ideal} = X_A \Delta G_A + X_B \Delta G_B + RT(X_A \ln(X_A) + X_B \ln(X_B)) \tag{3.10}$$

(2) *Regular solution model*

The regular solution model assumes a random distribution of atoms even though the enthalpy of mixing is not zero. In this model, the enthalpy of mixing, ΔH_{mix}, is obtained by counting the different kinds of nearest neighbor bonds when the atoms are mixed at random; this information together with the bonding energies give the required change in

enthalpy of mixing. The enthalpy of mixing depends only on the bond between adjacent atoms. For this assumption to be valid, it is necessary that the volume of pure A and B is equal and do not change during mixing so that the interatomic distances and bond energies are independent of composition [164].

$$\Delta G_{regular} = X_A \Delta G_A + X_B \Delta G_B + RT(X_A \ln(X_A) + X_B \ln(X_B)) + \Omega X_A X_B \qquad (3.11)$$

In equation 3.11, a positive Ω indicates that the similar atoms favor clustering, whereas, the negative values indicates that there is a tendency for the atoms to mix.

(3) *Modified quasichemical model*

In order to provide a good prediction for the thermodynamic properties of any system, it is necessary to choose the suitable model that describes the excess Gibbs energy. If a model based on random mixing is used for the liquid phase, higher order interaction parameters are needed to reproduce the liquidus around the intermetallic compounds, such as Mg_2Ca and Al_2Ca, and it often results in a less satisfactory liquidus at other compositions. According to Sommer [161] and Mishra *et al.* [162], there is a tendency for glass formation in the Mg-Ca system in the composition range 50-74 at.% Ca and partial glass formation in the composition ranges 10-50 and 74-85 at.% Ca. This indicates the tendency for short range ordering in the Mg-Ca liquid. Besides, in the Al-Ca system, the measured heat of mixing forms V-shape with the minimum value around 0.4 at.% Ca indicating a tendency for short-range ordering. Furthermore, according to You *et al.* [163], there is strong evidence for the existence of molecular, such as Al_2Ca, species that are called associates, in the liquid phase. To deal with short range ordering, the associates model was proposed in the literature [161]. However, this model is not physically sound, since it assumes that some molecules occupy specific atomic positions. Furthermore,

using a random solution model to treat liquids with short range ordering continues to appear in the literature. In reality, a random solution model is only expected at very high temperature when the entropy term overwhelms any tendency for ordering or clustering of atoms. It follows that the configurational entropy of mixing should vary with temperature. The quasichemical solution model has a better treatment of configurational entropy that accounts for a non-random distribution of atoms. Therefore, no model based on the random mixing can properly describe the influence of short-range ordering, as they do not solve the problem of the configurational entropy. The description of short-range ordering can be taken into account with bond energy models by considering the interactions between atoms that extend beyond the nearest neighbours approximation [191-192]. This problem has been treated using quasichemical model [21-22]. The model is so-called because it has a mass-action equation that is typical in chemical reaction theory.

The molar Gibbs energy for the liquid phase, derived from quasichemical theory [164], is described by equation 3.12:

$$G^{liq} = n_i {}^{\circ}G_i^{liq} + n_j {}^{\circ}G_j^{liq} - T\Delta S^{config} + \frac{n_{ij}}{2}\Delta^{exs}G^{liq} \qquad (3.12)$$

Where n_i and n_j are the number of moles of the components i and j, n_{ij} is the number of (i-j) pairs, ΔS^{config} is the configurational entropy of mixing given for randomly distributing the (i-i), (j-j), and (i-j) pairs, presented as:

$$\Delta S^{config} = -R[n_i \ln(x_i) + n_j \ln(x_j)] - R[n_{ii} \ln(\frac{x_{ii}}{y^2{}_i}) + n_{jj} \ln(\frac{x_{jj}}{y^2{}_j}) + n_{ij} \ln(\frac{x_{ij}}{2y_i y_j})] \qquad (3.13)$$

Where x_i and x_j are the overall mole fractions of the components i and j, respectively.

$$x_i = \frac{n_i}{n_i + n_j} \tag{3.14}$$

Pair fraction: $x_{ii} = \frac{n_{ii}}{n_{ii} + n_{jj} + n_{ij}}$ (3.15)

And the coordination-equivalent fractions: $y_i = \frac{Z_i n_i}{Z_i n_i + Z_j n_j}$ (3.16)

where Z is the coordination number.

The mass balance in the quasichemical model gives [165]:

$$Z_i n_i = 2n_{ii} + n_{ij} \tag{3.17}$$

$$Z_j n_j = 2n_{jj} + n_{ij} \tag{3.18}$$

Substituting equations 3.17 and 3.18 into equations 3.15 and 3.16 gives:

$$\begin{aligned} y_i &= x_{ii} + \frac{x_{ij}}{2} \\ y_j &= x_{jj} + \frac{x_{ij}}{2} \end{aligned} \tag{3.19}$$

The expansion of ${}^{ex}G^{liq}$ as a polynomial in terms of the pair fractions x_{ii}, x_{jj}, x_{ij} is represented by equation 3.20 [165]:

$$\Delta^{ex}G^{liq} = \Delta g^{\circ}_{ij} + \sum_{\substack{i\geq 1 \\ m\geq 1}} g_{ij}^{m\circ} x_{ii}^{m} + \sum_{\substack{j\geq 1 \\ n\geq 1}} g_{ij}^{\circ n} x_{ij}^{n} \tag{3.20}$$

The parameters, $\Delta g^{\circ}_{ij}, g_{ij}^{i\circ}$ and $g_{ij}^{\circ j}$ are to be optimized using experimental data.

Chartrand and Pelton [22] modified the quasichemical model in order to permit the coordination number to vary with compositions and is express as follows:

$$\begin{aligned} \frac{1}{Z_i} &= \frac{1}{Z_{ii}^{i}}\left(\frac{2n_{ii}}{2n_{ii} + n_{ij}}\right) + \frac{1}{Z_{ij}^{i}}\left(\frac{n_{ij}}{2n_{ii} + n_{ij}}\right) \\ \frac{1}{Z_j} &= \frac{1}{Z_{jj}^{j}}\left(\frac{2n_{jj}}{2n_{jj} + n_{ij}}\right) + \frac{1}{Z_{ji}^{j}}\left(\frac{n_{ij}}{2n_{jj} + n_{ij}}\right) \end{aligned} \tag{3.21}$$

Where Z_{ii}^{i} and Z_{ij}^{i} are the values of coordination number of i atom when all nearest neighbors are i's and j's, respectively.

Substituting equation 3.21 in equations 3.17 and 3.18 gives:

$$n_i = \frac{2n_{ii}}{Z_{ii}^{i}} + \frac{n_{ij}}{Z_{ij}^{i}}$$
$$n_j = \frac{2n_{jj}}{Z_{jj}^{i}} + \frac{n_{ij}}{Z_{ji}^{i}} \qquad (3.22)$$

The coordination number of the pure elements in the metallic liquid solution, $Z_{CaCa}^{Ca} = Z_{MgMg}^{Mg} = Z_{SrSr}^{Sr}$, is set to be 6 which is the same coordination number used by Pelton and Chartrand [21,22]. Whereas, the coordination number of the pairs; Z_{MgCa}^{Mg}, Z_{CaMg}^{Ca}, Z_{MgSr}^{Mg}, Z_{SrMg}^{Sr}, Z_{CaSr}^{Sr}, Z_{SrCa}^{Ca}, Z_{AlCa}^{Al}, Z_{CaAl}^{Ca}, Z_{AlSr}^{Sr}, Z_{SrAl}^{Al}, Z_{MgAl}^{Al} and Z_{AlMg}^{Mg} are chosen to permit the composition of maximum short range ordering in the binary system to be consistent with the composition that corresponds to the minimum heat of mixing. The tendency to maximum short range ordering near the composition 55 at.% Mg in the Mg-Ca system was obtained by setting $Z_{MgCa}^{Mg} = 5$ and $Z_{CaMg}^{Ca} = 4$. In the Mg-Sr and Al-Sr systems, the tendency to maximum short range ordering near the composition 40 at.% Sr was obtained by setting $Z_{MgSr}^{Mg} = 4$, $Z_{SrMg}^{Sr} = 6$ and $Z_{AlSr}^{Sr} = 4$, $Z_{SrAl}^{Al} = 6$, respectively. The tendency to maximum short range ordering near the composition 40 at.% Ca in the Al-Ca system was obtained by setting $Z_{AlCa}^{Al} = 6$ and $Z_{CaAl}^{Ca} = 4$. The positive heat of mixing in the Ca-Sr system is reflecting the fact that formation of Ca-Ca and Sr-Sr pairs is more favorable than formation of Ca-Sr pairs. This indicates that the coordination number for Ca-Sr pairs should be small. Hence the parameters Z_{CaSr}^{Sr} and Z_{SrCa}^{Ca} are set to be 3 in this work.

Thermodynamic optimization and calculation were performed in this work using FactSage program [166].

CHAPTER IV

Thermodynamic Modeling of the Mg-Al-Ca-Sr System

4.1 Thermodynamic Modeling of the Binary Sub-Systems

4.1.1 Mg-Ca Phase Diagram

The re-optimized Mg-Ca phase diagram along with all experimental data from the literature is shown in Figure 4.1. As can be seen from this figure the calculated liquidus and invariant points are in good agreement with the experimental data of Vosskühler [60], and Klemm and Dinkelacker [61] but differ slightly from the results of Baar [56]. A limited solid solubility of Ca in Mg is observed in the calculated phase diagram and shown in Figure 4.1(b). As can be seen from this figure the maximum solid solubility of Ca in Mg is 0.43 at.% at 517°C, this agrees with the results of Vosskühler [60] who reported 0.50 at.% at 516.8°C. Table 4.1 lists the thermodynamic model parameters obtained by optimization using the experimental thermodynamic and phase equilibrium data from the literature. The calculated invariant points in relation to the experimental data from the literature are presented in Table 4.2.

Table 4.1: *Optimized thermodynamic parameters of the Mg-Ca system (J/mol.atom).*

Phase	**The modified quasichemical model** $\Delta^{ex}G^{liq} = \Delta g^{\circ}_{ij} + \sum_{\substack{i\geq 1 \\ m\geq 1}} g^{m\circ}_{ij} x^{m}_{ii} + \sum_{\substack{j\geq 1 \\ n\geq 1}} g^{\circ n}_{ij} x^{n}_{ij}$	**Random solution model** $\Delta^{ex}G^{liq} = x_i x_j \sum_{n=0}^{n=m} {}^{n}L^{\phi}_{i,j}(x_i - x_j)^n$
Liquid (Mg,Ca)	$\Delta^{ex}G^{liq} = -706.33 + 0.37T + (323.40 - 1.20T)x_{Ca,Ca} + (508.82 - 0.89T)x_{Mg,Mg}$	$\Delta^{ex}G^{liq} = x_{Ca}x_{Mg}(-24018.6 + 1.94T) + x_{Ca}x_{Mg}(1785.73 + 4.47T)(x_{Ca} - x_{Mg}) + x_{Ca}x_{Mg}(14387.5 - 22.98T)(x_{Ca} - x_{Mg})^2$
Mg_2Ca	$G^{Mg_2Ca}_{Mg:Ca} = -13468.62 + 2.08T$	$G^{Mg_2Ca}_{Mg:Ca} = -12704.4 + 1.81T$

Table 4.2: *Comparison between calculated and experimental values of the invariant reactions in the Mg-Ca system.*

Reaction	at.% Mg	at.% Ca	T(°C)	Reference	Reaction Type
L↔Mg-hcp	100.00	0.00	650.0	[57]	Melting
	100.00	0.00	649.3	**[This work]**	
L↔Ca-bcc	0.00	100.00	842.0	[57]	Melting
	0.00	100.00	841.2	**[This work]**	
Ca-bcc↔Ca-fcc	0.00	100.00	443.0	[57]	Allotropic
	0.00	100.00	442.5	**[This work]**	
L↔Mg_2Ca+Ca-fcc	27.00	73.00	442	[61]	Eutectic
	26.58	73.42	460	[58]	
	33.00	67	445	[59]	
	30.86	69.14	446	[56]	
	29.44	70.56	445	**[This work]**	
L↔Mg_2Ca	66.67	33.33	717	[60]	Congruent
	66.67	33.33	714	[58]	
	66.67	33.33	725	[59]	
	66.67	33.33	721	[56]	
	66.67	33.33	714	**[This work]**	
L↔Mg_2Ca+ Mg-hcp	89.44	10.56	516	[60]	Eutectic
	89.51	10.49	517	[59]	
	88.95	11.05	525	[58]	
	87.75	12.25	518	[56]	
	89.44	10.56	514	**[This work]**	

The calculated enthalpy of mixing of liquid Mg-Ca at 877°C is plotted in Figure 4.2 together with experimental values from the literature [63,64]. As can be seen in this figure, the calculated enthalpy of mixing of liquid Mg-Ca agrees well with the experimental data of Sommer *et al.* [64], whereas, the measured enthalpy of mixing by Agarwal *et al.* [63] is twice as large as that measured by Sommer *et al.* [64] and, hence, considered not reliable. Figure 4.2 shows that the minimum value of the enthalpy of mixing is around 50 at.% Mg. Comparison between experimental enthalpy of mixing of Mg-Ca liquid at 877°C [63,64] and the calculations using the modified quasichemical model and random solution model is shown in Figure 4.2. Although the experimental

phase diagram was reproduced by both models and the same number of optimized parameters were used, as can be seen in Table 4.1, the quasichemical model resulted in better agreement with the experimental data of Sommer *et al.* [64].

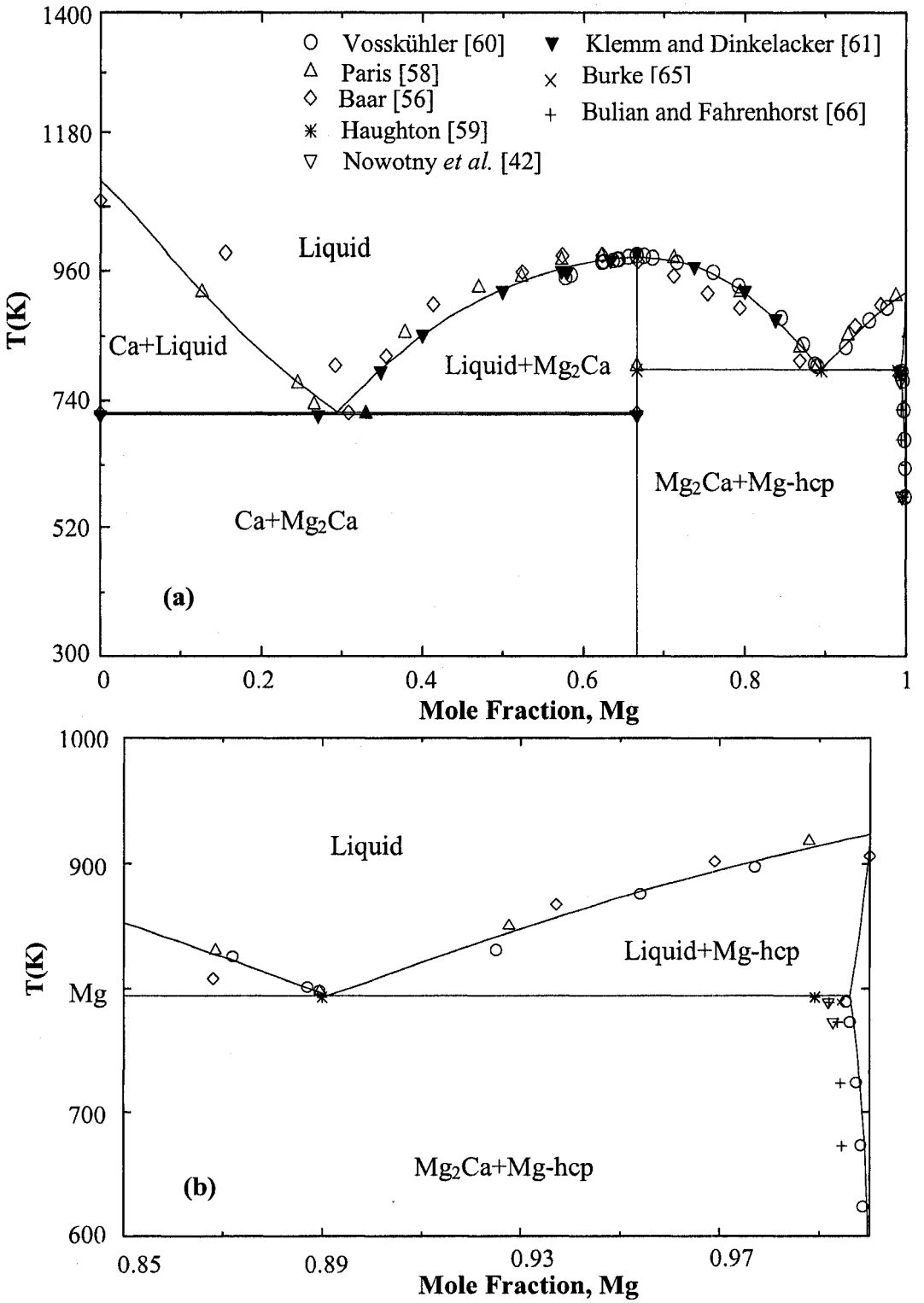

Figure 4.1: *(a) Re-optimized Mg-Ca System, (b) Mg-rich region of Mg-Ca system.*

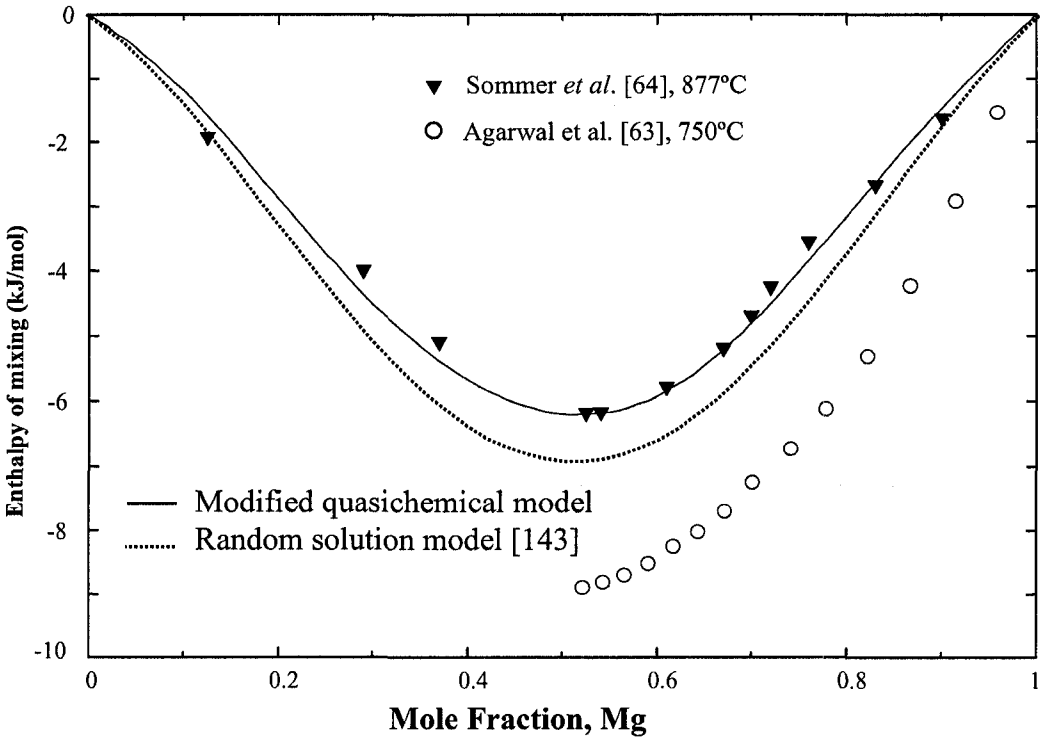

Figure 4.2: *Comparison between the calculated enthalpy of mixing of Mg-Ca liquid at 877°C using the modified quasichemical model and random solution model along with the experimental data [63,64].*

The entropy of mixing of the Mg-Ca liquid at 807°C calculated using the modified quasichemical model shows a minimum value near the composition 50 at.% Mg which corresponds to the composition where the enthalpy of mixing is minimum indicating a tendency for short range ordering in the Mg-Ca liquid as can be seen in Figure 4.3. This is in agreement with the work of Sommer [18] and Mishra *et al.* [19] who reported a tendency for glass formation close to this composition. Also, it can be seen from this figure that the indication for short range ordering in the liquid is more obvious in the curve obtained by the modified quasichemical model. Figure 4.4 presents the calculated activities of Ca and Mg in the liquid at 827°C in relation to the experimental data obtained by [74,75]. As can be seen in Figure 4.4, the calculated activities followed the

general trend of the experimental data. The deviation is within the uncertainty limits of the measured values especially since these data were obtained by vapor pressure measurements which usually show large degree of scatter.

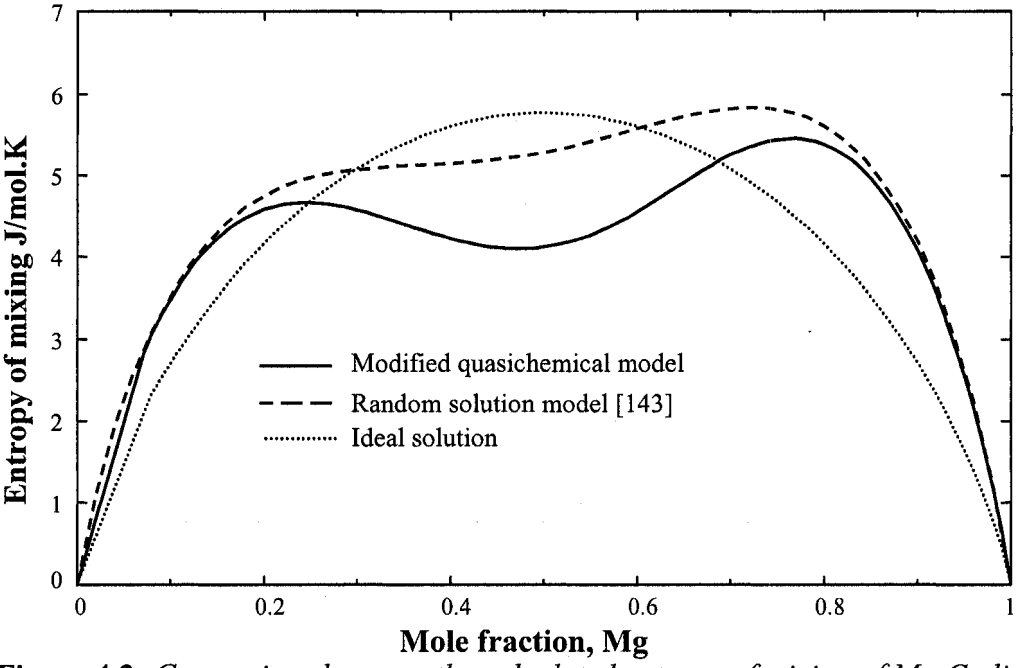

Figure 4.3: *Comparison between the calculated entropy of mixing of Mg-Ca liquid at 807°C using the modified quasichemical model and random solution model.*

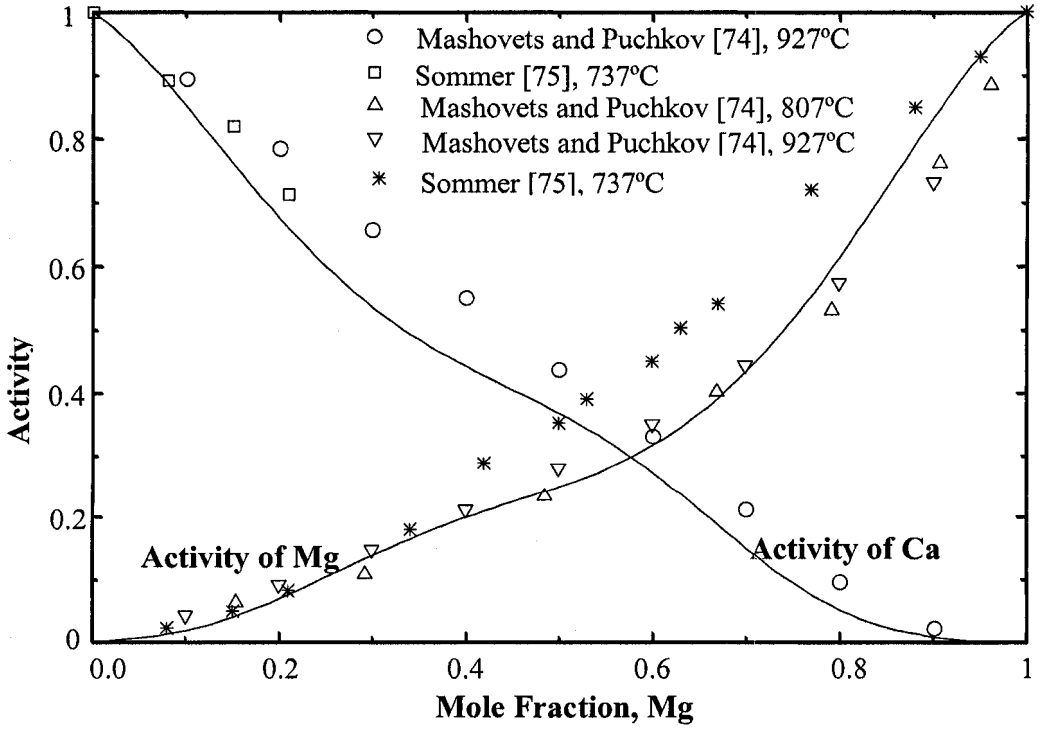

Figure 4.4: *Calculated activity of (a) Ca and (b) Mg in Mg-Ca liquid at 827°C (Reference state: Ca-liquid and Mg-liquid).*

In this work, the calculated heat of formation of Mg_2Ca is -13.47 kJ/mol.atom, which is in agreement with the heat of formation measured using tin solution calorimetry by King and Kleppa [73], and Davison and Smith [70] as -13.5±1.25 kJ/mol.atom and -13.17±2.63 kJ/mol.atom, respectively.

4.1.2 Mg-Sr Phase Diagram

Experimental phase diagram, enthalpy of mixing and the activities of Mg and Sr in the liquid phase were used to optimize the thermodynamic model parameters of the liquid and the intermetallic compounds in this system. The optimized model parameters as well as the binary invariant points are given in Tables 4.3 and 4.4, respectively. The re-optimized phase diagram of the Mg-Sr system in relation to the experimental data from the literature is shown in Figure 4.5. Good agreement between the re-optimized phase diagram and the measured liquidus points of [77-79,155] can be observed in this figure.

Table 4.3: *Optimized thermodynamic parameters of the Mg-Sr system (J/mol.atom).*

Phase	**The modified quasichemical model** $\Delta^{ex}G^{liq} = \Delta g_{ij}^{\circ} + \sum_{\substack{i\geq 1\\ m\geq 1}} g_{ij}^{m\circ} x_{ii}^{m} + \sum_{\substack{j\geq 1\\ n\geq 1}} g_{ij}^{\circ n} x_{ij}^{n}$
Liquid (Mg,Sr)	$\Delta^{ex}G^{liq} = -447.89 + 0.15T + (-355.16 - 0.05T)x_{Sr,Sr}$ $+ (170.42 - 0.07T)x_{Mg,Mg}$ $Z_{MgSr}^{Sr} = 4$ $Z_{SrMg}^{Mg} = 6$
Mg_2Sr	$G_{Mg:Sr}^{Mg2Sr} = -7950.79 + 0.038T$
$Mg_{38}Sr_9$	$G_{Mg:Sr}^{Mg38Sr9} = -12206.3 + 0.16T$
$Mg_{23}Sr_6$	$G_{Mg:Sr}^{Mg23Sr6} = -12125.28 + 0.24T$
$Mg_{17}Sr_2$	$G_{Mg:Sr}^{Mg17Sr2} = -12330.53 + 0.91T$

Table 4.4: *Comparison between calculated and experimental values of the invariant reactions in the Mg-Sr system.*

Reaction	at.% Mg	at.% Sr	T(°C)	Reference	Reaction Type
Sr-bcc ↔Sr-fcc	0.00	100.00	547.0	[57]	Allotropic
	0.00	100.00	547.0	**[This work]**	
L↔Mg_2Sr+Sr-fcc	35.00	65.00	842.0	[155]	Eutectic
	30.00	70.00	438.0	[79]	
	29.60	70.40	426.0	[78]	
	30.56	69.44	426.0	**[This work]**	
L↔Mg_2Sr	66.67	33.33	680.0	[155]	Congruent
	66.67	33.33	680.0	[79]	
	66.67	33.33	689.0	[78]	
	66.67	33.33	676.6	**[This work]**	
L+Mg_2Sr↔$Mg_{23}Sr_6$	80.90	19.10	608.0	[79]	Peritectic
	80.64	19.36	603.0	[78]	
	79.31	20.69	600.7	**[This work]**	
L+$Mg_{23}Sr_6$↔$Mg_{38}Sr_9$	82.56	17.44	599.0	[79]	Peritectic
	82.50	17.50	598.0	[155]	
	81.50	18.50	595.6	**[This work]**	
L↔$Mg_{17}Sr_2$+$Mg_{38}Sr_9$	84.90	15.10	592.0	[79]	Eutectic
	84.50	15.50	587.0	[155]	
	84.50	15.50	592.0	[77]	
	83.40	16.60	599.0	[78]	
	84.90	15.10	592.4	**[This work]**	
L↔$Mg_{17}Sr_2$	90.00	10.00	609.0	[79]	Congruent
	90.00	10.00	603.0	[155]	
	90.00	10.00	606.0	[77]	
	89.47	10.53	604.0	[78]	
	89.47	10.53	595.4	**[This work]**	
L↔(Mg)+$Mg_{17}Sr_2$	94.00	6.00	586.0	[79]	Eutectic
	94.00	6.00	585±2	[155]	
	94.10	5.90	582.0	[77]	
	93.55	6.45	585.0	[78]	
	93.34	6.66	586.8	**[This work]**	

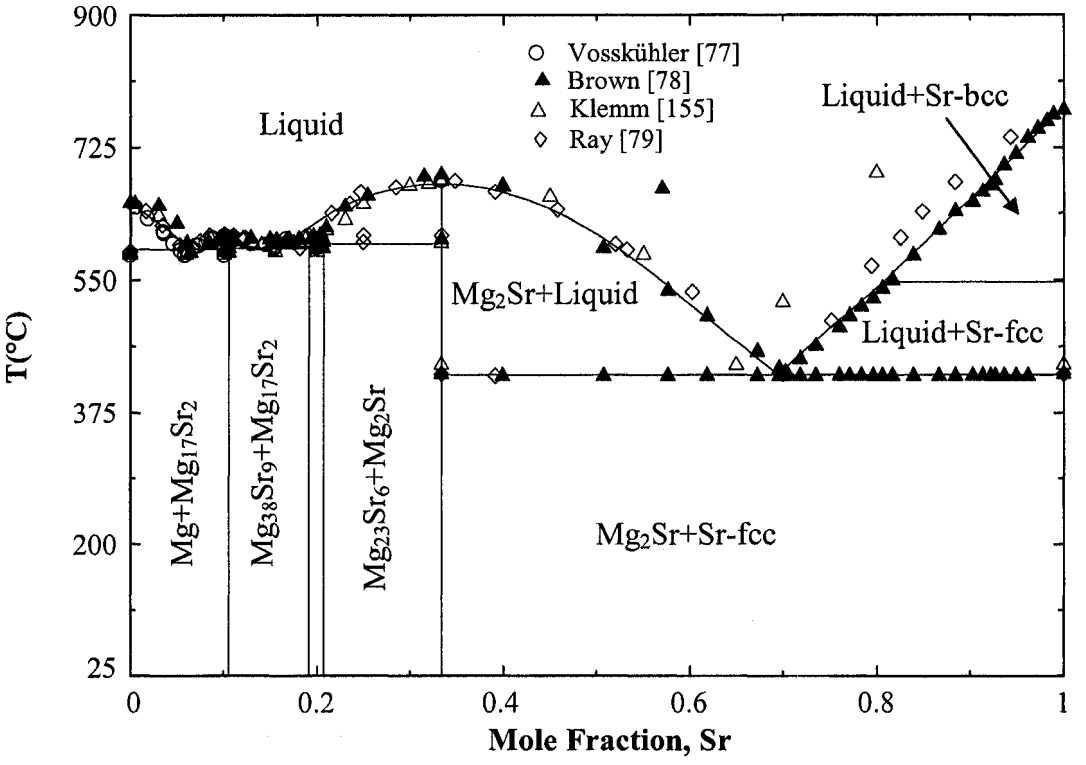

(a)

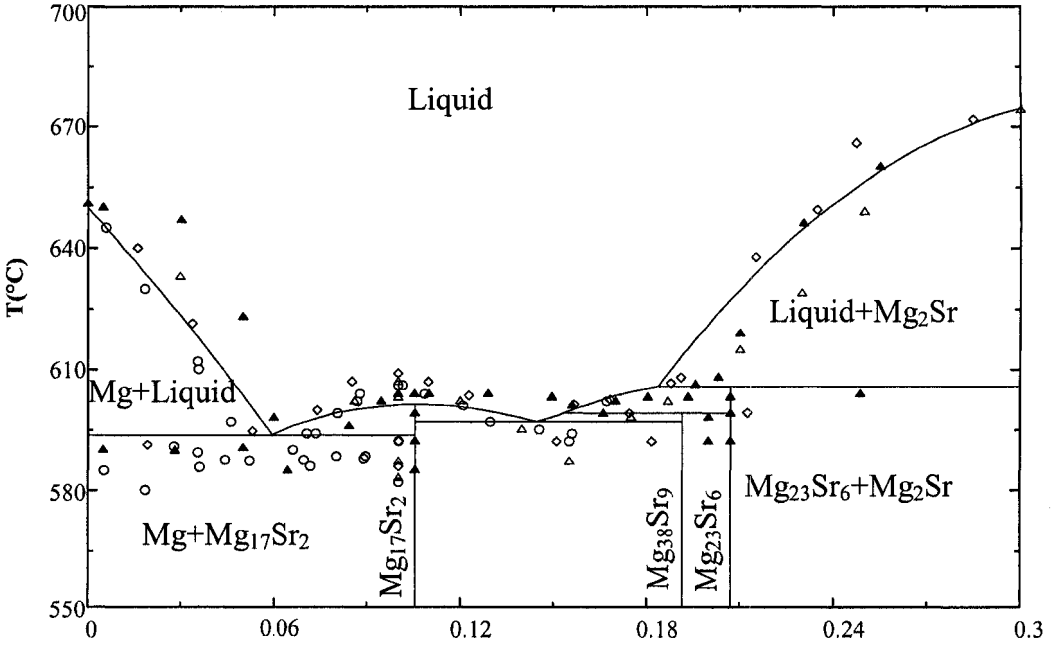

(b)

Figure 4.5: *(a) Re-optimized Mg-Sr system, (b) Mg-rich region of the Mg-Sr system.*

Also, good agreement between the calculated enthalpy of mixing at 807°C and the experimental data of Sommer *et al.* [64] can be observed in Figure 4.6. As can be seen in this figure, the enthalpy of mixing of Mg-Sr liquid at 807°C calculated using the modified quasichemical model is in better agreement with the experimental data than the random solution model. Figure 4.7 shows the calculated activities of Mg and Sr in the Mg-Sr liquid at 827°C along with the experimental data of [80]. The calculated activities show good agreement with the experimental data.

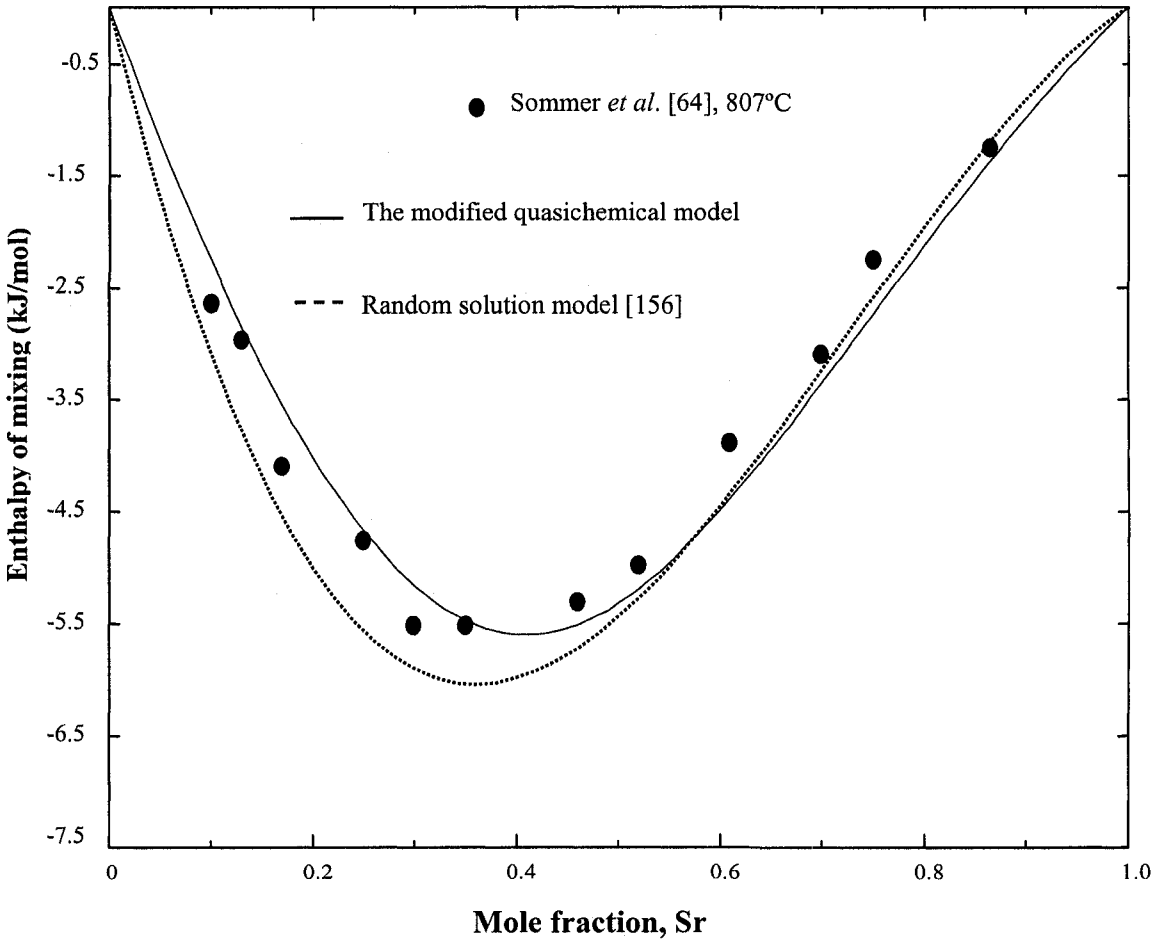

Figure 4.6: *Comparison between the calculated enthalpy of mixing of Mg-Sr liquid at 807°C using the modified quasichemical model and random solution model along with the experimental data of [64].*

The formation of an intermetallic compound from its components results in changes in the structure, bond type and strength. The Gibbs free energy of formation of the intermetallic compounds gives an indication of their stability. According to thermodynamic principles, the formation of an intermetallic compound results in small change in entropy that ranges from -10 to 10 J/mol.atom which depends on the configurational and vibrational contribution to the entropy of formation. Hence, an unreasonable prediction of the entropy of formation creates a less reliable value for the enthalpy of formation. In this work, the calculated enthalpy of formation of Mg_2Sr is -7.95 kJ/mol.atom, which is in agreement with the value of the enthalpy of formation measured from solid Mg and Sr using tin solution calorimetry by King and Kleppa [73] of -7.18 kJ/mol.atom, but is different from that of Zhong *et al.* [148] at -10.62 kJ/mol.atom. Figure 4.8 shows a comparison between the calculated enthalpy of formation from this work and the Zhong's *et al.* [148] results. In this work, the calculated entropy of formation of Mg_2Sr is 0.038 J/mol.atom compared to the Zhong *et al.* [148] calculations resulting in 3.03 J/mol.atom. This difference resulted in a less reliable value for the enthalpy of formation. The entropy of formation of other intermetallic compounds in the Mg-Sr system calculated by Zhong *et al.* [148] are also different from this work. For example, the entropy of formation of $Mg_{38}Sr_9$ is 54.73 J/mol.atom compared to the calculated value of 0.16 J/mol.atom. Therefore, this difference in the entropy of formation between the two works resulted in different values for the enthalpy of formation as can be seen in Figure 4.8.

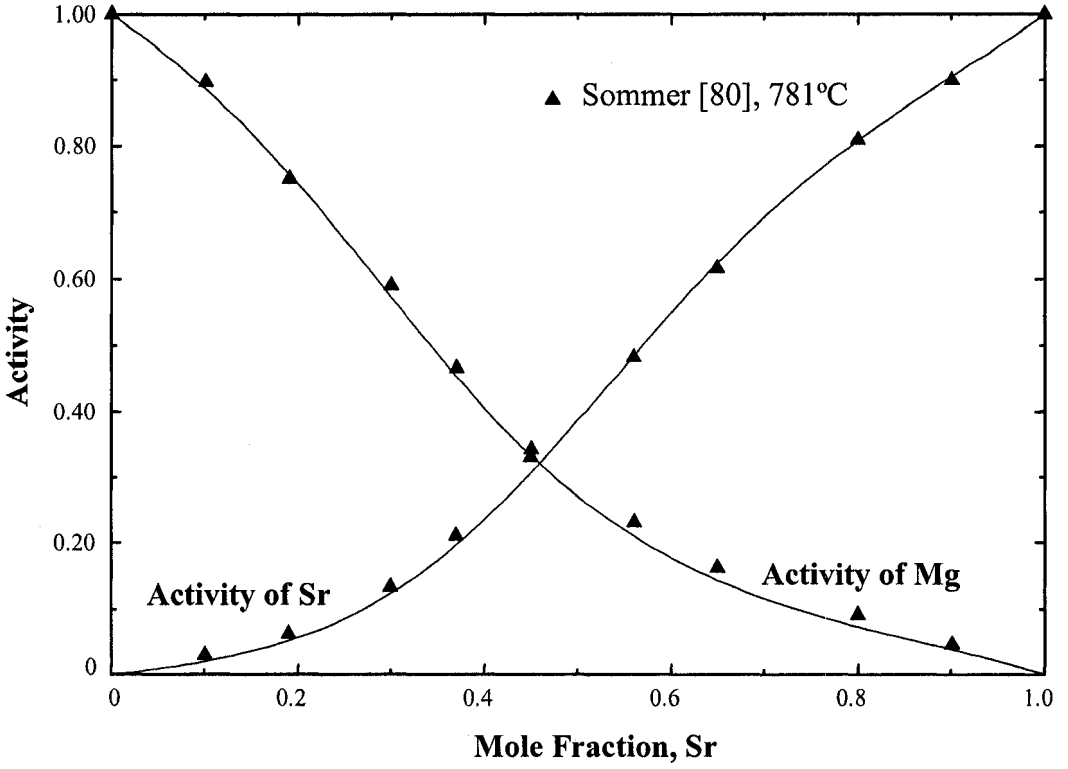

Figure 4.7: *Calculated activity of Mg and Sr in Mg-Sr liquid with the experimental data of [80] at 827°C (Reference state: Ca-liquid and Mg-liquid).*

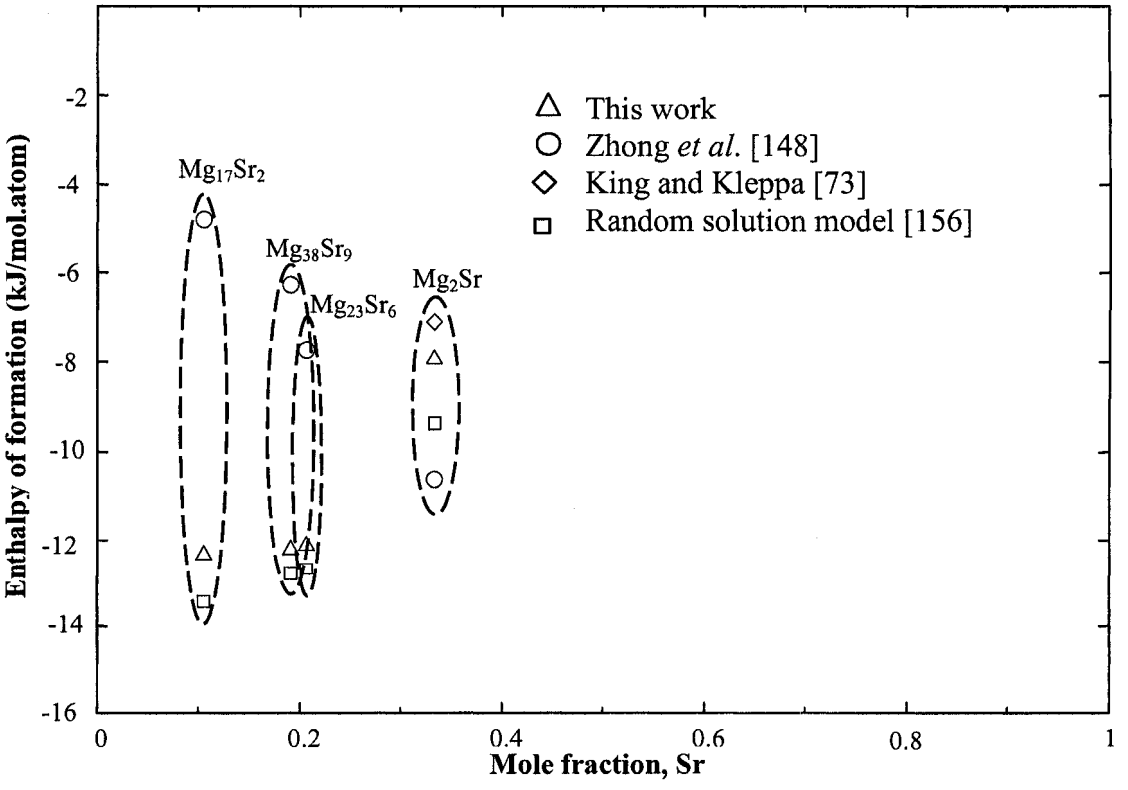

Figure 4.8: *Enthalpy of formation of different intermetallic compounds in the Mg-Sr system.*

For the Mg-Ca and Mg-Sr systems, it was found that the random solution model agrees reasonably well with the experimental phase diagram, but the modified quasichemical model gives better agreement with the experimental thermodynamic data and the experimental phase diagram. The modified quasichemical model can also describe the short range ordering better than random solution model. Therefore, the modified quasichemical model will be used to re-optimize the rest of binary sub-systems of the Mg-Al-Ca-Sr.

4.1.3 Al-Sr Phase Diagram

The re-optimized Al-Sr system along with all experimental data from the literature is shown in Figure 4.9. As can be seen from this figure, the calculated liquidus and invariant points are in good agreement with the experimental data of Closset *et al.* [26], and Bruzzone and Merlo [30] but differ slightly from those obtained by Vakhobov *et al.* [24] and Vakhobov *et al.* [25]. The results of Closset *et al.* [26] are supported with good description of the experimental methods and they are considered more reliable compared to [24,25] works which are in agreement with Chartrand and Pelton's [34] assessment.

Table 4.5: *Optimized thermodynamic parameters of the Al-Sr system (J/mol.atom).*

Phase	**The modified quasichemical model** $\Delta^{ex}G^{liq} = \Delta g^{\circ}_{ij} + \sum_{\substack{i\geq 1 \\ m\geq 1}} g^{m\circ}_{ij} x_{ii}^{m} + \sum_{\substack{j\geq 1 \\ n\geq 1}} g^{\circ n}_{ij} x_{ij}^{n}$
Liquid (Al,Sr)	$\Delta^{ex}G^{liq} = -1511.5 + 0.54T + (-187.10 - 0.269T)x_{Sr,Sr}$ $+ (442.76 - 0.108T)x_{Al,Al}$ $Z^{Sr}_{AlSr} = 4$ $Z^{Al}_{SrAl} = 6$
Al_4Sr	$G^{Al4Sr}_{Al:Sr} = -30853 + 1.4T$
Al_3Sr_8	$G^{Al3Sr8}_{Al:Sr} = -11868 + 0.4T$
Al_7Sr_8	$G^{Al7Sr8}_{Al:Sr} = -21198 + 0.25T$
Al_2Sr	$G^{Al2Sr}_{Al:Sr} = -30409 + 2.1T$

Table 4.5 lists the thermodynamic model parameters obtained by optimization using the experimental thermodynamic and phase equilibrium data from the literature. The calculated invariant points in relation to the experimental data from the literature are presented in Table 4.6. The calculated liquidus and invariant points of the Al-Sr system are in good agreement with the experimental data up to 60 at.% Sr as can be seen in Table 4.6 and Figure 4.9. It is noteworthy that discrepancies between experimental data in the Sr-rich region are due to the high reactivity of Sr.

Table 4.6: *Comparison between calculated and experimental values of the invariant*

Reaction	at.% Al	at.% Sr	T(°C)	Reference	Reaction Type
$L \leftrightarrow Al+Al_4Sr$	99.25	0.75	654	[26]	Eutectic
	99.15	0.85	654±1	[31]	
	98.70	1.30	653	[32]	
	99.36	0.64	656	[This work]	
$L \leftrightarrow Al_4Sr$	80.00	20.00	1000±20	[23]	Congruent
	80.00	20.00	1040	[30]	
	80.00	20.00	1025	[26]	
	80.00	20.00	1038	[25]	
	80.00	20.00	1029	[This work]	
$L+Al_4Sr \leftrightarrow Al_2Sr$	66.67	33.33	936	[30]	Peritectic
	66.67	33.33	920	[26]	
	66.67	33.33	923	[This work]	
$L+Al_2Sr \leftrightarrow Al_7Sr_8$	46.67	53.33	666	[30]	Peritectic
	46.67	53.33	664	[26]	
	46.67	53.33	667	[This work]	
$L \leftrightarrow$ Sr-bcc	0.00	100.00	769	[81]	Melting
	0.00	100.00	770	[This work]	
$L \leftrightarrow Al_7Sr_8+Al_3Sr_8$	27.50	72.50	593	[30]	Eutectic
	27.29	72.71	604	[This work]	
$L \leftrightarrow$ Sr-bcc$+Al_3Sr_8$	19.22	80.78	599	[This work]	Eutectic

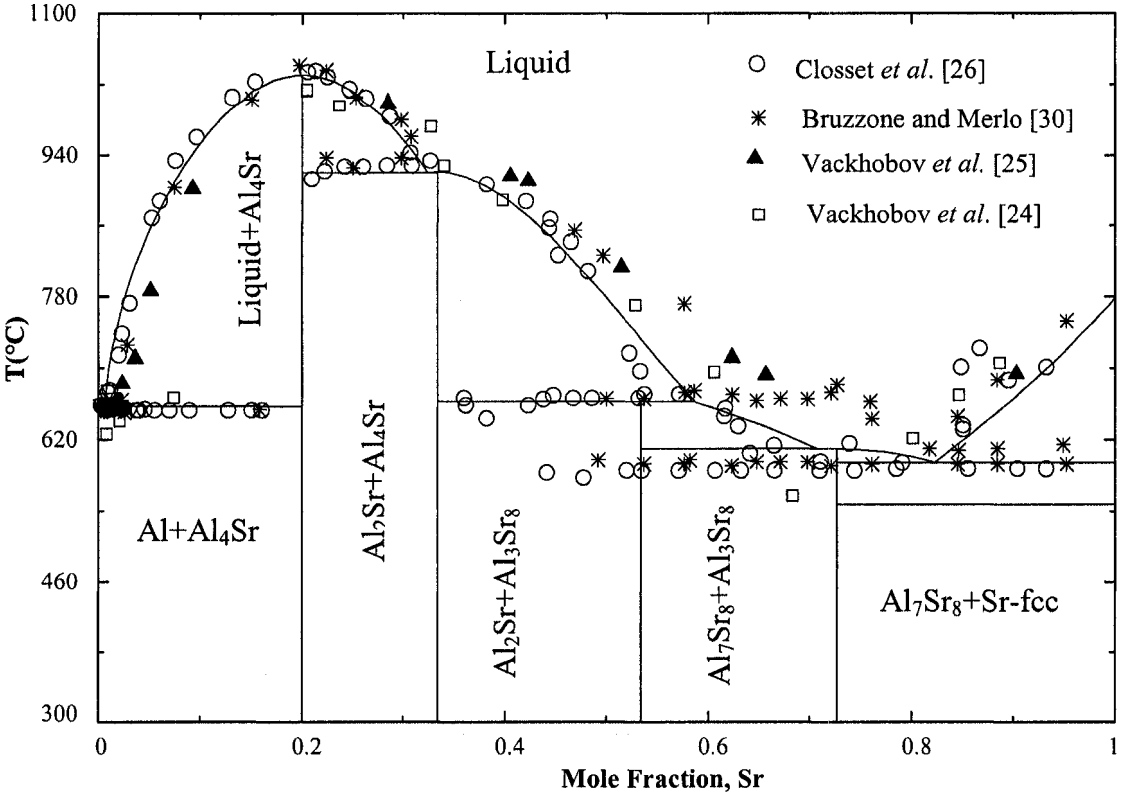

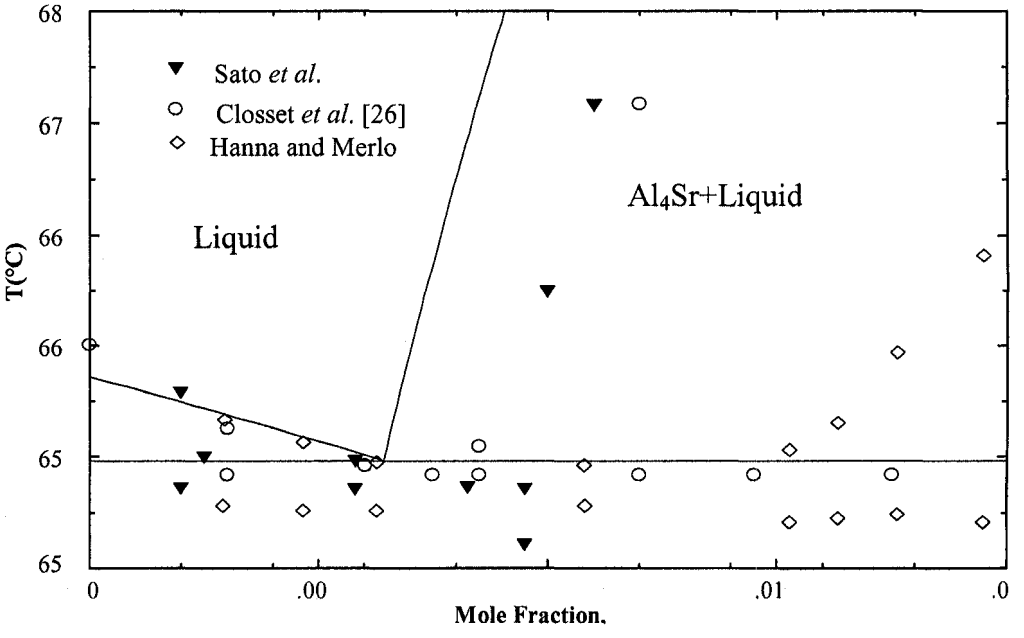

(b)

Figure 4.9: *(a) Re-optimized Al-Sr system, (b) Al-rich region of the Al-Sr system.*

The calculated enthalpy of mixing of Al-Sr liquid at 852°C is plotted in Figure 4.10 together with experimental values from the literature [37,38]. As can be seen in this

figure, the calculated enthalpy of mixing of Al-Sr liquid agrees well with the experimental data. The reported data are consistent over all the composition range and show no temperature dependence. Figure 4.10 shows that the minimum value of the enthalpy of mixing occurs around 40 at.% Sr which indicates high stability of the liquid and a tendency for short range ordering.

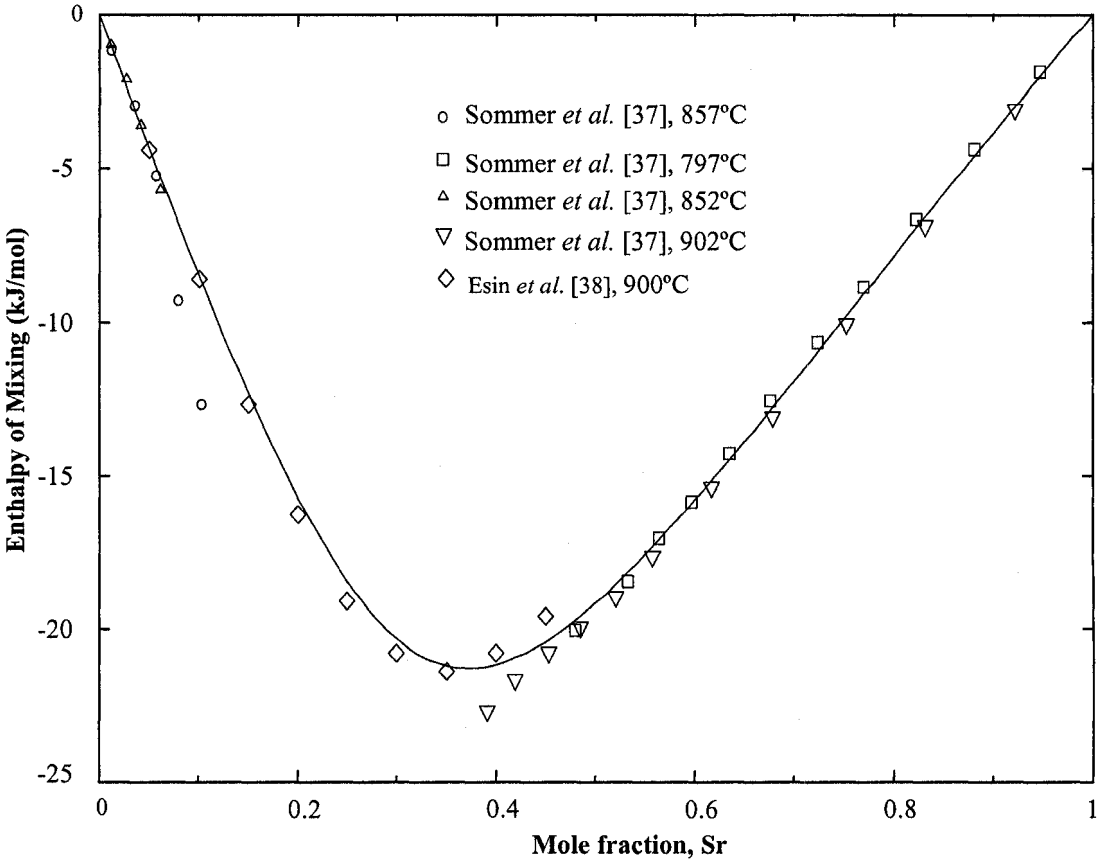

Figure 4.10: *Calculated enthalpy of mixing of Al-Sr liquid at 852°C (Reference state: Al-liquid and Sr-liquid).*

The experimentally measured Sr activity in the liquid phase [23,24,39] is compared with the calculation performed at 1050°C as shown in Figure 4.11. It can be seen in this figure that mixing up to 60 at.% of Sr in the Al-Sr liquid demonstrates

negative deviation from Raoult's ideal solution, but mixing 60-100 at.% Sr in the liquid obeys Raoult's model for the ideal solution.

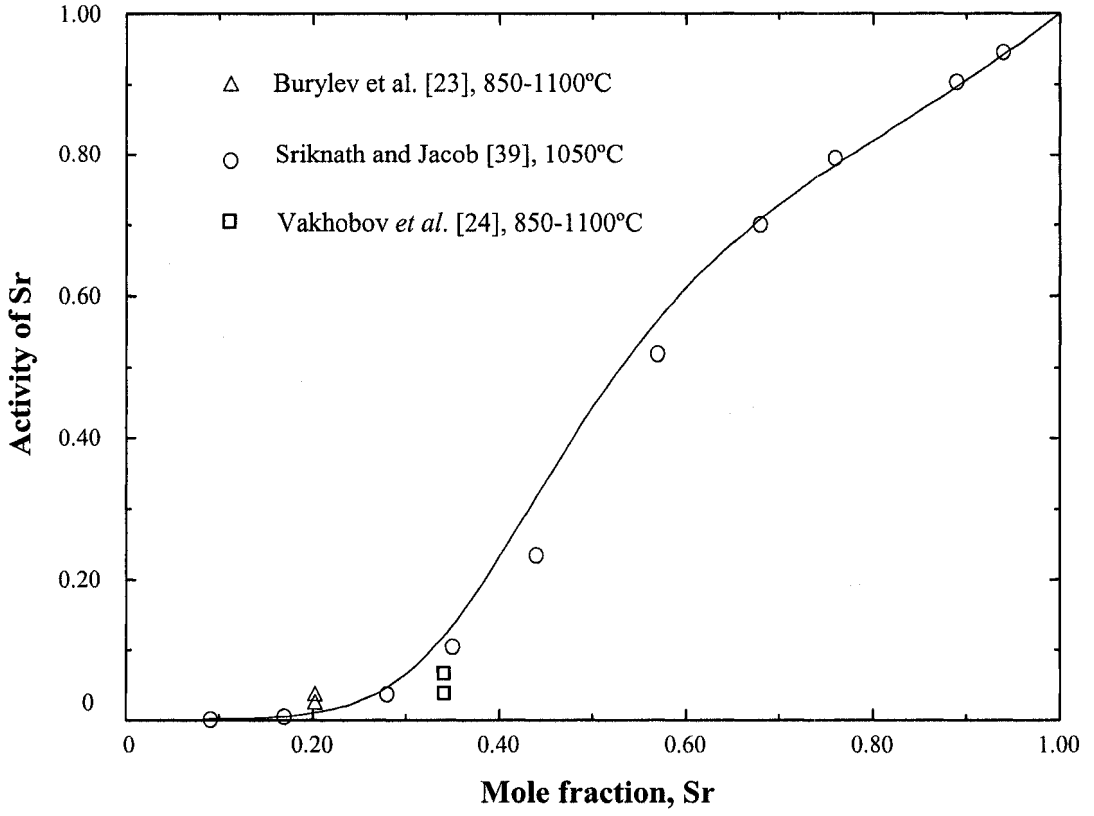

Figure 4.11: *Calculated activity of Sr in the Al-Sr liquid at 1050°C (Reference state: Al-liquid and Sr-liquid).*

4.1.4 Al-Ca Phase Diagram

The experimental phase diagram, enthalpy of mixing and the activities of Al and Ca in the liquid phase were used to optimize the thermodynamic model parameters of the liquid and the intermetallic compounds in this system. The optimized model parameters as well as the binary invariant points are given in Tables 4.7 and 4.8, respectively. The re-optimized phase diagram of the Al-Ca system in relation to the experimental data from the literature is shown in Figure 4.12. Good agreement between the re-optimized phase diagram and the measured liquidus points of [29,40,41] can be observed in this figure.

Table 4.7: *Optimized thermodynamic parameters of the Al-Ca system (J/mol.atom).*

Phase	**The modified quasichemical model** $\Delta^{ex}G^{liq} = \Delta g_{ij}^{\circ} + \sum_{\substack{i\geq 1 \\ m\geq 1}} g_{ij}^{m\circ} x_{ii}^{m} + \sum_{\substack{j\geq 1 \\ n\geq 1}} g_{ij}^{\circ n} x_{ij}^{n}$
Liquid (Al,Ca)	$\Delta^{ex}G^{liq} = -1296.4 + 0.48T + (-0.142T)x_{Ca,Ca} + (134.3 + 0.031T)x_{Al,Al}$ $Z_{AlCa}^{Al} = 6, Z_{CaAl}^{Ca} = 4$
Al_2Ca	$G_{Al:Ca}^{Al2Ca} = -28559 + 1.8T$
Al_4Ca	$G_{Al:Ca}^{Al4Ca} = -17327 + 0.46T$
Al_3Ca_8	$G_{Al:Ca}^{Al3Ca8} = -16309 + 0.21T$
$Al_{14}Ca_{13}$	$G_{Al:Ca}^{Al14Ca13} = -28209 + 0.18T$

Table 4.8: *Comparison between calculated and experimental values of the invariant reactions in the Al-Ca system.*

Reaction	at.% Al	at.% Ca	T(°C)	Reference	Reaction Type
L↔Al-fcc	100.00	0.00	661	[81]	Melting
	100.00	0.00	661	**[This work]**	
L↔Al-fcc+Al_4Ca	94.90	5.10	613	[29]	Eutectic
	94.80	5.20	616	[41]	
	94.50	5.50	610	[40]	
	95.22	4.78	612	**[This work]**	
L+Al_2Ca↔Al_4Ca	80.00	20.00	690	[40]	Peritectic
	80.00	20.00	700	[41]	
	80.00	20.00	700	[29]	
	80.00	20.00	700	**[This work]**	
L↔Al_2Ca	66.67	33.33	1079	[41]	Congruent
	66.67	33.33	1086	[29]	
	66.67	33.33	1083	**[This work]**	
L+Al_2Ca↔$Al_{14}Ca_{13}$	50.00	50.00	633	[29]	Peritectic
	51.85	48.15	631	**[This work]**	
L↔$Al_{14}Ca_{13}$+Al_3Ca_8	35.50	64.50	545	[41]	Eutectic
	33.70	66.30	556	[29]	
	33.10	66.90	550	[40]	
	33.44	66.56	557	**[This work]**	
L↔Ca-bcc+Al_3Ca_8	20.00	80.00	560	[29]	Eutectic
	20.44	79.56	554	**[This work]**	
L↔Al_3Ca_8	27.27	72.73	579	[29]	Congruent

The calculated enthalpy of mixing at 827°C and the experimental data of Sommer *et al.* [37] and Notin *et al.* [47] are shown in Figure 4.13. As can be seen from this figure, the calculated enthalpy of mixing of liquid Al-Ca is in good agreement with the experimental data. The calculated entropy of mixing of the Al-Ca liquid at 827°C shows a minimum value near the composition 40 at.% Ca which corresponds to the composition where the enthalpy of mixing is minimum indicating a tendency for short range ordering in the Al-Ca liquid as can be seen in Figure 4.14.

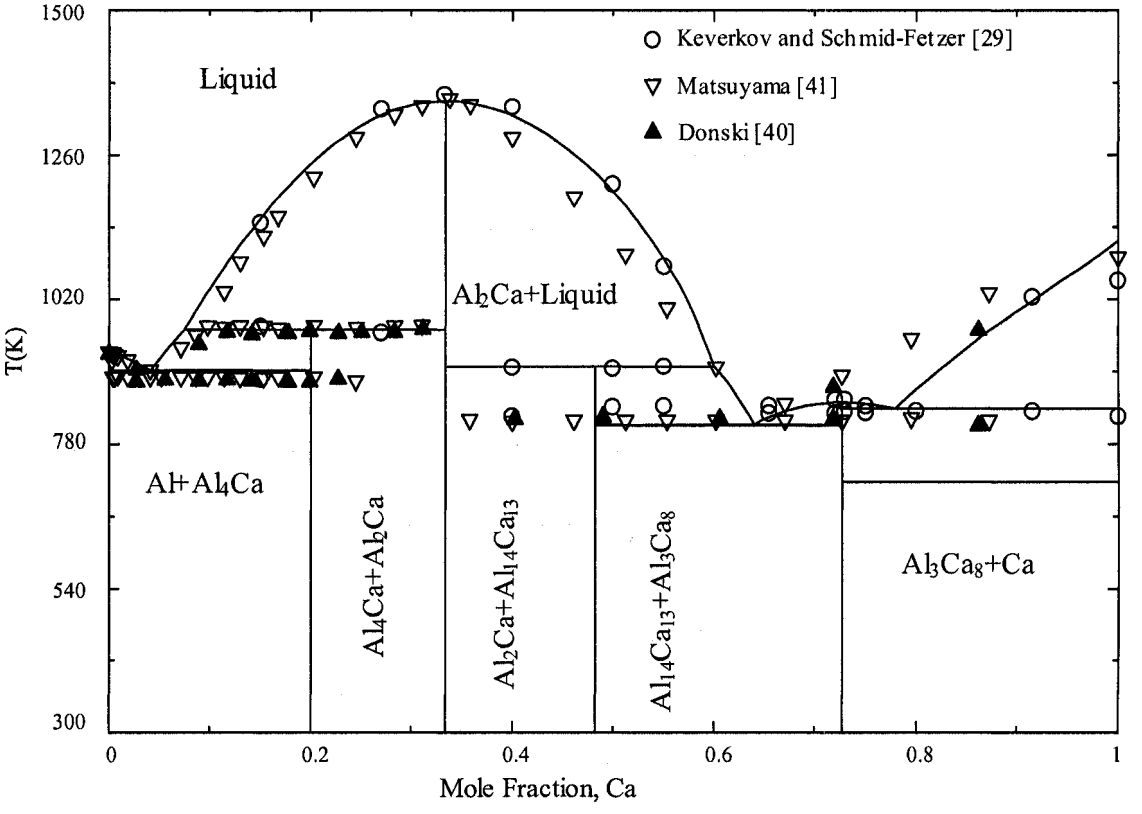

Figure 4.12: *Re-optimized Al-Ca system.*

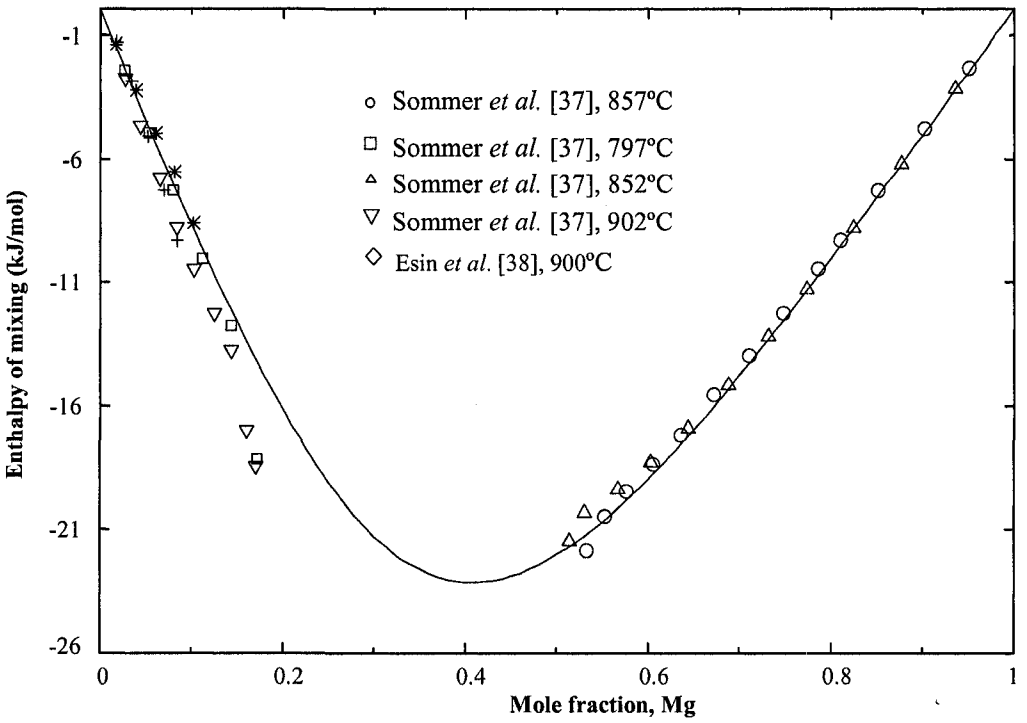

Figure 4.13: *Calculated enthalpy of mixing of Al-Ca liquid at 827°C (Reference state: Al-liquid and Ca-liquid).*

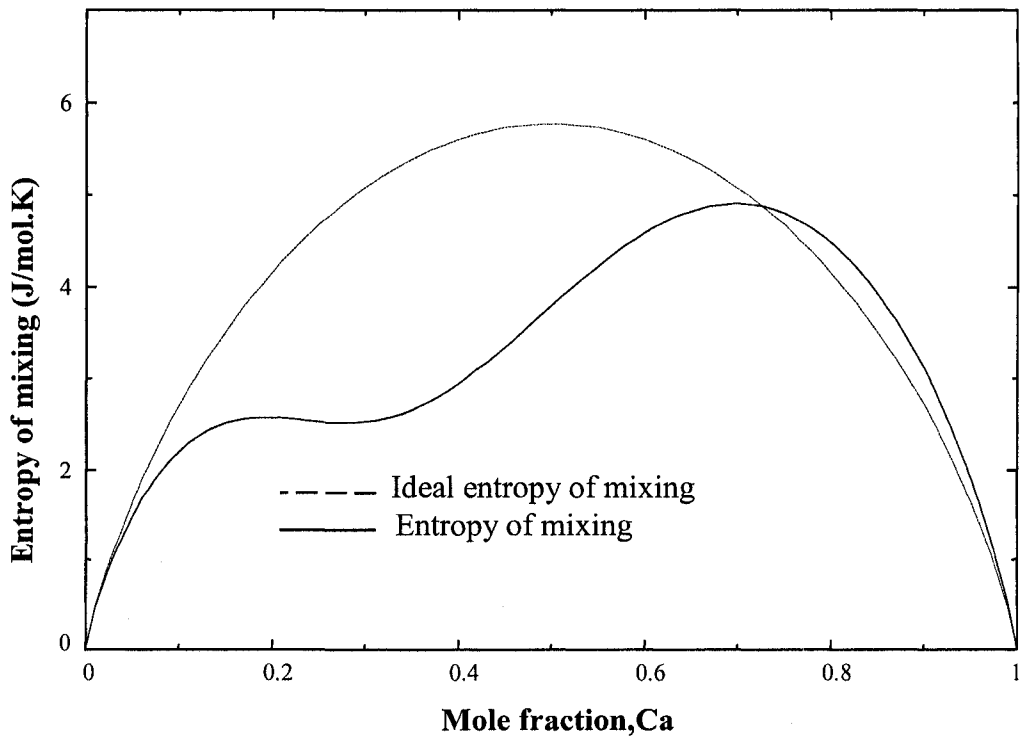

Figure 4.14: *Entropy of mixing of the Al-Ca liquid at 827°C.*

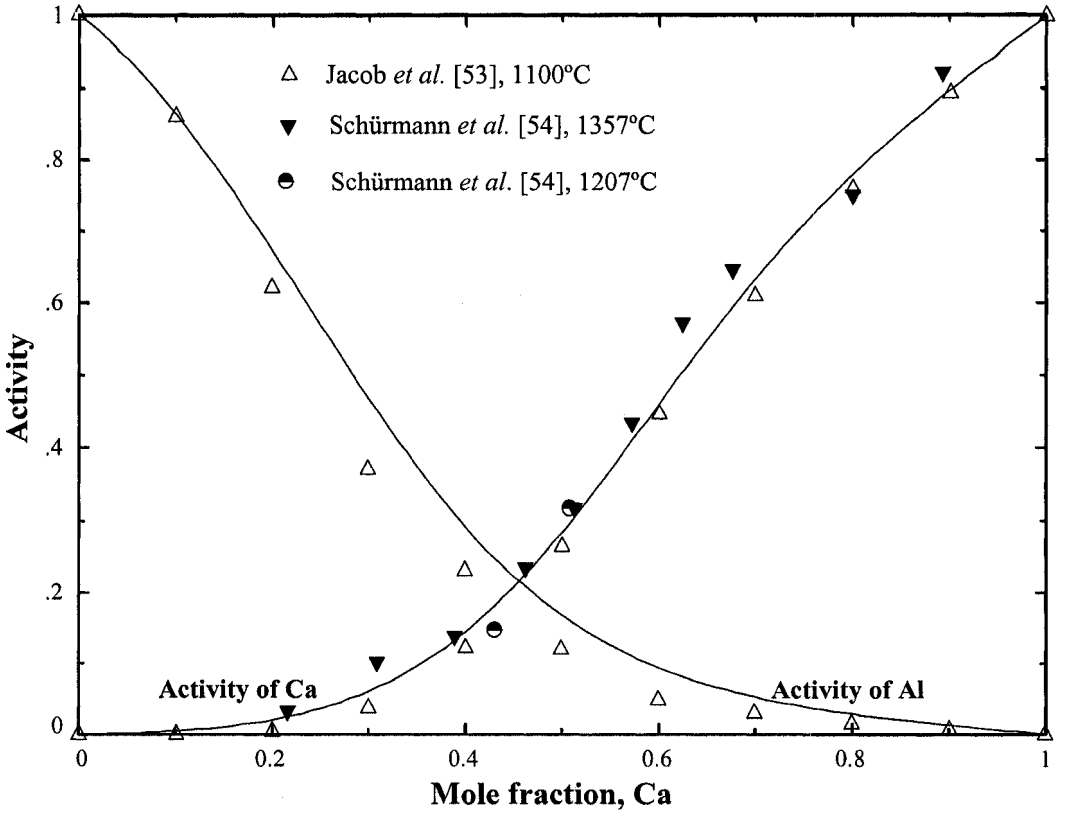

Figure 4.15: *Calculated activity of Ca and Al in the Al-Ca liquid at 1100°C (Reference state: Al-liquid, Ca-liquid).*

Figure 4.15 shows the calculated activities of Al and Ca in the Al-Ca liquid at 1100°C along with the experimental data of Jacob *et al.* [53] and Schürmann *et al.* [54]. The calculated activities show good agreement with the experimental data. The calculated heat of formation of the intermetallic compounds in the Al-Ca system along with the measured heat of formation is plotted in Figure 4.16. The calculated and the measured heat of formation of the compounds in the Al-Ca system are in accord.

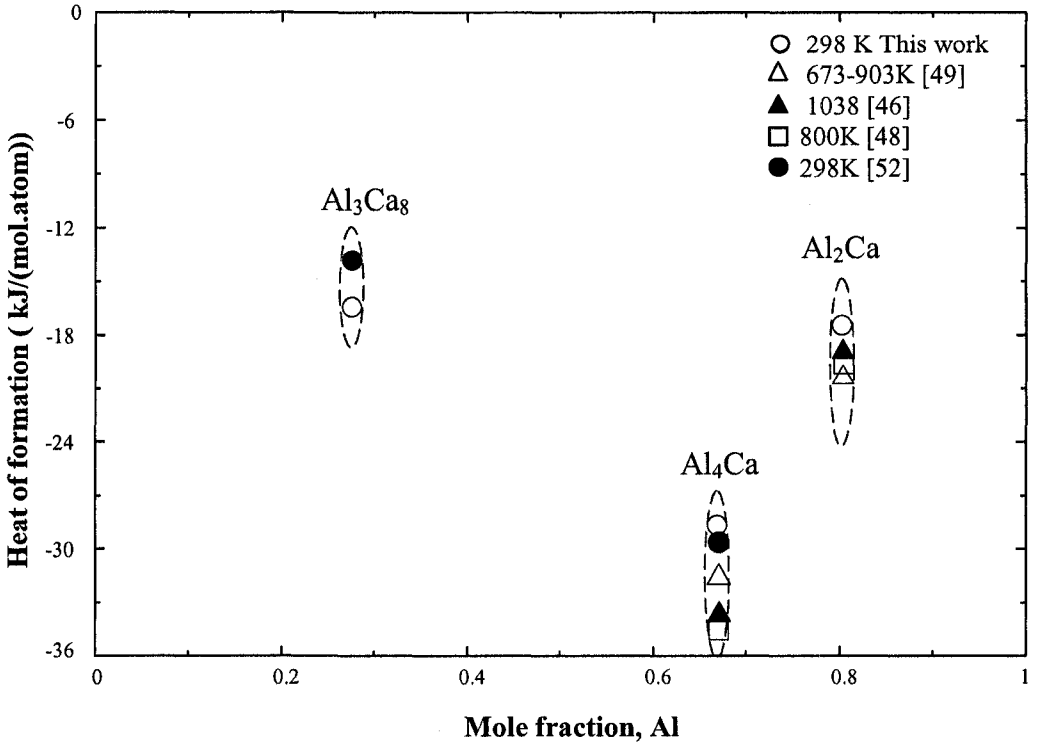

Figure 4.16: *Heat of formation of different intermetallic compounds in the Al-Ca system.*

4.1.5 Ca-Sr Phase Diagram

The experimental data of Schottmiller *et al.* [81], and Predel and Sommer [88] are used to re-optimize the Ca-Sr system. The stable phases in the present assessment of this system are liquid, fcc and bcc. Figure 4.17 shows the re-optimized phase diagram with the experimental data of Schottmiller *et al.* [81]. The re-optimized Ca-Sr system agrees well with the experimental data. The optimized model parameters are given in Table 4.9. Figure 4.18 shows good agreement between the calculated enthalpy of mixing and the experimental data of [88]. Physically, the positive enthalpy of mixing reflects the fact that the formation of Ca-Ca and Sr-Sr pairs is more favorable than the formation of Ca-Sr pairs. In this work, the excess entropy of mixing of the liquid alloys is relatively small with maximum value of +0.02 J/mol.K which is in agreement with the evaluation of

Alcock *et al.* [87]. Due to the lack of experimental thermodynamic data for the Ca-Sr system, its thermodynamic description was predicted based on the experimental work of Schottmiller *et al.* [81], and Predel and Sommer [88] only.

Table 4.9: *Optimized thermodynamic parameters of the Ca-Sr system (J/mol.atom).*

Phase	**The modified quasichemical model** $\Delta^{ex}G^{liq} = \Delta g^{\circ}_{ij} + \sum_{\substack{i\geq 1 \\ m\geq 1}} g^{m\circ}_{ij} x_{ii}^{m} + \sum_{\substack{j\geq 1 \\ n\geq 1}} g^{\circ n}_{ij} x_{ij}^{n}$
Liquid (Ca,Sr)	$\Delta^{ex}G^{liq} = 43.74 + 0.01T + 22.85x_{Ca,Ca} - 6.09x_{Sr,Sr}$ $Z^{Sr}_{CaSr} = 3$ $Z^{Ca}_{SrCa} = 3$
Bcc	$G^{bcc}_{Ca:Sr} = 3770.0 + 0.01T$
Fcc	$G^{fcc}_{Ca:Sr} = 3770.0 + 0.11T$

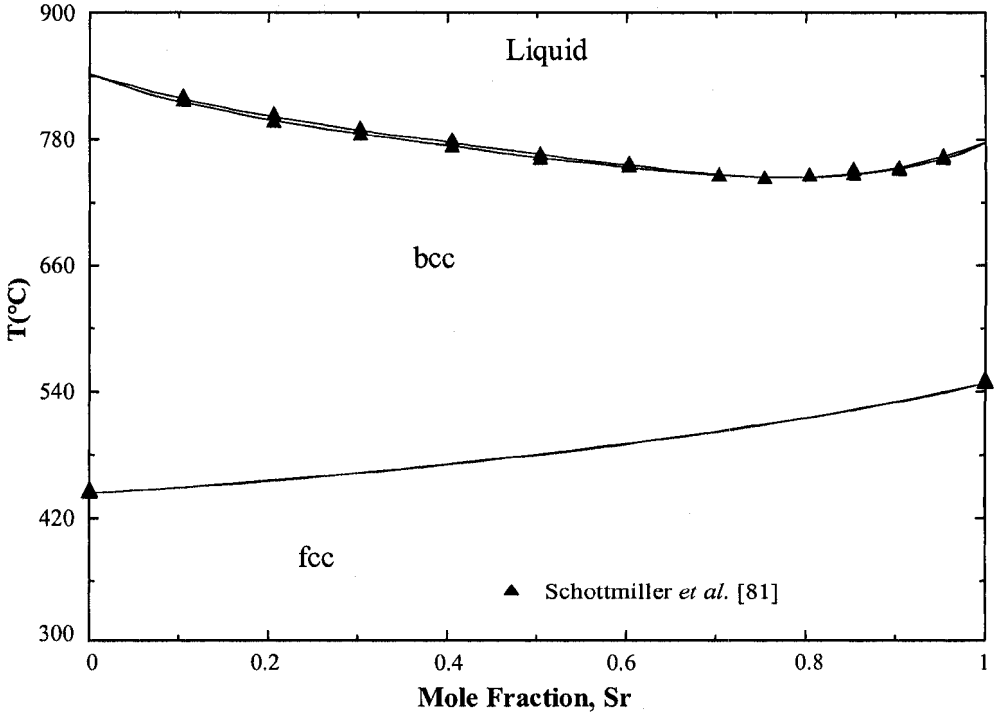

Figure 4.17: *Re-optimized Ca-Sr system.*

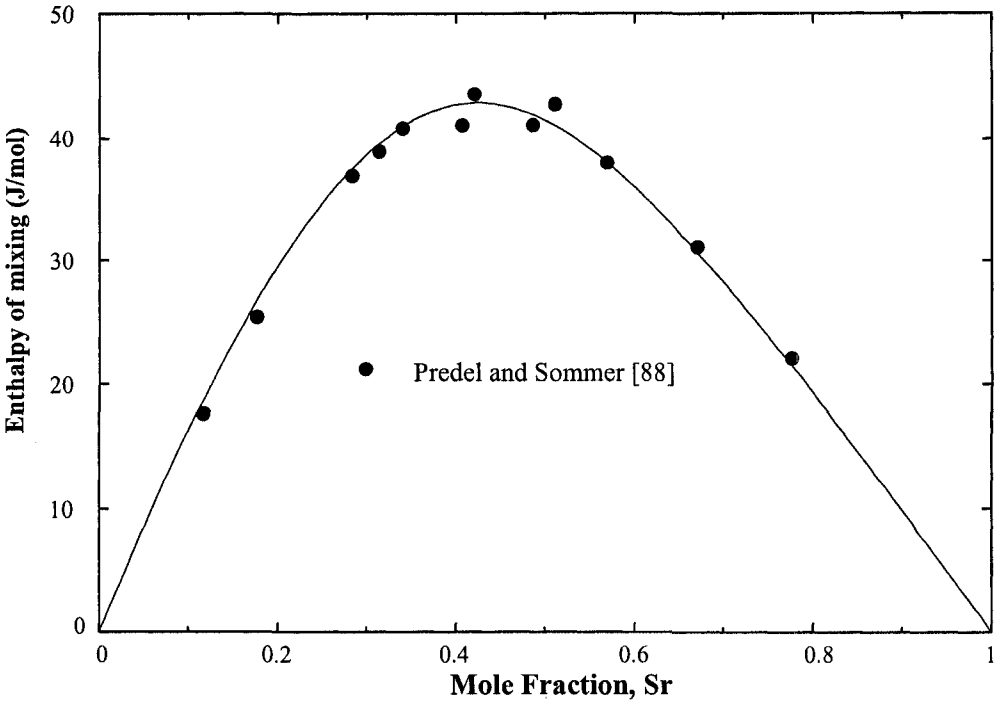

Figure 4.18: *Calculated heat of mixing of Ca-Sr liquid at 827°C (Reference state: Ca-liquid, Sr-liquid).*

4.1.6 Mg-Al Phase Diagram

The re-optimized Mg-Al phase diagram along with all experimental data from the literature is shown in Figure 4.19. As can be seen from this figure the calculated liquidus and invariant points are in good agreement with the experimental data. The optimized model parameters as well as the binary invariant points are given in Tables 4.10 and 4.11, respectively.

Good agreement between the re-optimized phase diagram and the measured liquidus points of [90,93,98,167,168,172,173] can be observed in this figure. Figure 4.20 presents the calculated activities of Mg in the liquid at 800°C in relation to the experimental data obtained by [105,107-109,112,114,182,183]. As can be seen in Figure 4.20, the calculated activity of Mg shows good agreement with the experimental data and small deviation from ideal solution.

Table 4.10: *Optimized thermodynamic parameters of the Mg-Al system (J/mol.atom).*

Phase	**The modified quasichemical model** $\Delta^{ex}G^{liq} = \Delta g_{ij}^{\circ} + \sum_{\substack{i\geq 1 \\ m\geq 1}} g_{ij}^{m\circ} x_{ii}^{m} + \sum_{\substack{j\geq 1 \\ n\geq 1}} g_{ij}^{\circ n} x_{ij}^{n}$
Liquid (Mg,Al)	$\Delta^{ex}G^{liq} = -256.7 + 0.16T + 24.94x_{Mg,Mg} + 41.83x_{Al,Al}$ $Z_{MgAl}^{Al} = 6$ $Z_{AlMg}^{Mg} = 6$
(Mg)	$G_{Mg:Al}^{(Mg)} = 1950 + 2T + (1480 - 2.1T)(x_{Mg} - x_{Al}) + 3500(x_{Mg} - x_{Al})^2$
(Al)	$G_{Mg:Al}^{(Al)} = 4971 - 3.5T + (900 + 0.423T)(x_{Mg} - x_{Al}) + 950(x_{Mg} - x_{Al})^2$
$Mg_{23}Al_{30}$	$G_{Mg:Al}^{Mg_{23}Al_{30}} = -991.8 + 173T$
$Mg_{89}Al_{140}$	$G_{Mg:Al}^{Mg_{89}Al_{140}} = -1075 + 675T$
γ	$G(Mg, Al : Al, Mg) = 113100 - 14.5T$ $G(Mg, Mg : Al, Mg) = 113100 - 14.5T$

Table 4.11: *Comparison between calculated and experimental values of the invariant reactions in the Mg-Al system.*

Reaction	at.% Mg	at.% Al	T(°C)	Reference	Reaction Type
L ↔Al-Fcc+$Mg_{89}Al_{140}$	38.10	61.90	448.0	[167]	Eutectic
	36.90	63.10	445.0	[98]	
	38.30	61.70	448.0	[90]	
	37.40	62.60	449.9	[94]	
	36.35	63.65	448.9	**[This work]**	
L ↔γ+$Mg_{89}Al_{140}$	42.50	57.50	449.8	[92]	Eutectic
	42.47	57.53	447.9	**[This work]**	
γ+$Mg_{89}Al_{140}$ ↔ $Mg_{23}Al_{30}$	43.38		410.1	**[This work]**	Peritectic
L ↔γ	58.70	41.30	463.0	[90]	Congruent melting
	53.00	47.00	460±1	[99]	
	53.89	46.11	462.5	**[This work]**	
L ↔γ+Mg-Hcp	70.00	30.00	437	[167]	Eutectic
	69.95	30.05	437.2	[168]	
	70.10	29.90	437	[90]	
	68.89	31.11	434.3	**[This work]**	
L↔Al-Fcc	0.00	100.00	661	[57]	melting

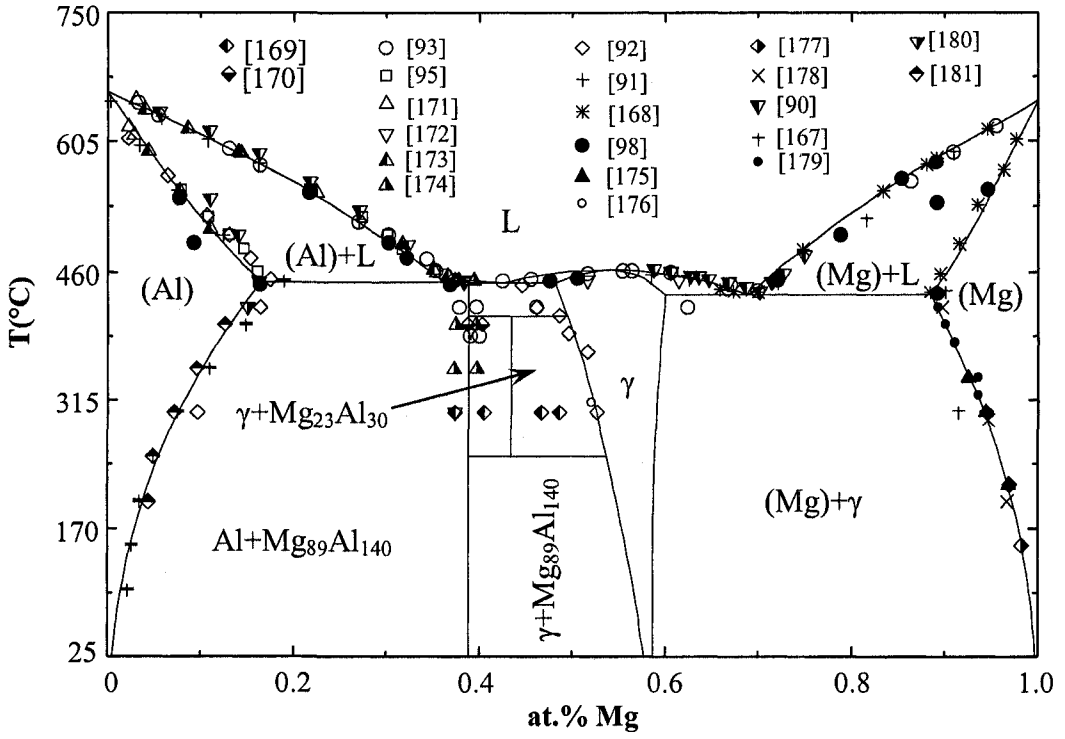

Figure 4.19: *Re-optimized Mg-Al system.*

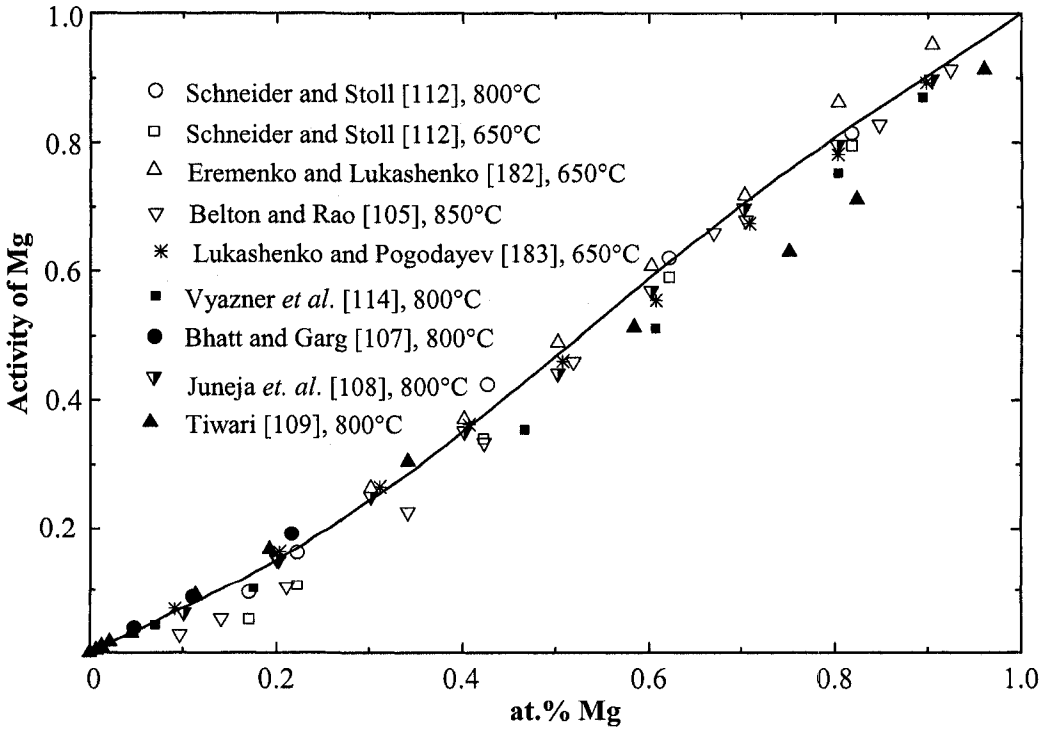

Figure 4.20: *Calculated activity of Mg in Mg-Al liquid with the experimental data at 800°C (Reference state: Al-liquid and Mg-liquid).*

Figure 4.21 shows the calculated enthalpy of mixing at 675°C compared with the experimental data from the literature. As can be seen in this figure, the minimum value of the heat of mixing is about -3 kJ/mol and at 50 at.% Mg. Thus, the contribution of the configurational entropy of mixing is negligible compared to that of ideal entropy and, therefore, the activity has small deviation from ideal solution.

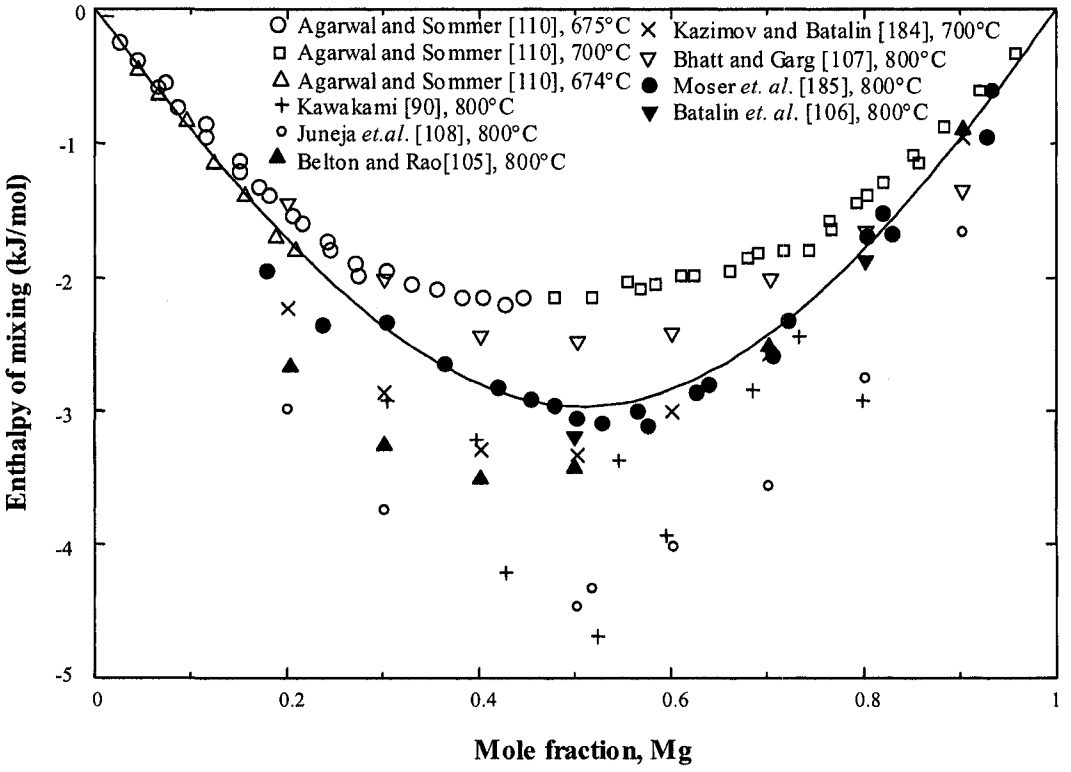

Figure 4.21: *Calculated enthalpy of mixing of Mg-Al liquid at 800°C (Reference state: Mg-liquid, Al-liquid).*

4.2 Thermodynamic Modeling of the Ternary Sub-systems

4.2.1 Mg-Al-Sr Phase Diagram

The thermodynamic properties of the liquid were estimated from the optimized binary parameters using Toop extrapolation [187]. This is an asymmetric extrapolation method

that is used in this work because Mg and Al have similar properties which are different from those of Sr. For this purpose, Mg and Al were placed in the same group while Sr was in a different group. Ternary adjustable terms were added based on the experimental data for the Mg-Al-Sr system obtained from this work and the literature. Ternary thermodynamic parameters of the Mg-Al-Sr system are presented in Table 4.12. The database was then used to calculate polythermic projections of the liquidus surfaces shown in Figure 4.22. The Mg-Al-Sr ternary system is presented as a projection using Gibbs triangle at various temperature and constant pressure. The liquidus projection of the Mg-Al-Sr system is divided into fifteen primary crystallization fields: Al_4Sr, Al_2Sr, Al_3Sr_8, Al_7Sr_8, $Mg_{17}Sr_2$, $Mg_{23}Sr_6$, $Mg_{38}Sr_9$, Mg_2Sr, $Mg_{58}Al_{38}Sr_4$, Al, Mg, γ, β, Sr-fcc, and Sr-bcc. The model predicted five saddle points, eight quasi-peritectics and five ternary eutectics. The respective reactions of these points are listed in Table 4.13.

Table 4.12: *Ternary thermodynamic parameters of the Mg-Al-Sr system.*

Phase	Parameter (J/mol.atom)
Liquid	$L^{0,liquid}_{Mg:Al:Sr} = -45187 + 42T$
(Mg_2Sr)	$G^{0,(Mg,Al)_2Sr}_{Al:Sr} = -82019 + 20T$
($Mg_{23}Sr_6$)	$G^{0,(Mg,Al)_{23}Sr_6}_{Al:Sr} = -840775 + 498T$ $L^{0,(Mg,Al)_{23}Sr_6}_{Mg,Al:Sr} = -160712$
($Mg_{38}Sr_9$)	$G^{0,(Mg,Al)_{38}Sr_9}_{Al:Sr} = -1394933 + 803T$ $L^{0,(Mg,Al)_{38}Sr_9}_{Mg,Al:Sr} = -178160$
($Mg_{17}Sr_2$)	$G^{0,(Mg,Al)_{17}Sr_2}_{Al:Sr} = -250061 + 70T$ $L^{0,(Mg,Al)_{17}Sr_2}_{Mg,Al:Sr} = -20171$
(Al_4Sr)	$G^{0,(Mg,Al)_4Sr}_{Mg:Sr} = -45104 + 50T$
(Al_2Sr)	$G^{0,(Mg,Al)_2Sr}_{Mg:Sr} = -30209 + 8.5T$ $L^{0,(Mg,Al)_2Sr}_{Mg,Al:Sr} = 900$
$Mg_{58}Al_{38}Sr_4$	$G^{0,Mg_{58}Al_{38}Sr_4}_{Mg:Al:Sr} = -6010 + 200T$

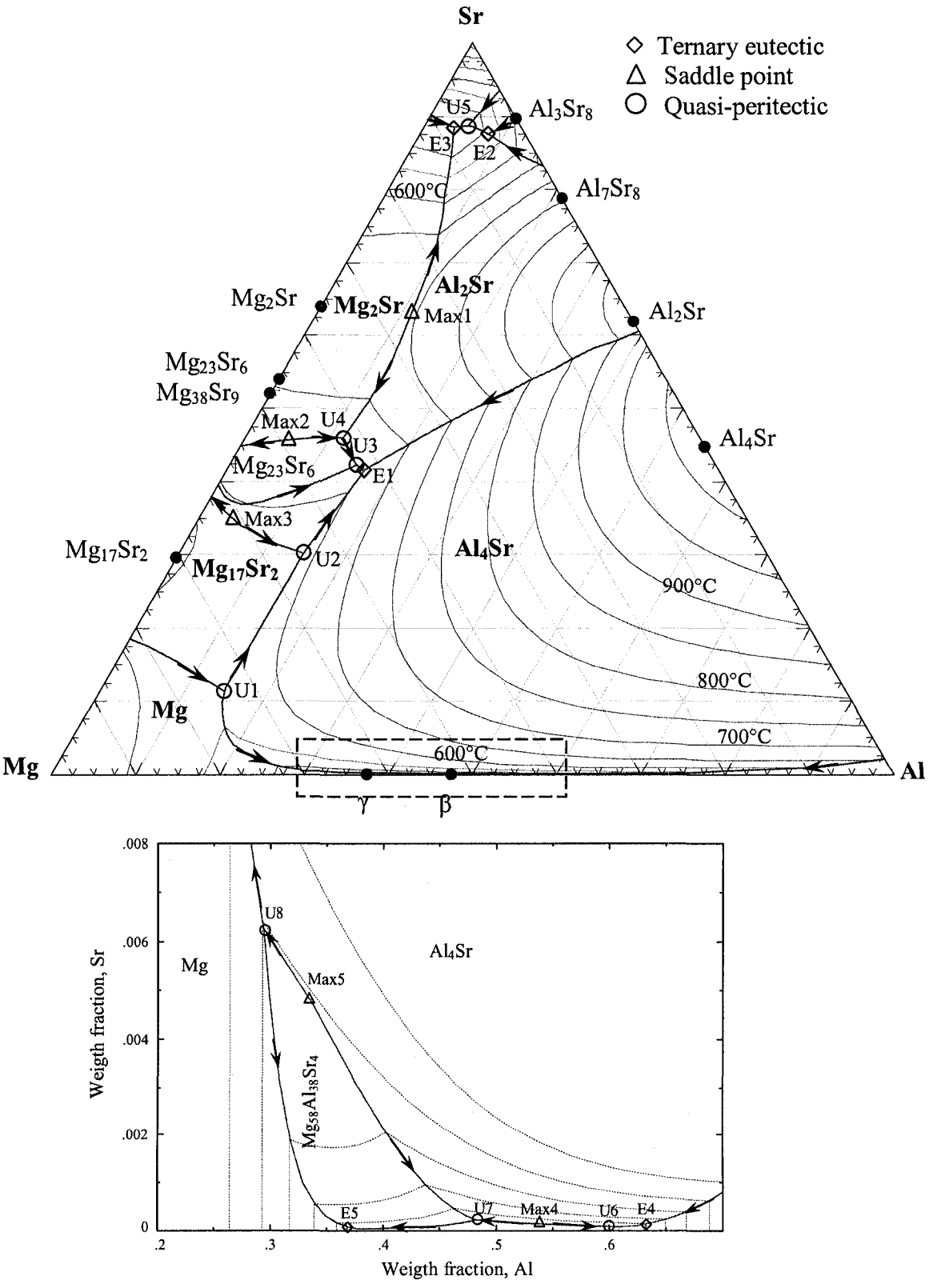

Figure 4.22: *Calculated liquidus projection of the Mg-Al-Sr system in wt.%.*

Table 4.13: *Ternary invariant points of the Mg-Al-Sr system and compared with experimental data from the literature (wt.%).*

Reaction	wt.% Mg	wt.% Al	wt.% Sr	Predicted T(°C)	Reaction	Measured T(°C)
$L+Mg_{17}Sr_2 \leftrightarrow Mg+Al_4Sr$	73.79	14.76	11.45	530	U1	533 **[This work]**
						527 [130]
						521 [127]
$L+Mg_{38}Sr_9 \leftrightarrow Al_4Sr+Mg_{17}Sr_2$	56.10	14.75	29.15	584	U2	592 **[This work]**
						597 [130]
						607 [127]
$L \leftrightarrow Al_4Sr+Al_2Sr+Mg_{38}Sr_9$	42.30	16.29	41.41	603	E1	603 **[This work]**
$L+Mg_{38}Sr_9 \leftrightarrow Al_2Sr+Mg_{23}Sr_6$	42.61	15.05	42.34	604	U3	
$L+Mg_2Sr \leftrightarrow Al_2Sr+Mg_{23}Sr_6$	42.60	11.49	46.45	611	U4	609 **[This work]**
$L+Al_2Sr \leftrightarrow Al_3Sr_8+Al_7Sr_8$	4.33	7.99	87.68	510	E2	
$L+Al_2Sr \leftrightarrow Sr+Al_3Sr_8$	6.18	5.05	88.77	450	U5	
$L+Al_2Sr \leftrightarrow Sr+Mg_2Sr$	7.87	3.61	88.52	426	E3	
$L \leftrightarrow Mg_2Sr+Al_2Sr$	24.06	11.28	64.66	697	Max1	
$L \leftrightarrow Mg_{17}Sr_2+Mg_{38}Sr_9$	61.72	2.24	36.03	597	Max2	
$L \leftrightarrow Mg_2Sr+Mg_{23}Sr_6$	46.35	7.78	45.87	613	Max3	
$L \leftrightarrow Al+Al_4Sr+\beta$	36.78	63.21	0.01	420	E4	
$L+Al_4Sr \leftrightarrow \gamma+\beta$	40.02	59.97	8.7e-3	404	U6	
$L+Al_4Sr \leftrightarrow \gamma+Mg_{58}Al_{38}Sr_4$	51.70	48.28	0.02	408	U7	
$L \leftrightarrow \gamma+Mg+Mg_{58}Al_{38}Sr_4$	63.15	36.84	8.5e-3	402	E5	
$L+Mg \leftrightarrow Al_4Sr+Mg_{58}Al_{38}Sr_4$	69.99	29.38	0.63	478	U8	
$L \leftrightarrow Al_4Sr+\gamma$	49.35	50.63	0.02	403	Max4	
$L \leftrightarrow Al_4Sr+Mg_{58}Al_{38}Sr_4$	68.01	31.44	0.55	473	Max5	

**E denotes ternary eutectic reaction; U denotes ternary quasi-peritectic reaction and Max denotes saddle point*

Based on the experimental data from this work, the location of the pertinent solid phases of the Mg-Al-Sr system at 400°C is presented in the calculated isothermal section,

as can be seen in Figure 4.23. The solubility limits of the binary compounds are in accord with the experimental work of Janz *et al.* [127].

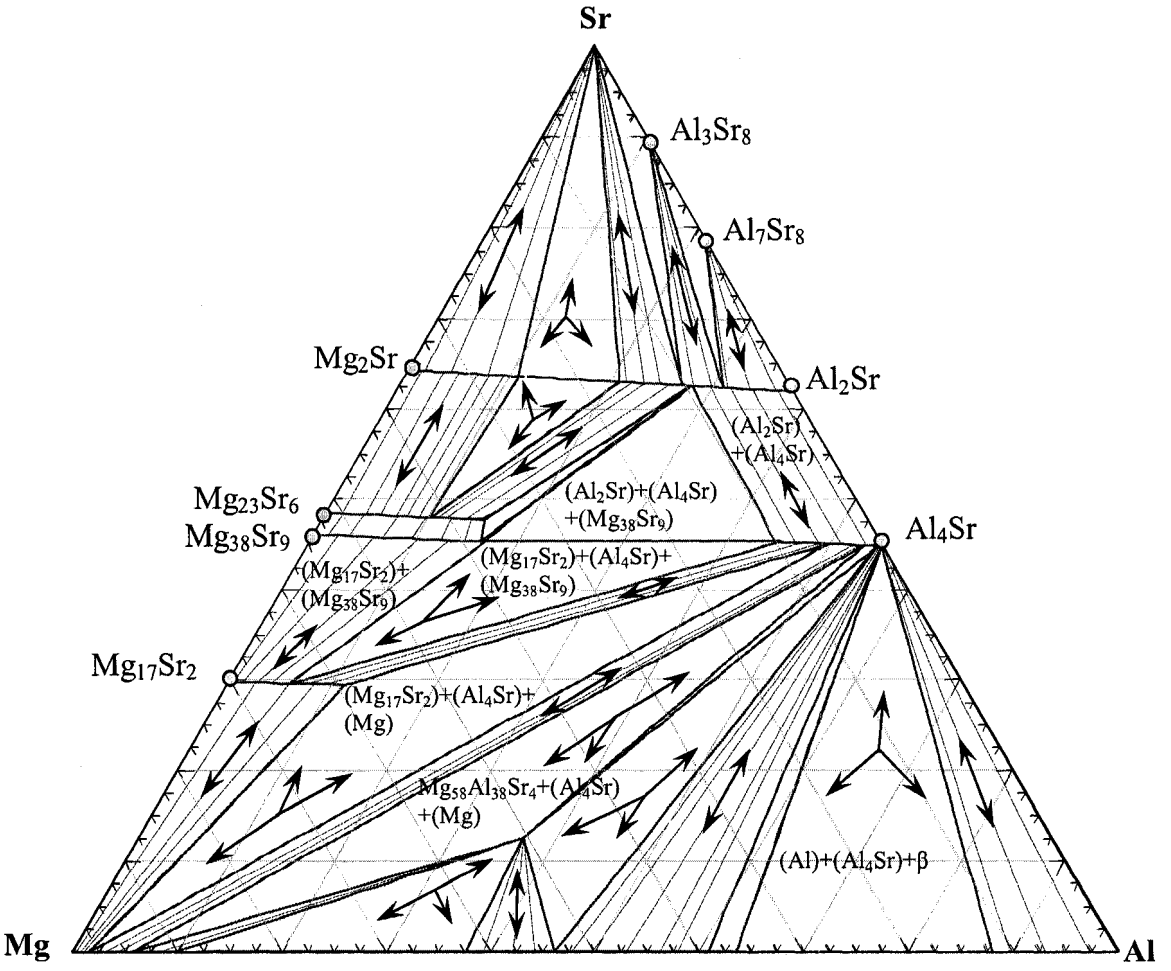

Figure 4.23: *Calculated isothermal section of the Mg-Al-Sr (wt.%) at 400°C.*

4.2.2 Mg-Al-Ca Phase Diagram

The thermodynamic properties of the liquid were estimated from the optimized binary parameters using Toop extrapolation [187]. This is an asymmetric extrapolation method used in this work due to the difference in atomic structure of Mg and Al compared to Ca. Ternary adjustable terms were added based on the experimental data for the Mg-Al-Ca system obtained in this work and the literature. The database was then used to calculate

polythermic projections of the liquidus surfaces as shown in Figure 4.24. The calculated liquidus projection is divided into thirteen primary crystallization fields: Al_4Ca, Al_2Ca, Al_3Ca_8, $Al_{14}Ca_{13}$, Mg_2Ca, Al, Mg, Al, γ, β, $Mg_2Al_4Ca_3$, Ca-bcc, and Ca-fcc. The model predicted four saddle points, four quasi-peritectics, one peritectic and five ternary eutectics. The respective reactions of these points are listed in Table 4.14. Ternary thermodynamic parameters of the Mg-Al-Sr system are presented in Table 4.15.

Table 4.14: *Ternary invariant points of the Mg-Al-Ca system and compared with experimental data from the literature (wt.%).*

Reaction	wt.% Mg	wt.% Al	wt.% Ca	Predicted T(°C)	Measured T(°C)	Reaction
$L \leftrightarrow Ca+Al_3Ca_8+Mg_2Ca$	17.05	2.37	80.58	441	451 [This work]	E1
$L \leftrightarrow Al_{14}Ca_{13}+Al_3Ca_8+Al_2Ca$	1.31	27.91	70.78	613		E2
$L \leftrightarrow Mg+C36+Mg_2Ca$	78.94	4.79	16.27	504	513 [17]	E3
					514 [157]	
$L \leftrightarrow Mg+\gamma+Al_2Ca$	65.45	33.33	1.22	429		E4
$L \leftrightarrow Al+\gamma+Al_2Ca$	27.72	70.53	1.75	485		E5
$L+Mg_2Ca \leftrightarrow C36+Al_3Ca_8$	24.15	9.97	65.88	584		U1
$L+Al_3Ca_8+Al_2Ca \leftrightarrow C36$	11.21	19.81	68.98	649		P1
$L+Mg+C36 \leftrightarrow Al_2Ca$	74.13	20.57	5.30	502	515 [This work]	P2
$L+\gamma+\beta \leftrightarrow Al_2Ca$	38.51	60.37	1.12	446		P3
$L+Al+Al_4Ca \leftrightarrow Al_2Ca$	25.30	72.60	2.10	420		P4
$L \leftrightarrow Mg_2Ca+C36$	47.59	7.25	45.16	671		Max1
$L \leftrightarrow Al_2Ca+Al_3Ca_8$	7.45	22.56	69.9	654		Max2
$L \leftrightarrow Mg+C36$	78.62	10.86	10.52	524	534 [157]	Max3
$L \leftrightarrow \gamma+Al_2Ca$	49.39	49.39	1.22	456	450 [This work]	Max4

Table 4.15: *Optimized thermodynamic parameters of the ternary compound and solid solubilities (J/mol.atom).*

Phase	Parameter (J/mol.atom)
(Mg_2Ca)	$G^{0,Mg_2Ca}_{Al:Ca} = 439$ $L^{0,Mg_2Ca}_{Mg,Al:Ca} = -363297 + 39T$
(Al_2Ca)	$G^{0,Al_2Ca}_{Mg:Ca} = 41840$ $L^{0,Al_2Ca}_{Mg,Al:Ca} = -100834$
(Al_3Ca_8)	$G^{0,Al_3Ca_8}_{Mg:Al} = 418400$ $L^{0,Al_3Ca_8}_{Ca,Al:Mg} = -920480$
$Mg_2Al_4Ca_3$	$G^{0,C36}_{Mg:Al:Ca} = -26044 - 36 * T$

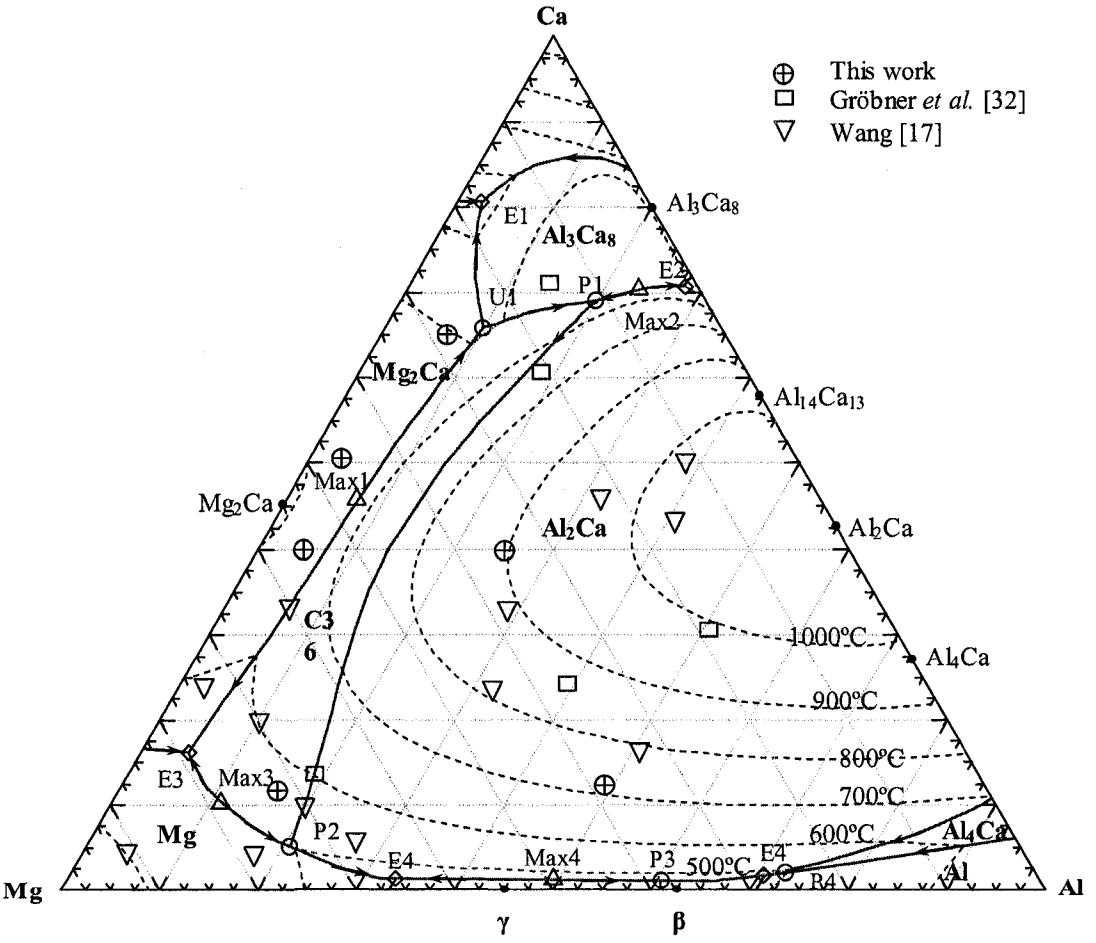

Figure 4.24: *Calculated liquidus projection of the Mg-Al-Ca system (wt.%).*

Based on the results of the thermodynamic modeling of this work, the predicted eutectic reaction (E3: L↔Mg+C36+Mg_2Ca) in the Mg-rich region, as can be seen in Table 4.14, occurs at 504°C compared to the results of Wang [17] and Suzuki *et al.* [157] who obtained values of 513 and 514°C, respectively. In addition, the saddle point predicted in this work (Max3: L↔Mg+C36) occurs at 524°C which is in accord with Suzuki's *et al.* [157] value of 534°C. Therefore, phase equilibria in the Mg-rich region obtained in this work is very well supported with experimental data.

The calculated isothermal section of the Mg-Al-Ca system at 300°C is shown in Figure 4.25. As can be noticed in this figure, the maximum solubility of Mg in Al_2Ca is found to be 7.6 at.%, compared to our own experimental work and Gröbner's *et al.* [135] result as 8.6 and 5.0 at.%, respectively. In addition, Al_3Ca_8 dissolved 11.8 at.% Mg, compared to the values of the experiments in the current work and of Gröbner's *et al.* [135] at 10.0 and 13.5 at.% Mg, respectively. The calculations observed that Mg_2Ca dissolved 15.8 at.% Al compared to the value measured in this work and by Gröbner *et al.* [135] at 22.3 and 22.0 at.% Al, respectively. The samples designed to measure the extended solubility of the $Al_{14}Ca_{13}$ binary compound in the ternary system were not successful because of the slow kinetics of formation of this compound.

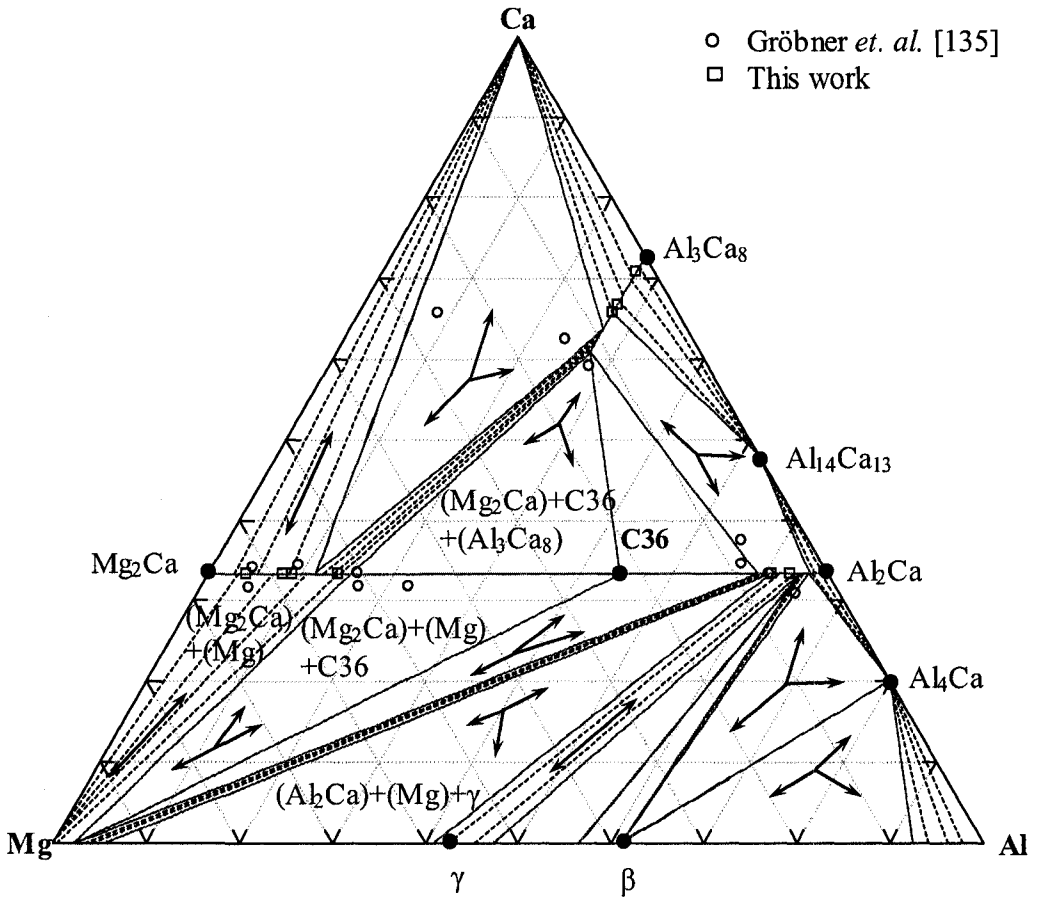

Figure 4.25: *Calculated isothermal section of the Mg-Al-Ca (at.%)*

4.2.3 Mg-Ca-Sr Phase Diagram

The thermodynamic properties of the liquid were estimated from the optimized binary parameters using Toop extrapolation [189]. No ternary adjustable terms were added since experimental phase equilibrium and thermodynamic data for the Mg-Ca-Sr system could not be found in the literature. The calculated liquidus projection in Figure 4.26 is divided into eight primary crystallization fields: (Mg), $Mg_{17}Sr_2$, Mg_2Sr, $Mg_{23}Sr_6$, $Mg_{38}Sr_9$, fcc, Mg_2Ca, and bcc. The crystallization fields of $Mg_{23}Sr_6$ and $Mg_{38}Sr_9$ are more extended in the ternary diagram than these predicted in the work of Zhong *et al.* [148]. Liquidus surfaces of bcc and Mg_2Ca dominate the phase diagram.

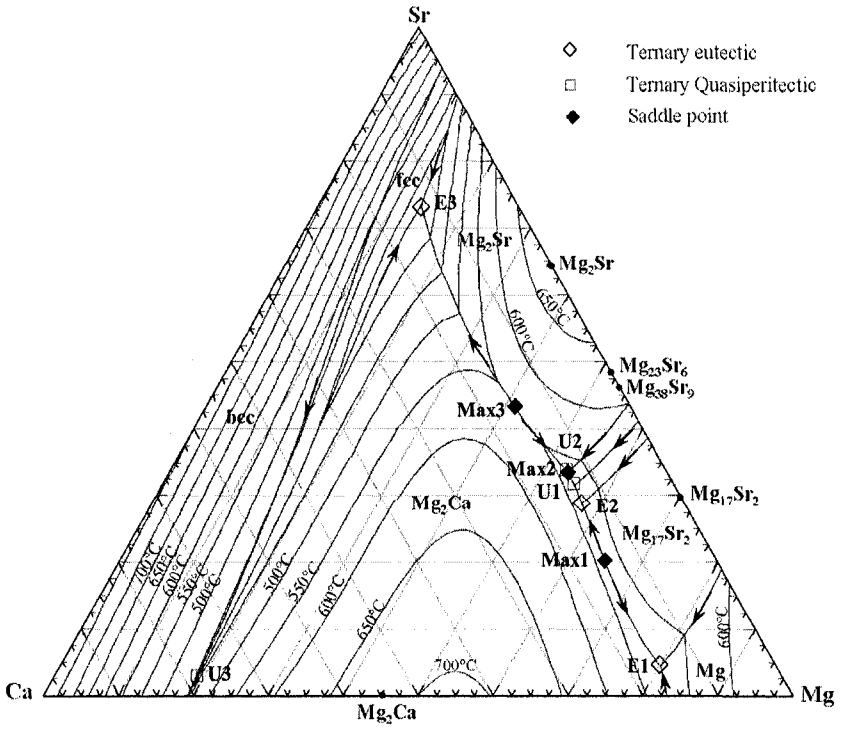

Figure 4.26: *Ternary liquidus projection of the Mg-Ca-Sr system in weight fraction with invariant points calculated using the modified quasichemical model assuming limited solubility between Mg_2Ca and Mg_2Sr.*

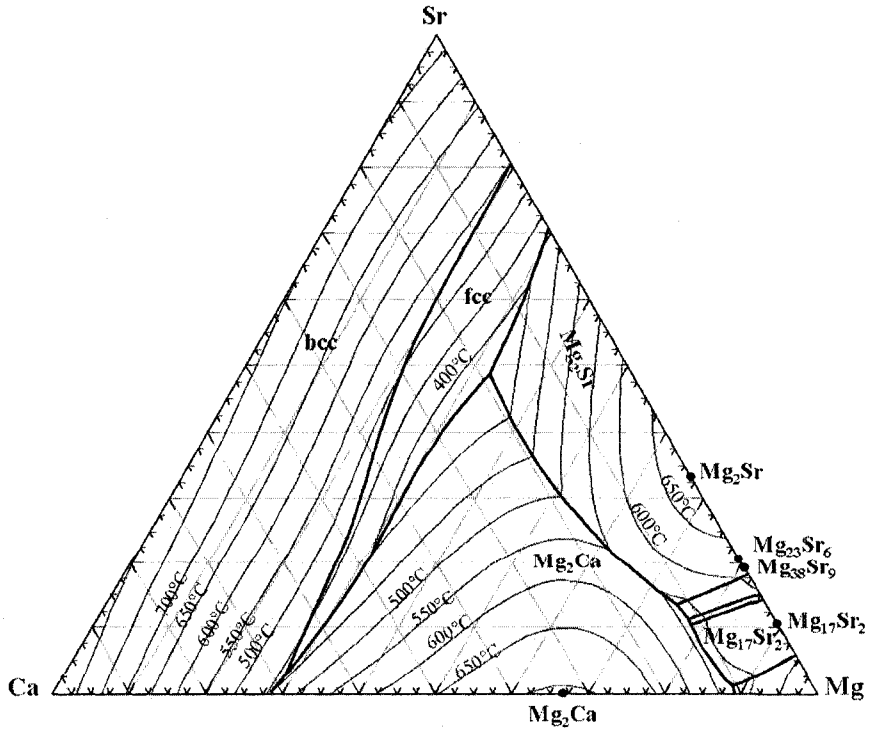

Figure 4.27: *Ternary liquidus projection of the Mg-Ca-Sr system in mole fraction calculated using the modified quasichemical model assuming limited solubility between Mg_2Ca and Mg_2Sr.*

The model predicted three saddle points, three quasi-peritectic and three ternary eutectics. The respective reactions of these points are listed in Table 4.16. A comparison between liquidus projections calculated using random solution model and the modified quasichemical model is presented in Figure 4.28.

Table 4.16: *Ternary invariant points of the Mg-Ca-Sr system for the case of no solid solubility between Mg_2Ca and Mg_2Sr (wt.%).*

Reaction	wt.% Mg	wt.% Ca	wt.% Sr	T(K)	Reaction type*
L ↔ Mg_2Ca+ Mg +$Mg_{17}Sr_2$	79.96	15.45	4.59	792.2	E1
L↔$Mg_{17}Sr_2$+$Mg_{38}Sr_9$+Mg_2Ca	57.40	13.68	28.92	809.9	E2
L ↔ Mg_2Ca+ fcc +Mg_2Sr	13.77	13.02	73.21	622.5	E3
L+$Mg_{23}Sr_6$↔Mg_2Ca+$Mg_{38}Sr_9$	54.99	13.40	31.61	819.64	U1
L+Mg_2Sr↔Mg_2Ca+$Mg_{23}Sr_6$	52.89	13.36	33.75	814.02	U2
L+ bcc ↔ Mg_2Ca+fcc	19.17	78.02	2.81	718.6	U3
L ↔ Mg_2Ca + $Mg_{17}Sr_2$	64.73	14.98	20.29	813.4	Max1
L ↔ Mg_2Ca + $Mg_{23}Sr_6$	53.21	13.32	33.47	811.8	Max2
L ↔ Mg_2Ca + Mg_2Sr	41.25	15.37	43.38	839.0	Max3

**E denotes ternary eutectic reaction; U denotes ternary quasi-peritectic reaction and S denotes saddle point*

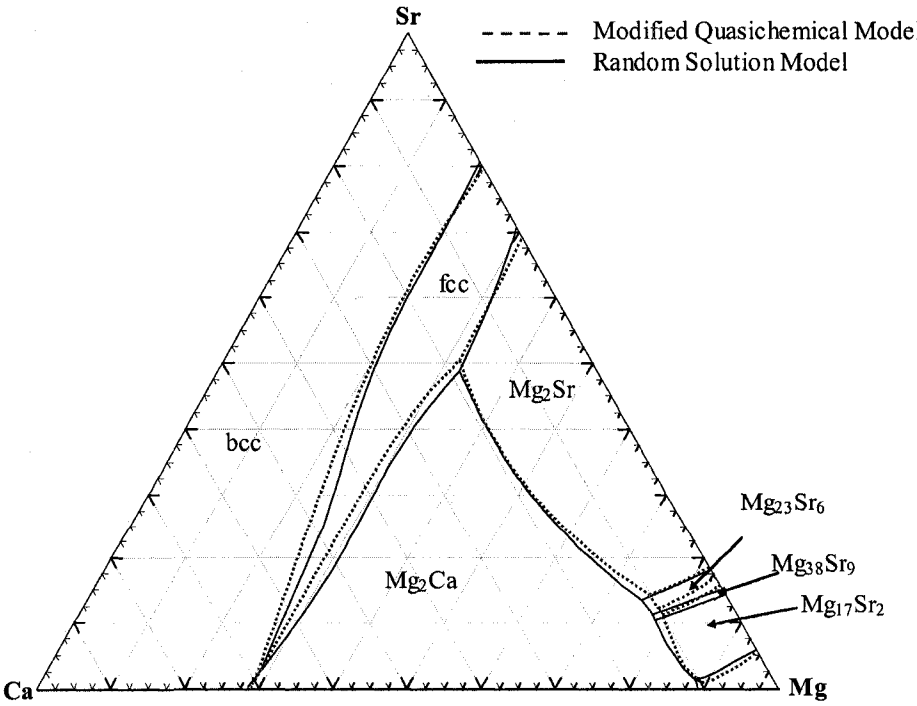

Figure 4.28: *Ternary liquidus projection of the Mg-Ca-Sr system in mole fraction calculated using the modified quasichemical model and random solution model assuming mutual solubility between Mg_2Ca and Mg_2Sr.*

Although the random solution and the modified quasichemical models resulted in similar Mg-rich corner, the two models predicted slightly different liquidus projection for the Mg-Ca-Sr system. Since there is no experimental data to prove the existence of unlimited solubility between Mg_2Ca and Mg_2Sr, mutual solubility between Mg_2Ca and Mg_2Sr in the ternary phase diagram to form C14 solid solution is considered. C14 is modeled using two sublattices with Mg atoms occupying the first sublattice. In view of the fact that atomic size and crystal structure of Ca and Sr are similar, these two elements replace each other and their mixing is allowed on the second sublattice.

The Gibbs energy of C14 is modeled using compound energy formalism and presented in the following equation:

$$G^{C14} = y_{Ca}G^{0,C14}_{Mg:Ca} + y_{Sr}G^{0,C14}_{Mg:Sr} + y_{Ca}G^{0,C14}_{Va:Ca} + y_{Sr}G^{0,C14}_{Va:Sr} + \frac{2}{3}RT(y_{Ca}\ln y_{Ca} + y_{Sr}\ln y_{Sr}) + y_{Ca}y_{Sr}L^{0.C14}_{Ca,Sr:Mg}$$

Where $G^{0,C14}_{Mg:Ca}$ and $G^{0,C14}_{Mg:Sr}$ are the Gibbs energy of formation of Mg_2Ca and Mg_2Sr compounds in the binary Mg-Ca and Mg-Sr systems. $G^{0,C14}_{Va:Ca}$ and $G^{0,C14}_{Va:Sr}$ represent the metastable end members of the solid solution and they were given high positive values (10^5 J/mol). $L^{0.C14}_{Ca,Sr:Mg}$ describes the ternary interaction parameter within the sublattice which is assumed to be negligible due to lack of the experimental data for this system.

The liquidus projection for the case of mutual solubility between Mg_2Ca and Mg_2Sr is drawn in Figure 4.29. The model predicted two quasi-peritectic and two ternary eutectics. Comparison between the calculated invariant points in this analysis and the work of Zhong *et al.* [148] is listed in Table 4.17. Isothermal section of the Mg-Ca-Sr system at 450°C using the modified quasichemical model for the mutual solubility between Mg_2Ca

and Mg_2Sr is drawn in Figure 4.30. Taking into account the mutual solubility between Mg_2Ca and Mg_2Sr resulted in a different liquidus projection and different invariant points. This demands experimental investigation in order to verify the mutual solubility and the invariant points in this system.

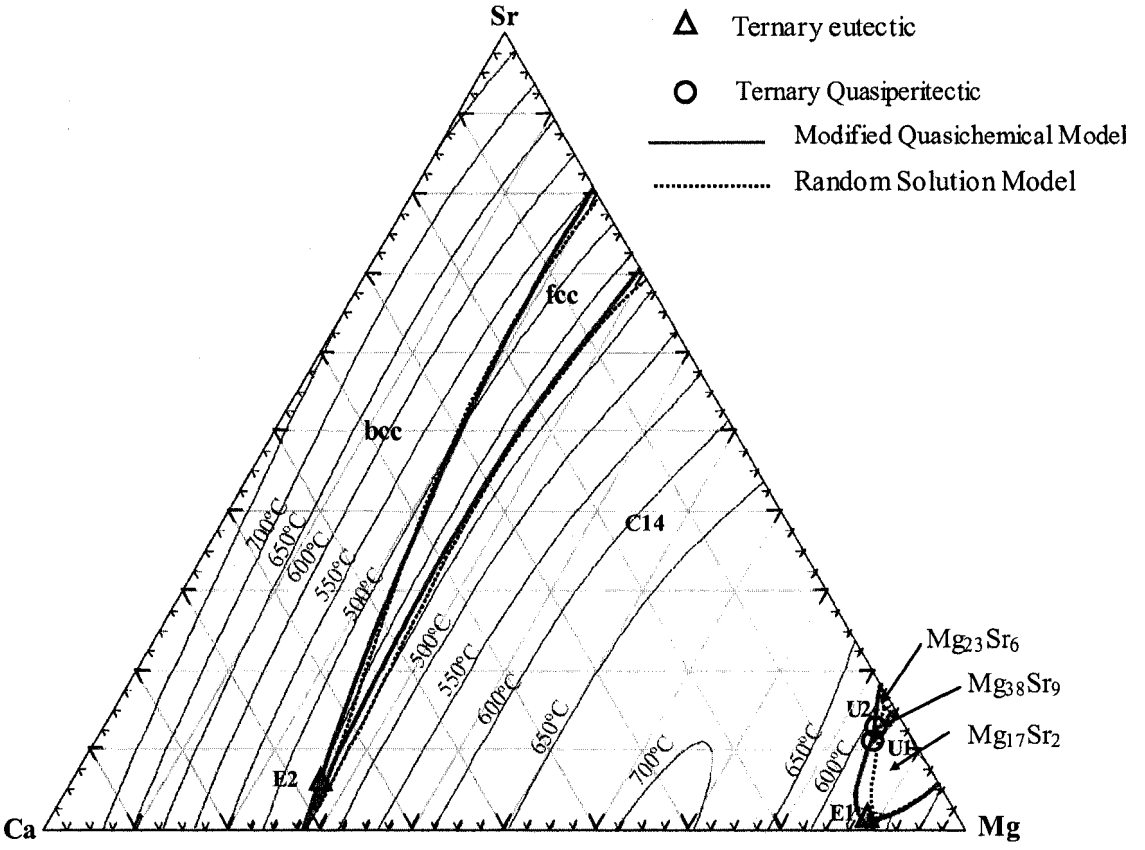

Figure 4.29: *Ternary liquidus projection of the Mg-Ca-Sr system in mole fraction calculated using the modified quasichemical model and random solution model assuming mutual solubility between Mg_2Ca and Mg_2Sr.*

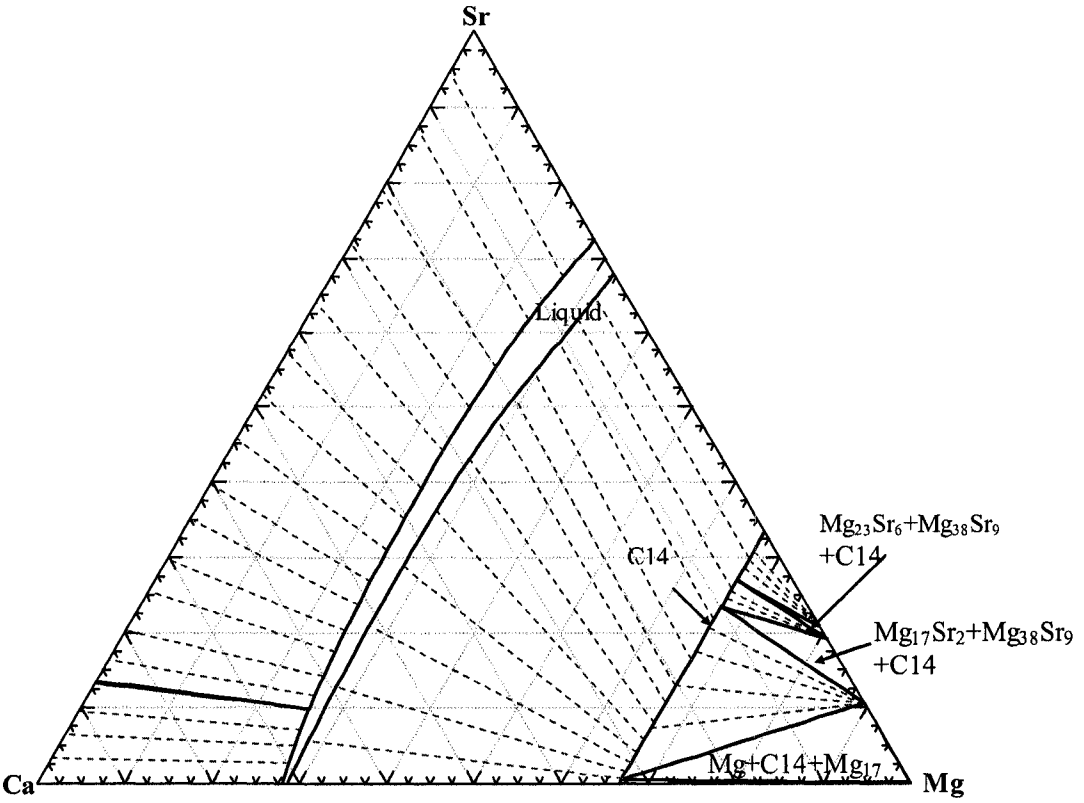

Figure 4.30: *Isothermal section of the Mg-Ca-Sr system in mole fraction at 450°C calculated using the modified quasichemical model assuming mutual solubility between Mg_2Ca and Mg_2Sr.*

Table 4.17: *Ternary invariant points of the Mg-Ca-Sr system for the case of complete solid solubility between Mg_2Ca and Mg_2Sr (at.%).*

Reaction	at.% Mg	at.% Ca	at.% Sr	T(K)	Reference	Reaction type*
L ↔ C14+Mg +$Mg_{17}Sr_2$	88.95	8.43	2.75	783.90	[148]	E1
	89.05	10.20	0.75	792.97	**This work**	
L+$Mg_{38}Sr_9$↔$Mg_{17}Sr_2$ +C14	83.32	3.60	13.08	841.90	[148]	U1
	84.34	4.61	11.05	852.66	**This work**	
L+$Mg_{23}Sr_6$↔C14+ $Mg_{38}Sr_9$	81.95	1.95	16.10	859.50	[148]	U2
	83.83	3.74	12.43	858.07	**This work**	
L ↔ C14+fcc+ bcc	29.24	69.23	1.53	717.00	[148]	E2
	27.53	68.61	3.86	718.29	**This work**	

**E denotes ternary eutectic reaction; U denotes ternary quasi-peritectic reaction and S denotes saddle point*

4.2.4 Al-Ca-Sr Phase Diagram

The thermodynamic properties of the Al-Ca-Sr liquid were estimated from the optimized binary parameters using Toop extrapolation [189]. Ternary adjustable terms were not added since experimental thermodynamic and equilibrium data for the Al-Ca-Sr system could not be found in the literature. The database was then used to calculate polythermic projections of the liquidus surfaces shown in Figures 4.31 and 4.32. The calculated liquidus projection is divided into eleven primary crystallization fields: Al_4Sr, Al_2Sr, Al_3Sr_8, Al_7Sr_8, Al_2Ca, Al_4Ca, Al_3Ca_8, $Al_{14}Ca_{13}$, Al, fcc, and bcc. The model predicted one saddle point, one peritectic, seven quasi-peritectics and two ternary eutectics. The respective reactions of these points are listed in Table 4.18.

Table 4.18: *Ternary invariant points of the Al-Ca-Sr system (at.%).*

Reaction	at.% Al	at.% Ca	at.% Sr	T / K	Reaction type*
$L \leftrightarrow Al+Al_4Sr+Al_4Ca$	95.39	4.13	0.48	898.55	E1
$L \leftrightarrow fcc+Al_3Ca_8+Al_7Sr_8$	34.29	37.78	27.93	585.85	E2
$L+ Al_3Ca_8 \leftrightarrow fcc+bcc$	25.21	56.72	18.07	726.65	U1
$L+Al_7Sr_8 \leftrightarrow Al_3Ca_8+Al_2Sr$	35.02	37.72	27.26	587.65	U2
$L+ Al_3Ca_8 \leftrightarrow Al_2Sr+Al_{14}Ca_{13}$	38.14	41.24	20.62	620.75	U3
$L+ Al_2Sr \leftrightarrow Al_2Ca+Al_{14}Ca_{13}$	42.12	40.23	17.65	710.95	U4
$L+Al_2Ca \leftrightarrow Al_2Sr+Al_4Sr$	59.47	20.46	20.07	1030.85	U5
$L+Al_4Sr \leftrightarrow Al_4Ca+Al_2Ca$	91.89	7.05	1.06	962.45	U6
$L+Al_3Sr_8 \leftrightarrow fcc+Al_7Sr_8$	30.40	17.58	52.02	758.25	U7
$L+ bcc+ Al_3Sr_8 \leftrightarrow fcc$	24.45	8.94	66.61	810.75	P
$L \leftrightarrow Al_4Sr+Al_2Ca$	73.62	16.02	10.36	962.65	S

**E denotes ternary eutectic reaction; U denotes ternary quasi-peritectic reaction and S denotes saddle point*

In view of the fact that atomic size and crystal structure of Ca and Sr are similar, a possible ternary solid solubility of the third element in the Al-Ca and Al-Sr intermetallic

compounds exists. This demands experimental investigation in order to determine their solubility limit and the invariant points.

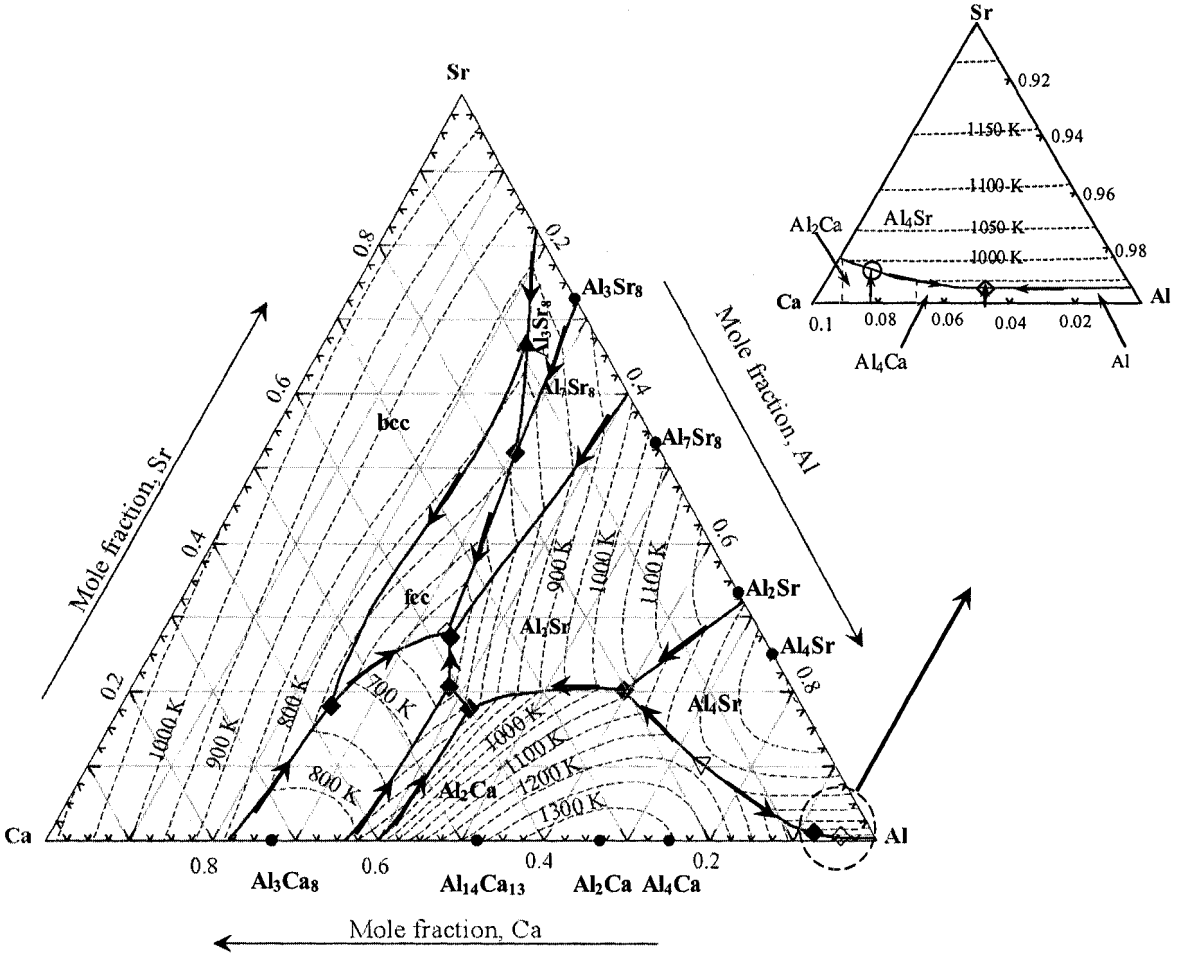

Figure 4.31: *Ternary liquidus projection of the Al-Ca-Sr system in mole fraction with invariant points.* ○ *Ternary quasi-peritetic,* ◇ *Ternary eutectic,* ▽ *Saddle point,* ◆ *Ternary peritectic).*

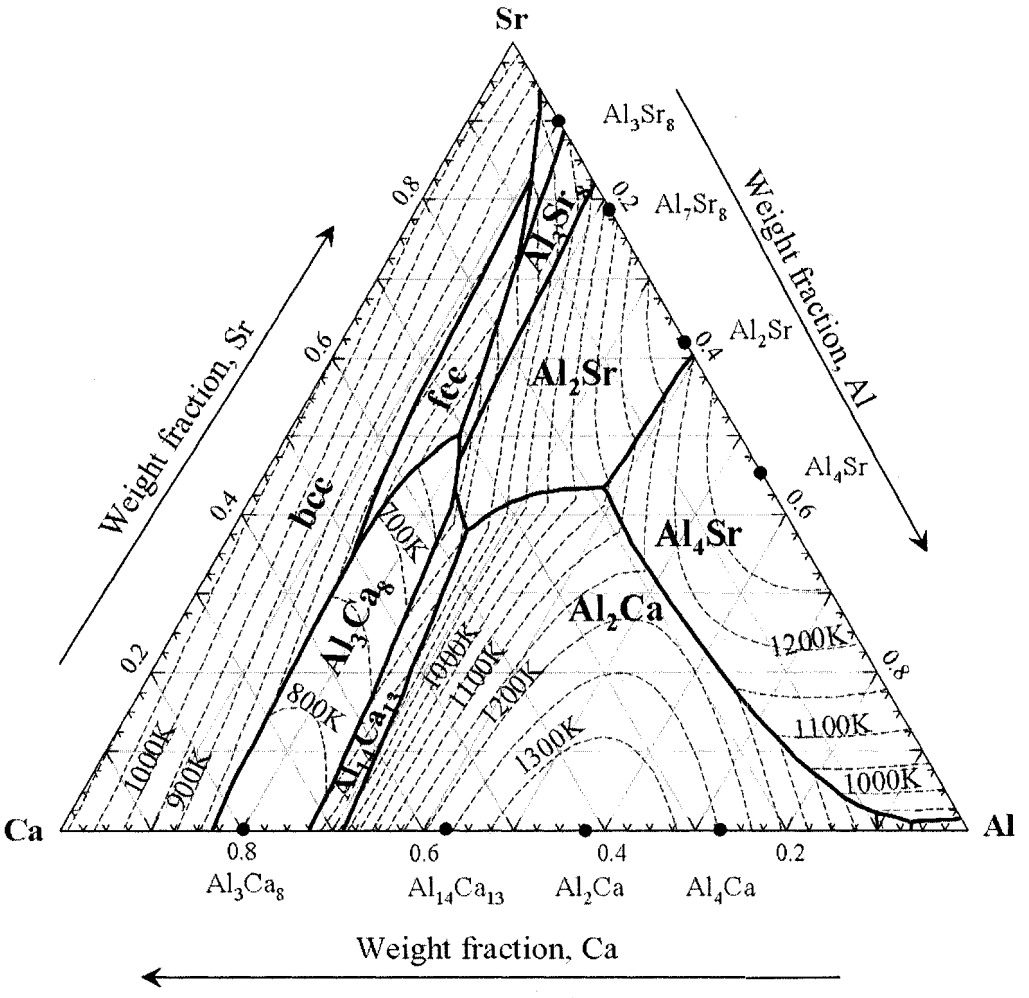

Figure 4.32: *Ternary liquidus projection of the Al-Ca-Sr system in weight fraction.*

4.3 Mg-Al-Ca-Sr Quaternary System

The Mg-Al-Sr, Mg-Al-Ca, Al-Ca-Sr and Mg-Ca-Sr ternary systems are combined to represent the quaternary system, no quaternary interaction parameters were used because of the lack of experimental data. As an example, the liquidus projections at fixed Sr content of 10 and 30 at.% are plotted in Figures 4.33 and 4.34, respectively.

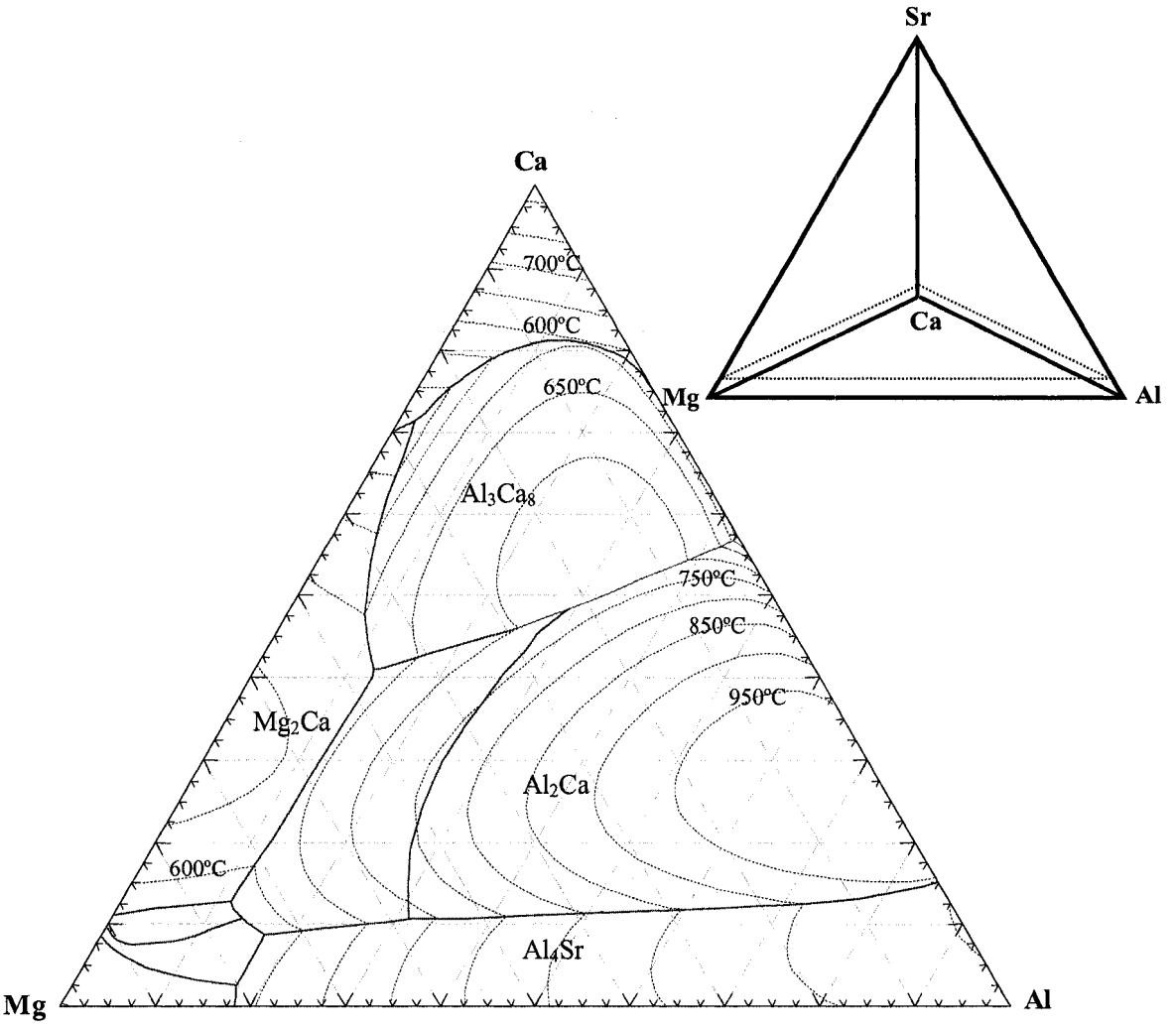

Figure 4.33: *Liquids projection of the Mg-Al-Ca-Sr at 10 at.% Sr*

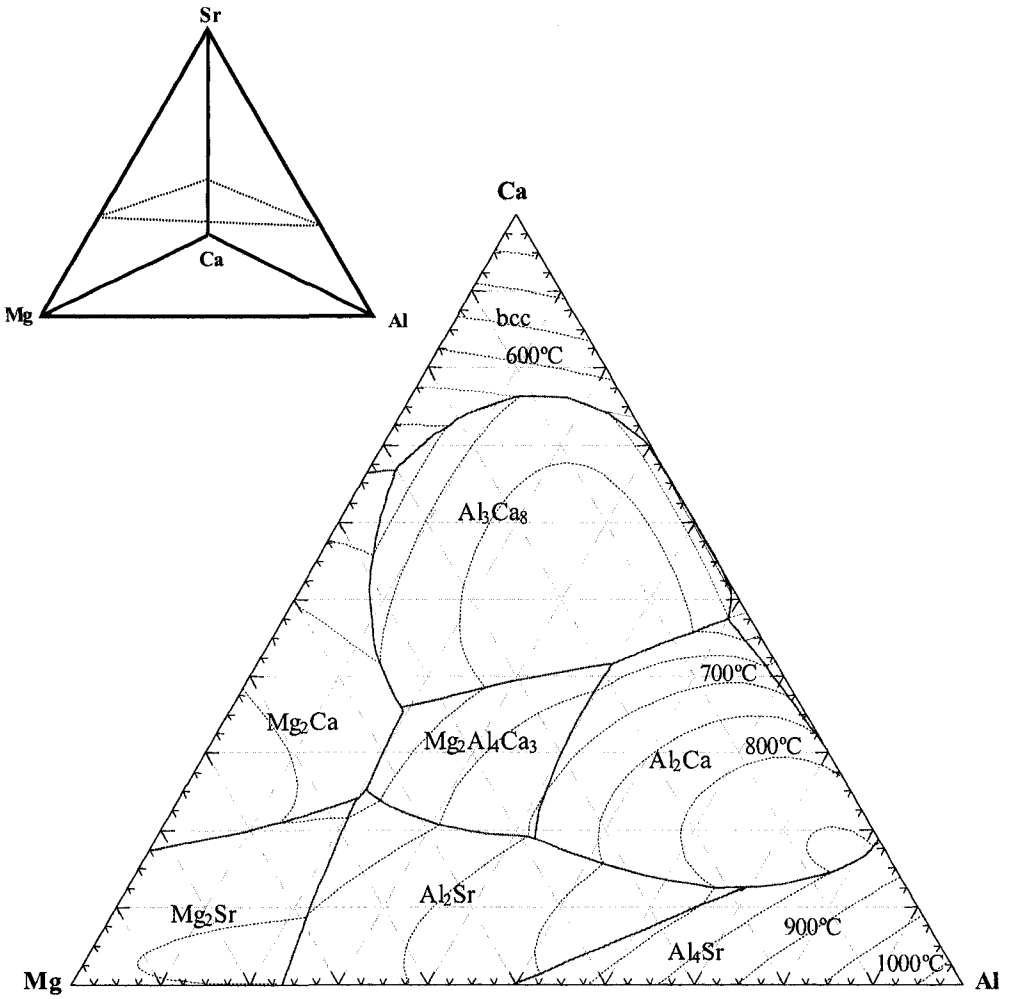

Figure 4.34: *Liquids projection of the Mg-Al-Ca-Sr at 30 at.% Sr*

In the Mg-rich region, the addition of 10 at.% Sr to the Mg-Al-Ca resulted in precipitation of thermally high stable compounds; Al_4Sr and $Mg_{17}Sr_2$ in the Mg-matrix as can be seen in Figure 4.33. Whereas, alloying the Mg-Al-Ca with 30 at.% Sr consumed Mg-matrix. At 10 at.% Sr, two compounds Al_2Ca and Al_4Sr extended in the quaternary system more than that at 30 at.% Sr.

Since there is no experimental data could be found in the literature for the Mg-Al-Ca-Sr system, Schiel simulation for the Mg-5.7Al-3.1Ca-0.15Sr alloy is drawn and compared to that reported by Ozturk *et al.* [126]. Taking the ternary solubility of Mg_2Ca and Al_2Ca into account resulted in different simulation curves, as can be seen in Figure 4.35, since Ozturk *et al.* [126] did not include in his modeling any ternary solubility or ternary compound. Using the modified quasichemical model resulted in different liquidus curve than the one predicted from Ozturk's *et al.* [126] work who used random solution model.

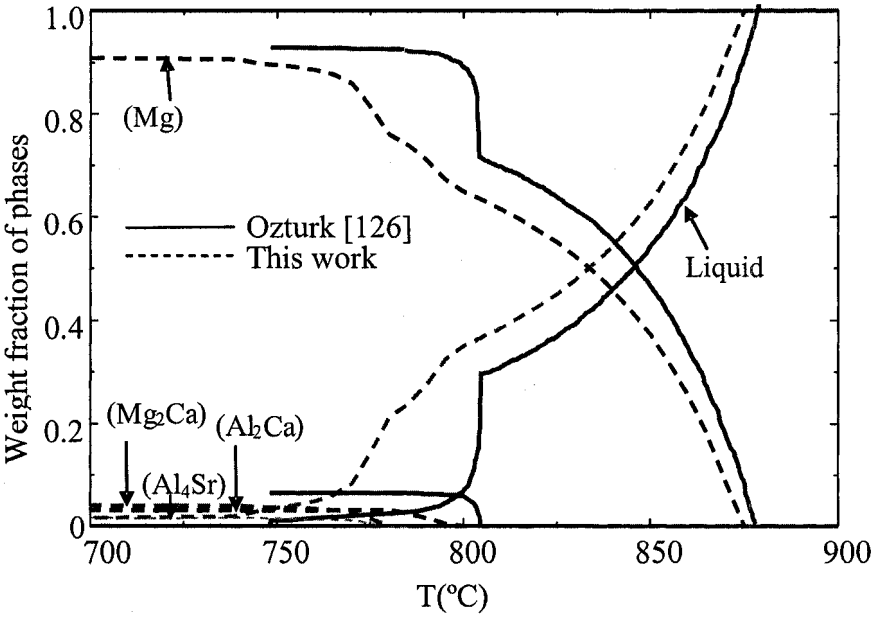

Figure 4.35: *Phase fractions as a function of temperature for Mg-5.7Al-3.1Ca-0.15Sr wt.%.*

A practical example, on the use of the multi-components dbase constructed in this work, is presented in Figure 4.36 showing the alloying effect of Ca addition to AJ62 (Mg-6Al-2.4Sr, wt.%) alloy. As can be seen from this figure, addition up to 4 wt.% Ca to the AJ62 forms thermally stable compounds at room temperature such as (Al_4Sr), (Al_2Ca) and ($Mg_{17}Sr_2$) which improve the microstructure stability and, in turn, enhance the creep

resistance of this alloy. Alloying with 4.7-21.4 wt.% Ca into AJ62, on the other hand, precipitates (Al_2Ca), (Mg_2Ca) and ($Mg_{17}Sr_2$) in Mg-matrix. According to Gröbner *et. al.* [135], the existence of both Mg_2Ca and Al_2Ca resulted in a brittle alloy. Therefore, alloying AJ62 with up to 4 wt.% Ca is preferred.

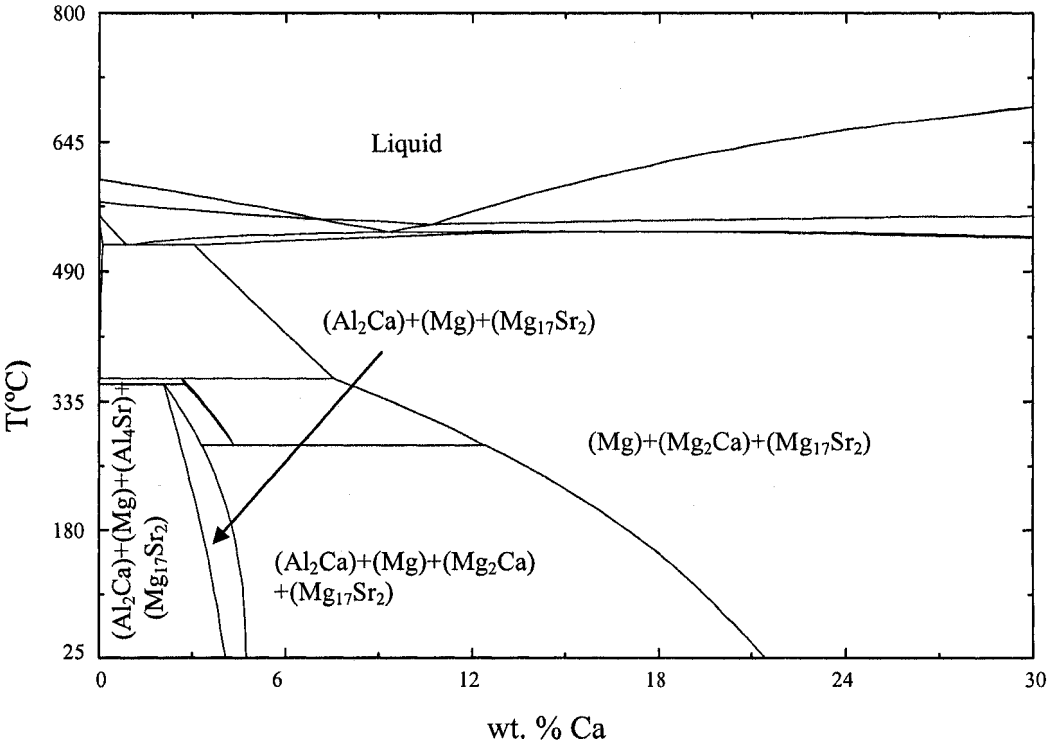

Figure 4.36: *Calculated vertical section of AJ62 with Ca.*

CHAPTER V

Experimental Procedure

5.1 Experimental Methods

Thermal and analytical investigations, phase identification, and microstructural characterization were carried out for the Mg-Al-(Ca,Sr) alloys. For the Mg-Al-Sr system, fifteen alloys and for Mg-Al-Ca system, thirteen alloys were chosen by critical assessment of the experimental and thermodynamic datasets that are available in the literature. The samples were prepared and analyzed chemically at MTL-CANMET and the actual compositions are shown in Tables 5.1 and 5.2.

Table 5.1: *Chemical composition of as-cast Mg-Al-Sr alloys in wt.%.*

Sample No.	Mg	Al	Sr
1	87.29	9.39	3.32
2	76.15	15.20	8.65
3	65.45	27.67	6.88
4	48.57	28.95	22.48
5	43.75	33.72	22.53
6	30.00	46.00	24.00
7	22.00	46.00	32.00
8	54.39	22.83	22.78
9	42.89	29.28	27.83
10	40.00	50.50	9.50
11	30.00	59.00	11.00
12	15.00	62.00	23.00
13	72.00	8.10	19.90
14	60.55	6.71	32.74
15	40.6	16.8	42.6

Sample No.	Mg	Al	Sr
16	31.8	24.4	43.8
17	43.3	11.9	44.8
18	29	19.2	51.8
19	34.2	13.6	52.2
20	50.2	18.5	31.3
21	41.1	8.6	50.3
22	44.8	30.2	25
23	78.3	11.5	10.2
24	52.3	25.5	22.2
25	12	37	51
26	30.2	9.3	60.5
27	26	11.1	62.9
28	14.7	18.6	66.7
29	19.1	16.1	64.8

Table 5.2: *Chemical composition of as-cast Mg-Al-Ca alloys in wt.%.*

Sample No.	Mg	Al	Ca
1	16.8	45.0	38.2
2	35.4	28.2	36.4
3	57.0	4.3	38.7
4	10.7	42.1	47.2
5	28.4	20.4	51.2
6	49.4	0.6	50.0
7	16.9	46.3	30.9
8	7.2	55.8	37.0
9	41.4	27.4	31.2
10	38.7	48.7	12.6
11	71.2	16.1	12.7
12	4.4	55.4	40.2
13	33.1	27.0	39.9

Mg-Al-Sr and Mg-Al-Ca ternary diagrams with the investigated compositions in weight percentage are given in Figures 5.1 and 5.2. Samples were prepared from 99.8 wt% magnesium, 99.9 wt.% aluminium, 99 wt.% strontium, and 99 wt.% calcium to achieve the target compositions.

In the Mg-Al-Sr system, special attention was directed to the $Mg_{17}Sr_2$+$Mg_{38}Sr_9$+Al_4Sr phase field to measure the maximum solubilities of these phases and their triangulations. In order to study the phase triangulations of Al_4Sr and $Mg_{17}Sr_2$ with Mg, and Al_4Sr with Mg and γ, samples containing these phases were also chosen. This will help in determining the extent of the Mg_2Sr, $Mg_{23}Sr_6$, $Mg_{38}Sr_9$, $Mg_{17}Sr_2$, Al_2Sr and Al_4Sr phase fields in the ternary system and their solubilities.

Since Mg_2Ca and Al_2Ca give the thermal stability to the alloys in the Mg-Al-Ca system, samples containing these phases were chosen. These samples will help determine the extended solubilities of Mg_2Ca and Al_2Ca in the ternary system. In addition, three

samples in the Al_3Ca_8+Mg_2Ca phase field were chosen, as can be seen in Figure 5.2, to measure the maximum solubilities of the Al_3Ca_8 and its triangulation.

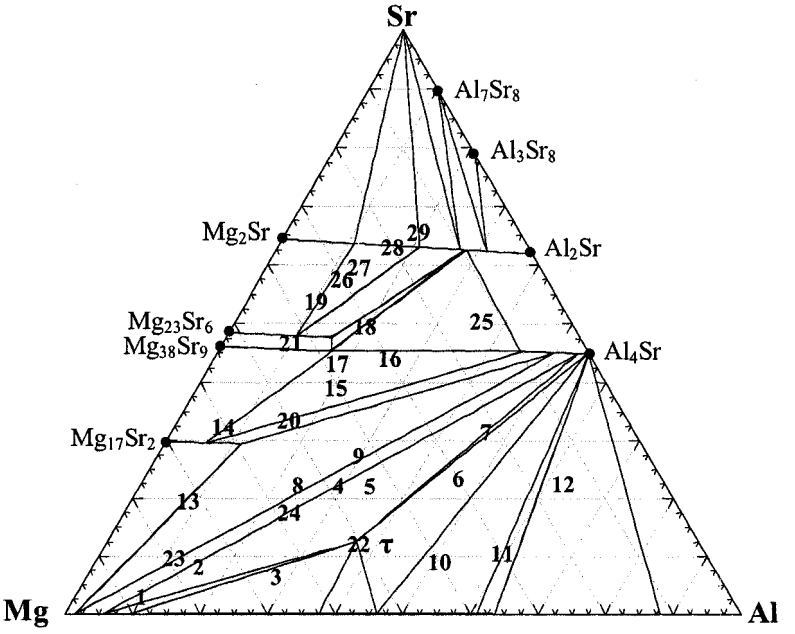

Figure 5.1: *Mg-Al-Sr isothermal section at 400°C, based on this work, showing the investigated compositions in wt.%.*

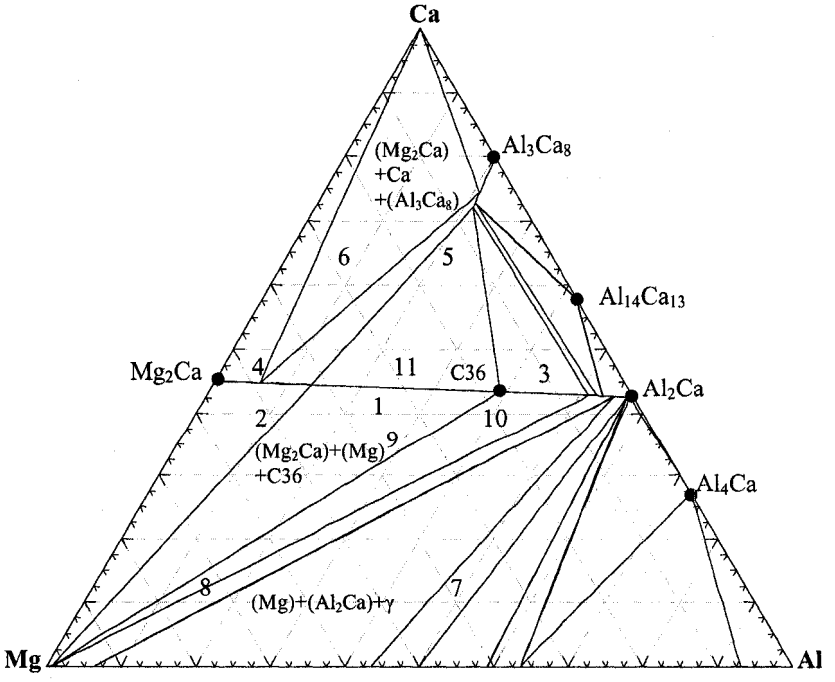

Figure 5.2: *Calculated isothermal section of the Mg-Al-Ca system at 300°C.*

5.2 Alloy Preparation

Aluminium and magnesium of proper portions were charged into a graphite crucible, which has 150 g capacity. The crucible was then placed inside an induction furnace under flowing argon with 1%SF_6 to protect the melt from oxidation. After the metals melted in the crucible, strontium or calcium was plunged using a graphite rod, followed with stirring. Once the strontium/calcium melted, the melt was again stirred using the graphite rod for a minimum of 120 seconds to attain homogeneity. After that the induction furnace was turned off and the melt was cooled under flowing argon. Every alloy was melted three times to achieve homogeneity.

The Mg-Al-Ca and Mg-Al-Sr samples were cut into two; one half was used for thermal analysis using DSC, the other half was used for heat treatment to study the isothermal sections at 400 and 300°C for Mg-Al-Sr and Mg-Al-Ca, respectively. XRD, SEM, and EPMA were used to analyze the heat-treated samples. The Mg-Al-Sr alloys were annealed at 400°C under flowing argon for 48 hours followed by water quenching. It was found in many cases that the samples disintegrated into powders when quenched in water due to the reaction of Mg. In order to avoid this Mg-Al-Ca alloy samples were heat-treated at 300°C for 24 hours under flowing argon and then quenched in oil to obtain non-powder samples.

In order to verify the final alloy composition after melting, the chemical compositions of the as-cast alloy were analyzed using the Inductively Coupled Plasma-Atomic Emission Spectrometry (ICP-AES) method. Small amounts of Ca/Sr and Al were subject to vaporization losses in alloys containing high Ca/Sr and Al; the loss of Ca/Sr was below 3 wt.% for alloys containing less than 40 wt.% Ca/Sr. In alloys containing

more than 40 wt.% Ca/Sr, the loss of these elements were in the range of 4-5 wt.%. In addition a loss of Al not exceeding 2 wt.% was found in alloys containing more than 50 wt.% Al. Nevertheless, the actual composition was used for the analysis in this work.

Four alloys with high-Sr concentration; samples 26, 27, 28 and 29 disintegrated into powders after casting. Post heat treatment analysis on these samples was not performed.

5.3 Sample Preparation for Optical Microscopy

Samples from the annealed alloys were carefully cut using a hex-saw to avoid contamination. They were then cold mounted under vacuum in epoxy resin. Microstructural observations were made using optical microscope (Olympus BX60M). The samples were polished with 1 μm α-Al_2O_3 suspension. The samples were etched using 1vol% nital solution (HNO_3 in ethanol). Etching was performed only by applying the etchant on the surface for a short period of time (~ 5s) to prevent dissolving Mg grains.

5.4 SEM and EPMA Analysis

SEM and EPMA were used to examine the phase compositions of the alloys. Chemical composition of the phases was determined using a CAMECA SX51 EPMA at MTL-CANMET by which the measurements were carried out on three locations for each phase and the average was used in the present analysis. Magnesium alloys have low stopping power to the primary electron beam, thus, a lower acceleration voltage is desired to reduce beam-specimen interaction volume. However, the acceleration voltage must be high enough to excite characteristic X-rays from the elements of interest. In this study, an acceleration voltage of 12 kV and a beam current of 10 nA were used for the analysis

to ensure a high-count rate and reasonable imaging resolution. Pure Mg, Al_4Ca and Al_4Sr standards were used for the EPMA quantitative analysis.

5.5 X-Ray Diffraction

Phase identification was carried out by X-ray diffraction (XRD) with a Philips diffractometer (Cu$K\alpha$ radiation) equipped with a PW 1050/25 focusing goniometer with steps 0.02° of 2θ diffraction angle and 1s exposure time. All the samples were investigated in the powder form in the heat-treated condition. For the calibration of the X-ray diffractometer, powder was made from pure Mg supplied by Noranda and diffraction patterns were obtained and compared with the literature. The relative peak intensity and the position matched completely. The obtained diffraction patterns were refined and analyzed using the Rietveld method in comparison with simulated X-ray spectra using PowderCell 2.3 [186]. The patterns were examined for known oxide phases such as MgO, Al_2O_3 and $MgAl_2O_4$ for any possible oxide formation. For the Mg-Al-Sr samples, XRD was done in the Chemistry Department at Concordia University and, for the Mg-Al-Ca samples the XRD were prepared in the Mining, Metals and Materials Department at McGill University.

The crystal structure and the atom positions in the unit cell must be known in order to calculate a diffraction pattern. The intensity of a diffracted beam depends on the structure factor, which is determined by the arrangement of atoms within a unit cell (Wyckoff position). After gathering the required information from the literature [154], the diffraction patterns were calculated using PowderCell 2.3 program. The crystal structure, the atoms positions and the corresponding XRD patterns for the known phases in the Mg-Al-Ca and Mg-Al-Sr systems are presented in Appendix A.

5.6 Differential Scanning Calorimetry (DSC)

Thermal analysis of the Mg-Al-(Ca,Sr) system was performed using a Setaram Setsys DSC-1200 instrument. The temperature calibration of the DSC equipment was done using pure Mg and Al. The samples were cut and mechanically polished to remove any possible contaminated surface layers. Afterwards, they were cleaned with acetone and placed in a graphite crucible with a lid to contain Mg vapours and protect the apparatus. To avoid oxidation, multiple evacuations followed by flushing with pure argon, were done. The DSC measurements were carried out at heating and cooling rates of 5°C/min. Slower heating rates were tried and were not found to reveal additional thermal arrests. The weight of the sample was 40~50 mg. During the calibration, it was verified that the geometrical mass (40~80 mg) and the surface quality did not show any significant effects on DSC spectra. The reproducibility of every measurement was confirmed by collecting the data from three heating and cooling cycles. The estimated error between the repetitive heating and cooling is ±1°C or less. However, the solidification behavior can be revealed much better using the cooling scans.

Figure 5.3 shows the general shape of the DSC spectra during cooling and heating of a pure element. On heating, melting requires heat and the downward peak is endothermic. On cooling, solidifying release heat and the upward peak is exothermic. Peak shapes have a linear portion up to the maximum deflection from the baseline followed by an exponential return to the baseline. The initial deflection during heating/cooling is indicated by the beginning of the linear portion of the peak and is used for temperature calibration [193]. Based on that, the onset temperature will be used for phase field boundaries and invariant reactions.

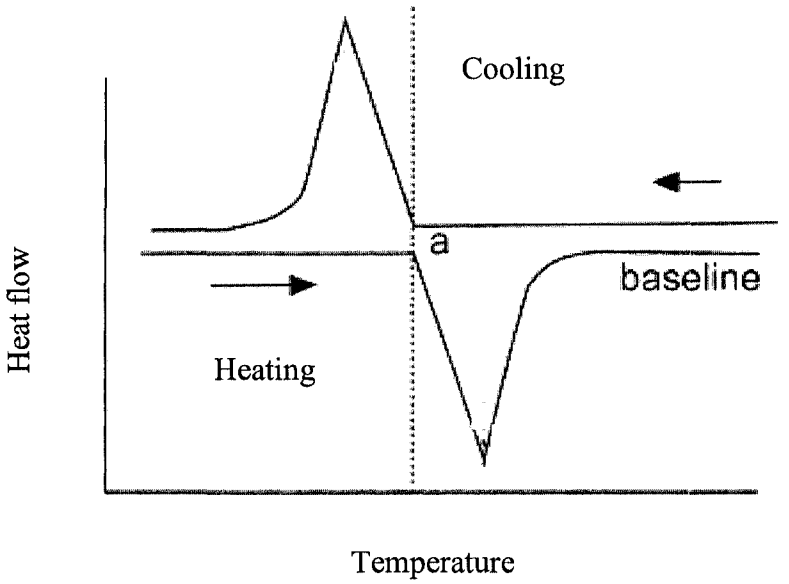

Figure 5.3: *DSC spectra during heating and cooling of a pure element.*

CHAPTER VI

Experimental Investigation of the Mg-Al-Sr System

Parvez *et al.* [128-131], from our group, investigated the Mg-Al-Sr system with twenty two different alloys using DSC, XRD and optical microscopy. They reported four new ternary intermetallic compounds or solid solutions. The stoichiometry of these new phases is not clearly identified and different from the earlier reported compounds by Makhmudov *et al.* [121] and Baril *et al.* [16]. This encouraged us to do further analysis of fourteen of Parvez's [149] samples using SEM and EPMA analyses to identify the phases in the Mg-Al-Sr system and to determine their compositions and answers many questions that were raised in previous articles [128-131]. Using the DSC results of Parvez [149], the solidification curves were obtained as described in the following section.

6.1 Solidification Curve Deduced from DSC

The solidification curves established from the DSC measurements are based on the heat transfer between the sample and the reference as shown by Tian equation [150,151]. Heat flux generated inside the sample (reaction, transition) can be written as:

$$\phi_r = -\phi - (C_s - C_r)\frac{dT_r}{dt} - R_{fs}C_s\frac{d\phi}{dt} \tag{6.1}$$

Where $\phi = \phi_{fr} - \phi_{fs}$ is the difference in heat flux between the sample and the reference which is directly measured by the DSC, t is the time, R_{fs} and C_s are the heat transfer resistance and heat capacity of the sample. The second term, $(C_s - C_r)\frac{dT_r}{dt}$, takes the difference in the heat capacities of the sample and reference into account and is assumed

to be negligible. This assumption is valid because the DSC curve is adjusted so that the baseline is flat. The third term considers the contribution of the thermal inertia of the system.

The heat flux generated by a reaction or phase transformation in the sample ϕ_r can be expressed by the heat evolution, h, which occurs in the sample: $\phi_r = \frac{dh}{dt}$. Chen *et al.* [152] assumed a linear dependence of the rate of heat evolution during solidification on the rate of solid phase fraction, $\frac{dh}{dt} = H\frac{d(1-f_l)}{dt}$, the total latent heat of solidification, H, is assumed to be constant. Equation 6.1 can be rewritten as:

$$H\frac{d(1-f_l)}{dt} = -\phi - RC\frac{d\phi}{dt} \tag{6.2}$$

The terms H and RC were treated as adjustable parameters determined from the measured DSC curve of the sample. H is obtained by integration of the area under DSC curve after the baseline was subtracted, and the term RC, time constant τ of the DSC, is iteratively obtained from the after reaction part of the DSC curve because there is no reaction heat input or output in the sample cell then [153].

6.2 Experimental Study of the Mg-Al-Sr System

Composition 1 (3.32/87.29/9.39 Sr/Mg/Al wt.%) is located close to the Mg-rich corner in the primary precipitation field of Mg and in the Mg+Al_4Sr+γ phase field as can be seen in Figure 6.1. Figure 6.2 shows the SEM image, EPMA analysis and solidification curve of this composition. The SEM image indicates that: (i) the matrix region (A) contained magnesium and a small amount of aluminum; (ii) the grain boundary region (B) contained magnesium as well as aluminum and strontium. Table 6.1 summarizes the

compositions and the phases at room temperature identified by SEM/EDS, EPMA and XRD analyses. Two phases, (Mg) and (Al_4Sr), were positively identified in the microstructure. The round brackets denote solid solubility. The SEM image shows that the dark Mg-matrix phase was separated by bright precipitates and the grain boundary network is not continuous. The network is connected via Mg-matrix bridges. The $Mg_{17}Al_{12}$ (γ) phase was not identified positively in the XRD pattern. The (Al_4Sr) phase is located at the grain boundary region and appears to be lamellae. The AJ51x, AJ62x and AJ62Lx alloys developed by Noranda also showed this phase [11]. Large ternary solid solubilities were observed in this alloy.

Table 6.1: *Composition and room temperature phase content of the investigated samples in the Mg+Al_4Sr+γ.*

Composition				Identified phases		Solubilities (at.%) (EPMA)
No.	(wt.%)					
	Sr	Mg	Al	EPMA and SEM/EDS	XRD	
1	3.32	87.29	9.39	(Mg) and (Al_4Sr)	(Mg) and (Al_4Sr)	Mg dissolves 4.8 at.% Al and Al_4Sr dissolves 23.2 at.% Mg
2	8.65	76.15	15.20	(Mg), (Al_4Sr) and ($Mg_{17}Sr_2$)	(Mg) and (Al_4Sr)	Mg dissolves 7.4 at.% Al , $Mg_{17}Sr_2$ dissolves 19 at.% Al
3	6.88	65.45	27.67	(Mg), (Al_4Sr) and γ	(Mg), (Al_4Sr) and γ	Mg dissolves 11.4 at.% Al, Al_4Sr dissolves 7.9 at.% Mg.
4	22.48	48.57	28.95	(Al_4Sr) and γ	(Mg), (Al_4Sr) and γ	Al_4Sr dissolves 10.8 at.% Mg
5	22.53	43.75	33.72	(Mg), (Al_4Sr) and γ	(Mg), (Al_4Sr) and γ	Mg dissolves 10.6 at.% Al, Al_4Sr dissolves 9.2 at.% Mg.
6	24.00	30.00	46.00	(Al_4Sr) and γ	(Al_4Sr), γ and τ	Al_4Sr dissolves 4.9 at.% Mg.
7	32.00	22.00	46.00	(Al_4Sr) and γ	(Al_4Sr) and γ	Al_4Sr dissolves 5.1 at.% Mg.

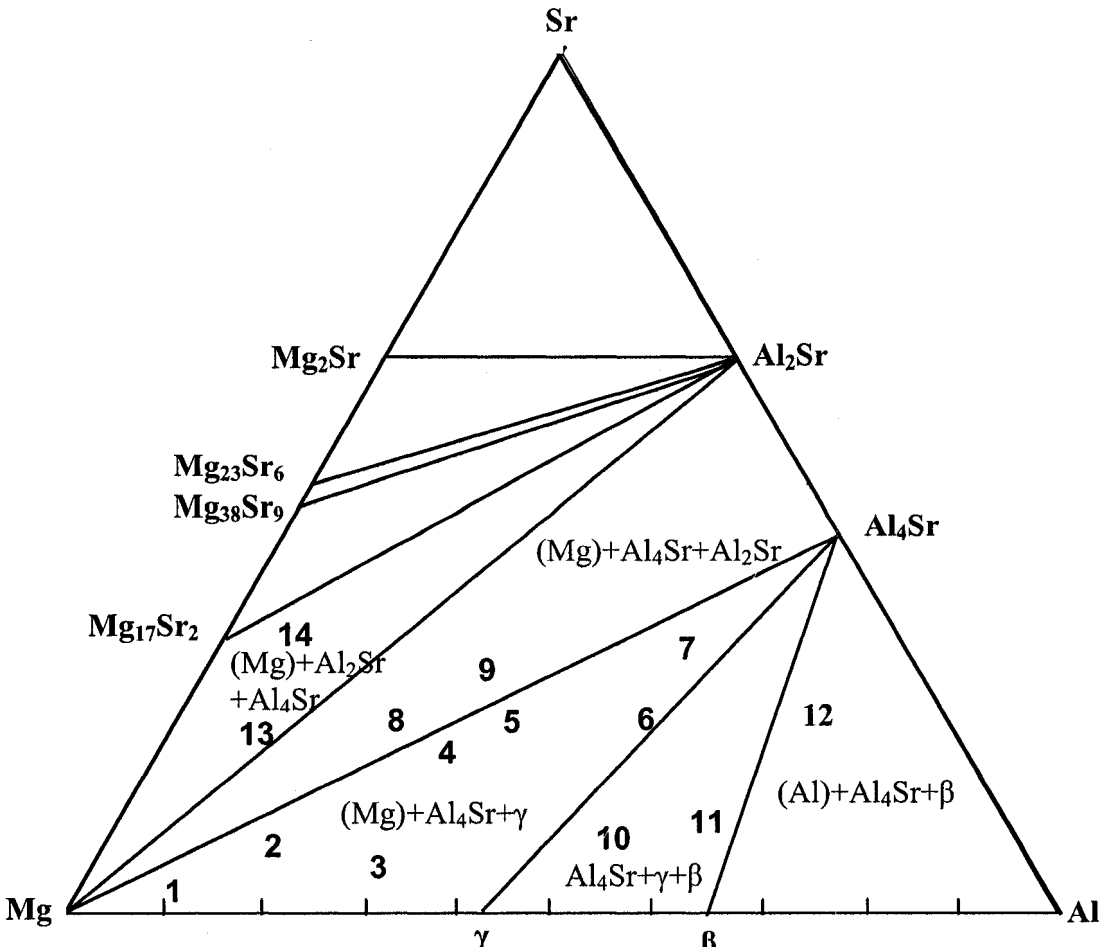

Figure 6.1: *Mg-Al-Sr ternary isothermal section at 25°C showing the investigated compositions in wt.% based on the thermodynamic model of [34].*

Quantitative EPMA analysis in Figure 6.2(IV) shows that Mg dissolves 4.8 at.% Al, whereas Al_4Sr dissolves 23.2 at.% Mg. As can be seen in Figure 6.2(III), that the solidification curve deduced from the DSC measurement shows that (Mg) starts to solidify at 602°C consuming 67 wt.% of the liquid and, binary and ternary invariant reactions occur at 517°C and 525°C, respectively, precipitating (Mg) and (Al_4Sr) from the remaining liquid at the grain boundary of the Mg-matrix (Figure 6.2(I)). A very good agreement between the SEM, XRD and EPMA analyses was observed in terms of phase identification.

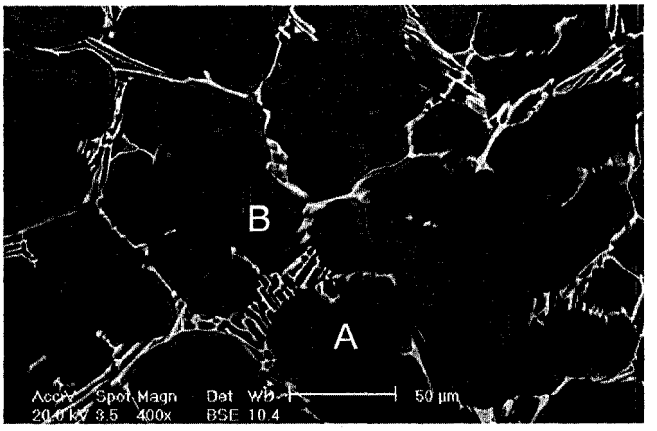

(I)

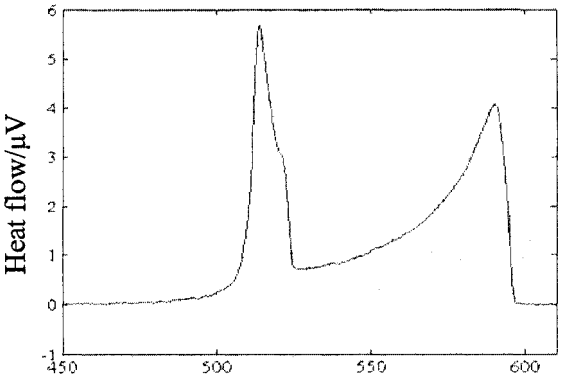

(II)

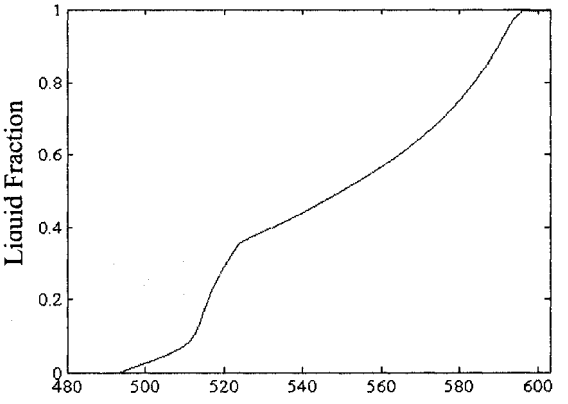

(III)

Location	at.% Mg	at.% Al	at.% Sr	Phases
A	95.2	4.8	0.0	(Mg)
B	23.2	58.2	18.6	(Al_4Sr)

(IV)

Figure 6.2: *(I) SEM image; (II) DSC spectra; (III) Solidification curve and (IV) EPMA analysis of composition 1.*

Spot analysis of composition 2 (8.65/76.15/15.20 Sr/Mg/Al wt.%) was carried out at two different locations as shown in Figure 6.3. The microstructure is characterized as dendrites and two types of secondary phases were observed.

Both types of secondary phases contain all three elements; Mg, Al and Sr. The eutectic morphology is more evident in this alloy than for composition 1 as shown in

Figure 6.3(II). Moreover, the solidification curve, as can be seen in Figure 6.3(III), shows that (Mg) starts to solidify at 530°C down to 516°C consuming more than 17 wt.% of the liquid, (Mg) and (Al_4Sr) precipitate at 516°C then a ternary invariant reaction occurs at 507°C precipitating (Mg), (Al_4Sr) and ($Mg_{17}Sr_2$) consuming the remaining liquid.

It can be seen by the EPMA analysis, as shown in Figure 6.3 and Table 6.1, that the dark phase is Mg dissolving 7.4 at.% Al and the grey bulky phase is $Mg_{17}Sr_2$ dissolving 19.3 at.% Al. Al_4Sr was predicted by the thermodynamic calculation of this alloy and confirmed by the XRD measurement but due to the small size of the precipitates it was difficult to detect this phase using EPMA.

In the present EPMA analysis, the large precipitate (spot B) shown in Figure 6.3(IV) is identified as $Mg_{17}Sr_2$ dissolving 19.3 at.% Al. Baril *et al.* [16] reported the existence of a bulky phase with chemical composition 78.10 ± 1.18 at.% Mg, 4.58 ± 0.37 at.% Sr and 17.32 ± 0.99 at.% Al in AJ52x alloy. This is not close to the chemical composition of the large precipitate observed in sample 2. However, the stoichiometry of this bulky phase was not clearly identified and they [16] tentatively designated the phase as $Al_3Mg_{13}Sr$. According to the present study, the extent of the ($Mg_{17}Sr_2$) phase field in the calculated ternary Mg-Al-Sr system reported by [34] and [126] is predicted to be narrower than what it should be and the system has therefore been be re-optimized during the current work.

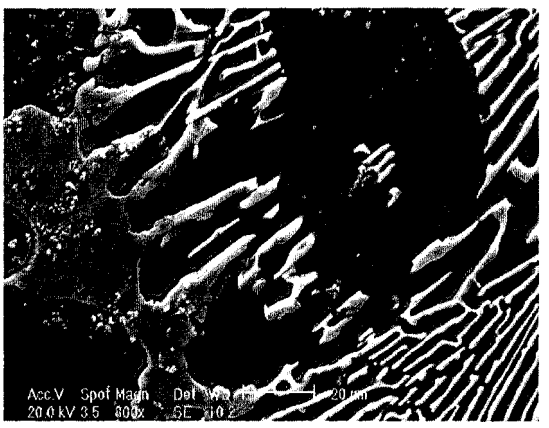

(I)

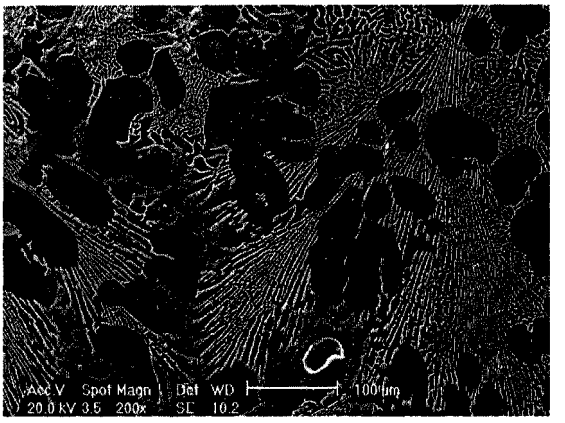

(II)

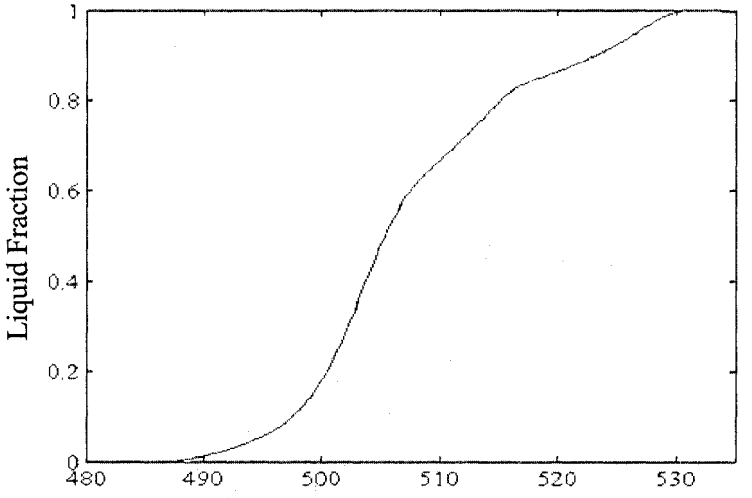

(III)

Location	at.% Mg	at.% Al	at.% Sr	Phases
A	92.6	7.4	0.0	(Mg)
B	71.4	19.3	9.3	($Mg_{17}Sr_2$)

(IV)

Figure 6.3: *SEM image (I) 800 x; (II) 200 x; (III) Solidification curve and (IV) EPMA analysis of composition 2.*

Figure 6.4 shows SEM image, EPMA analysis at three different locations and the solidification curve of composition 3 (6.88/65.45/27.67 Sr/Mg/Al wt.%). The plate-like phase is identified as (Al_4Sr) while the darker phase is designated as (Mg) according to

the EPMA and XRD analysis as summarized in Table 6.1. γ-Phase detected in region (C) was identified positively in both XRD and EPMA analyses. Ternary solid solubilities were measured by quantitative EPMA analysis. It can be seen in Figure 6.4(II) that Mg dissolves 11.4 at.% Al whilst the binary compound Al_4Sr dissolves 7.9 at.% Mg. A very small amount of Sr was detected in region (C) and negligible amount in region (B). Moreover, the solidification curve of sample 3 in Figure 6.4(III) shows three phase transformations: first occurs at 525°C forming (Al_4Sr) consuming around 10 wt.% of the liquid, second at 472°C forming (Al_4Sr) and (Mg) and the third one at 429°C precipitating (Al_4Sr), (Mg) and γ from the remaining liquid.

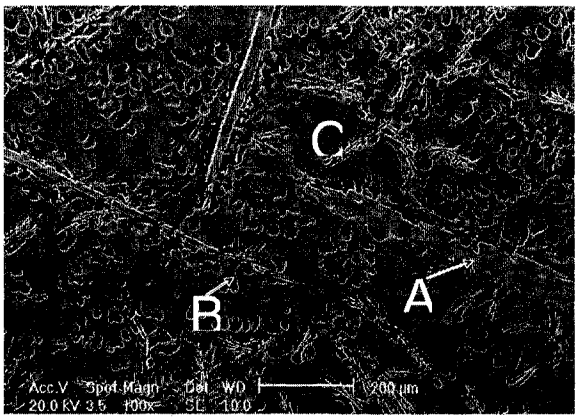

(I)

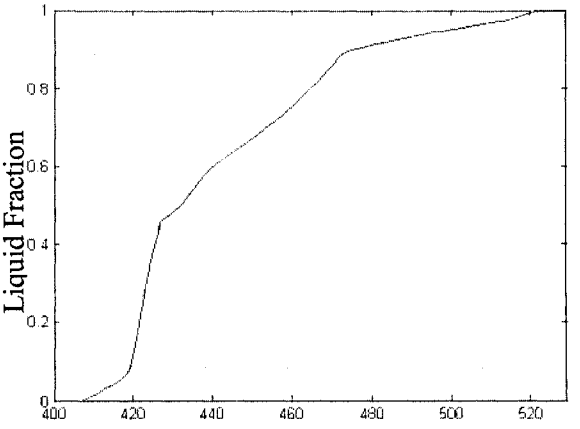

(III)

Location	at.% Mg	at.% Al	at.% Sr	Phases
A	7.9	70.3	21.8	(Al_4Sr)
B	88.6	11.4	0.0	(Mg)
C	59.2	40.6	0.2	γ

(II)

Figure 6.4: *(I) SEM image; (II) EPMA analysis and (III) Solidification curve of composition 3.*

Composition 4 (22.48/48.57/28.95 Sr/Mg/Al wt.%) has a plate-like, eutectic morphology and a dark matrix as shown in Figure 6.5. The plates are larger than those observed in composition 3. It can be seen in Table 6.1 that both (Mg), (Al_4Sr) were

identified by XRD and EPMA analyses whereas γ phase was not detected in the XRD pattern. In this sample, Al_4Sr dissolves 10.8 at.% Mg as shown in Figure 6.5(II). A very negligible amount of Sr was detected in region (B) by EPMA analysis.

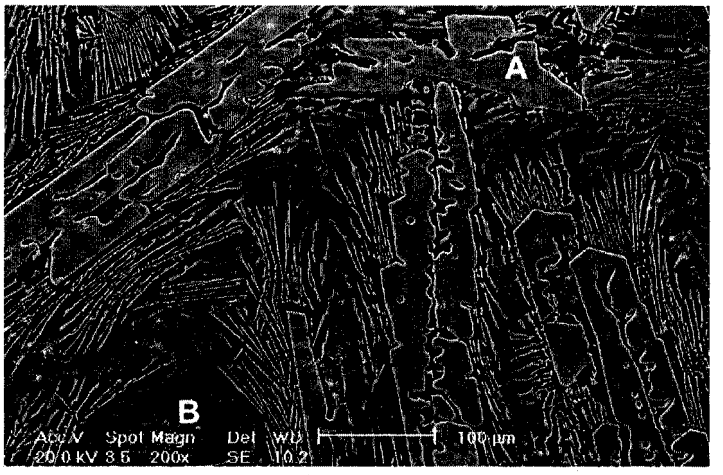

(I)

Location	at.% Mg	at.% Al	at.% Sr	Phases
A	10.8	68.3	20.9	(Al_4Sr)
B	63.4	36.3	0.3	γ

(II)

Figure 6.5: *(I) SEM image and (II) EPMA analysis of composition 4.*

Composition 5 (22.53/43.75/33.72 Sr/Mg/Al wt.%) is located very close to the boundary of two three-phase regions; Mg+Al_4Sr+γ and Mg+Al_4Sr+Al_2Sr as shown in Figure 6.1. It can be seen in Figure 6.6(I) that the amount of plate-like phase is somewhat higher than for compositions 2 and 4. This phase is identified as (Al_4Sr) by XRD and EPMA analyses as shown in Table 6.1 and Figure 6.6(II), respectively. Also, the solidification curve of sample 5 in Figure 6.6(III) shows that formation of (Al_4Sr) consumed more than 60 wt.% of the liquid. This is evident from its relative amount shown in the SEM image in Figure 6.6(I). γ-Phase is identified in region (B) which

appeared with higher contents in alloy 5 than in alloy 4. The matrix in region (C) was identified as (Mg) and supported by XRD analysis as shown in Table 6.1. A very good agreement between XRD and EPMA analyses was observed.

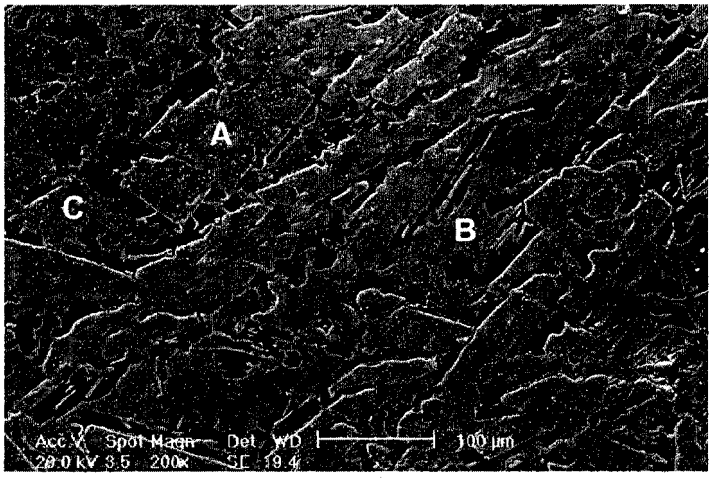

(I)

Location	at.% Mg	at.% Al	at.% Sr	Phases
A	9.2	69.8	21.0	(Al_4Sr)
B	61.3	38.6	0.1	γ
C	89.4	10.6	0.0	(Mg)

(II)

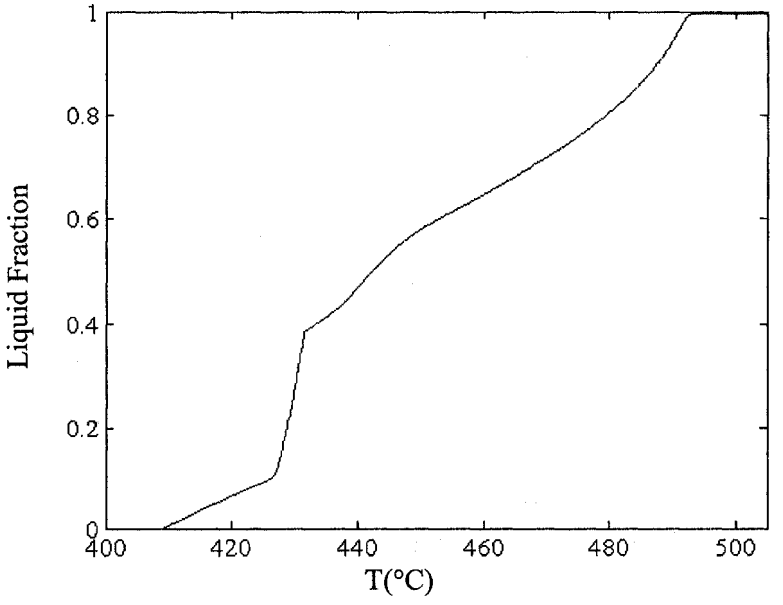

(III)

Figure 6.6: *(I) SEM image; (II) EPMA analysis and (III) Solidification curve of composition 5.*

Composition 6 (24/30/46 Sr/Mg/Al wt.%) is located faraway from Mg-rich region and very close to the boundary of two three-phase regions; Mg+Al_4Sr+γ and Al_4Sr+γ+β. In the XRD and EPMA analyses positively identified γ and (Al_4Sr) as shown in Table 6.1 and Figure 6.7(II). Here, Al_4Sr dissolves 4.9 at.% Mg. Some distinct peaks that are not associated with the known phases in the Mg-Al-Sr system have been observed in the XRD pattern and were confirmed by SEM image (region D). This phase was tentatively designated as τ, a ternary compound or solid solution, which however could not be identified and confirmed by EPMA due to the small size of the precipitates.

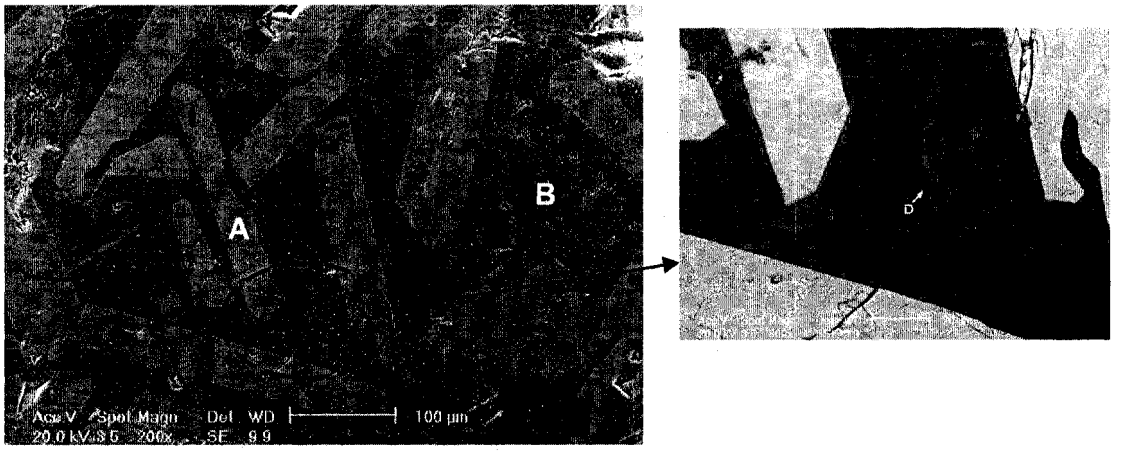

(I)

Location	at.% Mg	at.% Al	at.% Sr	Phases
A	4.9	74.0	21.1	(Al_4Sr)
B	56.5	43.4	0.1	γ

(II)

Figure 6.7: *(I) SEM image and (III) EPMA analysis of composition 6.*

SEM image and EPMA analysis of composition 7 (32/22/46 Sr/Mg/Al wt.%) are shown in Figure 6.8. The plate-like phase is identified as Al_4Sr which dissolves 5.1 at.% Mg and the region B is identified as γ. The solubility of Sr in γ was also found negligible in this alloy.

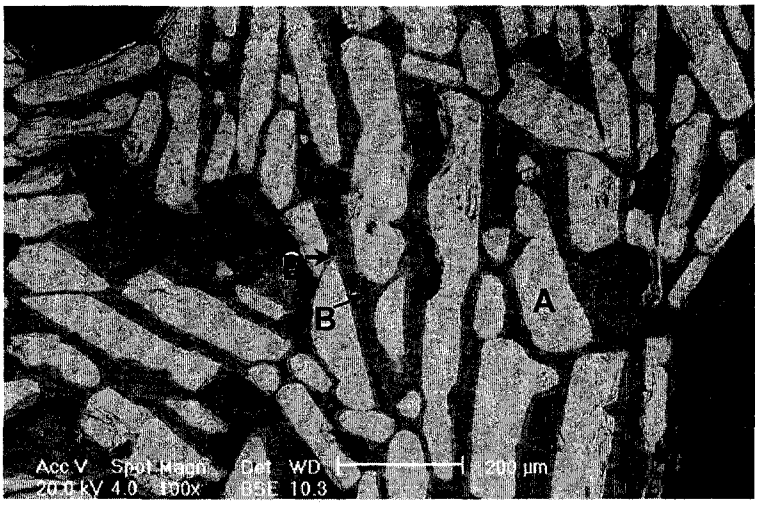

(I)

Location	at.% Mg	at.% Al	at.% Sr	Phases
A	5.1	74.5	20.4	(Al_4Sr)
B	57.5	42.4	0.1	γ

(II)

Figure 6.8: *(I) SEM image and (II) EPMA analysis of composition 7.*

It can be seen in Figure 6.1 that composition 8 (22.78/54.39/22.83 Sr/Mg/Al wt.%) is located in the Mg-rich corner close to composition 4, but the two alloys belong to two different phase fields. SEM image as shown in Figure 6.9(I) shows that the size of the plate-like phase is relatively smaller than in alloy 4 and it is distributed more evenly in the microstructure. Table 6.2 summarizes the compositions and room temperature phase contents identified by EPMA and XRD for the samples in this phase field.

Table 6.2: *Composition and room temperature phase content of the investigated samples In the Mg+Al_4Sr+Al_2Sr.*

No.	Composition (wt.%)			Identified phases		Solubilities (at.%) (EPMA)
	Sr	Mg	Al	EPMA and SEM/EDS	XRD	
8	22.78	54.39	22.83	(Mg), (Al_4Sr) and ($Mg_{17}Sr_2$)	(Mg), (Al_4Sr) and ($Mg_{17}Sr_2$)	Mg dissolves 11.2 at.% Al, Al_4Sr dissolves 14.1 at.% Mg and $Mg_{17}Sr_2$ dissolves 21.3 at.% Al.
9	27.83	42.89	29.28	(Mg), (Al_4Sr) and ($Mg_{17}Sr_2$)	(Mg), (Al_4Sr) and ($Mg_{17}Sr_2$)	Mg dissolves 11 at.% Al, Al_4Sr dissolves 12.5 at.% Mg and $Mg_{17}Sr_2$ dissolving 20.2 at.% Al.

(Mg), (Al_4Sr) and ($Mg_{17}Sr_2$) were identified in the diffraction patterns and by the EPMA analysis of regions (A), (B) and (C), respectively, as shown in Figure 6.9(I). From the EPMA analysis shown in Figure 6.9(III), Al_4Sr dissolves 14.1 at.% Mg. In contrast, 10.8 at.% of Mg is dissolved in Al_4Sr in alloy 4. In the present EPMA analysis, the light grey precipitate (spot C) is identified as $Mg_{17}Sr_2$ dissolving 21.3 at.% Al which is the maximum observed solubility of Al in $Mg_{17}Sr_2$. Moreover, sample 8 is located in the three-phase, (Mg), (Al_4Sr) and ($Mg_{17}Sr_2$), region which was, however, not predicted correctly by [34] and [126] as shown in Figure 6.1. The composition of the light grey phase is also not close to that of $Al_3Mg_{13}Sr$ observed by Baril *et al.* [16].

In Figure 6.9(III), the solidification curve shows that (Al_4Sr) precipitates between 613°C and 544°C consuming 23 wt.% of the liquid. At 544°C, both (Al_4Sr) and (Mg) are formed. Finally, a ternary invariant transformation occurs at 513°C forming (Al_4Sr), (Mg) and ($Mg_{17}Sr_2$).

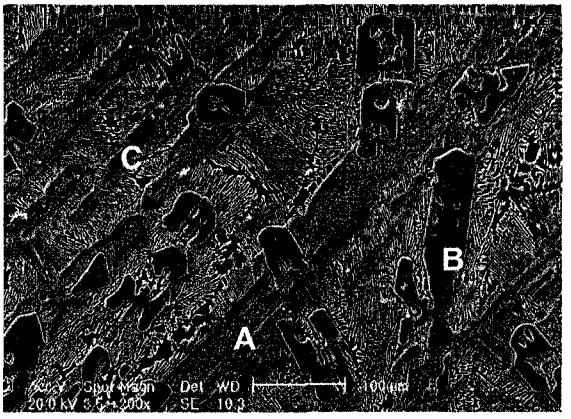

(I)

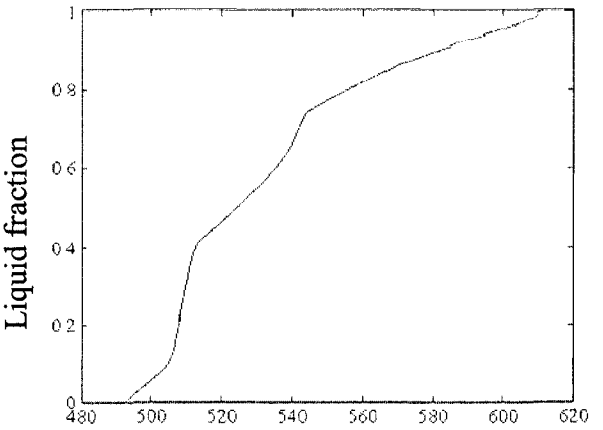

(II)

Location	at.% Mg	at.% Al	at.% Sr	Phases
A	88.6	11.2	0.2	(Mg)
B	14.1	64.5	21.4	(Al_4Sr)
C	70.0	21.3	8.7	($Mg_{17}Sr_2$)

(III)

Figure 6.9: *(I) SEM image; (II) Solidification curve and (III) EPMA analysis of composition 8.*

Composition 9 (27.83/42.89/29.28 Sr/Mg/Al wt.%) is located in the same three-phase region as composition 8. SEM image, EPMA analysis and solidification curve are shown in Figure 6.10. The microstructure of alloys 8 and 9 appeared to be quite similar. It is a plate-like structure with dark and light-grey phases. It can be seen in Table 6.2 that (Mg), (Al_4Sr) and ($Mg_{17}Sr_2$) have been identified in the XRD pattern; however, with the EPMA analysis only (Al_4Sr) and ($Mg_{17}Sr_2$) have been identified. The plate-like phase has been identified as Al_4Sr that dissolves 12.5 at.% Mg. According to the EPMA analysis shown in Figure 6.10(II), the light grey phase in region (B) is $Mg_{17}Sr_2$ dissolving 20.2 at.% Al. Similar ternary solid solubility has been observed in composition 8. It is obvious from the above discussion that a ternary solid solubility of $Mg_{17}Sr_2$ has been formed in the studied alloys and the phase region was not predicted correctly by [34] and [126].

The present study of the Mg-Al-Sr system shows that sample 9 is located in the three phase region of (Mg), (Al_4Sr) and ($Mg_{17}Sr_2$). It is worth noting, as shown in Figure 6.10(III), that the solidification curve suggests that (Al_4Sr) starts to solidify at 600°C down to 445°C consuming around 10 wt.% of the liquid, binary and ternary invariant reactions occur, respectively, at 545°C and 512°C precipitating (Al_4Sr), ($Mg_{17}Sr_2$) and γ from the remaining liquid.

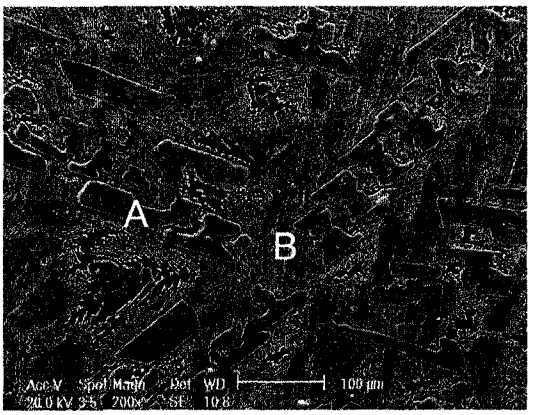

(I)

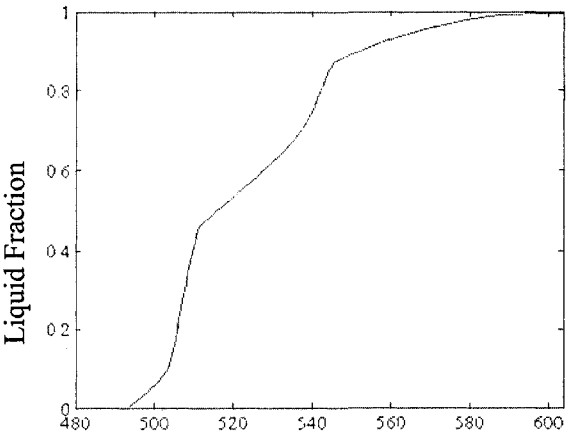

(III)

Location	at.% Mg	at.% Al	at.% Sr	Phases
A	12.5	66.6	20.9	(Al_4Sr)
B	70.6	20.2	9.2	($Mg_{17}Sr_2$)

(II)

Figure 6.10: *(I) SEM image; (II) EPMA analysis and (III) Solidification curve of composition 9.*

Table 6.3 summarizes the results of the investigated samples in this phase field. Figure 6.11 shows SEM image and EPMA analysis of composition 10 (9.5/40/50.5 Sr/Mg/Al wt.%). The microstructure of this alloy exhibits different morphology where the plate-like phase appears thinner. The XRD and EPMA analyses, shown in Table 6.3 and Figure 6.11(II), respectively, identified (Al_4Sr) and β positively. In the XRD pattern,

γ had a very small volume fraction and could not be detected in the EPMA analysis. In this sample, Al_4Sr phase dissolves 4.0 at.% of Mg as shown in Figure 6.11(II).

Table 6.3: *Composition and room temperature phase content of the investigated samples in the $Al_4Sr+\gamma+\beta$ phase field.*

Composition				Identified phases		Solubilities (at.%) (EPMA)
No.	(wt.%)					
	Sr	Mg	Al	EPMA and SEM/EDS	XRD	
10	9.50	40.00	50.50	(Al_4Sr) and β	(Al_4Sr), γ and β	Al_4Sr dissolves 4 at.% Mg.
11	11.00	30.00	59.00	(Al_4Sr)	(Al_4Sr), γ and β	Al_4Sr dissolves 2.1 at.% Mg.

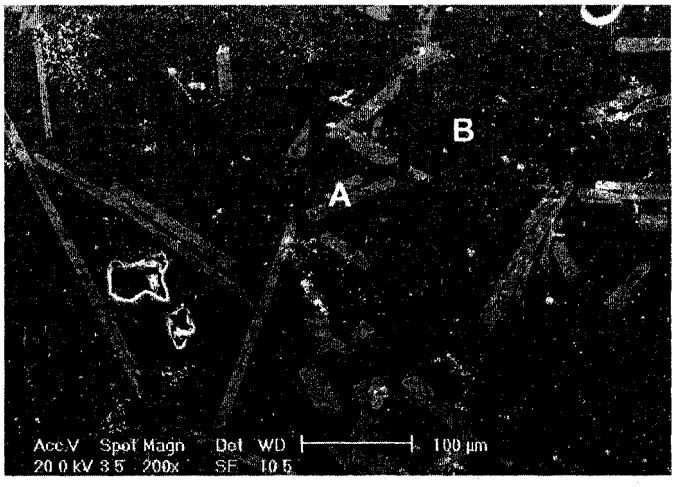

(I)

Location	at.% Mg	at.% Al	at.% Sr	Phases
A	4.0	75.4	20.6	(Al_4Sr)
B	49.1	50.7	0.2	β

(II)

Figure 6.11: *(I) SEM image and (II) EPMA analysis of composition 10.*

SEM image and EPMA analysis of composition 11 (11/30/59 Sr/Mg/Al wt.%) are shown in Figure 6.12. The microstructure is characterized by thick and thin plate-like structures and both of them have similar chemistry. The XRD analysis, reported in Table 6.3, identified three phases: (Al_4Sr), γ and β. The EPMA analysis, however, confirmed the existence of two phases (Al_4Sr) and β. It was observed that Al_4Sr dissolves 2.1 at.% of Mg in both regions (A) and (C) as can be seen in Figure 6.12(II).

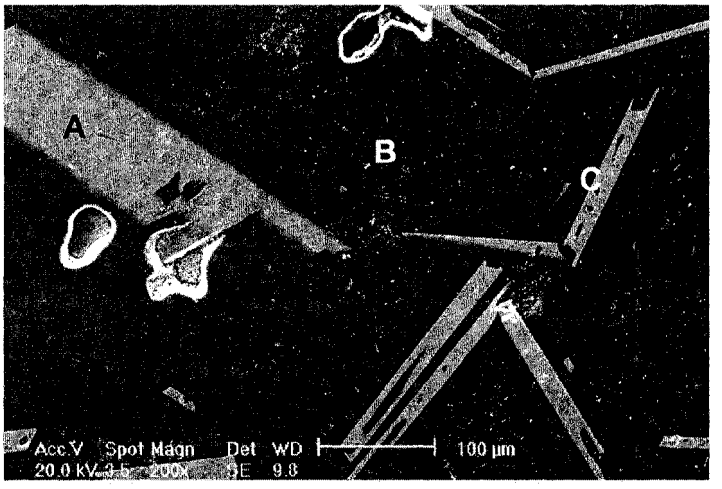

(I)

Location	at.% Mg	at.% Al	at.% Sr	Phases
A	2.1	77.0	20.9	(Al_4Sr)
B	38.9	61.1	0.0	β
C	2.1	76.8	21.1	(Al_4Sr)

(II)

Figure 6.12: *(I) SEM image and (II) EPMA analysis of composition 11.*

Figure 6.13 and Table 6.4 show SEM, XRD pattern and EPMA analyses of composition 12 (23/15/62 Sr/Mg/Al wt.%). The plate-like phase became thicker and larger as the alloy becomes closer to the Al_4Sr-rich region. Regions (A) and (B) were identified as (Al_4Sr) and β by EPMA analysis which was supported by the XRD results as shown in Table 6.4 and Figure 6.13(II). (Al) was identified only in the XRD pattern as

the microprobe analysis was conducted only in the two distinct regions of the micrograph shown in Figure 6.13(I). Quantitative EPMA analysis shows that Al_4Sr dissolves 1.7 at.% Mg, whilst the β-Phase does not show any solubility of Sr. In all the three alloys which contained β-Phase, the solubility of Sr in this phase was not detected by the EPMA analysis and considered to be negligible.

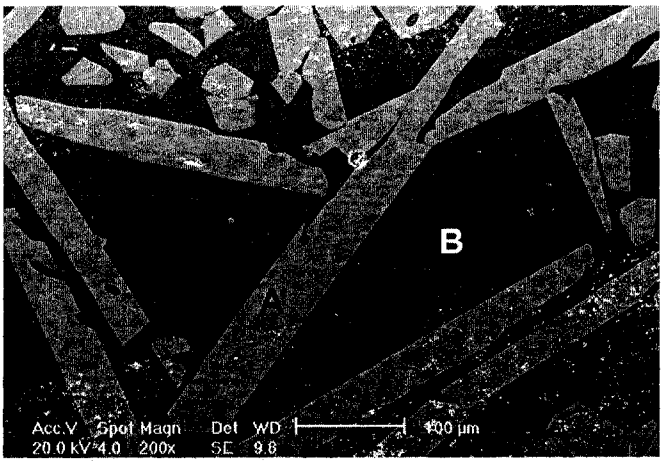

(I)

Location	at.% Mg	at.% Al	at.% Sr	Phases
A	1.7	77.2	21.1	(Al_4Sr)
B	37.4	62.5	0.0	β

(II)

Figure 6.13: *(I) SEM image and (II) EPMA analysis of composition 12.*

Table 6.4: *Composition and room temperature phase content of the investigated samples in the Al+Al_4Sr+β phase field.*

Composition				Identified phases		Solubilities (at.%) (EPMA)
No.	(wt.%)					
	Sr	Mg	Al	EPMA and SEM/EDS	XRD	
12	23	15	62	(Al_4Sr) and β	(Al), (Al_4Sr) and β	Al_4Sr dissolves 1.7 at.% Mg.

SEM image and EPMA analyses of composition 13 (19.9/72.0/8.1 Sr/Mg/Al wt.%) are shown in Figure 6.14. The microstructure is characterized as very bulky phase

surrounded by (Mg) matrix. XRD and EPMA analyses, as reported in Table 6.5, identified both (Mg) and ($Mg_{17}Sr_2$). According to SEM and EPMA analyses the dark phase was identified as Mg which dissolves 5.0 at.% Al. The large precipitates are identified as $Mg_{17}Sr_2$ that dissolve 8.5 at.% Al.

Table 6.5: *Composition and room temperature phase content of the investigated samples In the Mg+Al_2Sr+$Mg_{17}Sr_2$ phase field.*

No.	Composition (wt.%)			Identified phases		Solubilities (at.%) (EPMA)
	Sr	Mg	Al	EPMA and SEM/EDS	XRD	
13	19.90	72	8.1	(Mg) and ($Mg_{17}Sr_2$)	(Mg) and ($Mg_{17}Sr_2$)	Mg dissolves 5 at.% Al and $Mg_{17}Sr_2$ dissolves 8.5 at.% Al.
14	32.74	60.55	6.71	($Mg_{17}Sr_2$) and ($Mg_{38}Sr_9$)	($Mg_{17}Sr_2$) and ($Mg_{38}Sr_9$)	$Mg_{17}Sr_2$ dissolves 6.4 at.% Al and $Mg_{38}Sr_9$ dissolves 12.5 at.% Al.

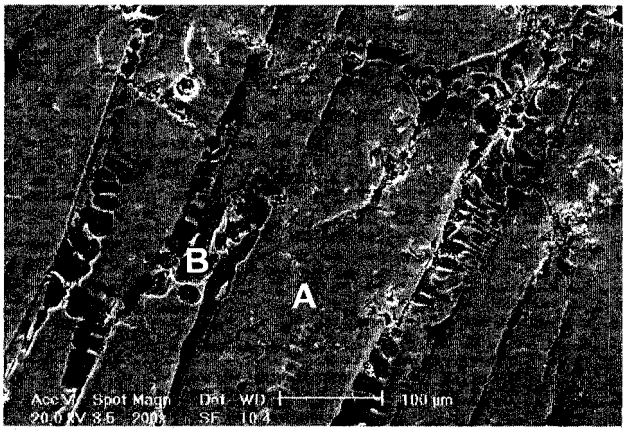

(I)

Location	at.% Mg	at.% Al	at.% Sr	Phases
A	81.7	8.5	9.8	($Mg_{17}Sr_2$)
B	94.9	5.0	0.1	(Mg)

(II)

Figure 6.14: *(I) SEM image and (II) EPMA analysis of composition 13.*

Figure 6.15 shows SEM and EPMA analyses at two different locations of composition 14 (32.74/60.55/6.71 Sr/Mg/Al wt.%). Two phases have been identified positively by XRD in sample 14 as shown in Table 6.5. EPMA analysis identified the phases in regions (A) and (B) as ($Mg_{17}Sr_2$) and ($Mg_{38}Sr_9$), respectively, as shown in Figure 6.15(II). In this alloy, EPMA analysis shows that $Mg_{17}Sr_2$ dissolves 6.4 at.% Al and $Mg_{38}Sr_9$ dissolves 12.5 at.% Al. This suggests, also, that the extent of the ($Mg_{38}Sr_9$) phase field in the ternary Mg-Al-Sr system is predicted narrower in the calculated phase diagrams reported in references [34] and [126] and thus the system needs to be re-optimized.

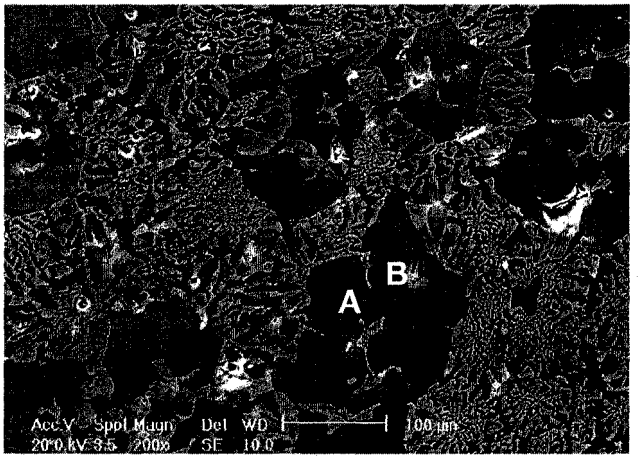

(I)

Location	at.% Mg	at.% Al	at.% Sr	Phases
A	83.0	6.4	10.6	($Mg_{17}Sr_2$)
B	70.8	12.5	16.7	($Mg_{38}Sr_9$)

(II)

Figure 6.15: *(I) SEM image and (II) EPMA analysis of composition 14.*

Based on the experimental results presented in this Chapter, a new Mg-Al-Sr isothermal section at 300 K was drawn and compared with that calculated from the thermodynamic modeling of [34]. It can be seen in Figure 6.16 that the extended

solubilities of the binary compounds, observed in this work, resulted in significant differences between the two isothermal sections.

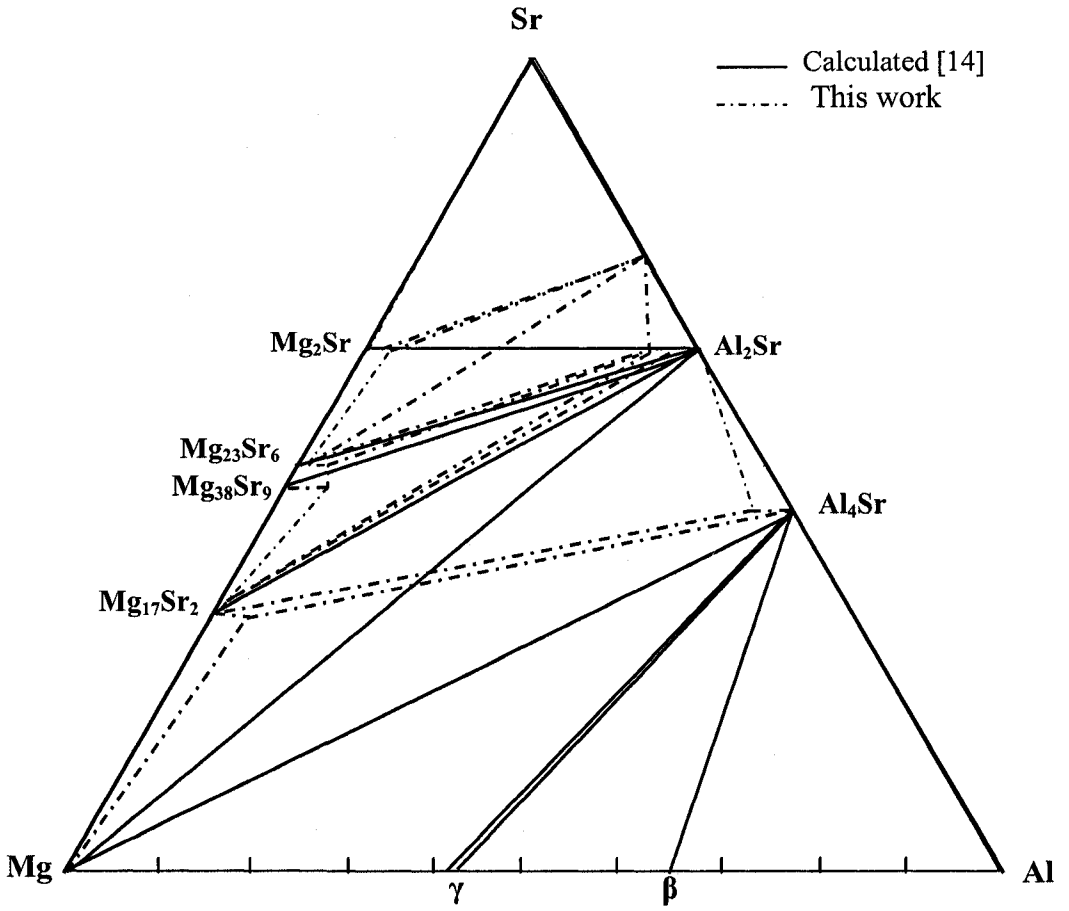

Figure 6.16: *Mg-Al-Sr isothermal section at 300 K.*

A solid solution of Mg in Al_4Sr was detected by XRD as well as EPMA. Solid solubility up to 23.2 at.% Mg in the Al_4Sr compound was detected in the investigated samples. Lattice parameter, as shown in Figure 6.17, increases linearly with Mg content as does the unit cell volume. The relation between lattice parameter *C* and Mg content is represented in equation 6.3 which describes the experimental data well with a coefficient of determination, R^2, 99.34 %. Such a behavior was expected considering the similar

atomic sizes of Mg and Al; the atomic radius of Mg is 0.160 nm against 0.143 nm for Al, i.e., a difference of about 11%.

$$C(x) = 0.039\ x + 11.082 \tag{6.3}$$

From the above equation, the extrapolated value at x = 0.0 is C = 11.082 Å. The experimental C lattice parameter of the Al_4Sr has been reported as 11.07Å [153]. This excellent agreement between the extrapolated and measured values confirms that the lattice parameter, C, of the $Mg_xAl_{4-x}Sr$ solid solution increases linearly with Mg content, x, obeying Vegard's law in the investigated samples. This solid solution is not a separate phase but it is due to the substitution of Al by Mg atoms in the Al_4Sr binary compound. Moreover, the solid solution of Mg in Al_4Sr must be considered as substitutional solid solution because of the following reasons: (i) Al/Sr ratio is not constant as proven by the EPMA analysis of all the samples containing this phase, and (ii) The numerical simulation of the X-ray spectra assuming substitutional solid solution using PowderCell 2.3 [186] agrees well with the experimental spectra but not if the solution is assumed to be interstitial. Further, it was observed that the other lattice parameter, a, remained constant.

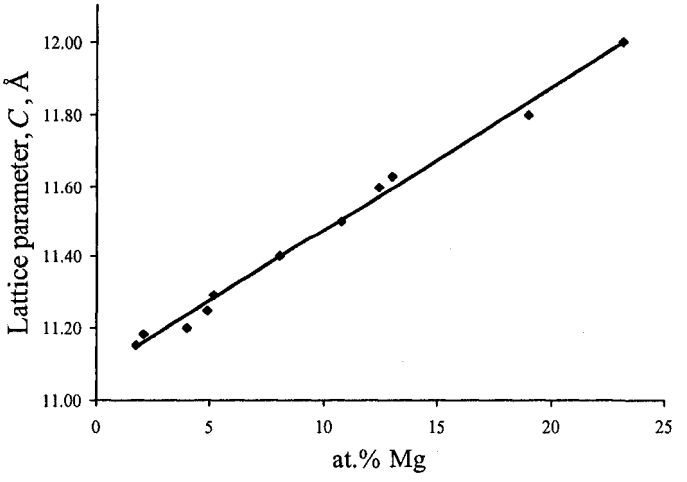

Figure 6.17: *Lattice parameter, C, of the $Mg_xAl_{4-x}Sr$ solid solution versus Mg content.*

6.3 Further Investigations on the Mg-Al-Sr System

Another set of Mg-Al-Sr samples was prepared to verify the thermodynamic model developed based on the first set of samples discussed in the previous section. Samples 15, 16 and 17 have been studied in the $(Mg_{17}Sr_2)$+(Al_4Sr)+$(Mg_{38}Sr_9)$ region to measure the maximum solubilities of Al in the binary compound $Mg_{38}Sr_9$ and Mg in Al_4Sr, as shown in Figure 6.18. The DSC spectra of sample 15 (40.3/20.1/39.6, Mg/Al/Sr) during heating and cooling events are shown in Figure 6.19. One exothermic peak appears in the cooling curve at 600°C which corresponds to the endothermic peak measured in the heating spectrum at 603°C. Another exothermic peak appeared in the heating curve at 644°C, but was not noticed in the cooling spectrum.

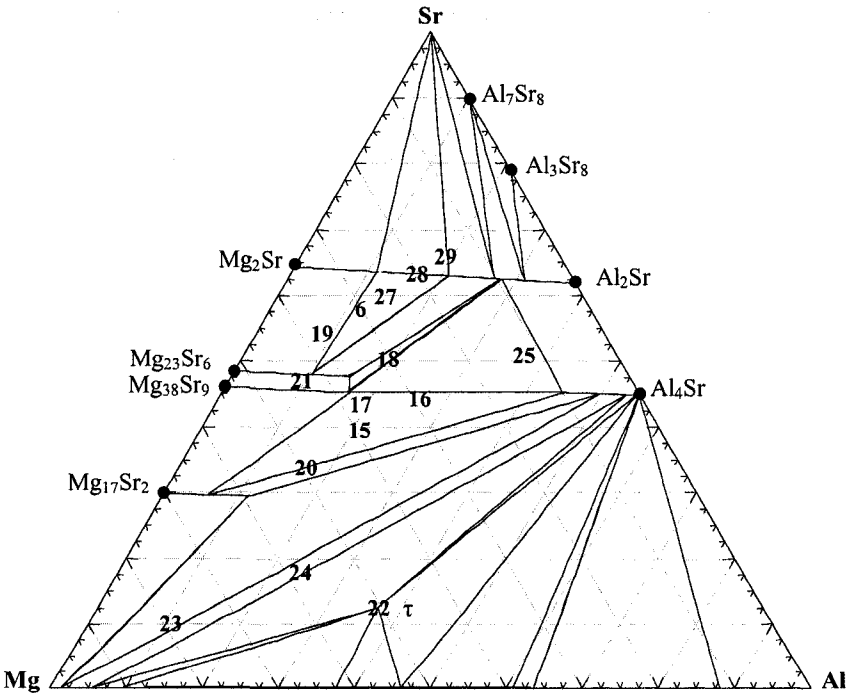

Figure 6.18: *Mg-Al-Sr isothermal section at 400°C, based on this work, showing the investigated compositions in wt.%.*

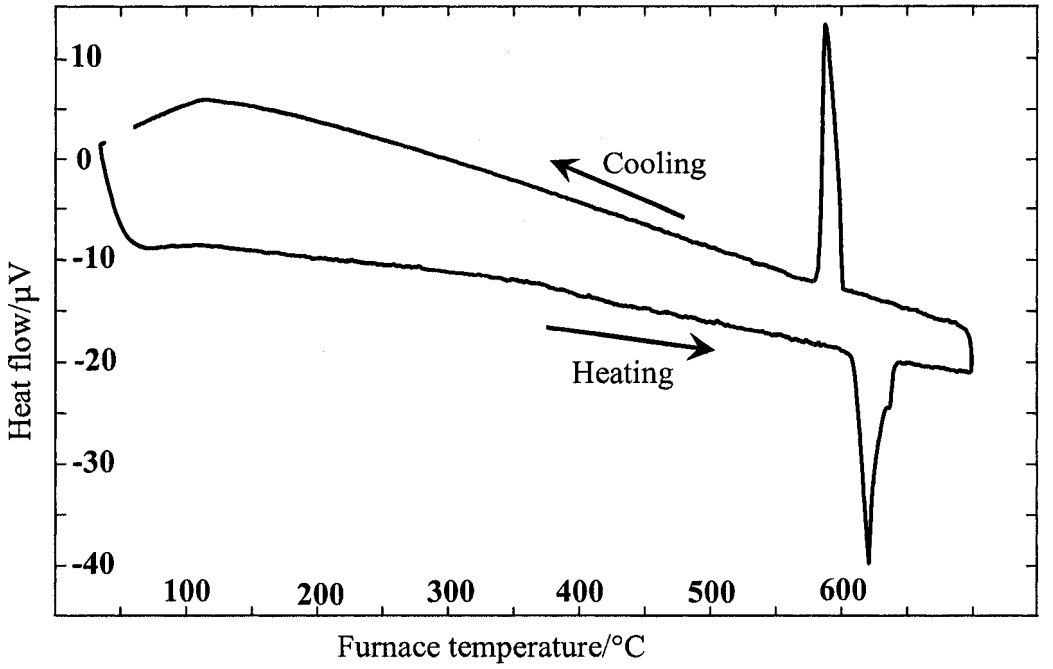

Figure 6.19: *DSC spectra of sample 15 (40.3/20.1/39.6, Mg/Al/Sr) during heating and cooling.*

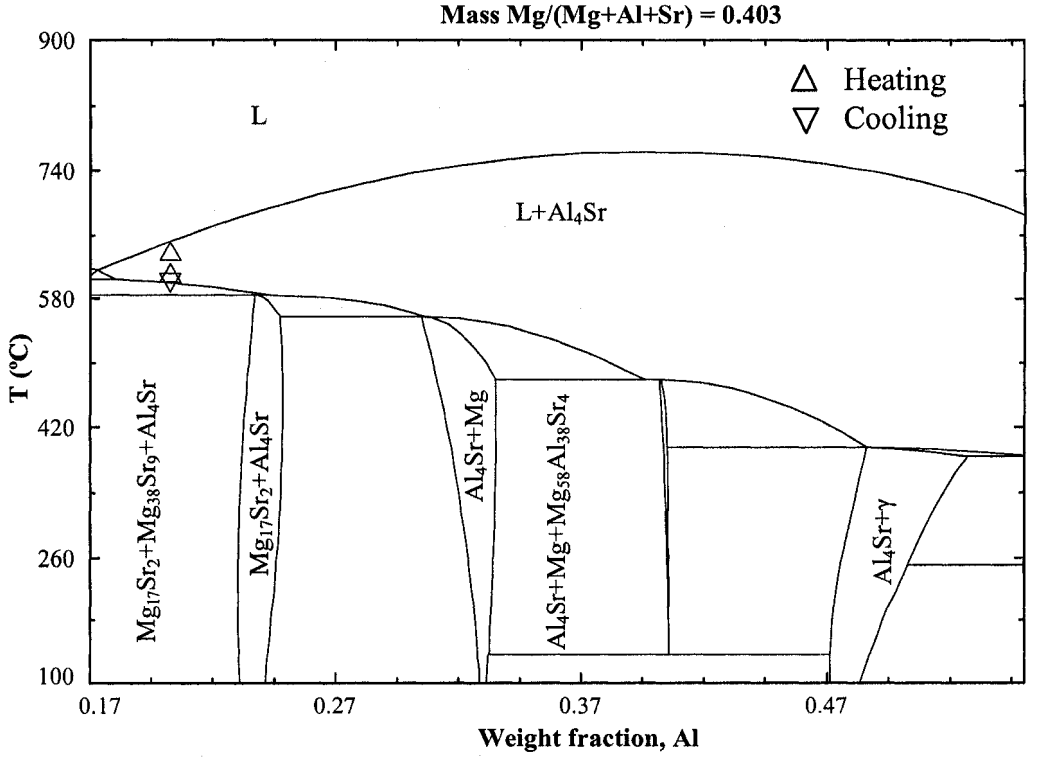

Figure 6.20: *Calculated vertical section at 40.3 wt.% Mg with DSC signals from heating and cooling curves of sample 15.*

It can be seen from this figure that the peaks appear more distinct in the heating than the cooling curve. This is due to the supercooling effect that causes more grain nucleation and energy accumulation. Supercooling arises from the fact that the undercooled phases require nucleation sites to start formation. Nucleation sites may be gas bubbles and/or rough foreign surfaces [194]. If such nucleating agents are not present in the liquid, then supercooling does not occur until the temperature drops lower than the equilibrium temperature. Since these phases start to form in a subcooled liquid, they will precipitate rapidly.

Figure 6.20 shows the calculated vertical section at 40.3 wt.% Mg with DSC signals of sample 15. As can be seen in this figure, the measured transformation temperatures correspond to the two phase boundaries in the vertical section: L/L+Al_4Sr/ L+Al_4Sr+$Mg_{38}Sr_9$ occurring at 644 and 603°C compared to 648 and 600°C predicted from thermodynamic calculation, respectively. Figure 6.21 shows SEM image, EPMA analysis and XRD pattern. SEM image indicates that both the matrix, region (A), and the gray phase in region (B) contained the three elements. According to the EPMA analysis, the matrix is ($Mg_{17}Sr_2$) dissolving 20.0±0.2 at.% Al and the gray phase is ($Mg_{38}Sr_9$) dissolving 20.3±0.1 at.% Al as shown in Figure 6.21(III). Three phases, ($Mg_{17}Sr_2$), (Al_4Sr), ($Mg_{38}Sr_9$), were positively identified in the XRD pattern. (Al_4Sr) was predicted from thermodynamic calculation for this alloy and confirmed by the XRD pattern as shown in Figure 6.21(II). Due to the small size of the precipitates it was difficult to detect this phase using EPMA. Good agreement between the SEM, XRD and thermodynamic modeling in terms of phase identification and phase transformation temperatures has been

achieved. It should be noted that the dark areas in most samples could be inclusion from casting or formed during annealing.

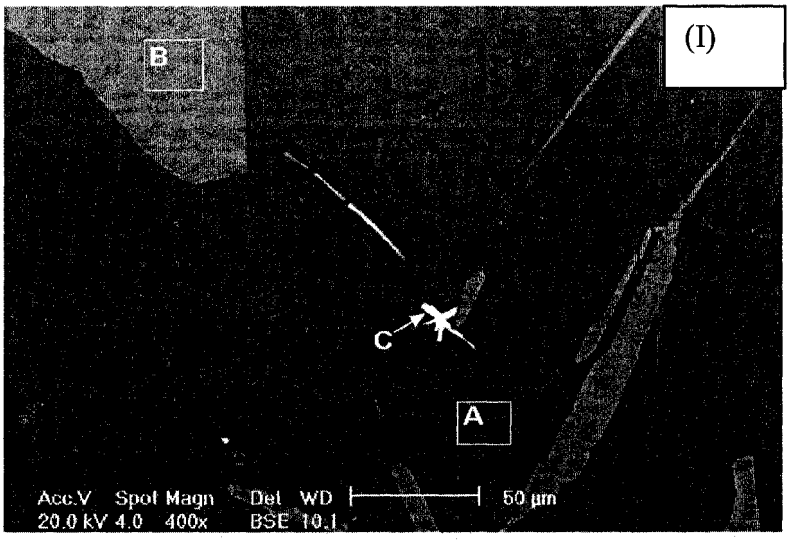

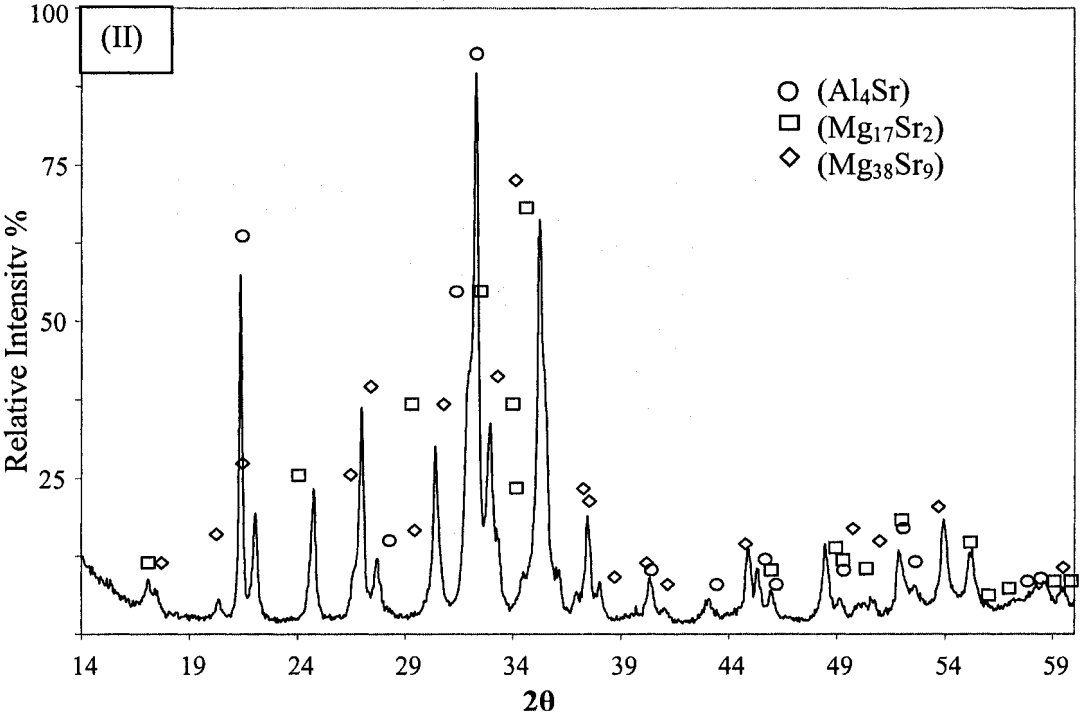

Location	at.% Mg	at.% Al	at.% Sr	Phases
A	64.1±0.1	20.0±0.2	15.9±0.1	$(Mg_{17}Sr_2)$
B	59.3±0.1	20.3±0.1	20.4±0.1	$(Mg_{38}Sr_9)$

(III)

Figure 6.21: *(I) SEM image; (II) XRD pattern and (III) EPMA analysis of composition 15.*

Sample 17 is located in the $Mg_{17}Sr_2$+$Mg_{38}Sr_9$+Al_4Sr phase field as shown in Figure 6.18. The DSC spectra of this sample exhibited three phase transformations during heating and cooling as can be seen in Figure 6.22. Three endothermic peaks appear in the heating curve at 627, 600 and 584°C that reoccurred during the cooling at 615, 601 and 581°C, respectively. The liquidus temperature was registered at 648°C.

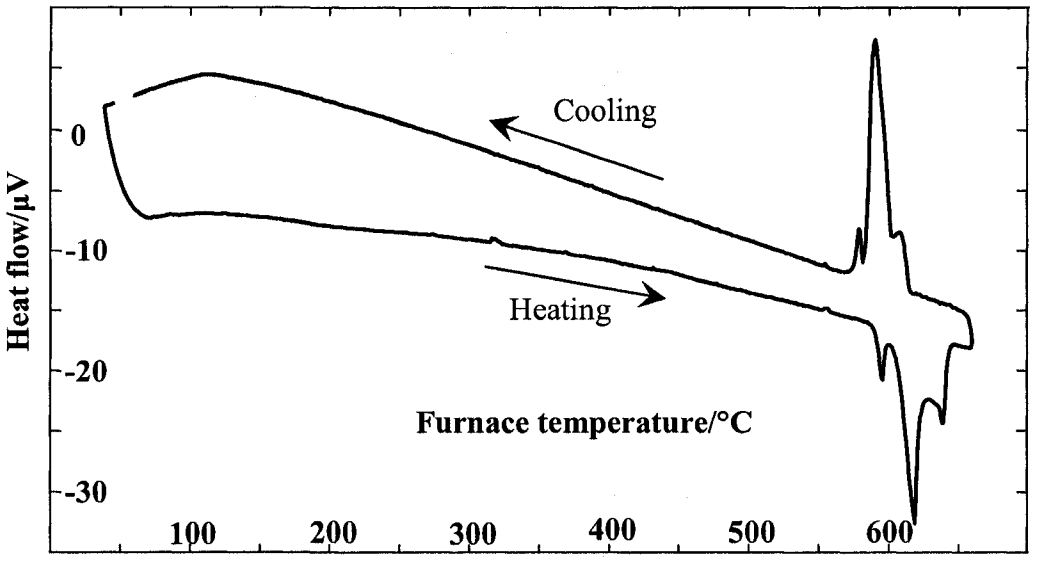

Figure 6.22: *DSC spectra of sample 17 (40.7/14.5/44.8, Mg/Al/Sr, wt.%) during heating and cooling.*

The calculated vertical section along with DSC signals of sample 17 is plotted in Figure 6.23. The solidification curve deduced from the DSC measurements in Figure 6.24 shows that (Al_4Sr) start to precipitate at 620°C down to 600°C consuming around 20 wt.% of the liquid, ($Mg_{17}Sr_2$) and (Al_4Sr) precipitate at 600°C consuming more than 65 wt.% of the liquid, then ($Mg_{38}Sr_9$), ($Mg_{17}Sr_2$) and (Al_4Sr) precipitate at 585°C consuming the remaining liquid. (Al_4Sr), ($Mg_{17}Sr_2$) and ($Mg_{38}Sr_9$) have been positively identified in the microstructure by EPMA and XRD analyses as can shown in Figure 6.25. According

to the EPMA analysis, $Mg_{38}Sr_9$ and $Mg_{17}Sr_2$ dissolve 15.6 and 7.7 at.% Al, respectively. In addition, Al_4Sr dissolves 16.2±0.1 at.% Mg.

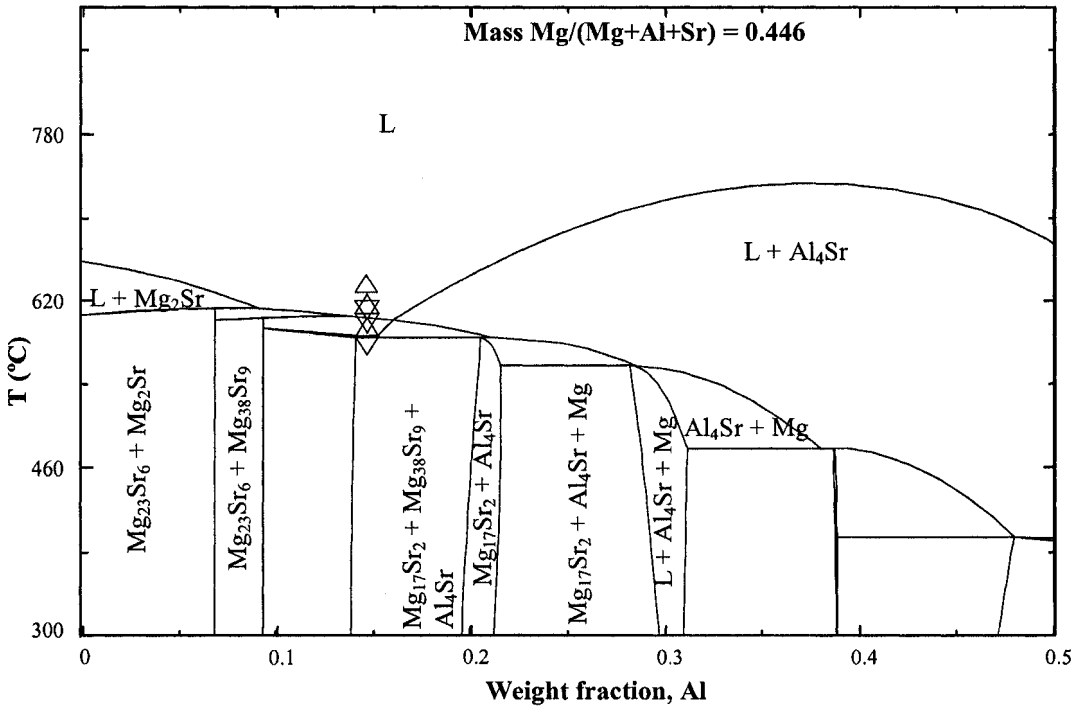

Figure 6.23: *Calculated vertical section at 44.6 wt.% Mg with DSC signals from heating and cooling curves of sample 17.*

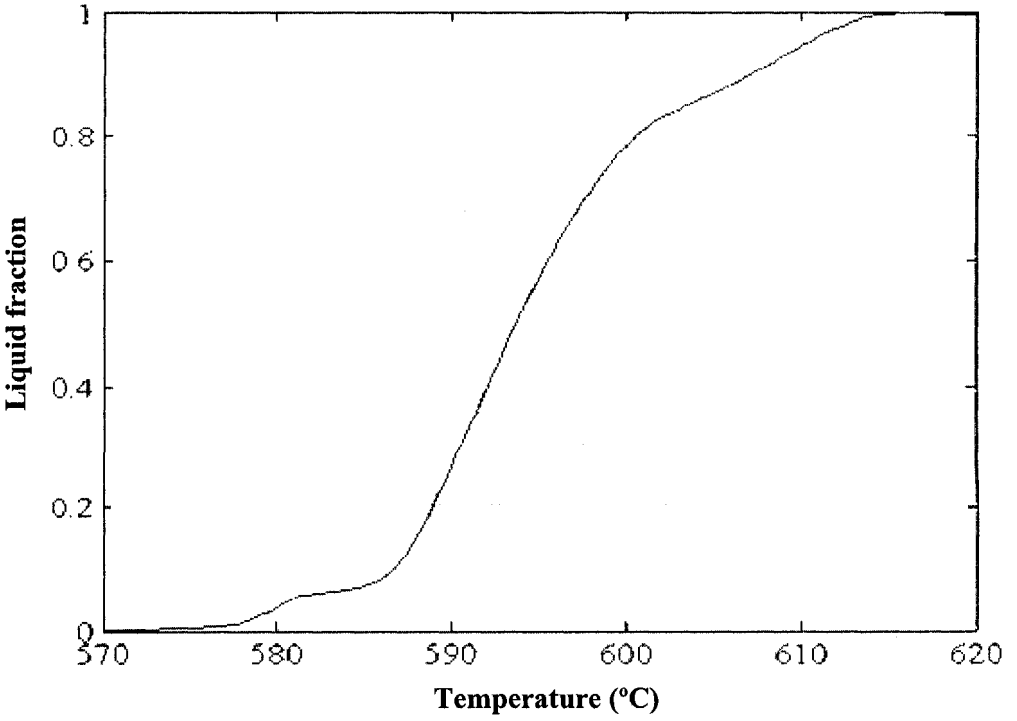

Figure 6.24: *Solidification curve of sample 17.*

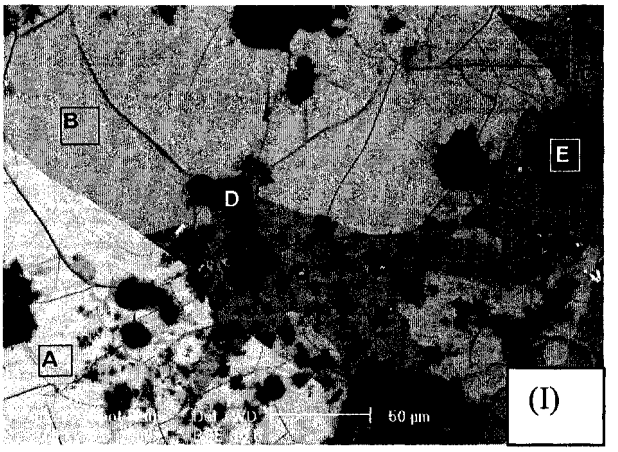

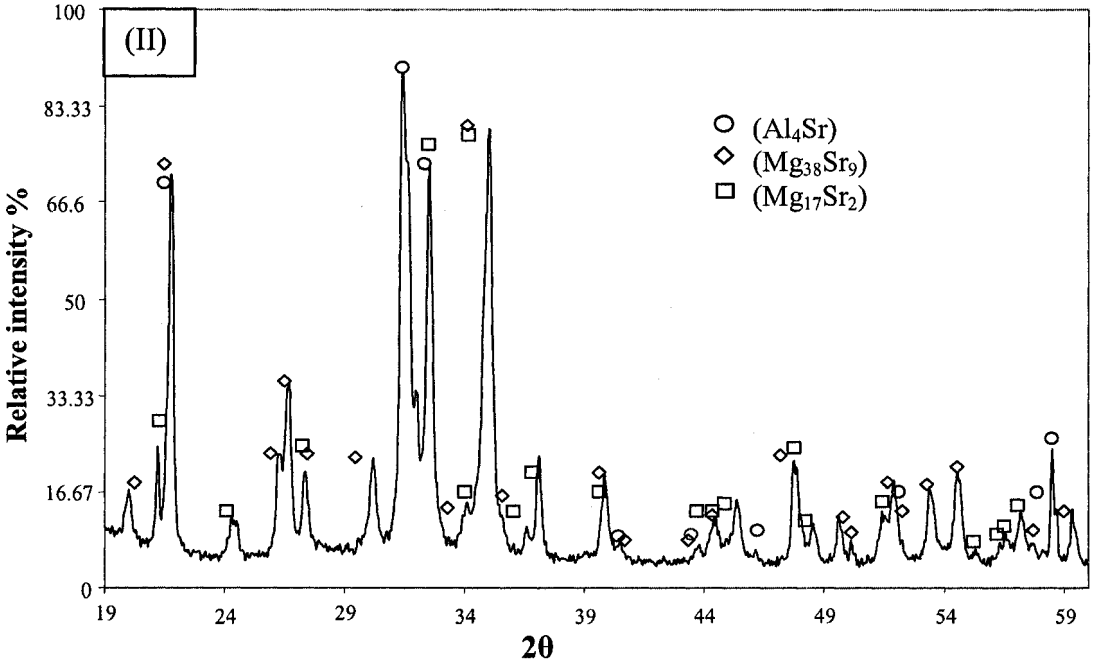

Location	at.% Mg	at.% Al	at.% Sr	Phases
A	16.2±0.1	63.0±0.1	20.8±0.1	(Al_4Sr)
B	68.2±0.4	15.6±0.4	16.2±0.1	$(Mg_{38}Sr_9)$
C	82.1±0.3	7.7±0.3	10.2±0.1	$(Mg_{17}Sr_2)$

(III)

Figure 6.25: *(I) SEM image; (II) XRD pattern and (III) EPMA analysis of composition 17.*

Sample 18 (29/23.3/47.7, Mg/Al/Sr) is located in the $Mg_{38}Sr_9$+Al_2Sr phase field. This sample has been chosen in order to measure the solubility of the $Mg_{38}Sr_9$ and Al_2Sr in the ternary system and to verify the phase triangulation in this region. The DSC spectra of sample 18 registered two peaks during heating that reoccurred in the cooling curve as

can be seen in Figure 6.26; the first peak occurs at 609 and 615°C in the cooling and heating sessions which corresponds to the thermodynamic calculations represented by the vertical section shown in Figure 6.27. The other peak occurs at 664 and 669°C in the cooling and heating curves, respectively. This represents a univariant reaction and its onset point corresponds to the liquidus as can be seen in Figure 6.27.

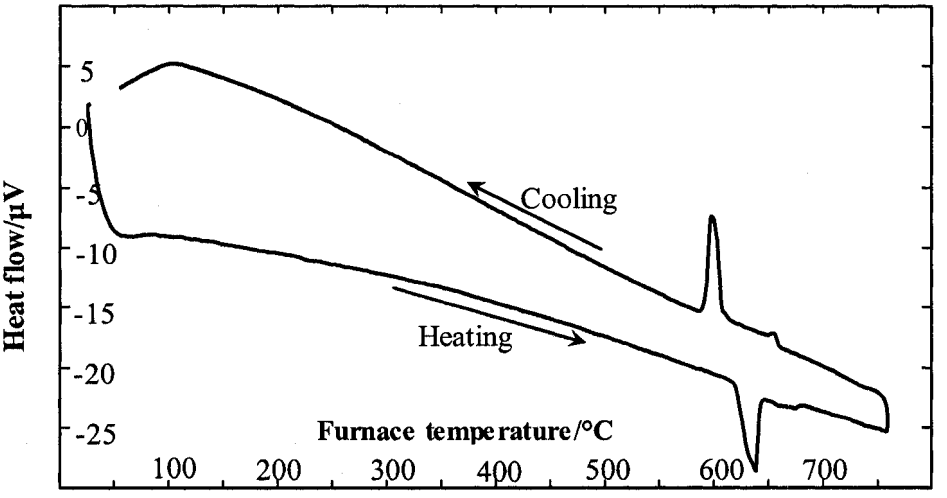

Figure 6.26: *DSC spectra of sample 18 (29/23.3/47.7, Mg/Al/Sr) during heating and cooling.*

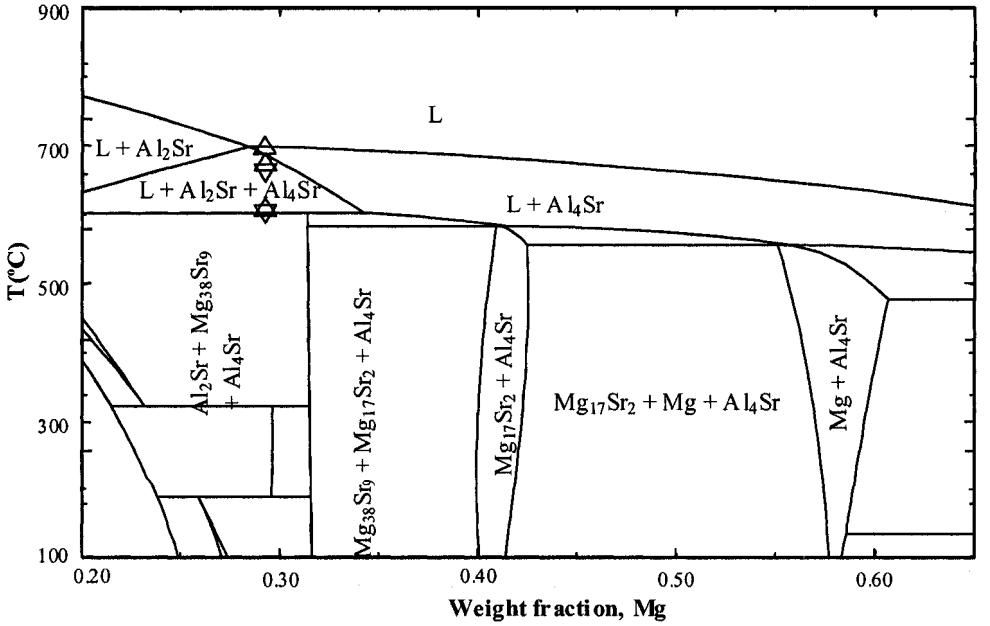

Figure 6.27: *Calculated vertical section at 23.3 wt.% Al with DSC signals from heating and cooling curves of sample 18.*

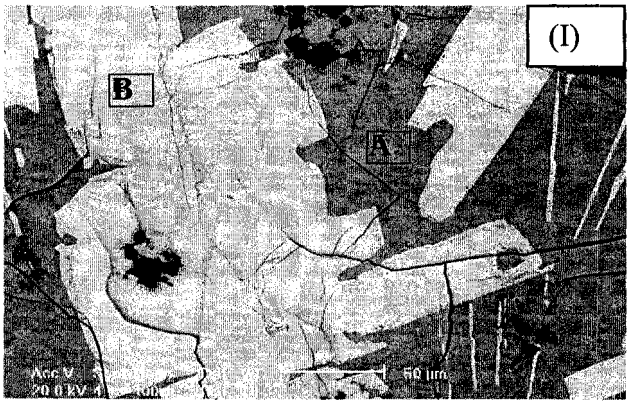

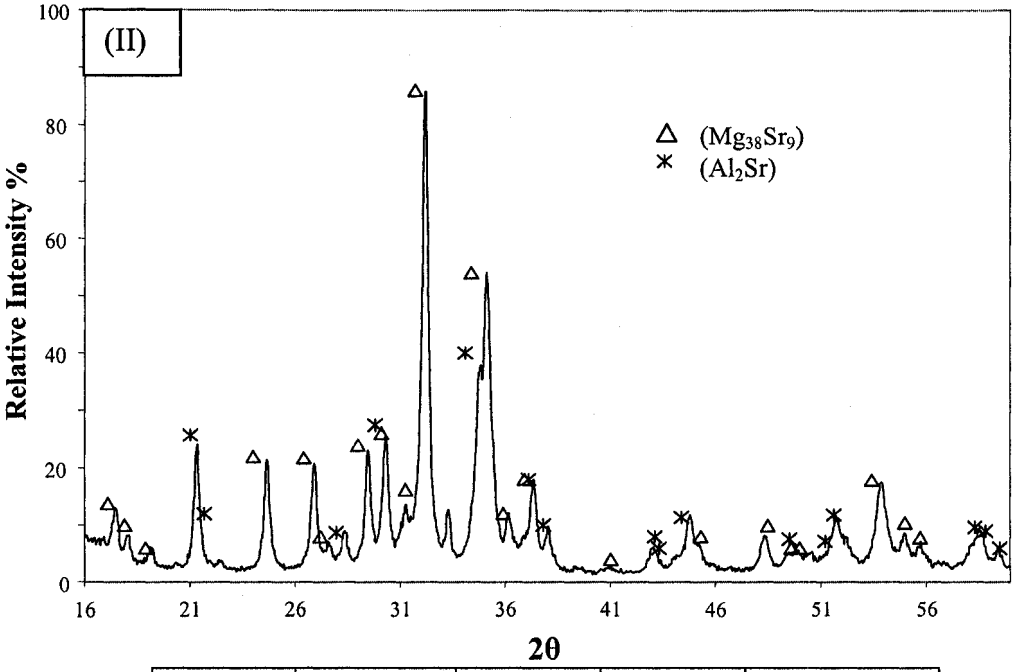

Location	at.% Mg	at.% Al	at.% Sr	Phases
A	58.7±0.1	20.4±0.2	20.9±0.1	$(Mg_{38}Sr_9)$
B	25.6±4.0	42.1±4.1	32.3±1.3	(Al_2Sr)

(III)

Figure 6.28: *(I) SEM image; (II) XRD pattern and (III) EPMA analysis of composition 18.*

SEM image identified two phases; plate-like phase and gray phase designated as (Al_2Sr) and $(Mg_{38}Sr_9)$, respectively. This is in close agreement with the XRD and EMPA results as can be seen in Figure 6.28(II) and (III). Figure 6.28(III) shows that $Mg_{38}Sr_9$ dissolves 20.4±0.2 at.% Al which is in agreement with samples 15 and 16. Whereas,

Al_2Sr dissolves 25.6 at.% Mg. The experimental results and thermodynamic calculations are consistent.

Sample 19 (34.2/13.6/54.3, Mg/Al/Sr wt.%) is located in $Mg_{23}Sr_6$+Mg_2Sr phase field and close to $Mg_{23}Sr_6$+Mg_2Sr+Al_2Sr phase field as shown in Figure 6.18. Referring to the DSC spectra of this sample shown in Figure 6.29, the cooling profile shows two thermal events at 639 and 608°C that reoccurred in the heating at 630 and 620°C, respectively. Note that the peak at 620°C overlaps with the peak at 630°C. These measured temperatures can be correlated to the calculated vertical section in Figure 6.30. The peak in the cooling curves occurs at 608°C tails back to the baseline that occurs due to the solidification of ($Mg_{23}Sr_6$) from the liquid which is in accordance with Figure 6.30.

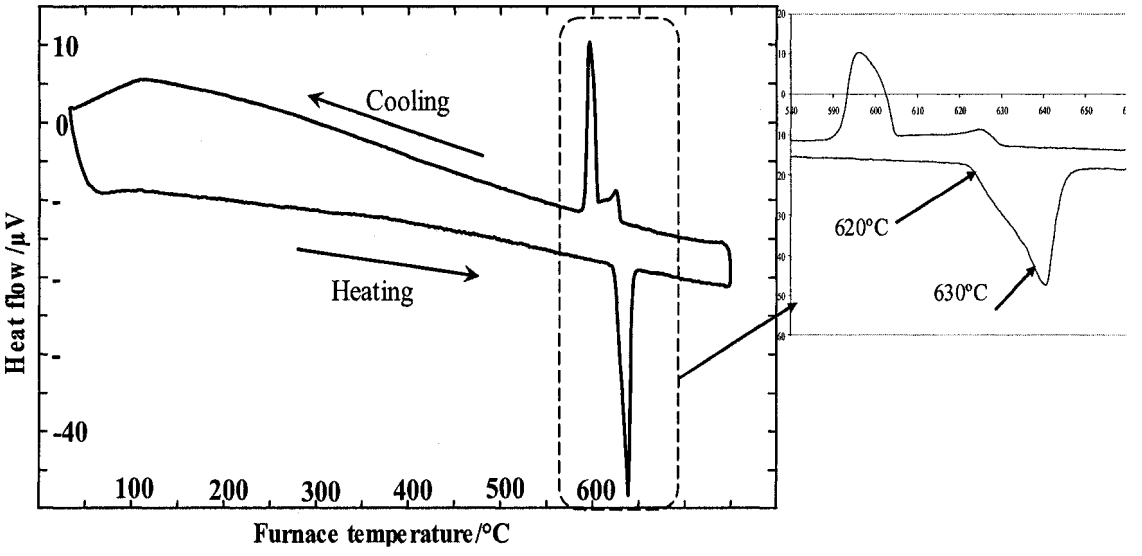

Figure 6.29: *DSC spectra of sample 19 (34.2/13.6/54.3, Mg/Al/Sr) during heating and cooling.*

It should be notedg that the solidification curve of sample 19 in Figure 6.31 shows that ($Mg_{23}Sr_6$) starts to precipitate at 650°C consuming around 20 wt.% of the liquid. ($Mg_{23}Sr_6$) and (Mg_2Sr) precipitate consuming the remaining liquid.

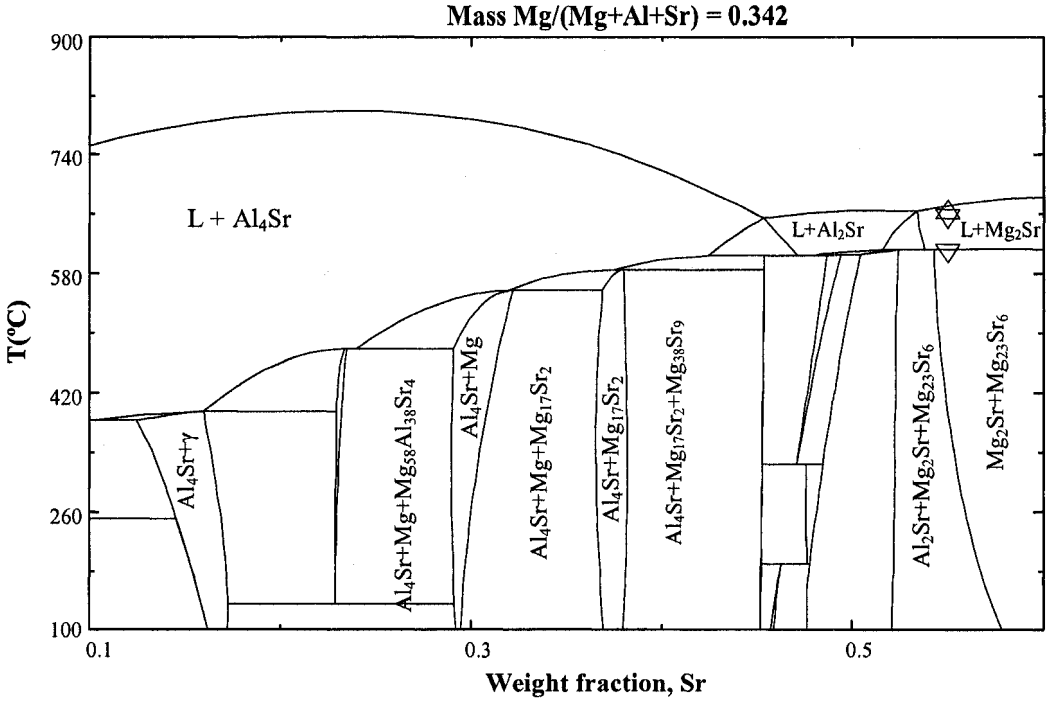

Figure 6.30: *Calculated vertical section at 34.2 wt.% Mg with DSC signals from heating and cooling curves of sample 19.*

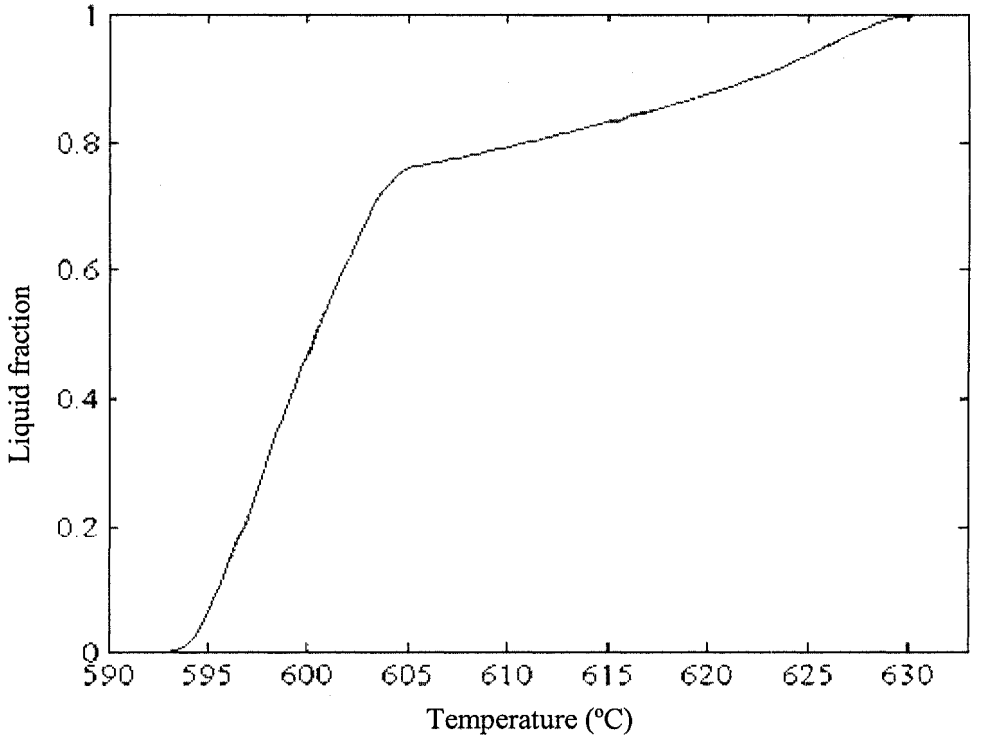

Figure 6.31: *Solidification curve of sample 19.*

($Mg_{23}Sr_6$) and (Mg_2Sr) have been positively identified in XRD and EPMA analysis as shown in Figure 6.32, whereas (Al_2Sr) could not be identified. This may be because this sample is away from (Al_2Sr) and close to phase boundary of the ($Mg_{23}Sr_6$)+ (Mg_2Sr) phase field. According to the EPMA analysis, $Mg_{23}Sr_6$ and Mg_2Sr dissolve 15.2±0.1 and 26.1±0.6 at.% Al, respectively.

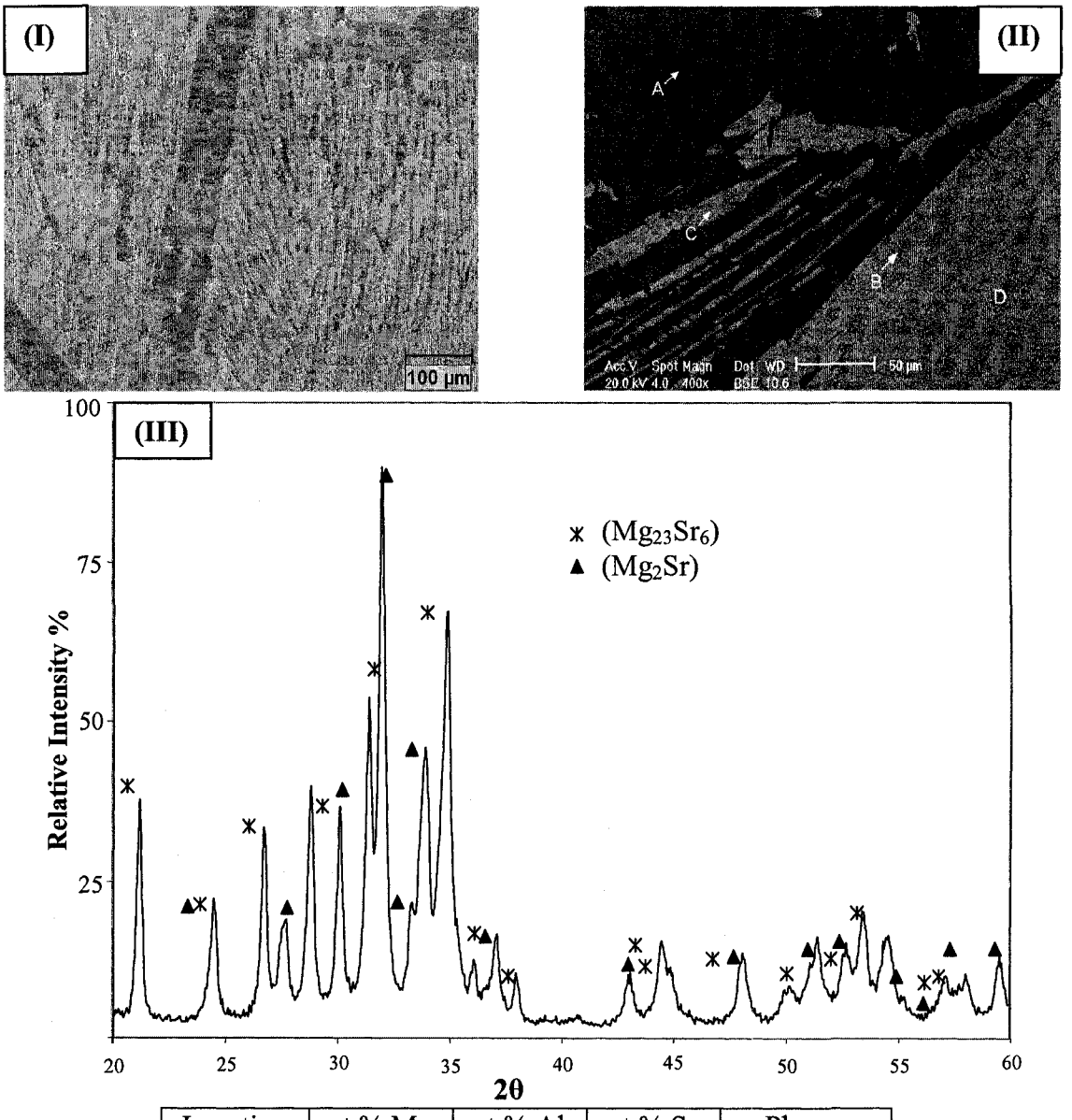

Location	at.% Mg	at.% Al	at.% Sr	Phases
A	63.5±0.1	15.2±0.1	21.3±0.1	($Mg_{23}Sr_6$)
B	40.0±0.6	26.1±0.6	33.9±0.1	(Mg_2Sr)

(IV)

Figure 6.32: *(I) Optical micrograph; (II) SEM image; (III) XRD pattern and (IV) EPMA analysis of composition 19.*

Sample 20 (34.2/13.6/54.3, Mg/Al/Sr) is located in the $Mg_{17}Sr_2$+$Mg_{38}Sr_9$+Al_4Sr phase field and close to phase boundary of the $Mg_{17}Sr_2$+Al_4Sr phase field as can be seen in Figure 6.18. The DSC spectra of this alloy registered two signals in heating that reoccurred in the cooling curve as shown in Figure 6.33. Figure 6.34 shows good agreement between the measured phase transformation temperatures with the calculated vertical section. Three phases; ($Mg_{17}Sr_2$), ($Mg_{38}Sr_9$) and (Al_4Sr) are positively identified in the XRD and SEM using EMPA analysis as can be seen in Figure 6.35(I) and (II). In this sample, $Mg_{17}Sr_2$ and $Mg_{38}Sr_9$ dissolve 12.6±0.2 and 20.0±0.1 at.% Al, respectively. Al_4Sr dissolves 19.9±0.9 at.% Mg as shown in Figure 6.35(III).

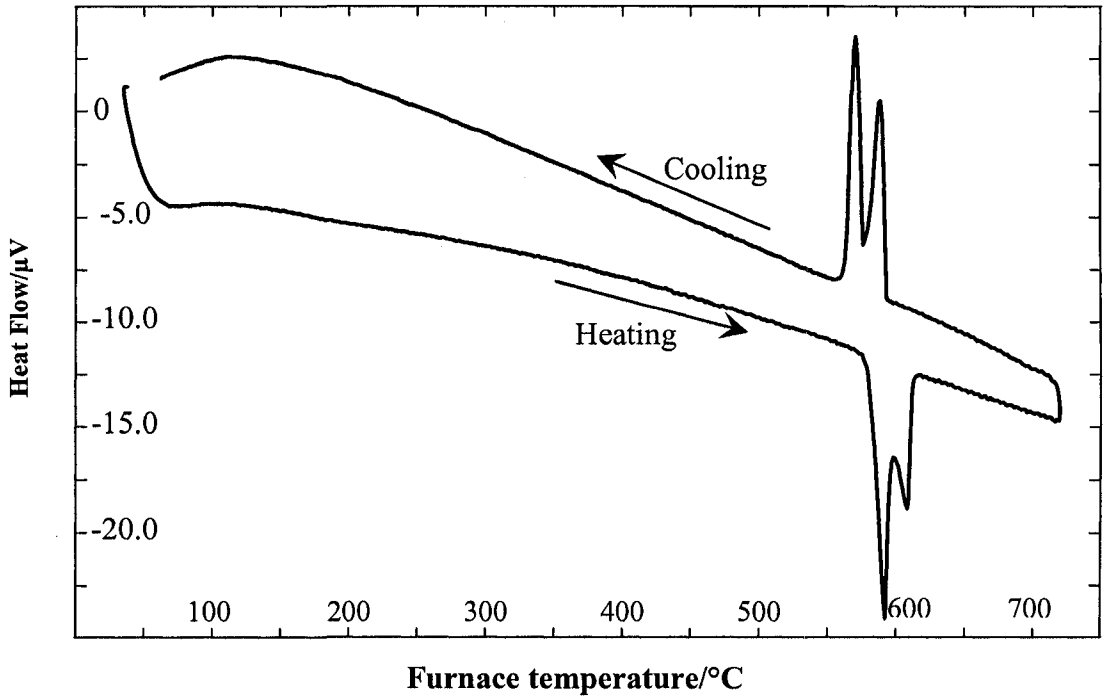

Figure 6.33: *DSC spectra of sample 20 (34.2/13.6/54.3, Mg/Al/Sr) during heating and cooling.*

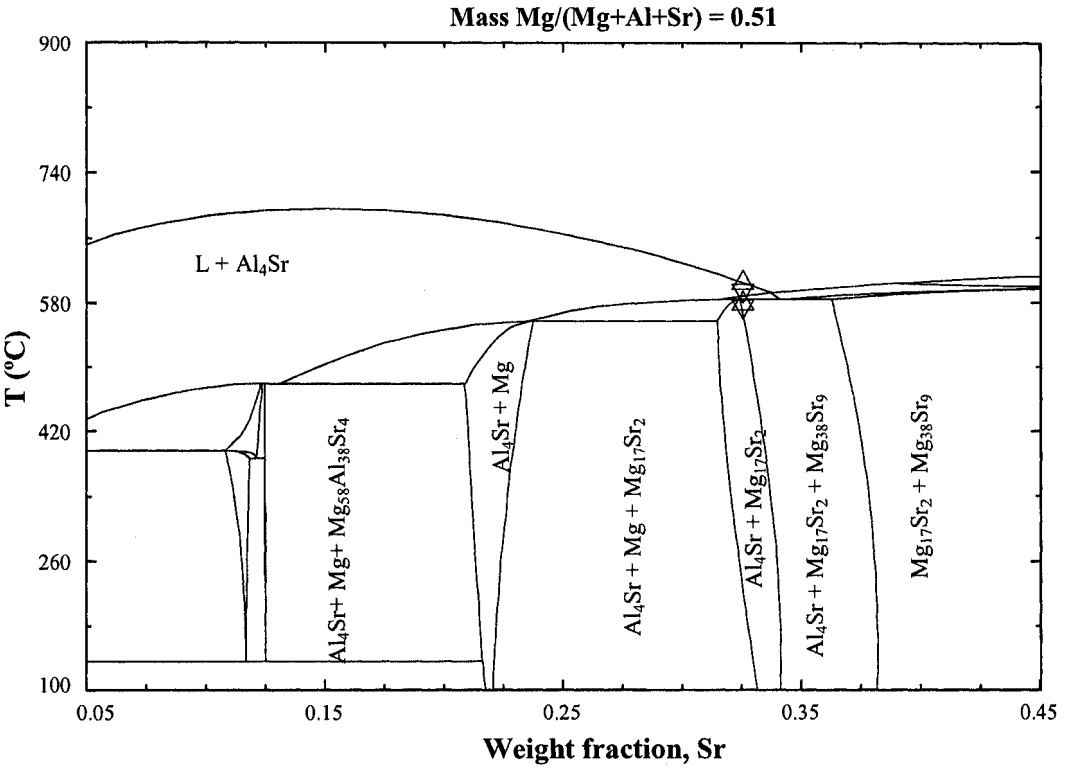

Figure 6.34: *Calculated vertical section at 51 wt.% Mg with DSC signals from heating and cooling curves of sample 20.*

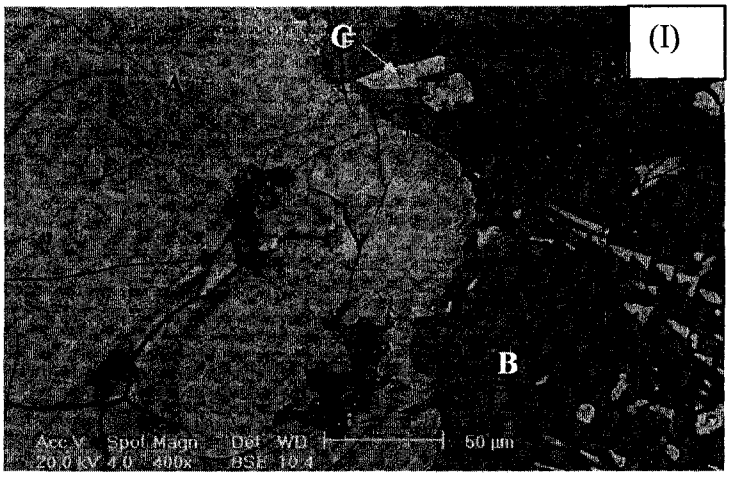

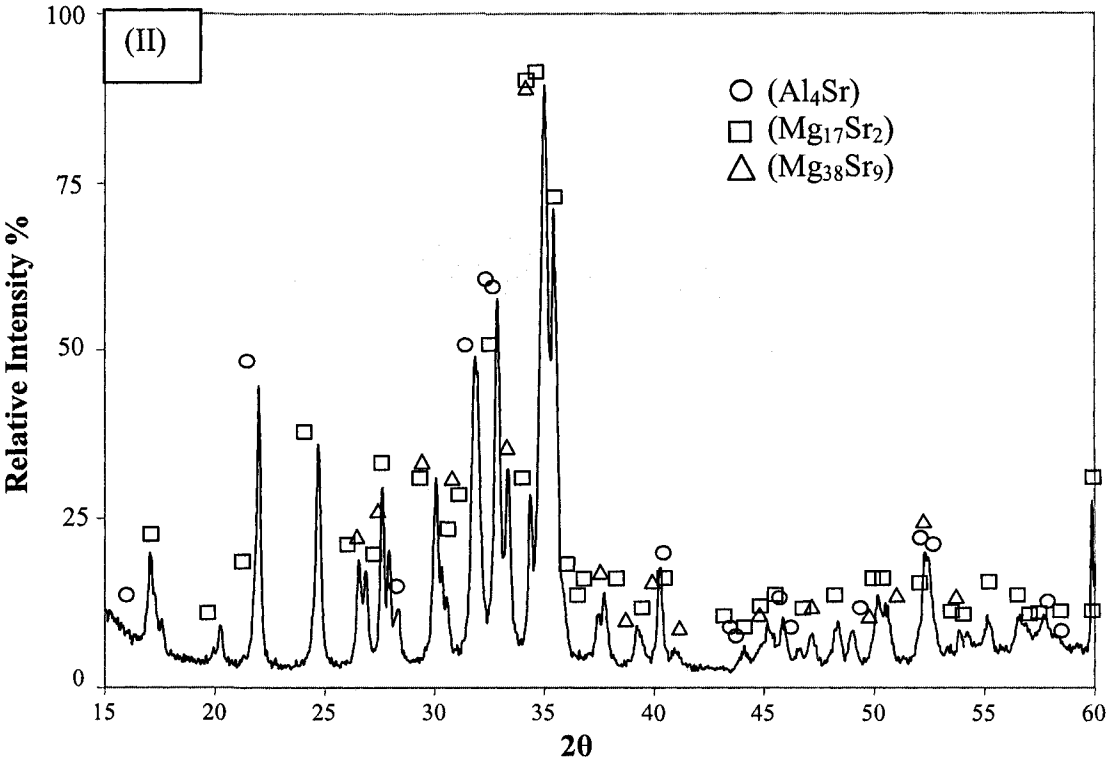

Location	at.% Mg	at.% Al	at.% Sr	Phases
A	64.3±0.2	20.0±0.1	15.7±0.1	$(Mg_{38}Sr_9)$
B	77.6±0.2	12.6±0.2	9.8±0.1	$(Mg_{17}Sr_2)$
C	19.9±0.9	58.2±1.1	21.9±0.3	(Al_4Sr)

(III)

Figure 6.35: *(I) SEM image; (II) XRD pattern and (III) EPMA analysis of composition 20.*

Sample 21 (43.3/9.5/47.2, Mg/Al/Sr wt.%) is located in two phase regions

$Mg_{23}Sr_6$+Mg_2Sr as can be seen in Figure 6.18. The DSC spectra shown in Figure 6.36 show a sharp and narrow peak suggesting the likelihood of an invariant transformation. This is consistent with the phase assemblage diagram in Figure 6.37 which shows that a liquid is transforming into two solids at around 600°C.

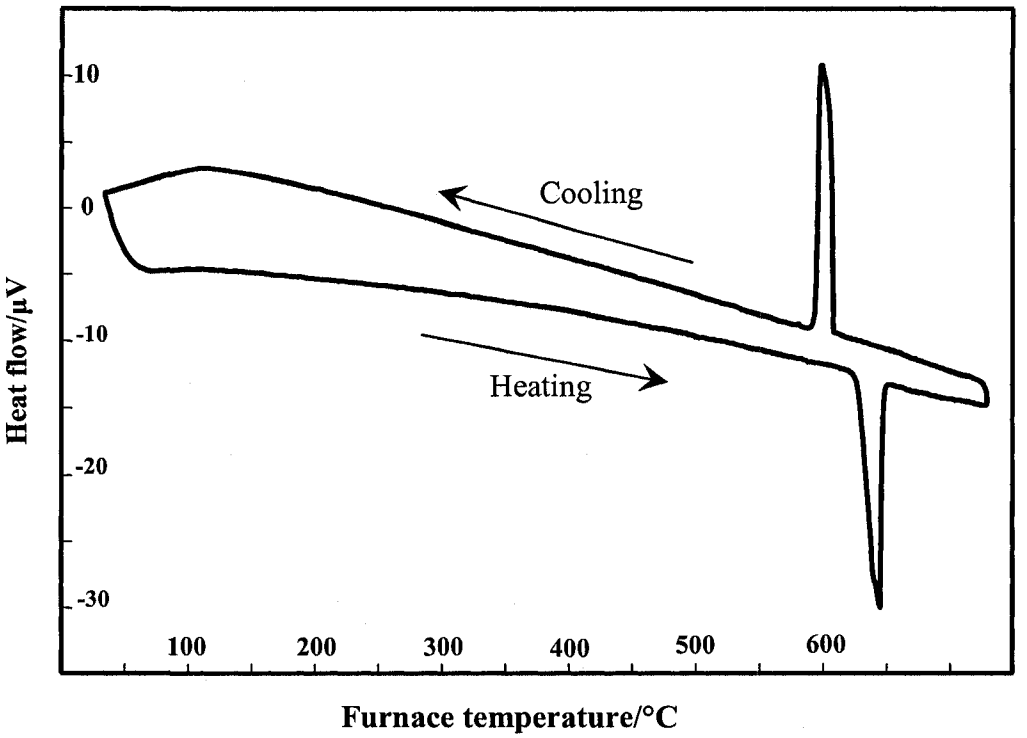

Figure 6.36: *DSC spectra of sample 21 (43.3/9.5/47.2, Mg/Al/Sr) during heating and cooling.*

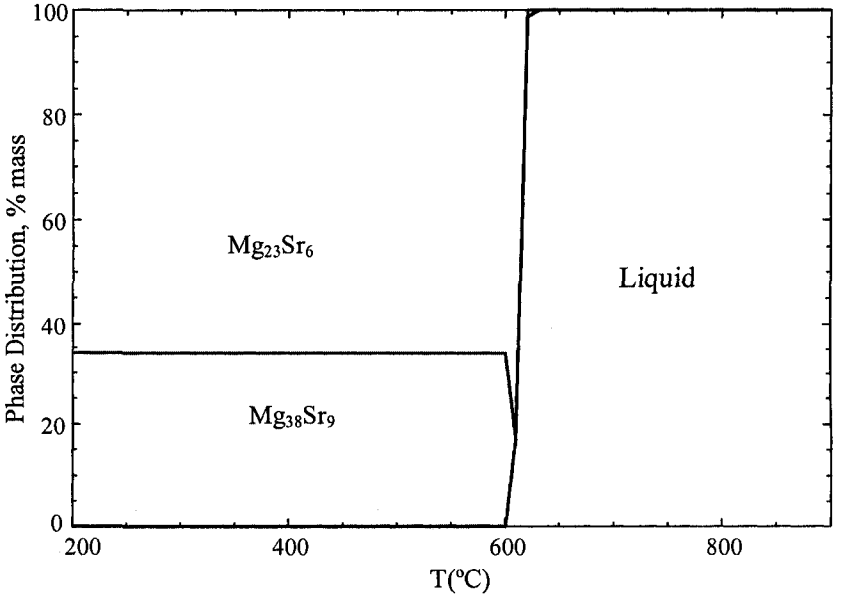

Figure 6.37: *Phase assemblage diagram of sample 21.*

SEM image of sample 21 in Figure 6.38(I) shows a fine eutectic morphology. ($Mg_{23}Sr_6$) and (Mg_2Sr) are identified by XRD and EPMA as shown in Figure 6.38(II) and (III), respectively. $Mg_{23}Sr_6$ and Mg_2Sr dissolve 9.8±0.2 and 6.0±0.1 at.% Al, respectively. These results agree very well with the thermodynamic calculations.

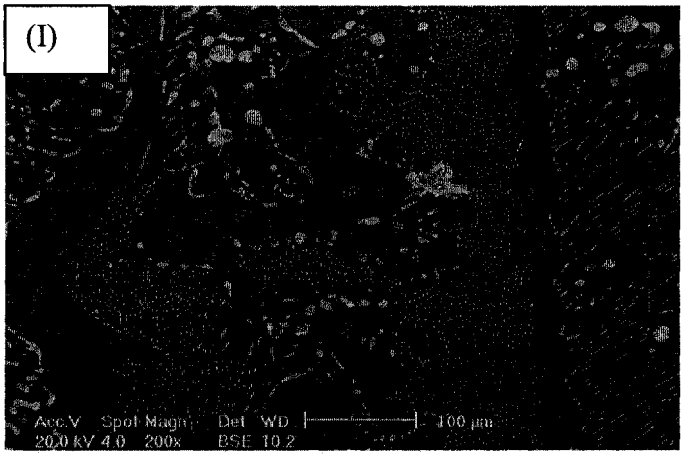

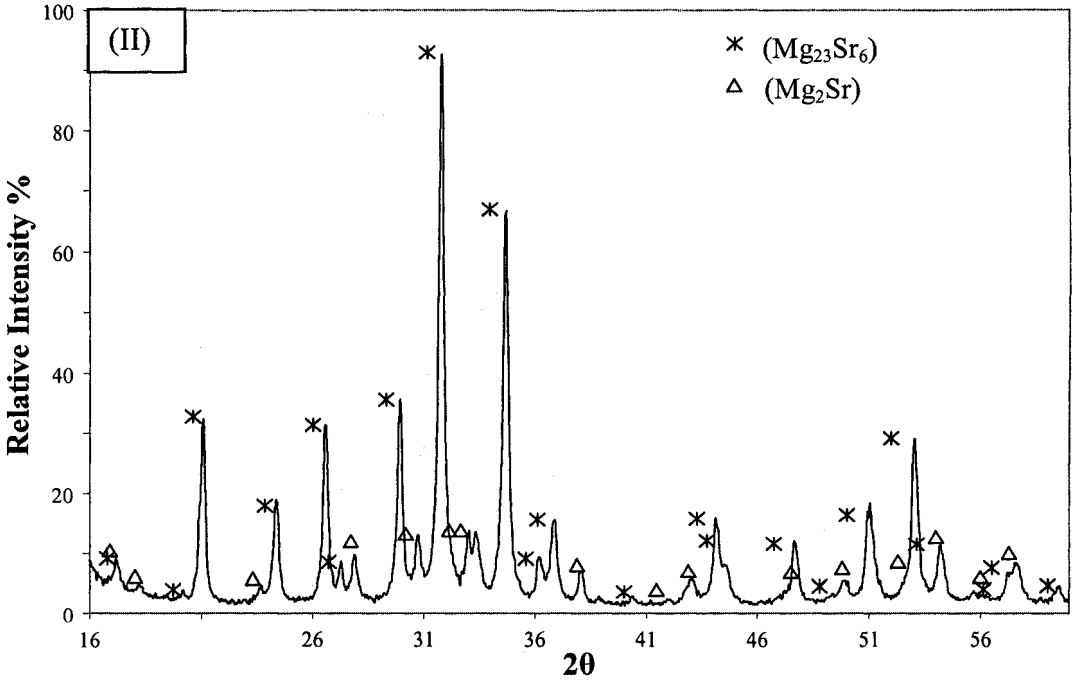

Location	at.% Mg	at.% Al	at.% Sr	Phases
A	58.7±2.1	6.0±0.1	35.3±2.4	(Mg_2Sr)
B	66.2±0.2	9.8±0.2	24.0±0.4	($Mg_{23}Sr_6$)

(III)

Figure 6.38: *(I) SEM image; (II) XRD pattern and (III) EPMA analysis of composition 21.*

Figure 6.39 shows the DSC spectra of sample 22 (50.4/37/12.6, Mg/Al/Sr). The calculated vertical section at 43.3 wt.% Mg along with the DSC signals is drawn in Figure 6.40. The predicted phase transformation temperatures are in accord with the DSC measurements.

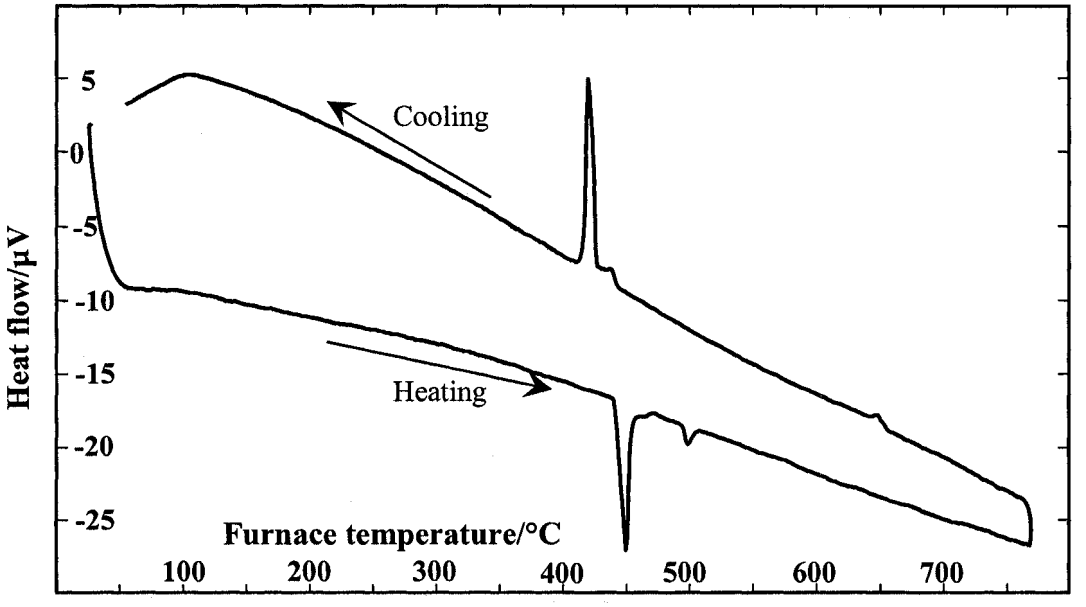

Figure 6.39: *DSC spectra of sample 22 (50.4/37/12.6, Mg/Al/Sr) during heating and cooling.*

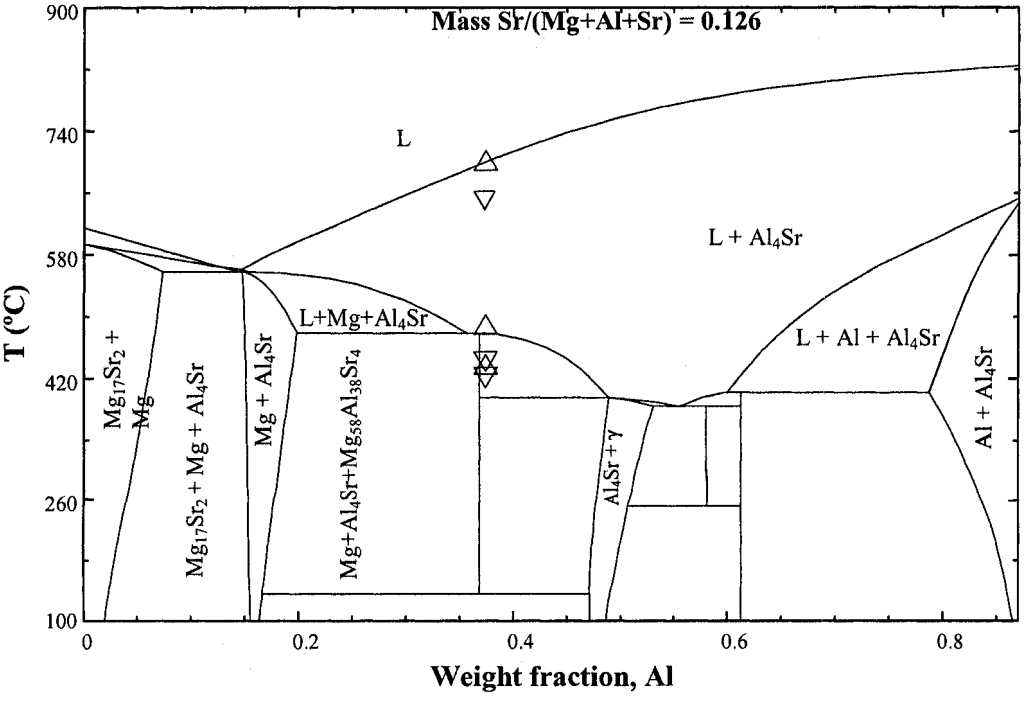

Figure 6.40: *Calculated vertical section at 12.6 wt.% Sr with DSC signals from heating and cooling curves of sample 22.*

Optical micrograph, SEM image, XRD and EMPA analyses of sample 22 are shown in Figure 6.41. SEM analysis indicates that both the plate-like phase, region (A), and the light gray phase in region (B) contained the three elements. According to the EPMA analysis, the plate-like phase is (Al_4Sr) dissolving 7.3±0.2 at.% Mg and the light gray phase is new ternary compound with the chemical composition of $Mg_{56}Al_{40}Sr_4$ as shown in Figure 6.41(III). Region (C) also is Mg dissolving 8.7 at.% Al. Furthermore, negligible amount of Sr was detected in γ-Phase in region (D). While analyzing the XRD, it was noticed that the lattice parameters of $Mg_{56}Al_{40}Sr_4$ are quite close to that of γ. Therefore, it was difficult to detect $Mg_{56}Al_{40}Sr_4$ by XRD. Besides, this ternary compound is a distinct phase and not a ternary solubility of γ-Phase. It is worth mentioning that the four phases were observed in the microstructure because of the slow kinetics of formation of $Mg_{56}Al_{40}Sr_4$.

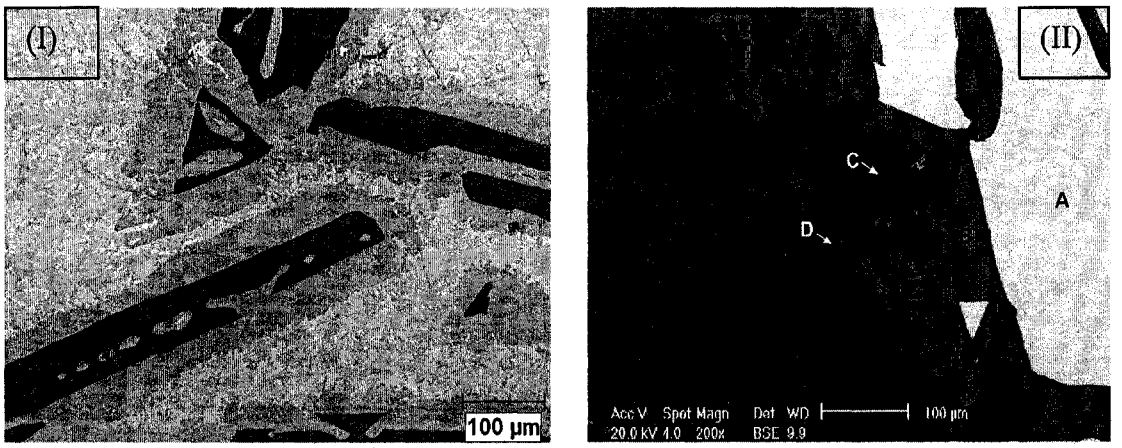

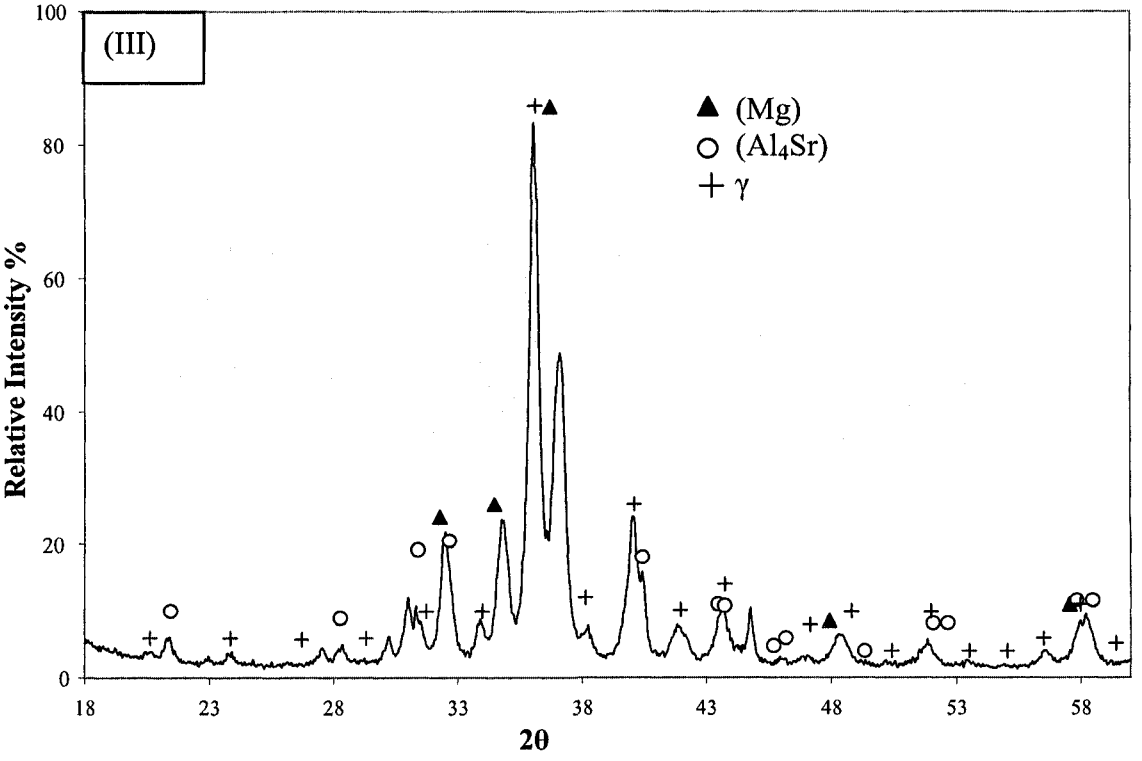

Location	at.% Mg	at.% Al	at.% Sr	Phases
A	7.3±0.2	72.2±0.1	20.5±0.1	(Al_4Sr)
B	39.6±0.2	56.2±0.2	4.2±0.1	$Mg_{58}Al_{38}Sr_4$
C	91.3±0.2	8.7±0.2	0.0	(Mg)
D	37.8±0.1	62.2±0.1	0.0	γ

(IV)

Figure 6.41: *(I) Optical micrograph; (II) SEM image; (III) XRD pattern and (IV) EPMA analysis of composition 22.*

Sample 23 is located in the $Mg+Al_4Sr+Mg_{17}Sr_2$ phase field, as shown in Figure 6.18. DSC spectra of this sample with heating and cooling runs are shown in Figure 6.42. There are three peaks during heating that were also encountered during cooling. During heating of this alloy, two thermal arrests, corresponding to the invariant reaction at 551°C and the univariant reaction at 534°C, were registered. The liquidus temperature also was observed during heating and cooling, and found to occur at 573 and 563°C, respectively.

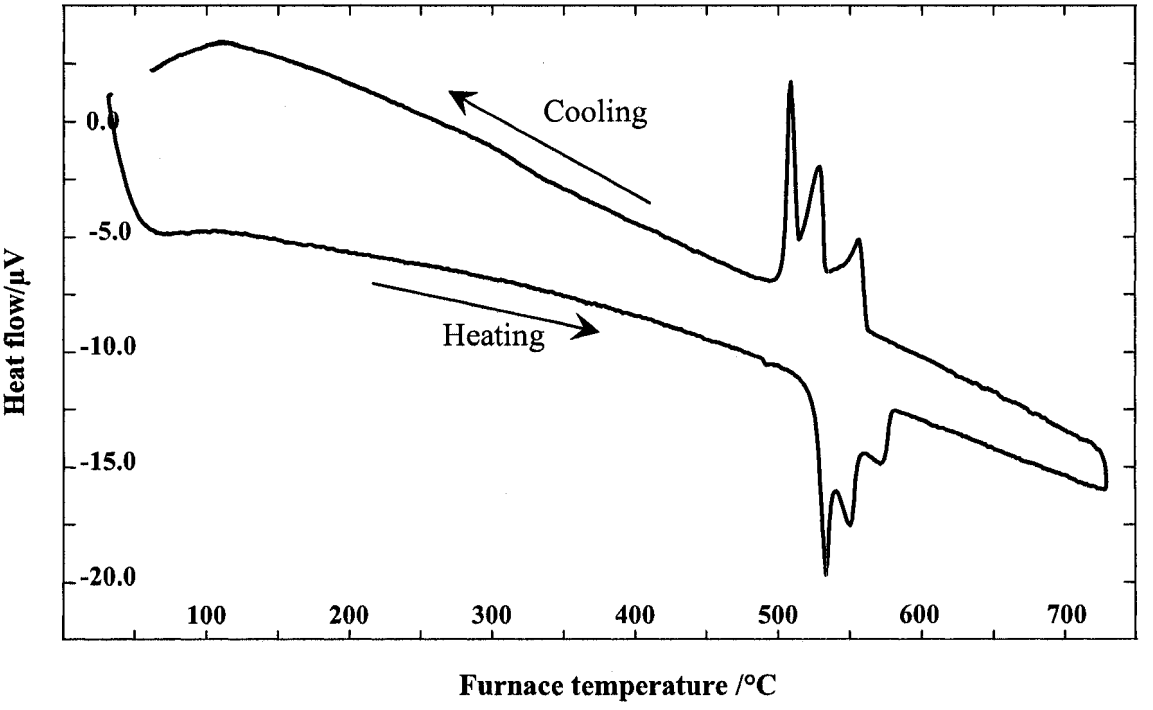

Figure 6.42: *DSC spectra of sample 23 (78/12.4/9.6, Mg/Al/Sr) during heating and cooling.*

Vertical section at 9.6 wt.% Sr with DSC signals from cooling and heating curves is drawn in Figure 6.43 to verify the calculated transformation temperatures along with the associated reactions. It can be observed that the liquidus and the subsolidus temperatures are consistent with the experimental values within the experimental uncertainty.

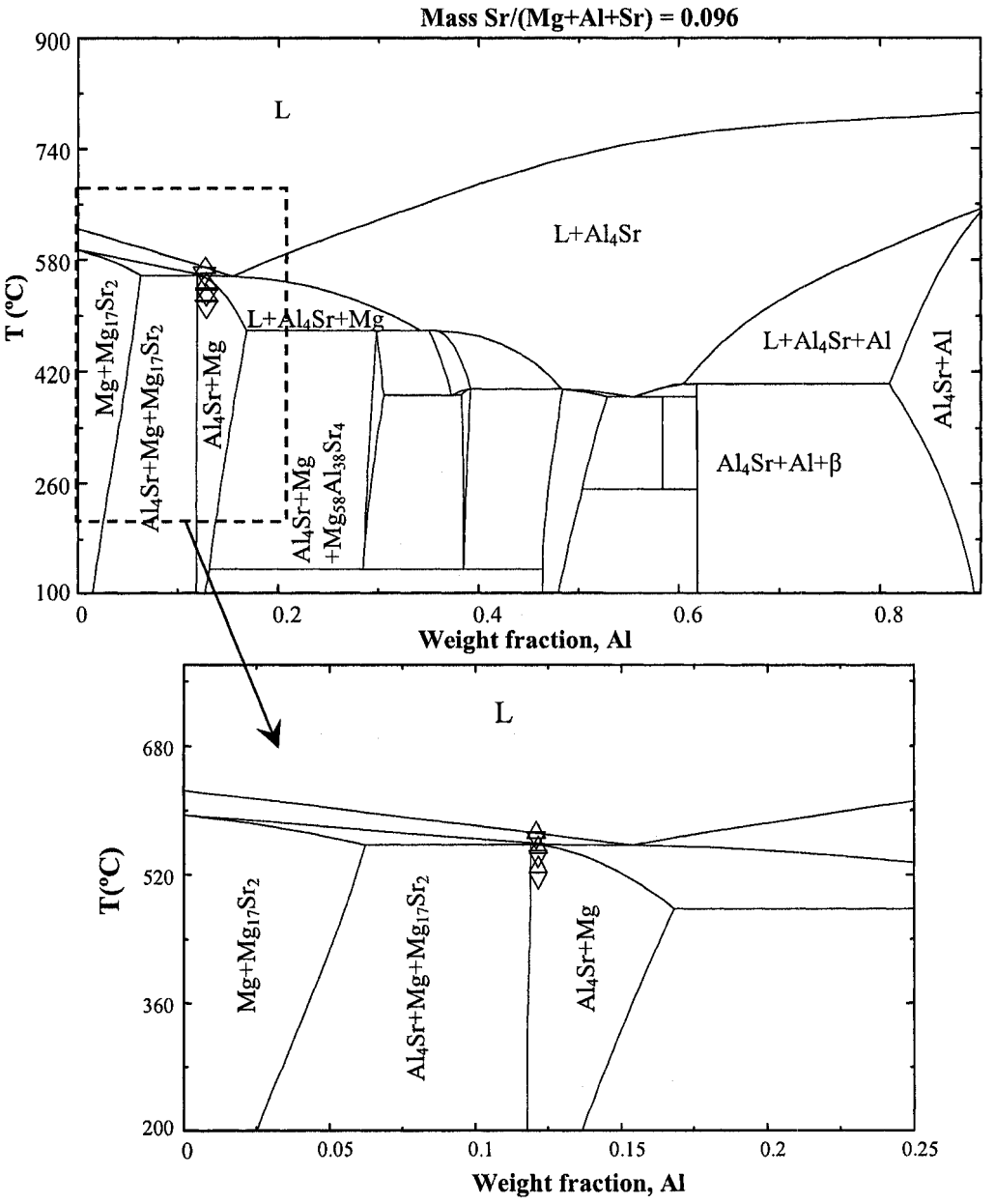

Figure 6.43: *Calculated vertical section at 9.6 wt.% Sr with DSC signals from heating and cooling curves of sample 23.*

Three phases; (Mg), (Al_4Sr) and ($Mg_{17}Sr_2$), were positively identified in the XRD and microstructure using EPMA as shown in Figure 6.44. SEM image shows that the dark Mg-matrix was separated by gray (region A) and bright precipitate (region C). (Al_4Sr) and ($Mg_{17}Sr_2$) are located at the grain boundaries region and appear to be lamellar. Quantitative EPMA analysis in Figure 6.44(IV) shows that Mg and $Mg_{17}Sr_2$

dissolve 2.0±0.3 and 14.2±0.1 at.% Al, while Al_4Sr dissolves 9.4±2.2 at.% Mg. These experimental results are consistent with the thermodynamic calculations.

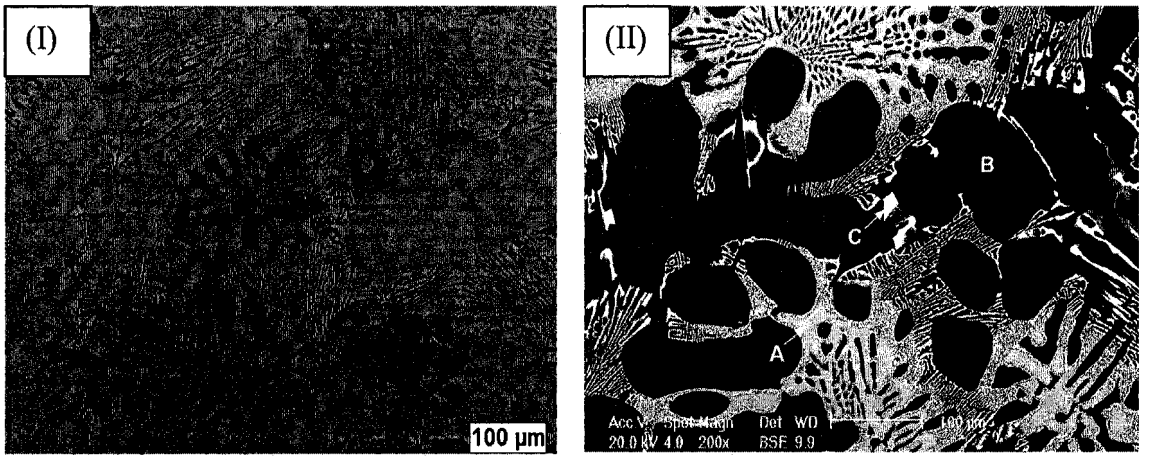

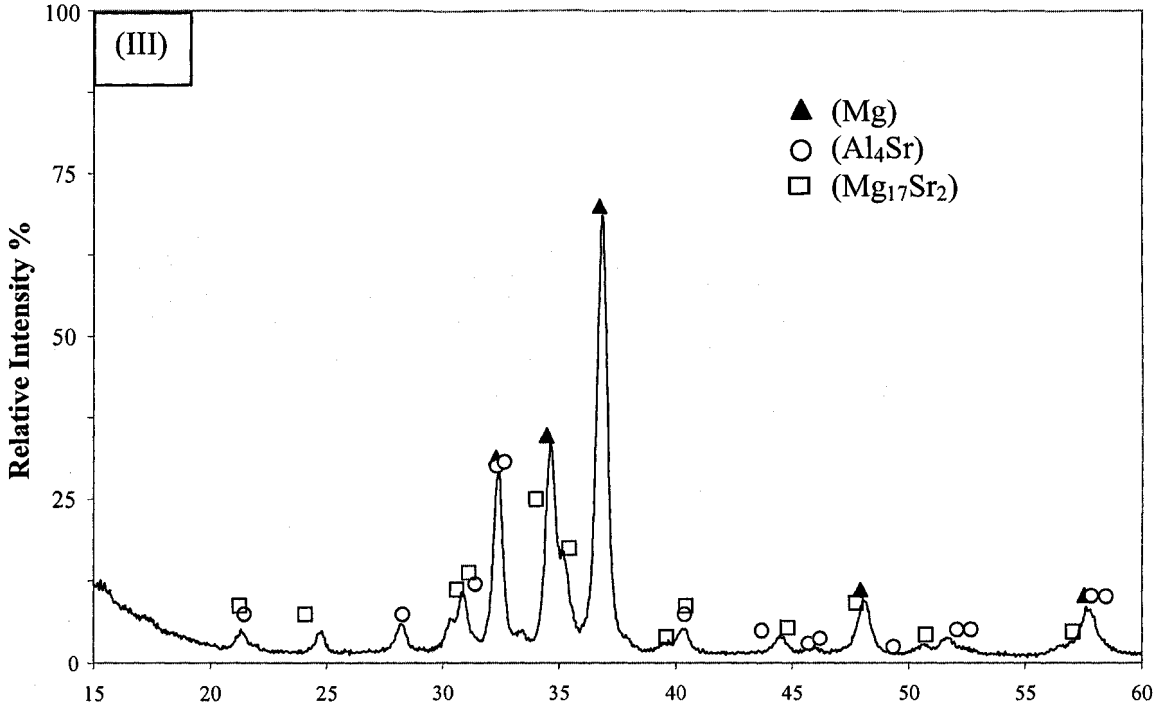

Location	at.% Mg	at.% Al	at.% Sr	Phases
A	76.2±0.2	14.2±0.1	9.6±0.1	$(Mg_{17}Sr_2)$
B	98.0±0.3	2.0±0.3	0.0	(Mg)
C	9.4±2.2	70.0±2.2	20.6±0.6	(Al_4Sr)

(IV)

Figure 6.44: *(I) Optical micrograph; (II) SEM image; (III) XRD pattern and (IV) EPMA analysis of composition 23.*

As can be seen in Figure 6.18, sample 24 (56/26/18, Mg/Al/Sr) is located in the Mg+Al_4Sr phase field and close to the borderline of the Mg+Al_4Sr+$Mg_{58}Al_{38}Sr_4$ phase field. The calculated vertical section at 18 wt.% Sr along with the thermal arrests during heating and cooling is plotted in Figure 6.46. The predicted phase transformation temperatures are in accord with the DSC measurements. The liquidus temperature is clearly observed during cooling and heating at 607°C and 634°C, respectively compared to the prediction from thermodynamic calculations as 650°C.

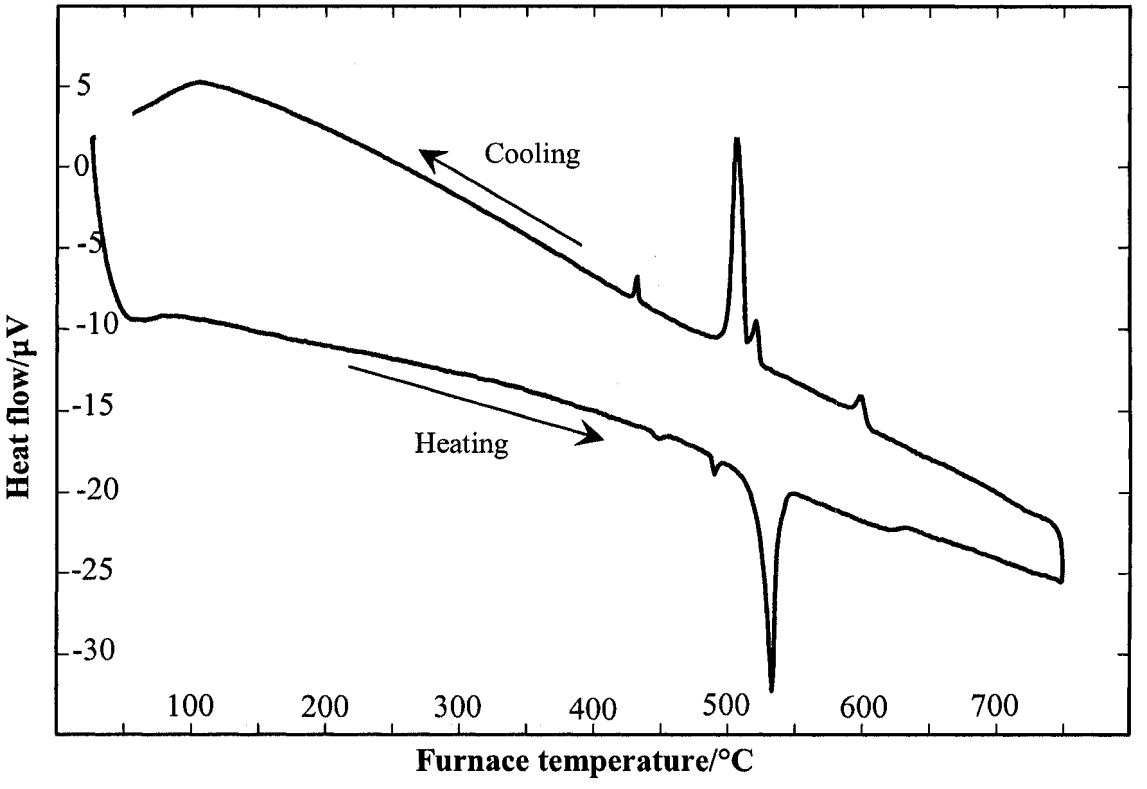

Figure 6.45: *DSC spectra of sample 24 (56/26/18, Mg/Al/Sr) during heating and cooling.*

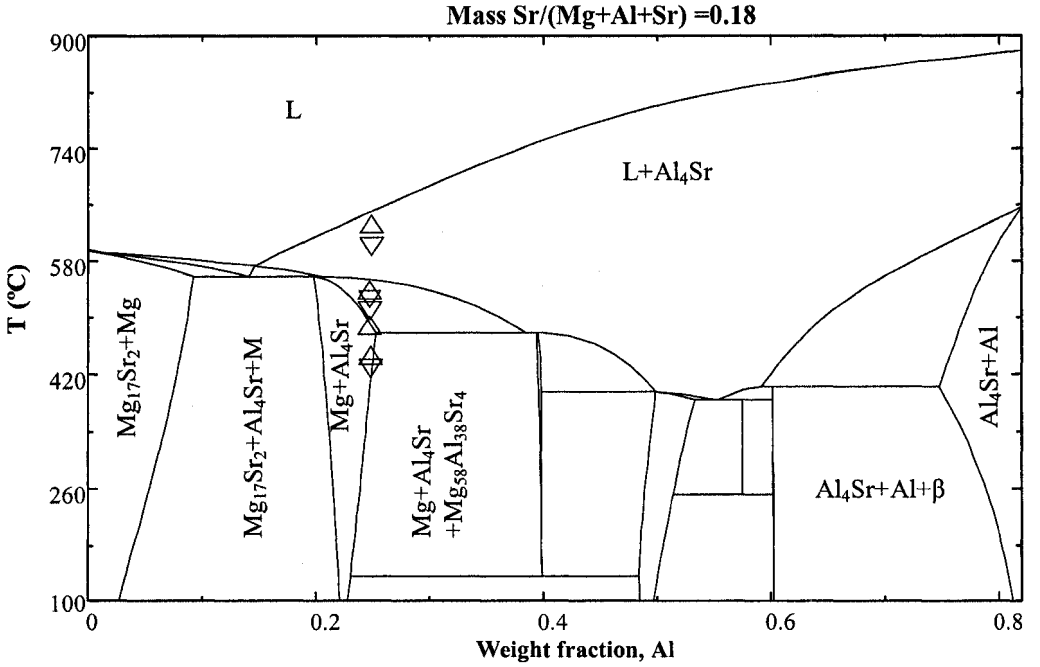

Figure 6.46: *Calculated vertical section at 18 wt.% Sr with DSC signals from heating and cooling curves of sample 24.*

Moreover, the solidification curve, as can be seen in Figure 6.47, shows that (Al_4Sr) starts to solidify at 620°C, (Mg) and (Al_4Sr) precipitate at 520°C, then a ternary invariant reaction occurs at 515°C down to 420°C consuming more than 60 wt.% of the liquid forming coarse and fine lamellae structures in Figures 6.50(I) and (II), and supported by the phase assemblage diagram in Figure 6.48.

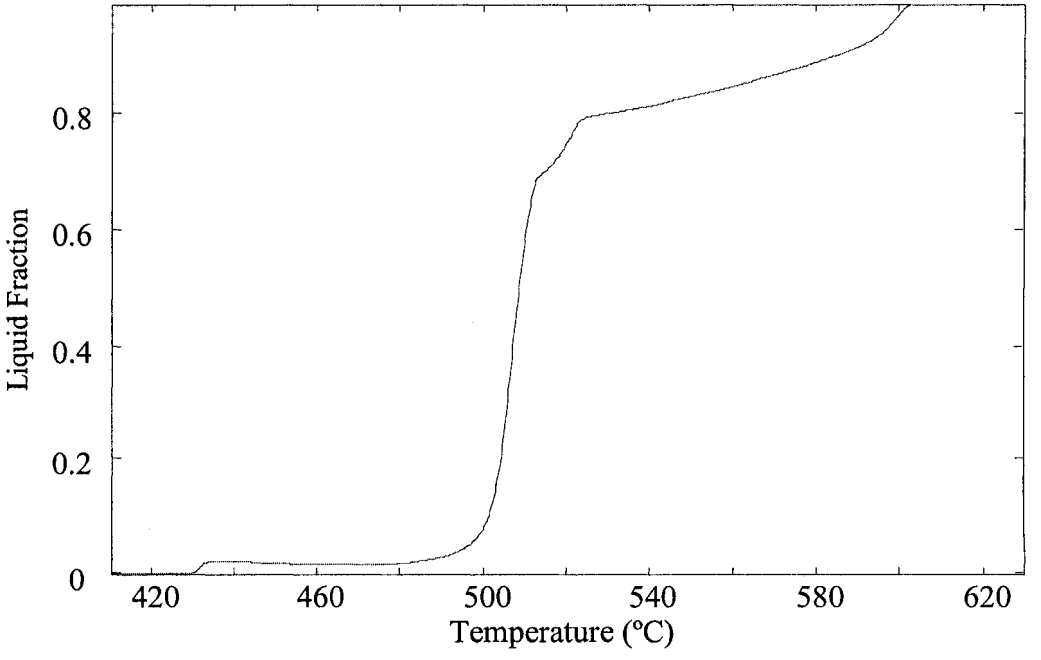

Figure 6.47: *Solidification curve of sample 24.*

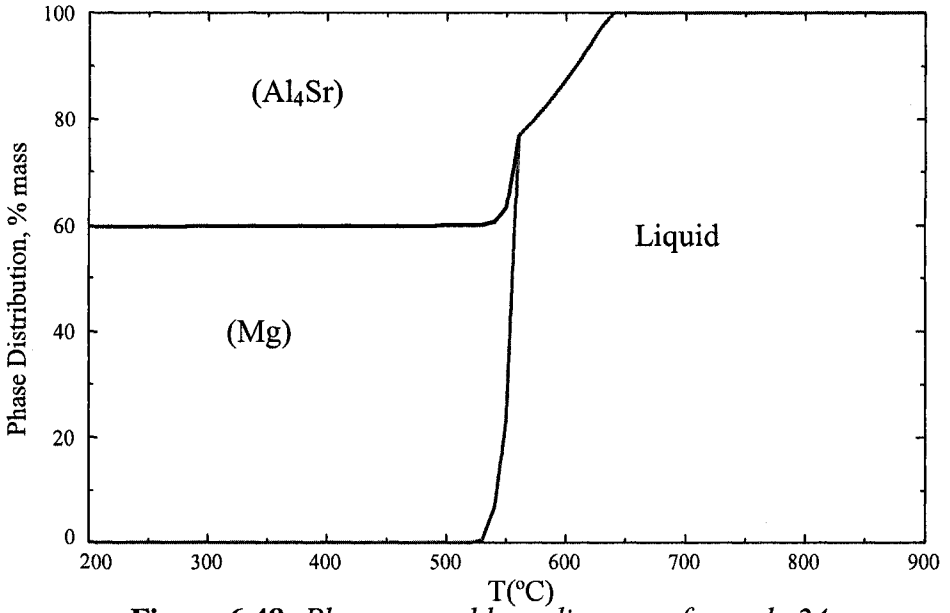

Figure 6.48: *Phase assemblage diagram of sample 24.*

Figure 6.49 shows optical micrograph, SEM, XRD and EMPA analyses of sample 24. SEM image shows that plate-like phase and dark region designated as (Al_4Sr) and (Mg), respectively and confirmed by EPMA analysis. Two lamellar structures are observed in this sample; one occurs at 520°C forming (Al_4Sr) in the coarse lamellae and the other one forms (Mg) in the fine lamellae at 432°C as shown in Figure 6.49(II).

SEM, XRD and EPMA analyses in Figure 6.49(II), (III) and (IV) identified positively (Mg) and (Al_4Sr) which is consistent with thermodynamic calculations. Whereas, $Mg_{58}Al_{38}Sr_4$ could not be identified, this may be because this sample is away from $Mg_{58}Al_{38}Sr_4$ and close to phase boundary of the Mg+Al_4Sr phase field. (Al_4Sr) dissolves 12.4±0.1 wt.% Mg, whereas, (Mg) dissolves 5.2±0.5 wt.% Al. The experimental results are consistent with the thermodynamic calculation in terms of phase identification and transformation temperatures.

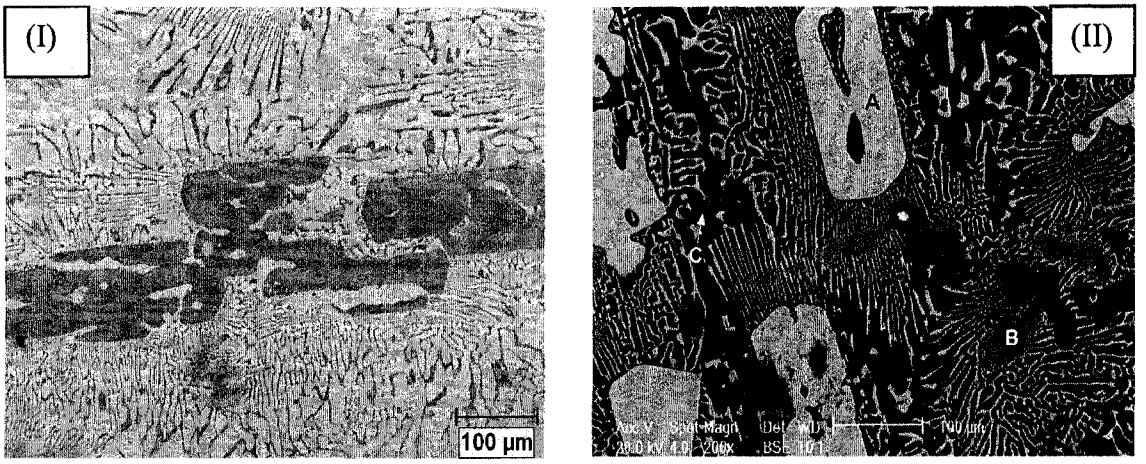

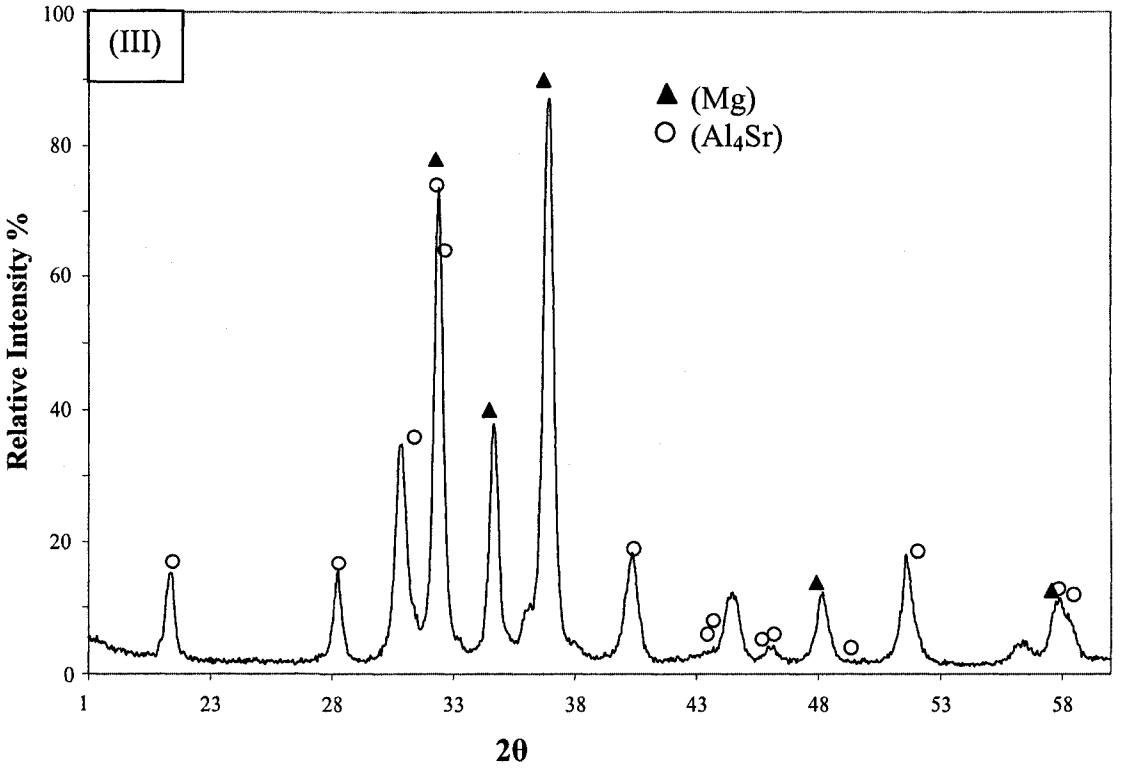

Location	at.% Mg	at.% Al	at.% Sr	Phases
A	12.4±0.1	66.7±0.5	20.9±0.5	(Al_4Sr)
B	60.9±0.5	30.0±0.5	9.1±0.5	(Al_4Sr)+(Mg)
C	94.8±0.5	5.2±0.5	0.0	(Mg)

(IV)

Figure 6.49: *(I) Optical micrograph; (II) SEM image; (III) XRD pattern and (IV) EPMA analysis of composition 24.*

As can be seen in Figure 4.50, the measured liquidus temperature obtained by DSC measurements and the predicted using thermodynamic modeling are consistent at lower temperatures. Whereas, there are small deviations between the predicted and measured liquidus temperatures due to high reactivity of Sr.

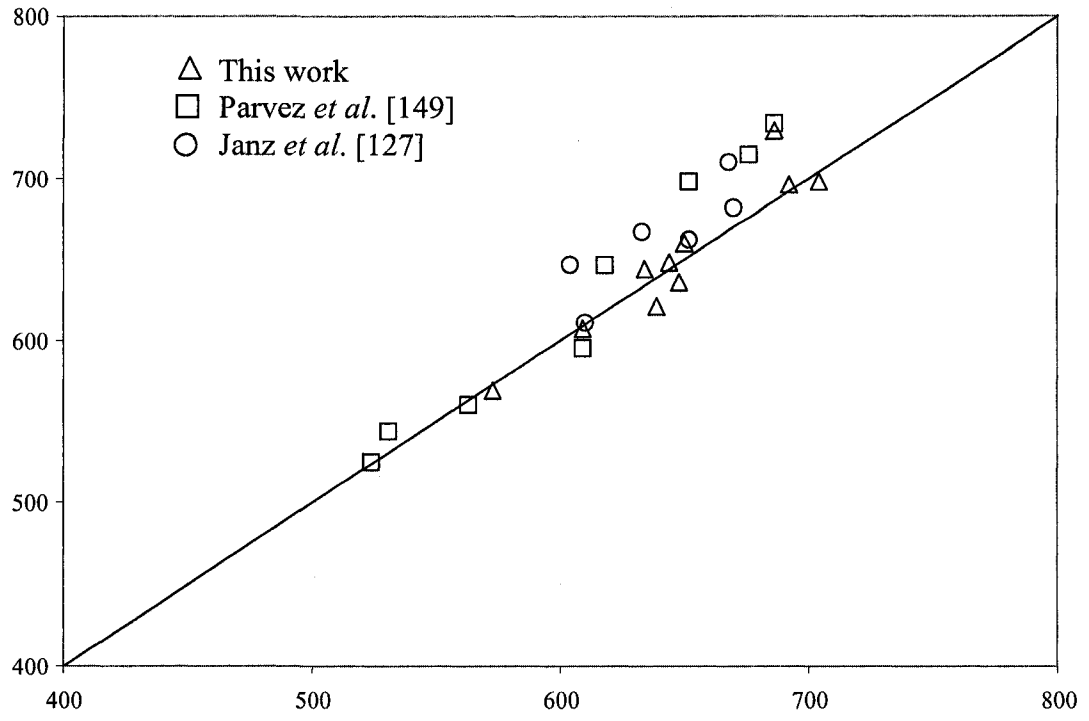

Figure 4.50: *Comparison between the predicted and measured temperatures.*

To conclude, solid solubility of six binary compounds in the Mg-Al-Sr system extending into the ternary system has been found and denoted as: (Al_4Sr), (Al_2Sr), ($Mg_{17}Sr_2$), ($Mg_{38}Sr_9$), ($Mg_{23}Sr_6$) and (Mg_2Sr) as can be seen in Table 6.7. These are not separate phases, but they are due to the substitution of Al by Mg atoms or vice versa in the binary compounds. In view of the relative atomic size of Al and Mg atoms, the ratio of Al radius to that of Mg is 1.12 indicating that there is a high chance for substitutional solid solubility. In addition, the solubility of Sr in γ-Phase was found negligible.

Table 6.6: *Comparison between the calculated and the measured solubility of the binary compounds in the Mg-Al-Sr system.*

Phase	Solubility of the third element in the binary compounds, at.%			
	[122]	[127]	This work	Calculation
Al_4Sr	25.0 at.% Mg	16.2 at.% Mg	19.9 at.% Mg	15.9
Al_2Sr	19.0 at.% Mg	33.6 at.% Mg	26.1 at.% Mg	30.8
$Mg_{17}Sr_2$	13.0 at.% Al	15.4 at.% Al	20.0 at.% Al	13.1
$Mg_{38}Sr_9$		17.5 at.% Al	20.3 at.% Al	22.3
$Mg_{23}Sr_6$	27.0 at.% Al	22.6 at.% Al		21.9
Mg_2Sr	12.0 at.% Al	22.2 at.% Al	26.1 at.% Al	18.6

In this work, the maximum solid solubility of Mg in Al_4Sr is found to be 19.9 at.%, compared to Makmadohv's *et al.* [122] and Janz's *et al.* [127] results as 25.0 at.% and 16.2 at.%, respectively. It was also observed that Al_2Sr dissolves 26.1 at.% Mg, whereas Makmadohv *et al.* [122] and Janz *et al.* [127] found that this solubility as 19.0 and 33.6 at.% Mg, respectively. The ternary solubility found in this has been used in the current thermodynamic modeling of the Mg-Al-Sr system.

Large solubilities of the Al in four binary compounds in the Mg-Sr system were observed. $Mg_{17}Sr_2$ dissolved 20.0 at.% Al which was found in sample 15 and 16, compared to Makmadohv's *et al.* [122] and Janz's *et al.* [127] values as 13.0 at.% and 15.4 at.% Al, respectively. In samples 15, 16 and 18, $Mg_{38}Sr_9$ dissolved 20.3 at.% Al compared to Janz's *et al.* [127] results as 17.5 at.% Al. Furthermore, It was found that Mg_2Sr dissolved 26.1 at.% Al, compared to Makmadohv's *et al.* [122] and Janz's *et al.* [127] results as 10.5 at.% and 22.2 at.% Al, respectively. Since the samples prepared to study the solubility of $Mg_{23}Sr_6$ were not successful because they were oxidized, the maximum solubility of Al in $Mg_{23}Sr_6$ was taken from the more recent work of Janz *et al.* [127] as 22.6 at.% Al. The maximum solid solubilities found in this work are reasonable because the samples were prepared from high purity elements and every sample was heat

treated at 400°C for 48 hours under flowing argon. Isothermal section at 400°C and liquidus projection of the Mg-Al-Sr system has been constructed based on these results as can be seen in Figure 4.23.

CHAPTER VII

Experimental Investigation of the Mg-Al-Ca System

7.1 Re-evaluation of the Experimental Data of the Mg-Al-Ca System

Further analysis has been performed of Wang's work [17] on the Mg-Al-Ca system. After analyzing all the X-ray diffraction using Rietveld method and PowderCell [186], the extended solubilities of Mg_2Ca, Al_2Ca and Al_3Ca_8 in the ternary have been confirmed. These phases were reported in Wang's work [17] as ternary phases. Two morphologies of eutectic structure were observed in the micrographs and supported by solidification curves; a coarse and a fine eutectic microstructures due to the existence of (Al_2Ca) and (Mg_2Ca), respectively [146].

7.2 Experimental Details

As with the Mg-Al-Sr system, the Mg-Al-Ca system was studied with key experiments to quantify the extended solubility of the Mg-Ca and Al-Ca binary compounds into the ternary system. A portion of the as-cast samples was used to measure phase transformation using DSC. The other portion was heat treated at 300°C for 24 hours, followed by oil quenching to construct the isothermal section of the Mg-Al-Ca system at this temperature. The heat treated samples were examined using XRD, microstructural characterization using optical microscopy, SEM and EPMA.

Sample 1 (35/25/40 wt.% Mg/Al/Ca) is located in the Mg+Mg_2Ca+C36 phase field and close to C36+Mg_2Ca+Al_3Ca_8 phase field as can be seen in Figure 7.1. The DSC spectra during heating and cooling are shown in Figure 7.2. Sharp and narrow peak appears in the cooling curve at 510°C which corresponds to the endothermic signal

measured in the heating spectrum at 511°C. This signal represents the phase transformation: $Mg_2Ca+Al_2Ca+Al_3Ca_8/Mg_2Ca+Al_2Ca+C36$ as can be seen in the calculated vertical section in Figure 7.3. Another exothermic signal was revealed on the heating curve at 702°C and appears in the cooling spectrum at 669°C. These signals are plotted in the vertical section in Figure 7.3. The melting point of this sample and the two samples in Wang's [17] work were not observed by heating up to 800°C, indicating that the melting points of these samples are higher than this temperature which is in quantitative agreement with the calculated vertical section.

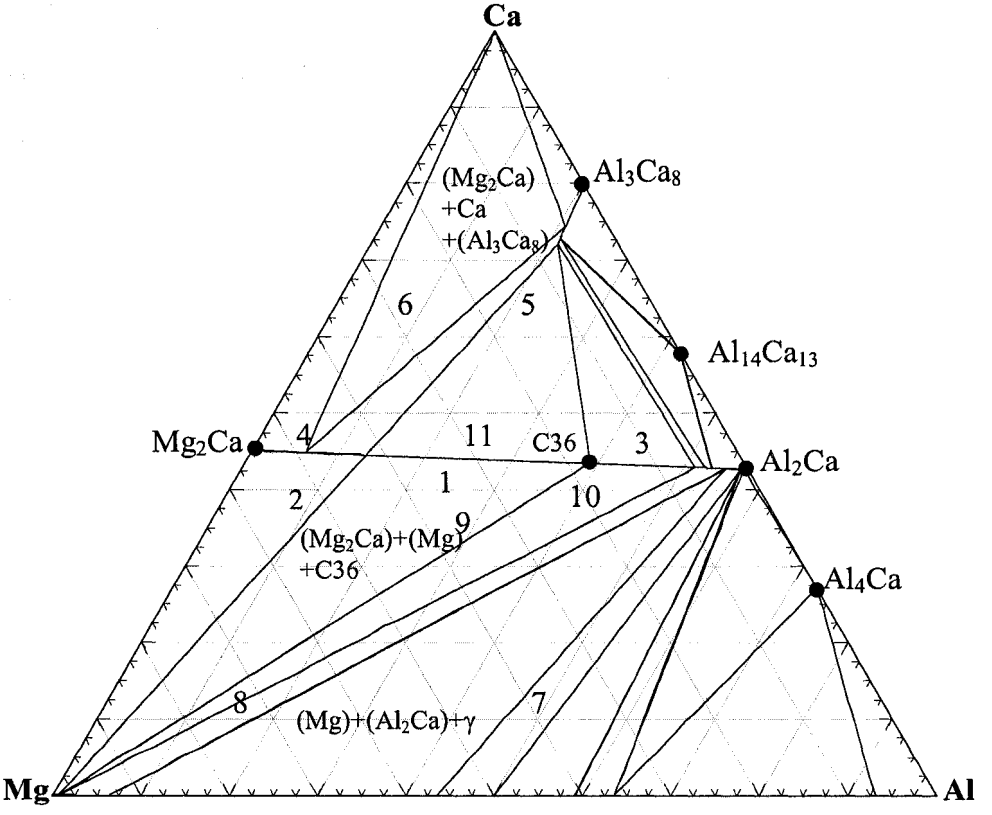

Figure 7.1: *Calculated isothermal section of the Mg-Al-Ca system at 300°C.*

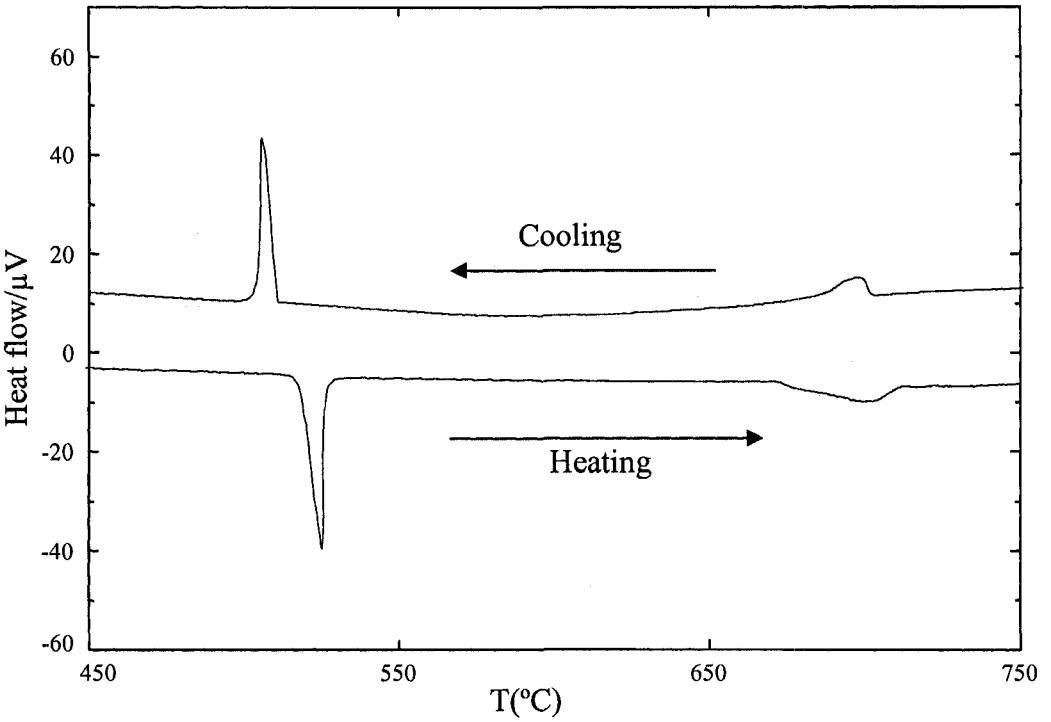

Figure 7.2: *DSC spectra of sample 1 (35/25/40 wt.% Mg/Al/Ca) during heating and cooling.*

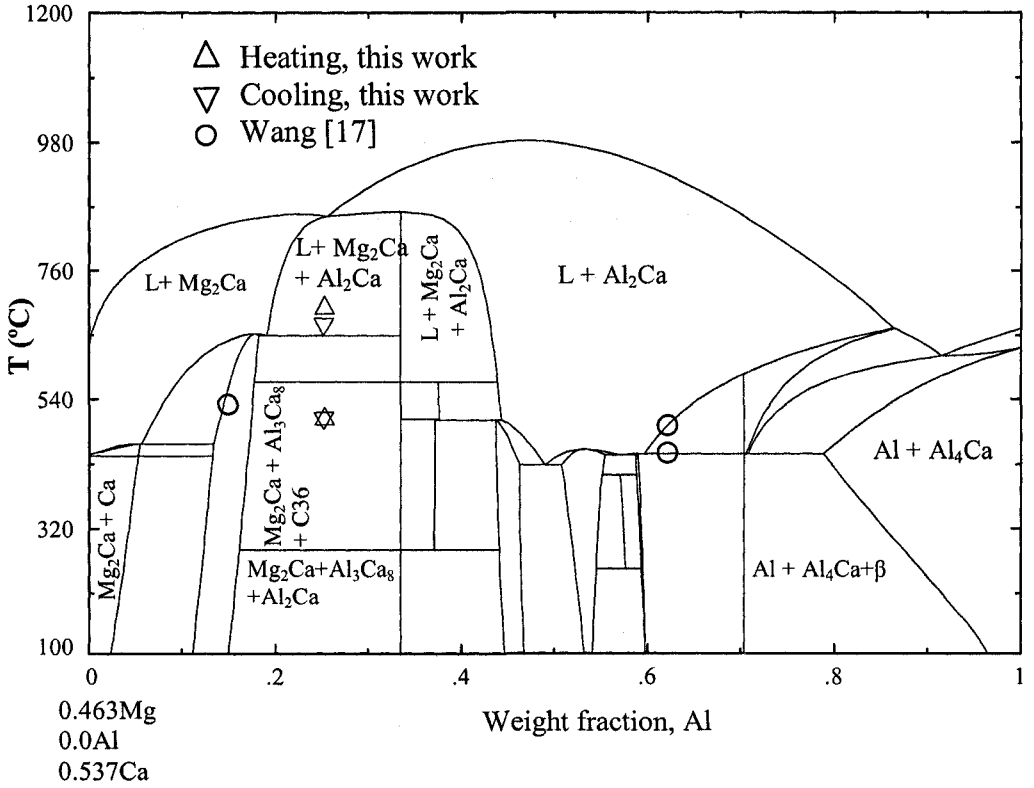

Figure 7.3: *Calculated vertical section with DSC signals from heating and cooling curves of sample 1.*

(Mg) and (Mg_2Ca) have been positively identified using XRD. Some distinct peaks that are associated with C36 have been observed. For the sake of comparison, the crystal structure and the chemical composition of C36 Laves phase has been adopted from Amerioun's *et al.* [188] work. In addition, Mg_2Ca dissolves 22.3±0.1 at.% Al as can be seen in Figure 7.4(III).

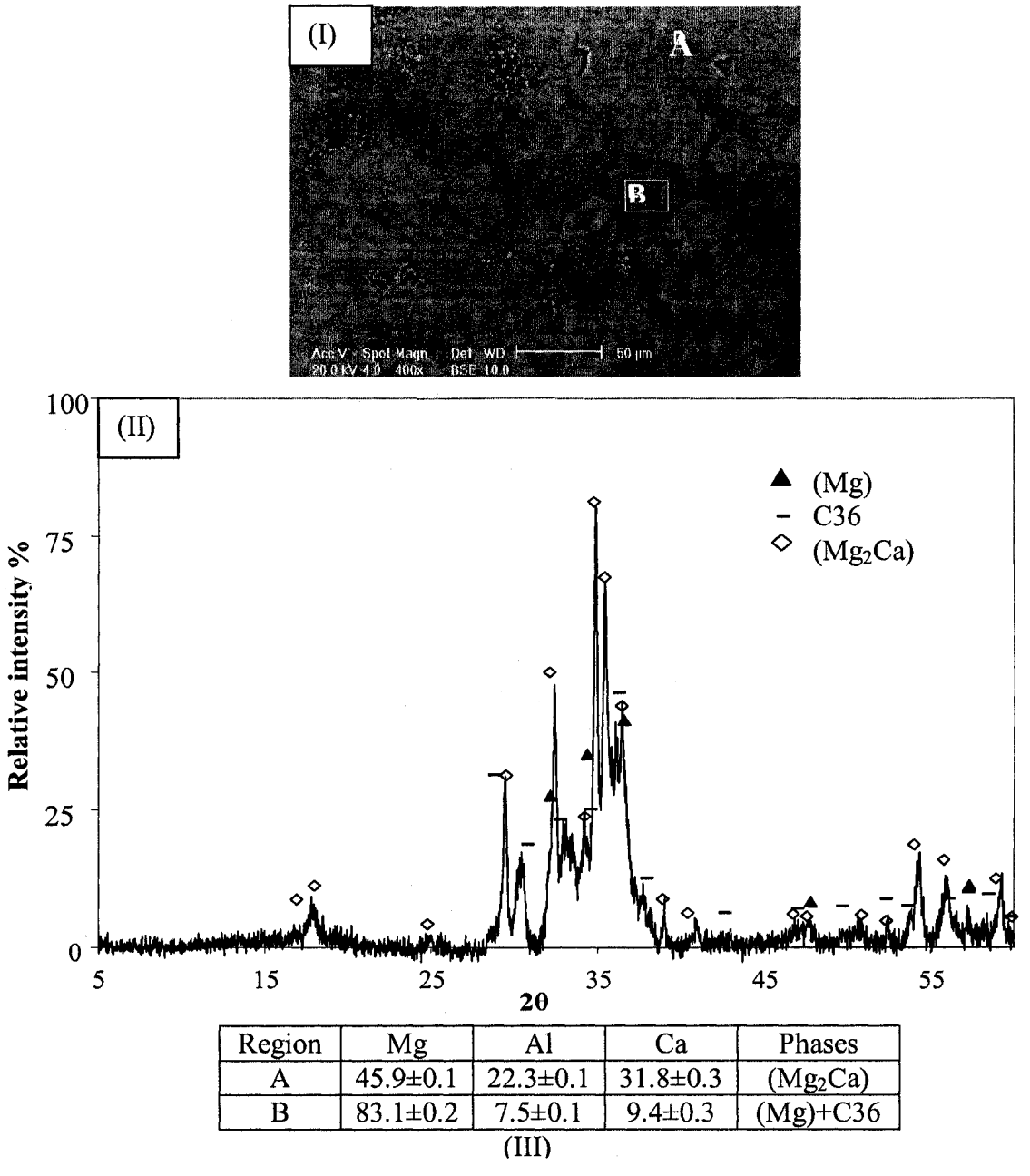

Region	Mg	Al	Ca	Phases
A	45.9±0.1	22.3±0.1	31.8±0.3	(Mg_2Ca)
B	83.1±0.2	7.5±0.1	9.4±0.3	(Mg)+C36

(III)

Figure 7.4: *(I) SEM image; (II) XRD pattern and (III) EPMA analysis of composition 1.*

Generally, the noise in the XRD background depends on the signal (peak) to noise ratio which, in turn, depends on the crystal structure of the phase. The samples that have noise are characterized by forming C36 or/and Al_3Ca_8 which generate many small peaks resulting in high noise in the background. Also, the highest number of counts was 150. The calculated XRD pattern of Al_3Ca_8 and C36 are shown in Figure 7.5.

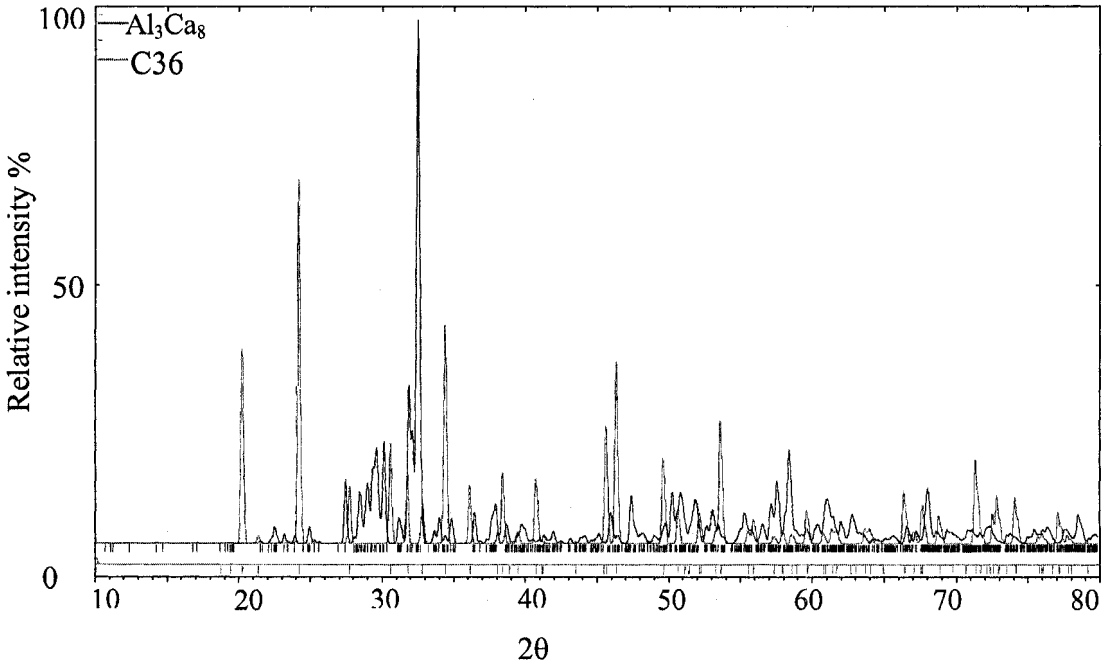

Figure 7.5: *Calculated XRD pattern of Al_3Ca_8 and C36.*

Sample 2 (55/5/40 wt.% Mg/Al/Ca) is located in the Mg_2Ca+Mg phase field as shown in Figure 7.1. Two transformation temperatures are registered by DSC spectra of this sample as shown in Figure 7.6; a sharp and narrow peak occurring at 510 and 523°C during cooling and heating, respectively. This corresponds to the phase transformation: L+Mg_2Ca+C36/Mg+Mg_2Ca+C36. The liquidus temperature was registered at 710 and 729°C during cooling and heating sessions. This finding can be correlated with the vertical section in Figure 7.7. Although the predicted liquidus temperature overestimates

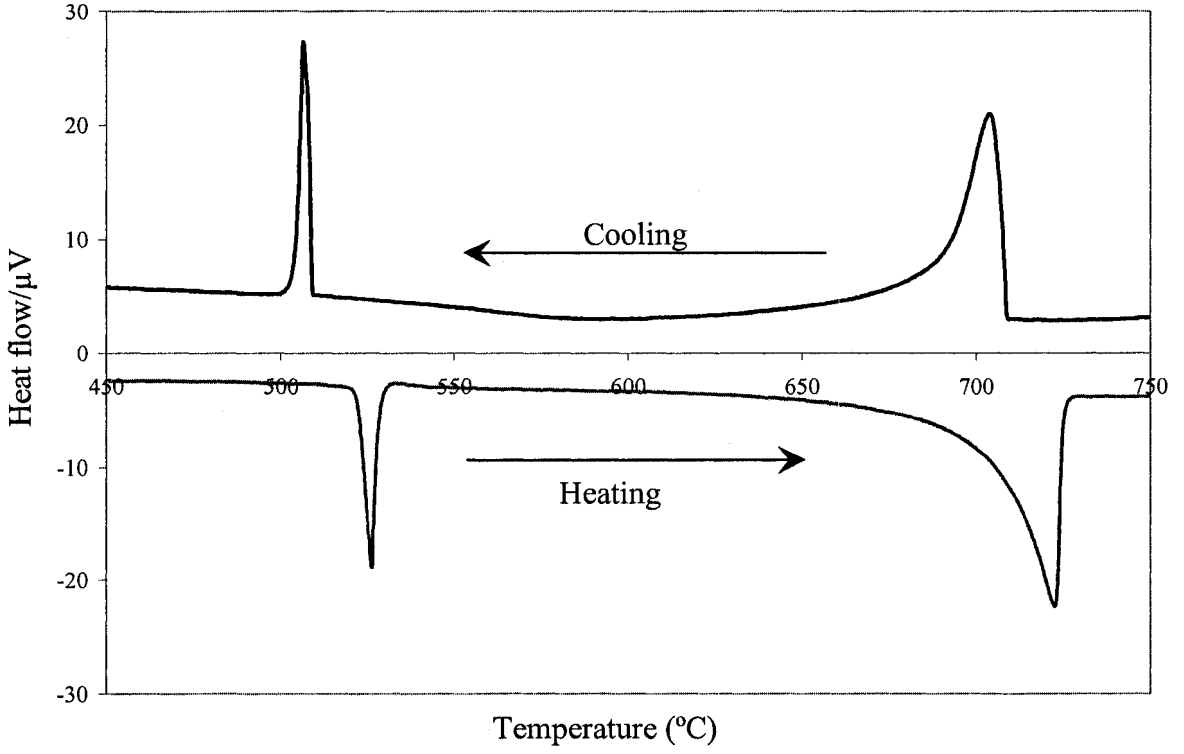

Figure 7.6: *DSC spectra of sample 2 (55/5/40 wt.% Mg/Al/Ca) during heating and cooling. (Baseline is subtracted)*

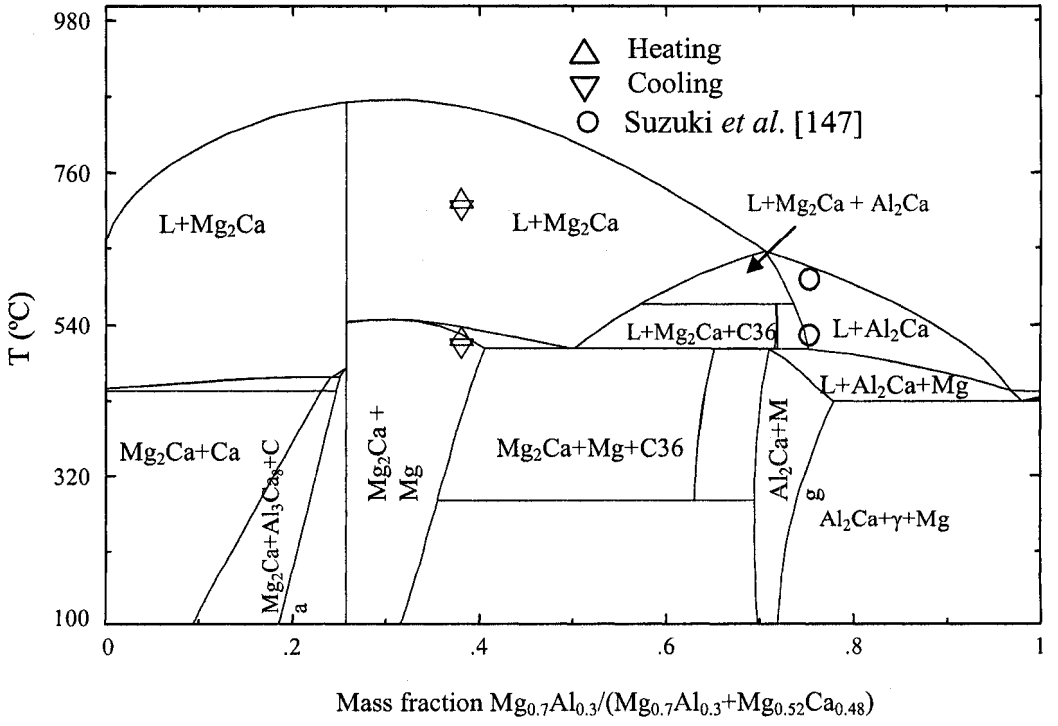

Figure 7.7: *Calculated vertical section with DSC signals from heating and cooling curves of sample 2.*

the measured liquidus temperature, a comparison between the measured transformation temperatures (melting and phase transformations) obtained by thermal analysis in this work and from the literature, and the predicted temperatures using the current thermodynamic modeling is presented in Figure 7.8. As can be noticed in this figure, the predicted and measured temperatures are in good agreement.

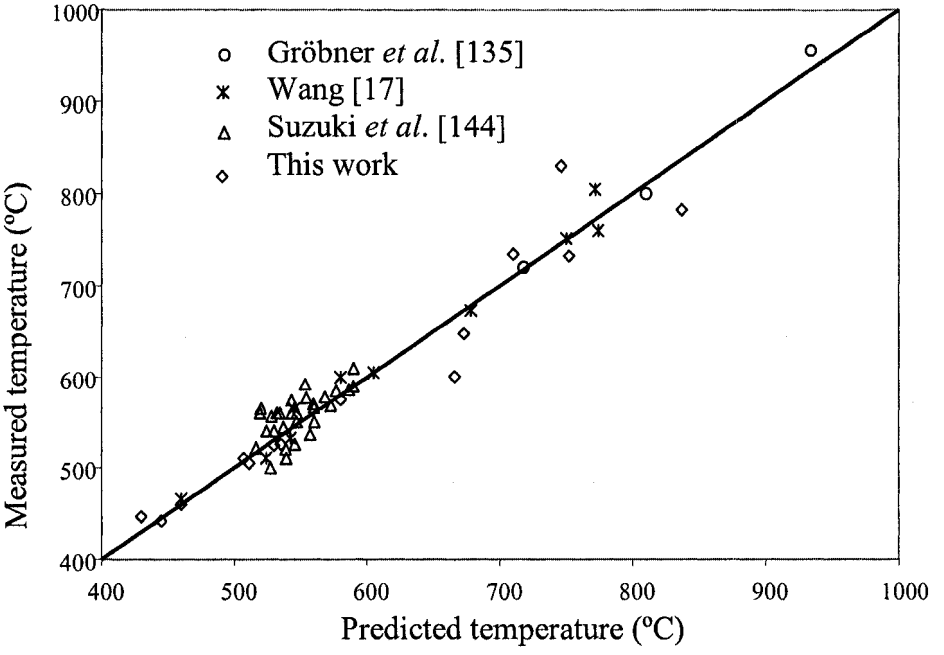

Figure 7.8: *Predicted transformation temperatures versus measured temperatures.*

XRD pattern of sample 2 identified positively two phases; (Mg) and (Mg_2Ca) as shown in Figure 7.9(IV). SEM image in Figure 7.9(I) shows two distinct phases; (Mg) and (Mg_2Ca) which are located in regions G and F, respectively and verified by EPMA analysis as can be seen in Figure 7.9(III). Good agreement between the calculated isothermal section at 300°C and the experimental work has been found in terms of phase identification. It is worth mention that in this sample Mg_2Ca dissolves 5.2±0.1 at.% Al.

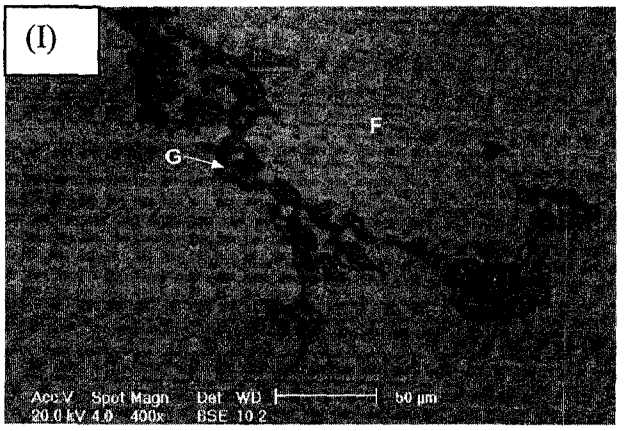

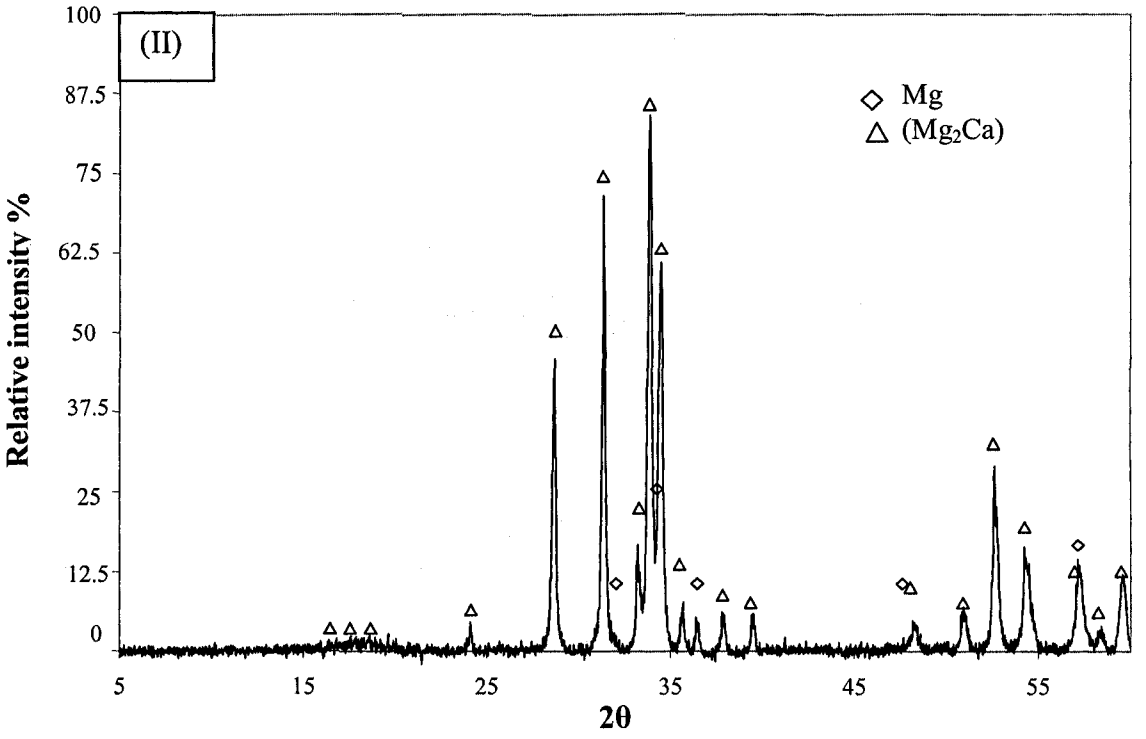

Region	at.% Mg	at.% Al	at.% Ca	Phases
F	63.2±0.3	5.2±0.1	31.6±0.3	(Mg_2Ca)
G	100.0	0.0	0.0	Mg

(III)

Figure 7.9: *(I) SEM image; (II) XRD pattern and (III) EPMA analysis of composition 2.*

Sample 3 (10/43/47 wt.% Mg/Al/Ca) is located in the Al_2Ca+Al_3Ca_8+C36 phase field, as shown in Figure 7.1. DSC spectra of this sample during heating and cooling runs are shown in Figure 7.10. There are two peaks which occur during heating at 448 and 495°C that were encountered at 460 and 481°C during cooling. These transformation temperatures along with the experimental data from the literature can be correlated to the calculated vertical section at 43 wt.% Ca in Figure 7.11. As can be seen in this figure, the predicted transformation temperatures are consistent with the measured temperatures by Suzuki *et al.* [144] in the Mg-rich region and deviates from the current work. These deviations between the experimental data in the current work and predictions from thermodynamic modeling are due to high reactivity of this sample because of high Ca content.

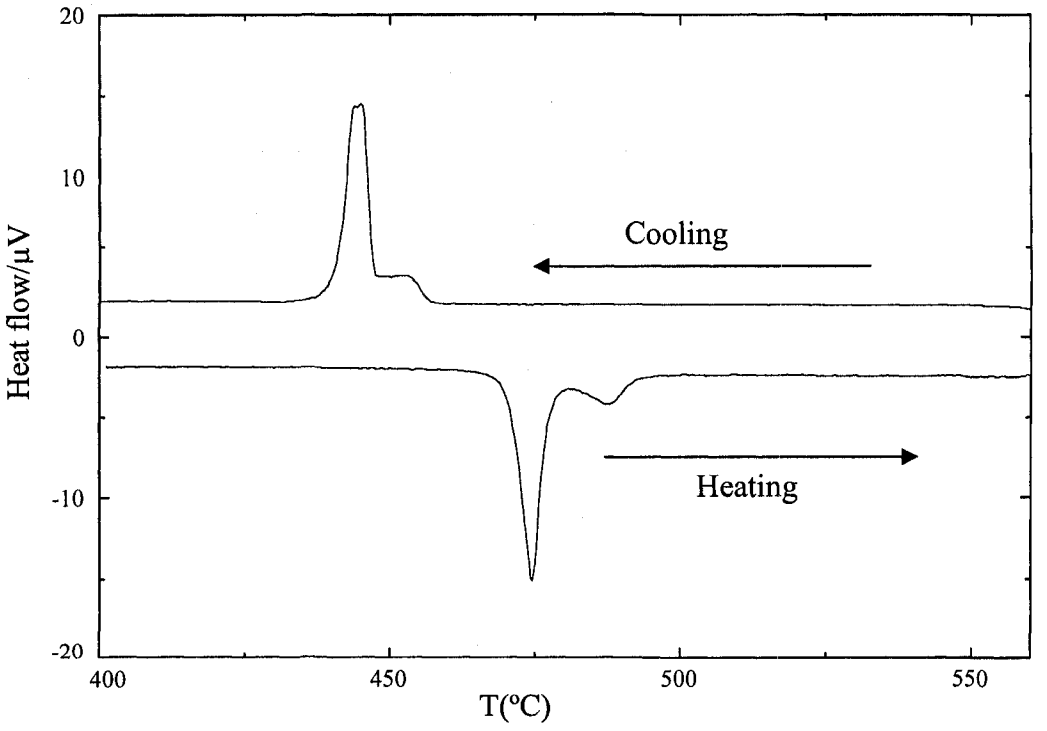

Figure 7.10: *DSC spectra of sample 3 (10/43/47 wt.% Mg/Al/Ca) during heating and cooling. (Baseline is subtracted)*

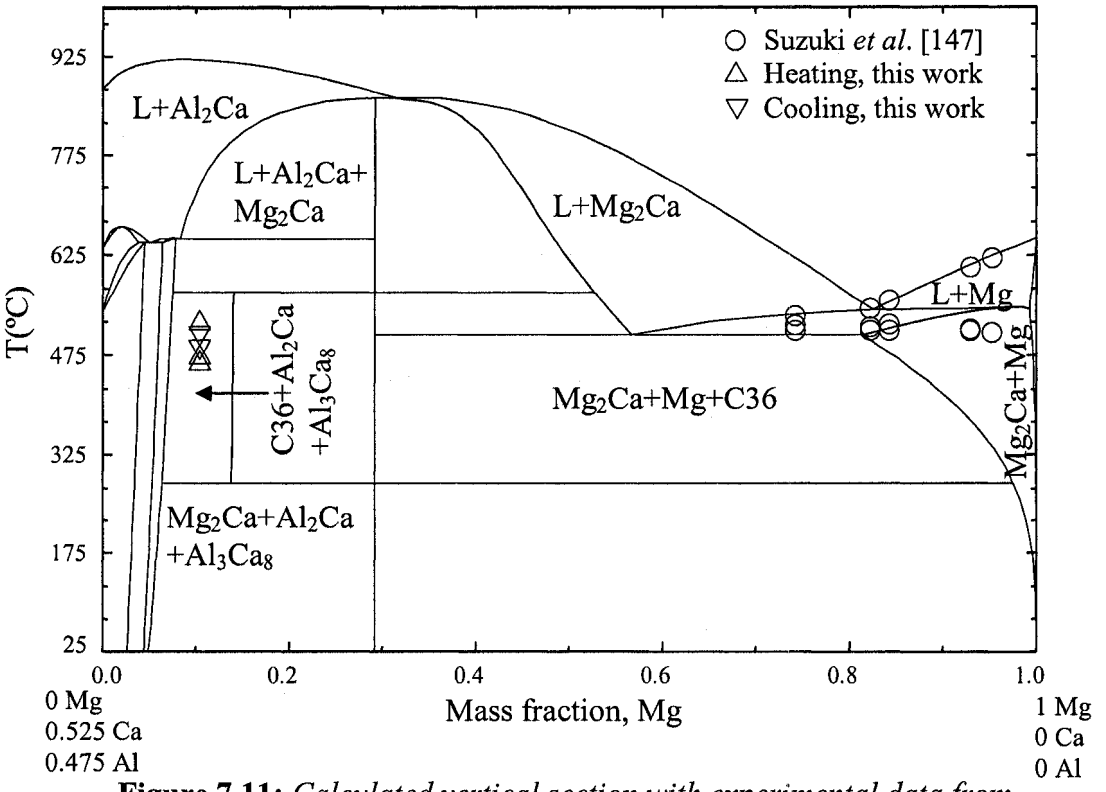

Figure 7.11: *Calculated vertical section with experimental data from this work and literature.*

Two phases, namely (Al_2Ca) and (Al_3Ca_8), are observed in the optical micrograph and SEM image as can be seen in Figures 7.12(I) and (II). The matrix, (Al_2Ca), in region H indicates that this alloy is located in the (Al_2Ca) crystallization field. XRD pattern of this sample in Figure 7.12(III) shows clearly the existence of (Al_2Ca) and (Al_3Ca_8) which is in agreement with EPMA analysis. It is noticed that (Al_2Ca) dissolves 8.6±0.1 at.% Mg and it is due to the substitution of Al by Mg atoms. Whereas, (Al_3Ca_8) dissolves 12.9±0.1 at.% Mg due to substitution of Ca by Mg atoms which is in accord with Gröbner's *et al.* [135] work.

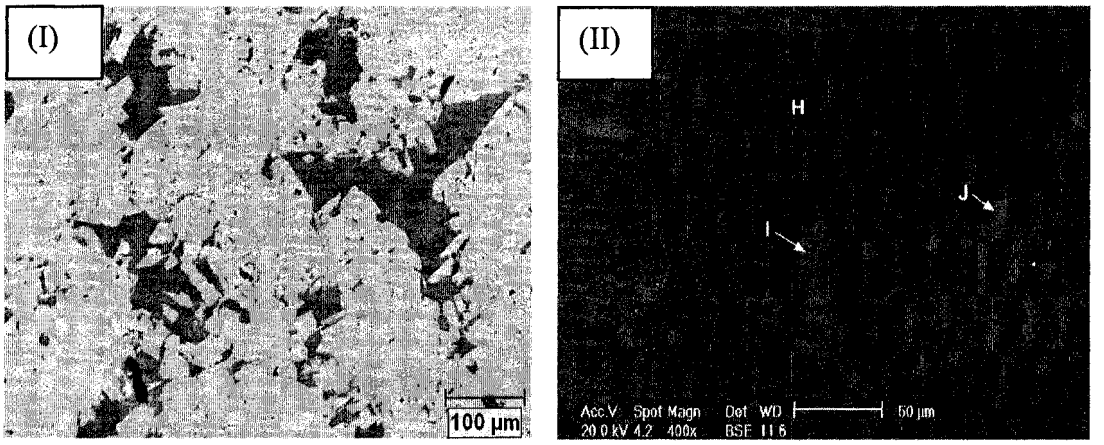

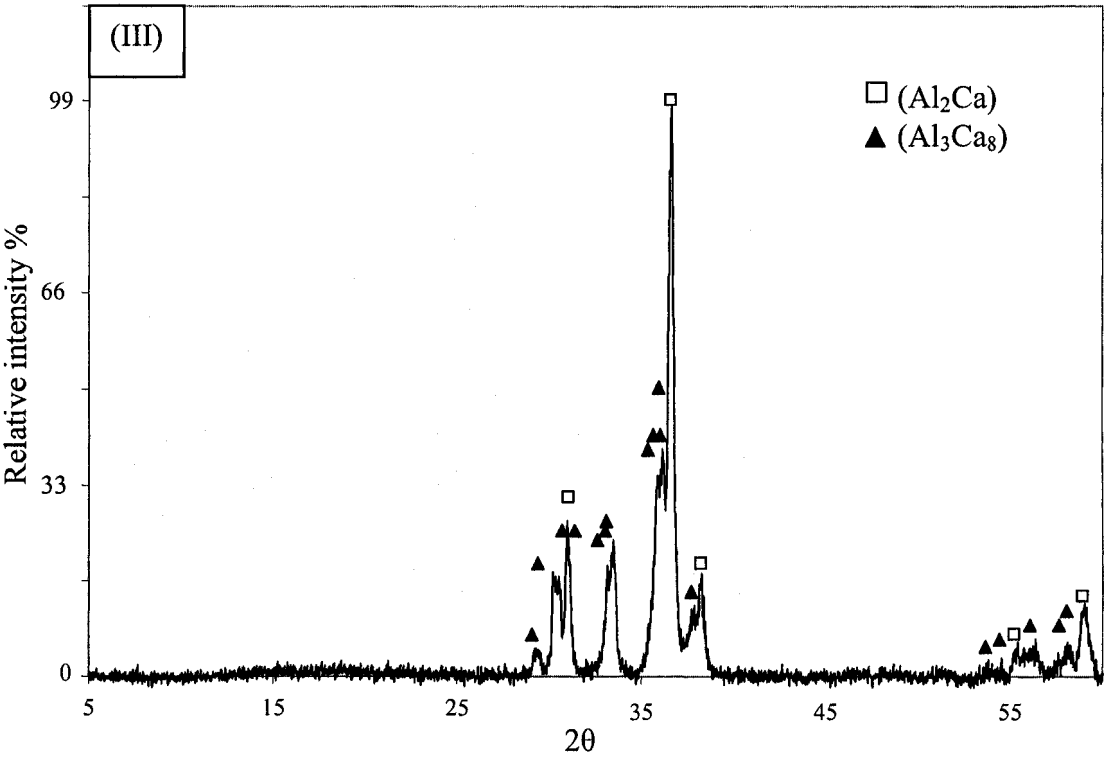

Region	Mg	Al	Ca	Phases
H	8.6±0.1	56.8±0.2	34.6±0.1	(Al_2Ca)
I	12.9±0.1	27.9±0.1	59.2±0.2	(Al_3Ca_8)

(IV)

Figure 7.12: *(I) Optical micrograph; (II) SEM image; (III) XRD pattern and (IV) EPMA analysis of composition 3.*

According to thermodynamic predictions, sample 4 (47/5/48 wt.%, Mg/Al/Ca) is located in the two phase field Mg_2Ca+Ca. The DSC heating and cooling curves of this sample are shown in Figure 7.13. Two exotherms appear in the cooling curve at 420°C and 742°C. This corresponds to the two endotherms that appear in the heating spectrum at 408°C and 723°C.

As can be seen in Figures 7.15(I) and (II), the binary compound (Mg_2Ca) dissolves 4.3±0.1 at.% Al. The XRD pattern positively identified two phases (Mg_2Ca) and pure Ca. However, due to the small size of precipitated Ca and the fact that this sample is far away from Ca and close to Mg_2Ca, it was difficult to detect Ca by EPMA analysis. On the other hand, the solidification curve, as can be seen in Figure 7.16, indicates that (Mg_2Ca) starts to solidify at 742°C down to 420°C consuming more than 95 wt.% of the liquid and, (Mg_2Ca) and pure Ca precipitate from the remaining liquid at 420°C.

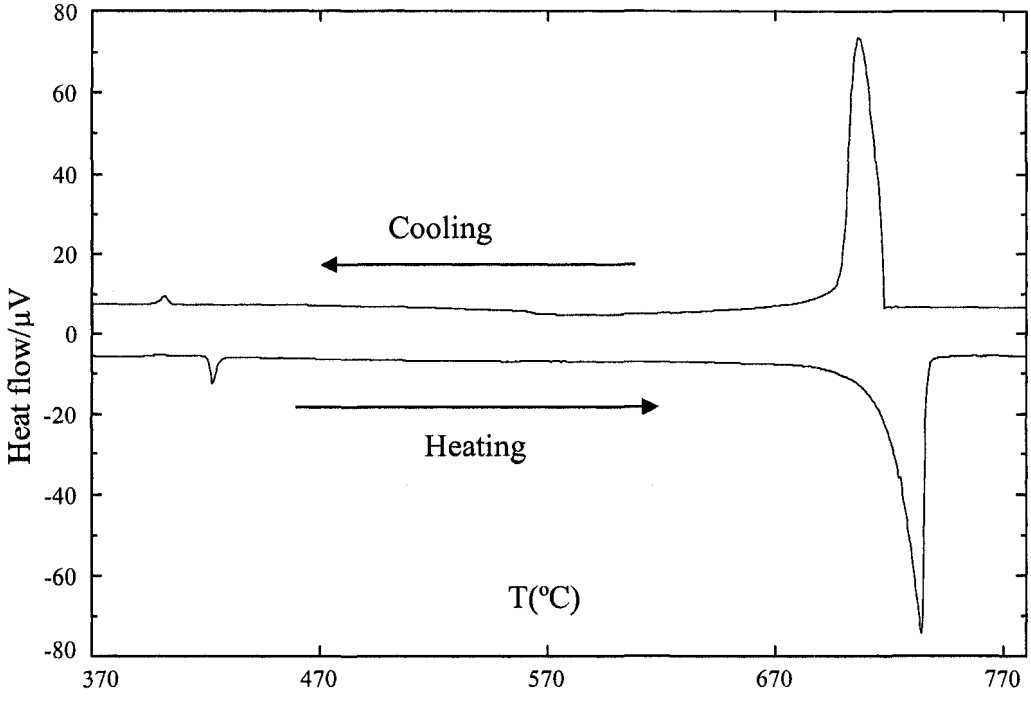

Figure 7.13: *DSC spectra of sample 4 (47/5/48 wt.% Mg/Al/Ca) during heating and cooling. (Baseline is subtracted)*

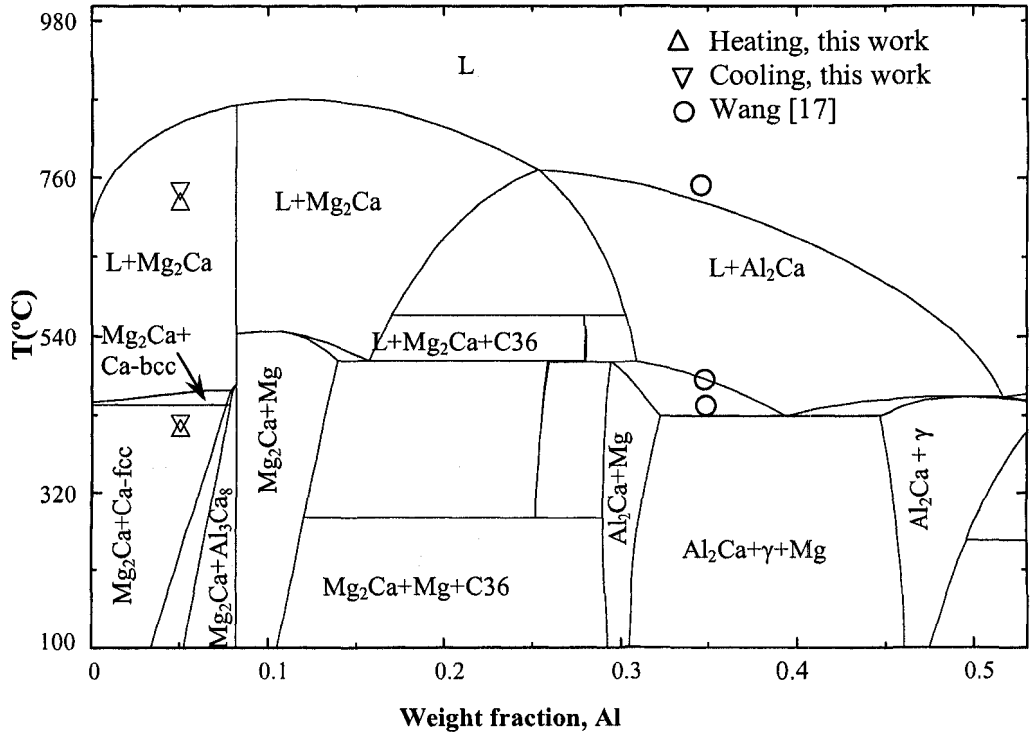

Figure 7.14: *Calculated vertical section at 47 wt.% Mg with DSC signals from heating and cooling curves of sample 4.*

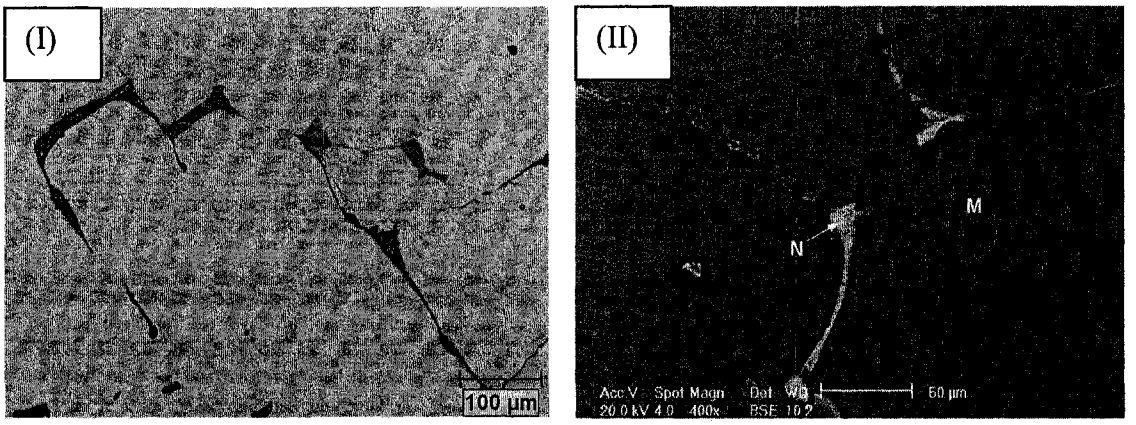

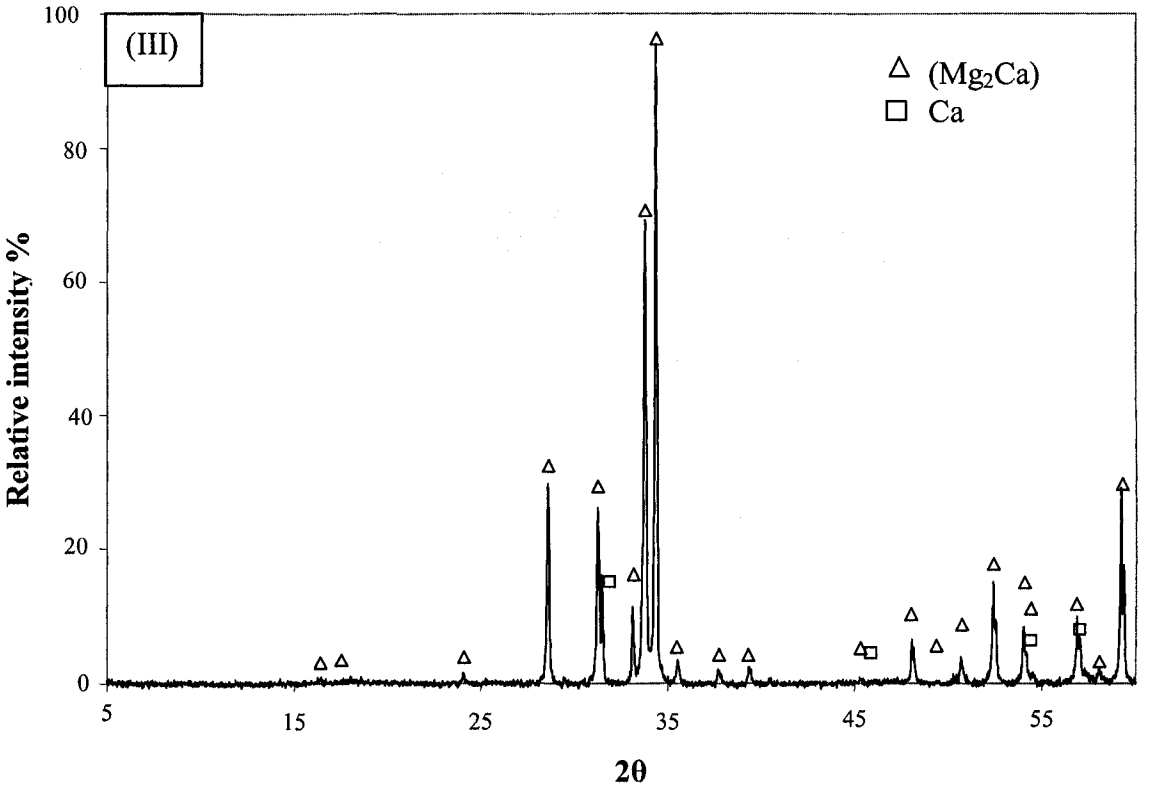

Region	Mg	Al	Ca	Phases
M	61.6±0.2	4.3±0.1	34.1±0.1	(Mg_2Ca)

(IV)

Figure 7.15: *(I) Optical micrograph; (II) SEM image; (III) XRD pattern and (IV) EPMA analysis of composition 4.*

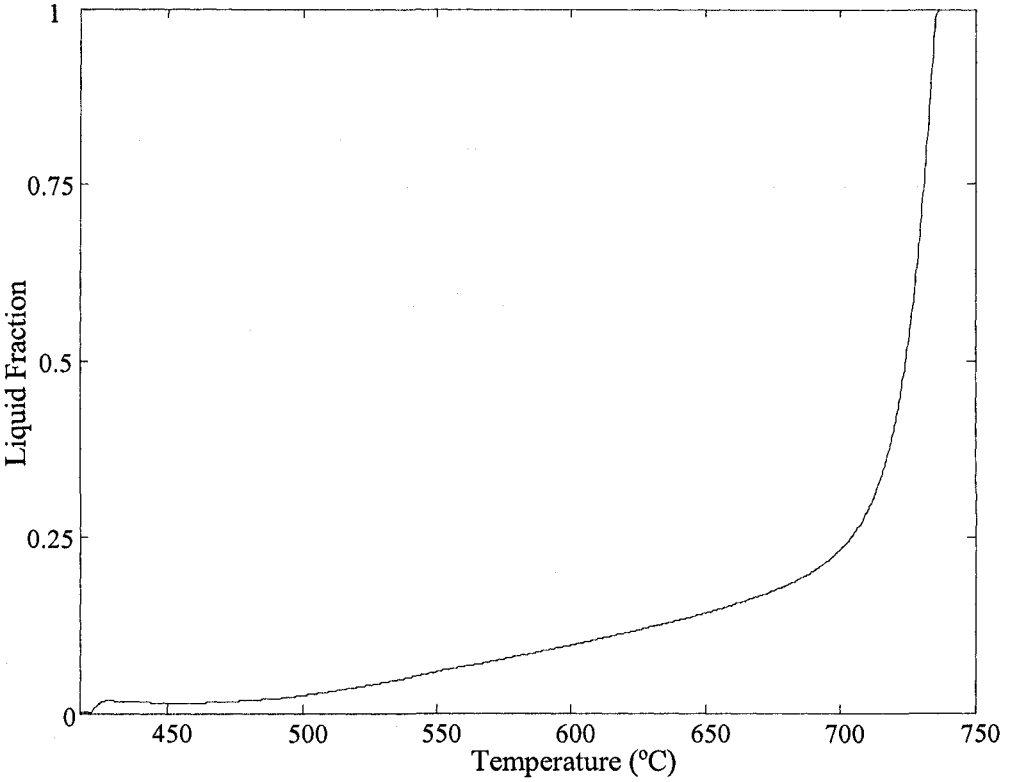

Figure 7.16: *Solidification curve deduced from DSC measurement of sample 4.*

SEM image, XRD pattern and EMPA analysis of sample 5 (14/21/65 wt.% Mg/Al/Ca) are shown in Figure 7.17. SEM image in Figure 7.17(I) shows clearly a dark gray region (U/V) which contains the three elements; Mg, Al and Ca. This region is designated as (Al_3Ca_8). The other two phases are precipitated at the grain boundaries of (Al_3Ca_8) and found to be (Mg_2Ca) and C36 according to XRD pattern. According to the EPMA analysis in Figure 7.17(III), (Al_3Ca_8) dissolves 8.5±0.2 at.% Al. Due to the small precipitates of (Mg_2Ca) and C36, it was difficult to detect these phases using EPMA analysis.

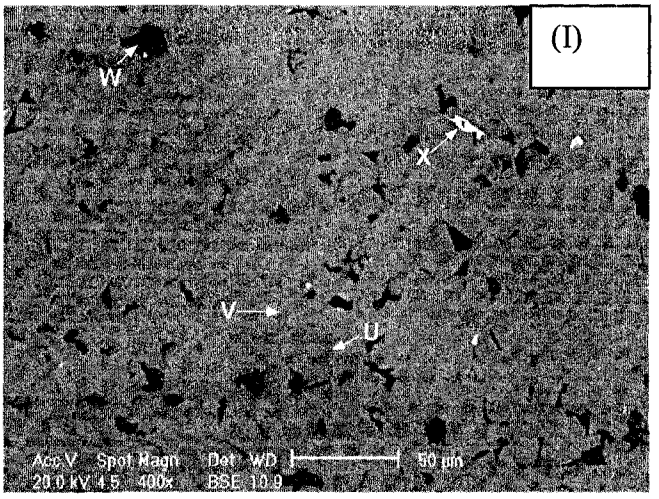

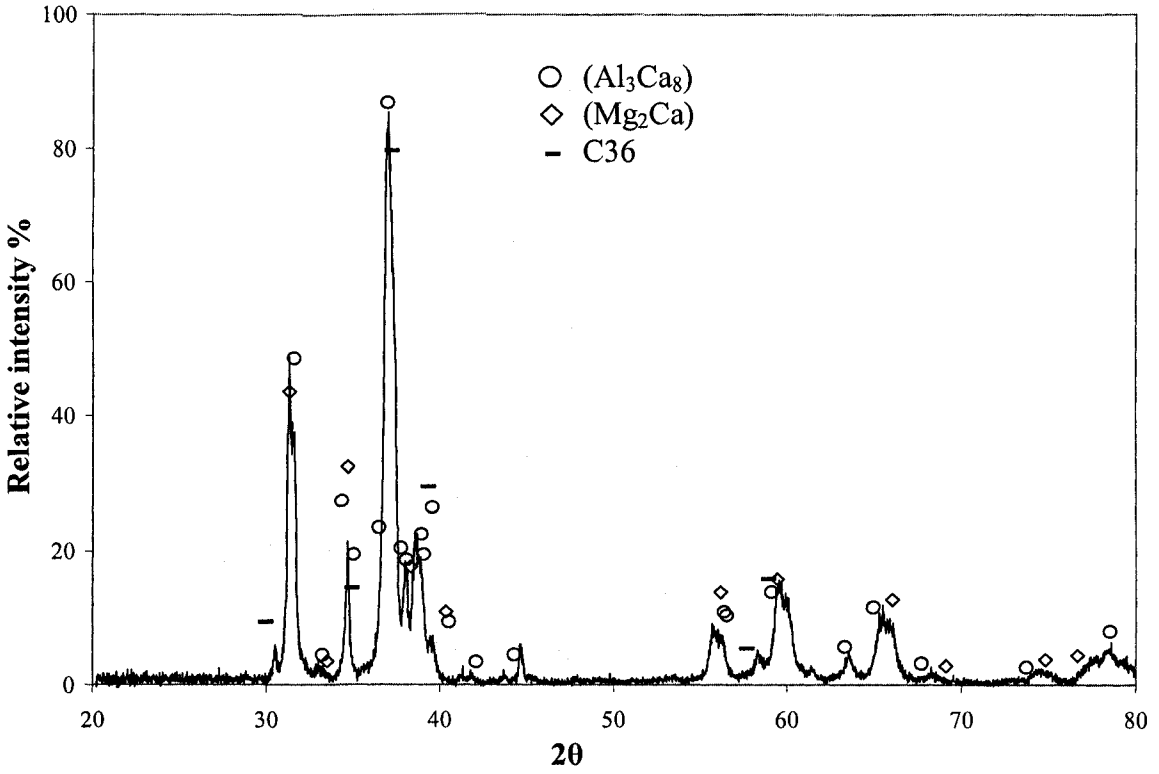

Region	Mg	Al	Ca	Phases
U or V	65.7±0.1	8.5±0.2	25.8±0.2	(Al_3Ca_8)
W	5.7±0.2	91.6±0.2	2.7±0.3	?

(III)

Figure 7.17: *(I) SEM image; (II) XRD pattern and (IV) EPMA analysis of composition 5 (14/21/65 wt.% Mg/Al/Ca).*

Sample 6 (28/7/65 wt.% Mg/Al/Ca) is located in the $Ca+Mg_2Ca+Al_3Ca_8$ phase field as can be seen in Figure 7.1. DSC spectra of this sample during heating and cooling runs are shown in Figure 7.18. Three peaks appear during heating that reoccurred during cooling. Correspondingly, the liquidus temperature was registered at 673°C. As can be seen in Figure 7.19, (Mg_2Ca) starts to solidify from the liquid at 675°C down to 451°C consuming around 80 % of the liquid then (Al_3Ca_8) precipitates consuming around 10% and an invariant reaction occurs at 406°C. SEM image shows two phases (Mg_2Ca) and (Al_3Ca_8) which is supported by XRD pattern and EPMA analysis as shown in Figure 7.21. According to EPMA analysis, Mg_2Ca and Al_3Ca_8 dissolve 9.1±0.1 at.% Al and 13.8±0.2 at.% Mg, respectively. The experimental results are consistent with the calculated isothermal section at 300°C, Figure 4.25, in terms of phase identification.

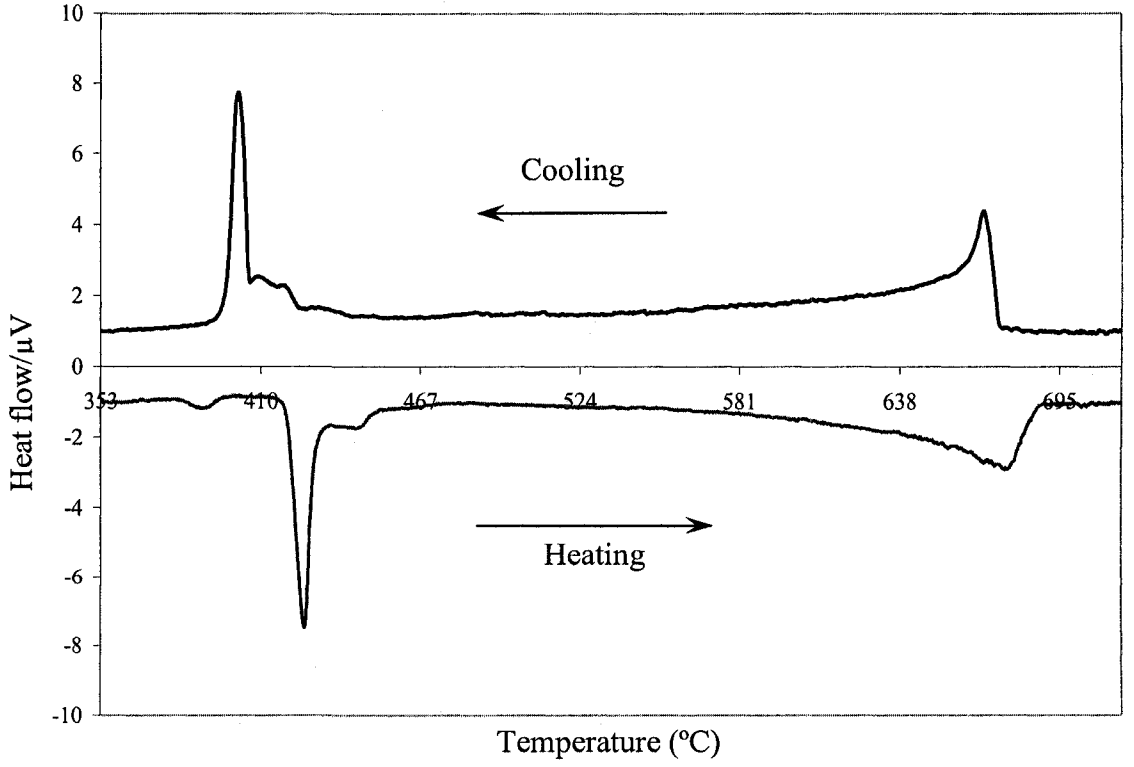

Figure 7.18: *DSC spectra of sample 6 (28/7/65 wt.% Mg/Al/Ca) during heating and cooling. (Baseline is subtracted)*

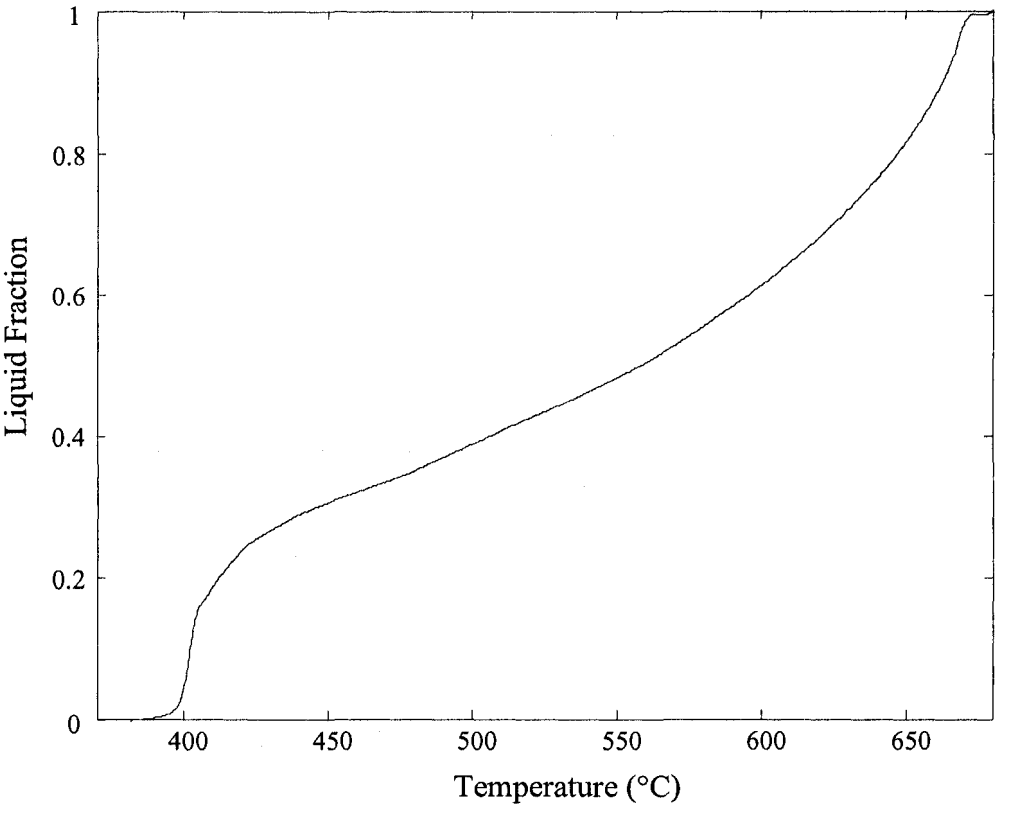

Figure 7.19: *Solidification curve deduced from DSC measurement of sample 6.*

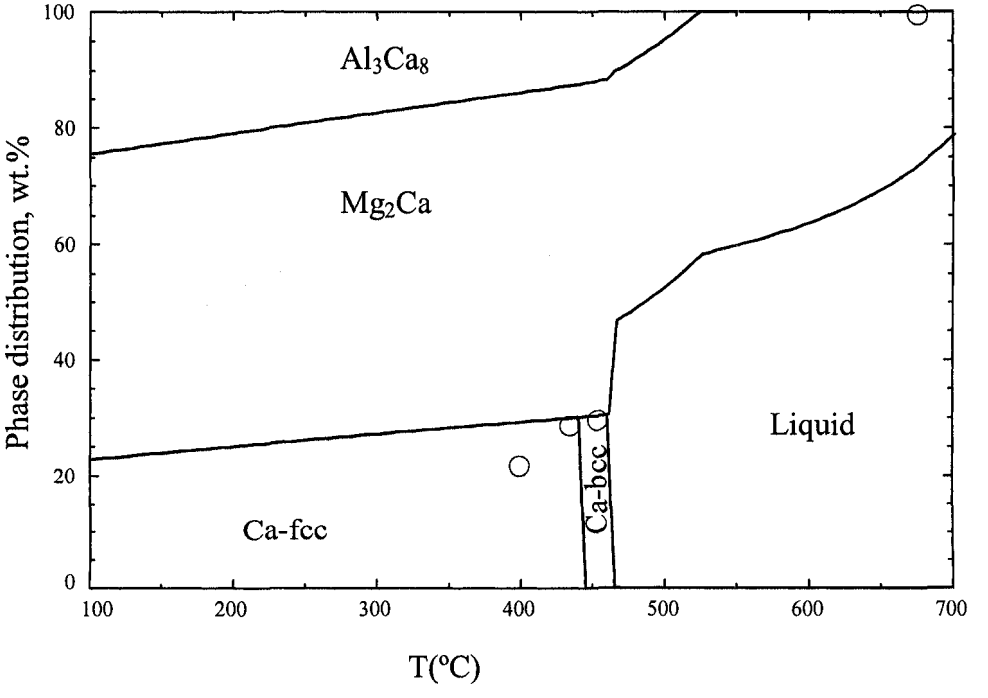

Figure 7.20: *Phase assemblage diagram of sample 6.*

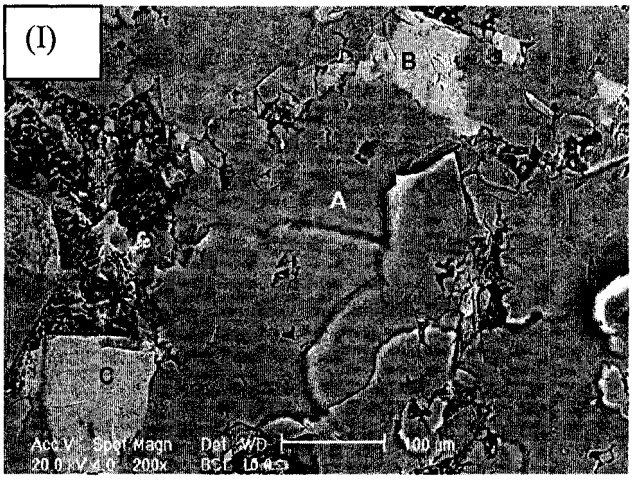

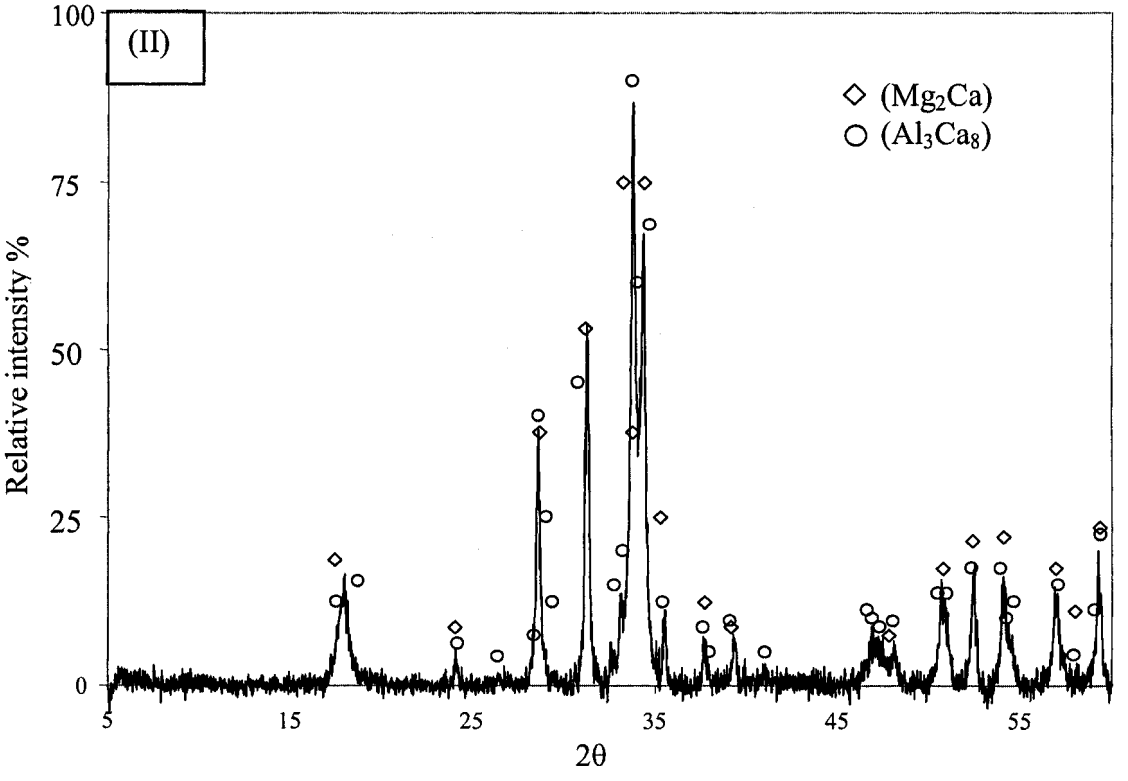

Region	Mg	Al	Ca	Phases
A	56.4±0.2	9.1±0.1	34.5±0.1	(Mg_2Ca)
B or C	13.8±0.2	23.8±0.1	62.4±0.1	(Al_3Ca_8)

(IV)

Figure 7.21: *(I) SEM image; (II) XRD pattern and (III) EPMA analysis of composition 6 (28/7/65 wt.% Mg/Al/Ca).*

According to the calculated isothermal section at 300°C in Figure 7.1, sample 7 (38/49/13 wt.% Mg/Al/Ca) is located in the Al_2Ca+γ phase field. DSC spectra of this sample in Figure 7.22 show sharp and narrow peak during heating occurring at 450°C and at 460°C during cooling. The liquidus temperature was registered at 750°C by a weak peak during heating. Labeling the DSC signals on the vertical section in Figure 7.23 shows a good agreement with the thermodynamic calculation.

SEM image, XRD pattern and EPMA analysis identified positively two phases (Al_2Ca) and γ as can be seen in Figure 7.24. According to EPMA analysis, (Al_2Ca) dissolves 4.8±0.1 at.% Mg, whereas, γ dissolves 1.4±0.1 at.% Ca. The experimental data agree with the calculated isothermal section in terms of phase identifications and phase transformation temperatures.

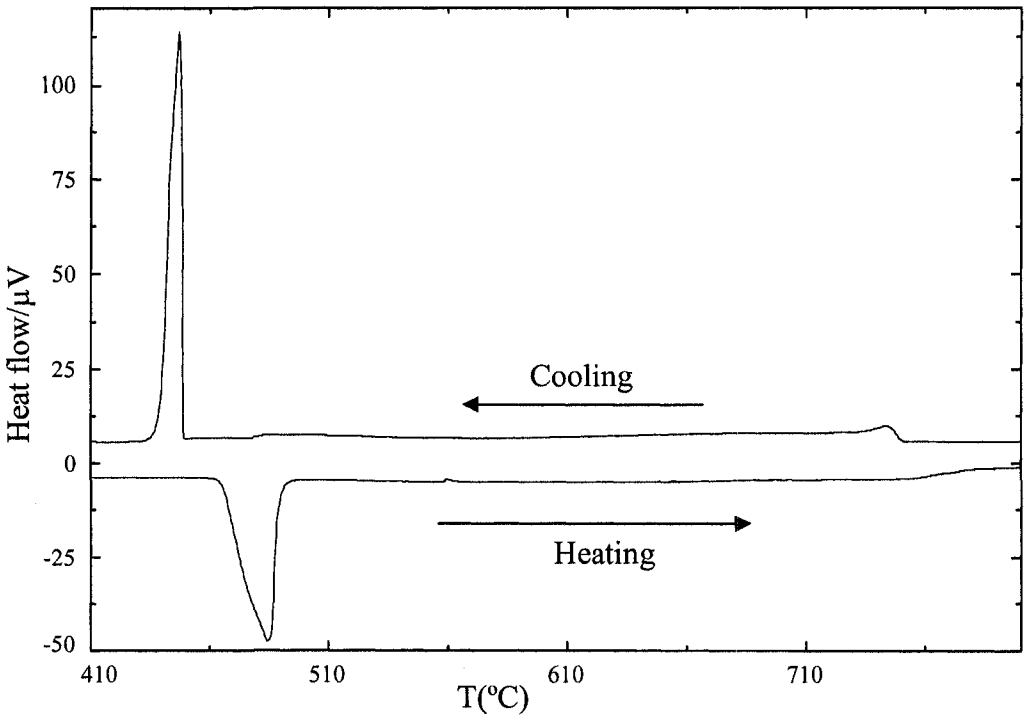

Figure 7.22: *DSC spectra of sample 7 (38/49/13 wt.% Mg/Al/Ca) during heating and cooling. (Baseline is subtracted)*

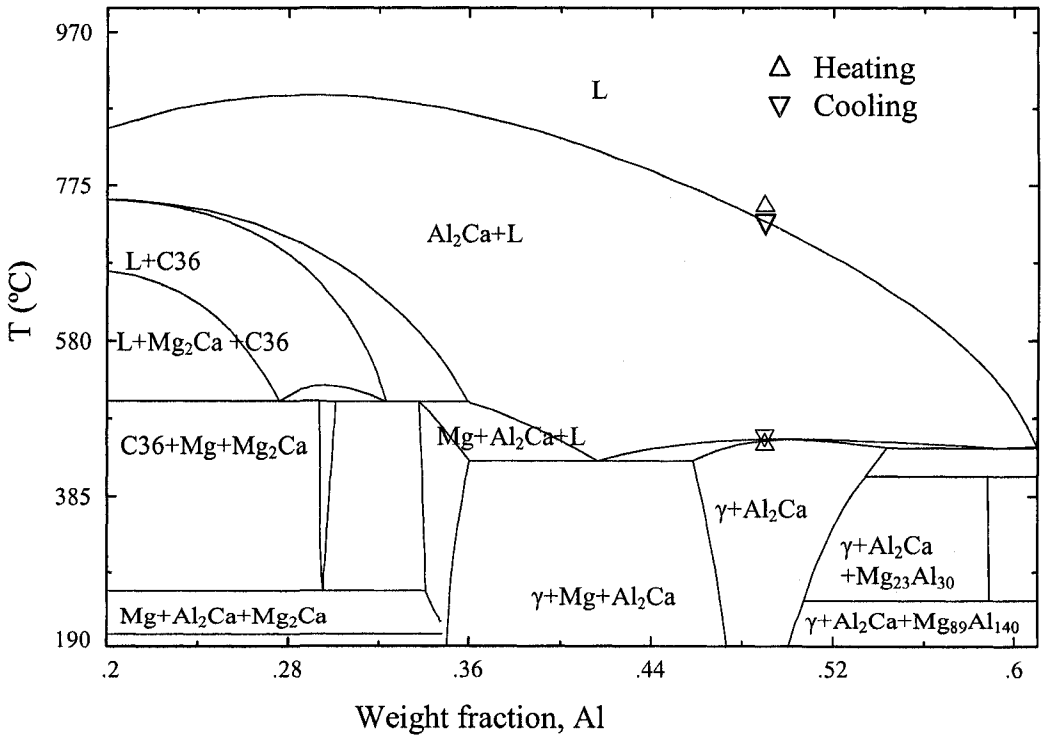

Figure 7.23: *Calculated vertical section at 38 wt.% Mg with DSC signals from heating and cooling curves of sample 7.*

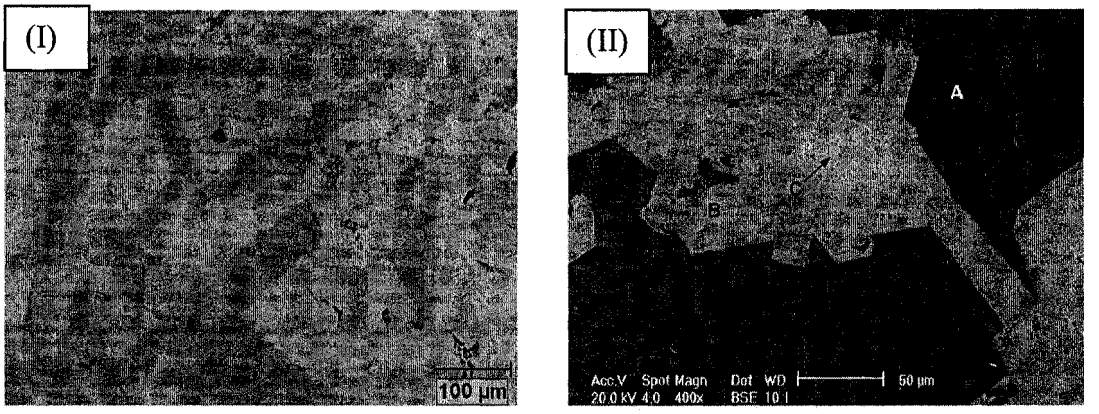

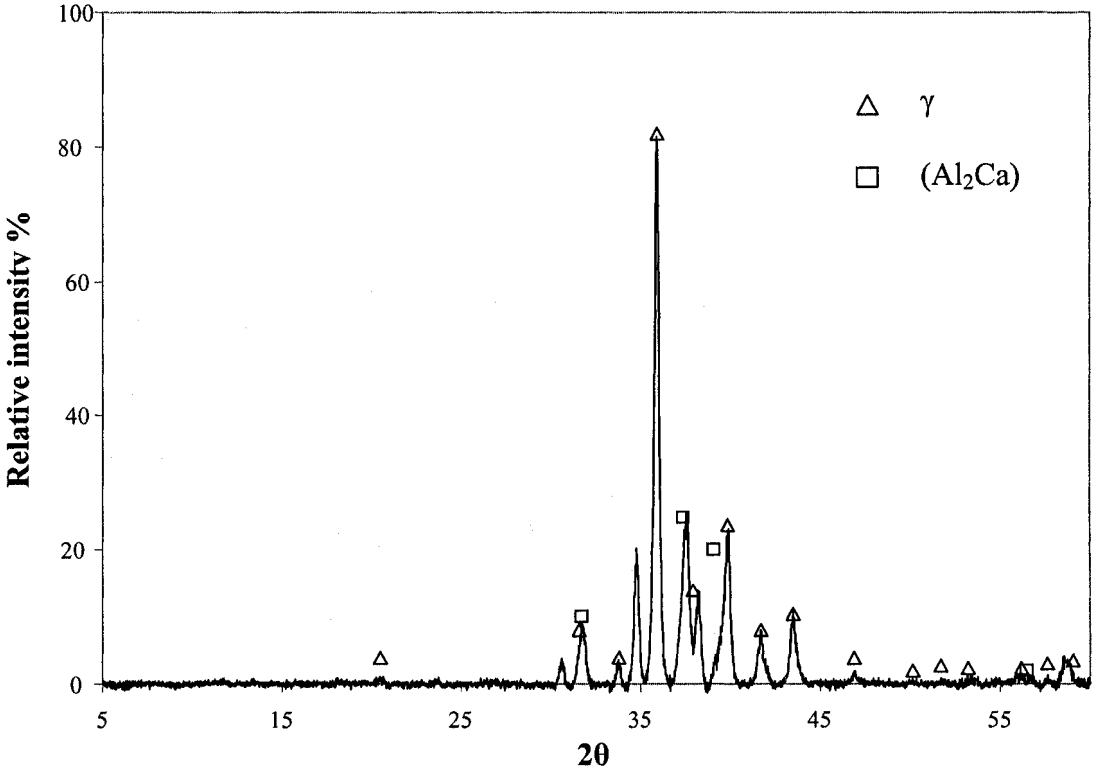

Region	Mg	Al	Ca	Phases
A	59.2±0.2	39.4±0.1	1.4±0.1	γ
C	4.8±0.1	64.4±0.1	30.8±0.1	(Al_2Ca)

(IV)

Figure 7.24: *(I) Optical micrograph; (II) SEM image; (III) XRD pattern and (IV) EPMA analysis of composition 7 (38/49/13 wt.% Mg/Al/Ca).*

Sample 8 (72/15/13 wt.% Mg/Al/Ca) is located in the Al_2Ca+Mg phase field and close to border line of the Al_2Ca+Mg+C36 phase field as can be seen in Figure 7.1. The phase transformation temperatures of this sample are obtained from the DSC spectra presented in Figure 7.25, which are labeled on the vertical sections shown in Figure 7.26. In this sample, the predicted phase transformation temperatures are consistent with the experimental results. Optical micrograph, SEM image, XRD pattern and EPMA analysis identified positively two phases (Al_2Ca) and (Mg) as can be seen in Figure 7.27.

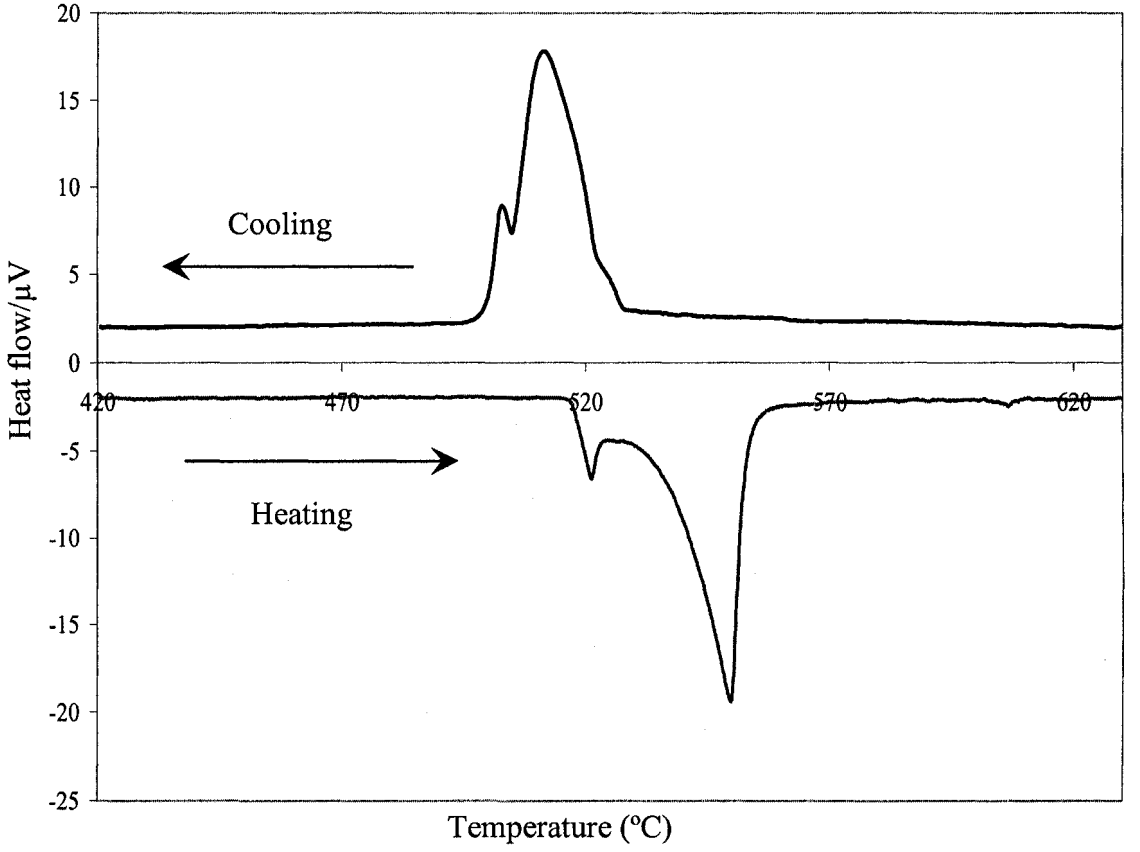

Figure 7.25: *DSC spectra of sample 8 (72/15/13 wt.% Mg/Al/Ca) during heating and cooling.*

It is worth noting, as can be seen in Figure 7.28, that the solidification curve deduced from the DSC measurement shows that C36 starts to solidify at 575°C down to

525°C consuming less than 10 wt.% of the liquid, then (Mg) and (Al_2Ca) start to solidify from the remaining liquid consuming more than 90 wt.% of the liquid.

The XRD pattern of sample 8 in Figure 7.27(III) indicates the presence of (Mg) and (Al_2Ca). This is in agreement with the SEM image and EPMA analysis. According to the EPMA analysis, (Al_2Ca) dissolves 6.3±0.2 at.% Mg, whereas, (Mg) dissolves 1.8±0.1 at.% Al. Due to the slow kinetics of formation, C36 was not observed in this sample. Thermodynamic predictions and the experimental results are consistent in terms of phase transformation temperatures.

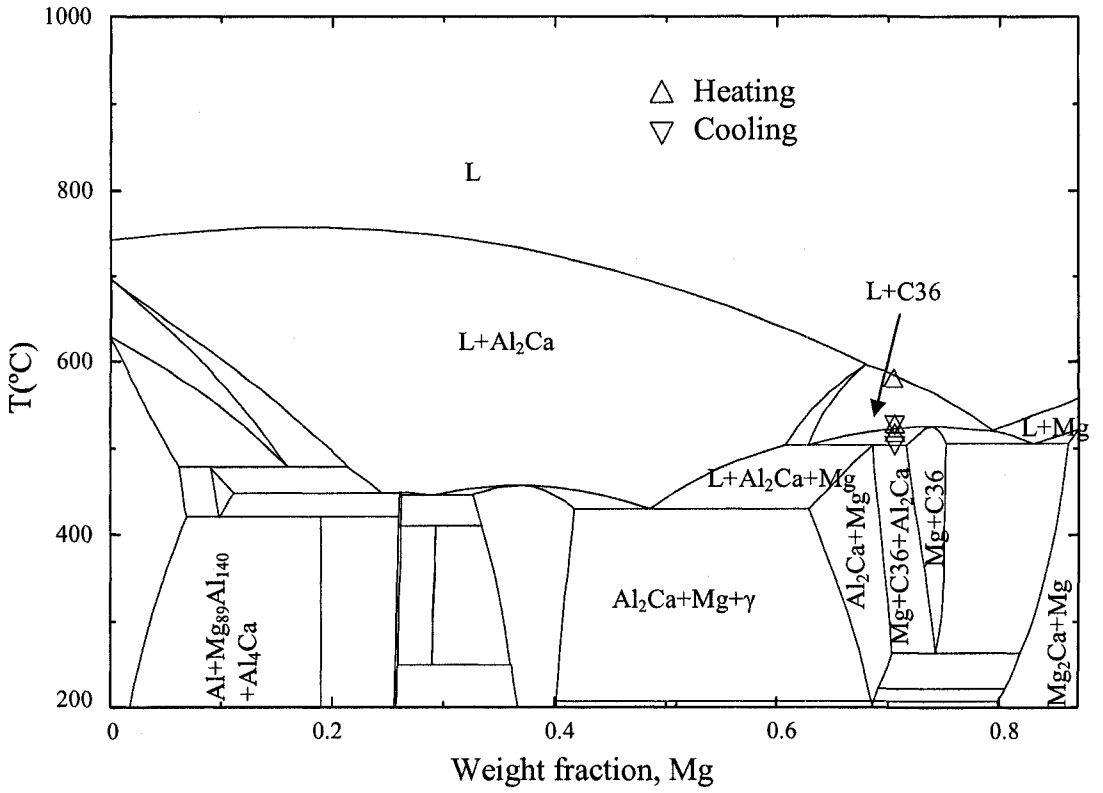

Figure 7.26: *Calculated vertical section at 13 wt.% Ca with DSC signals from heating and cooling curves of sample 8.*

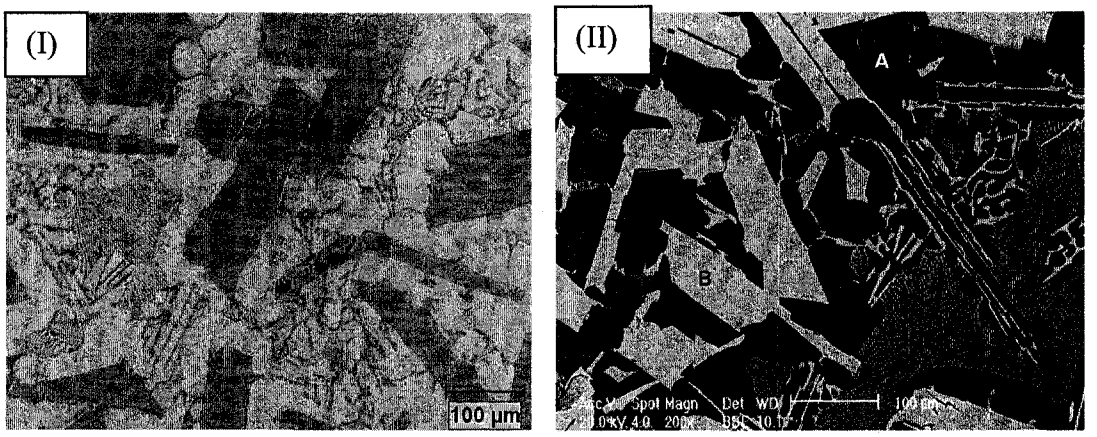

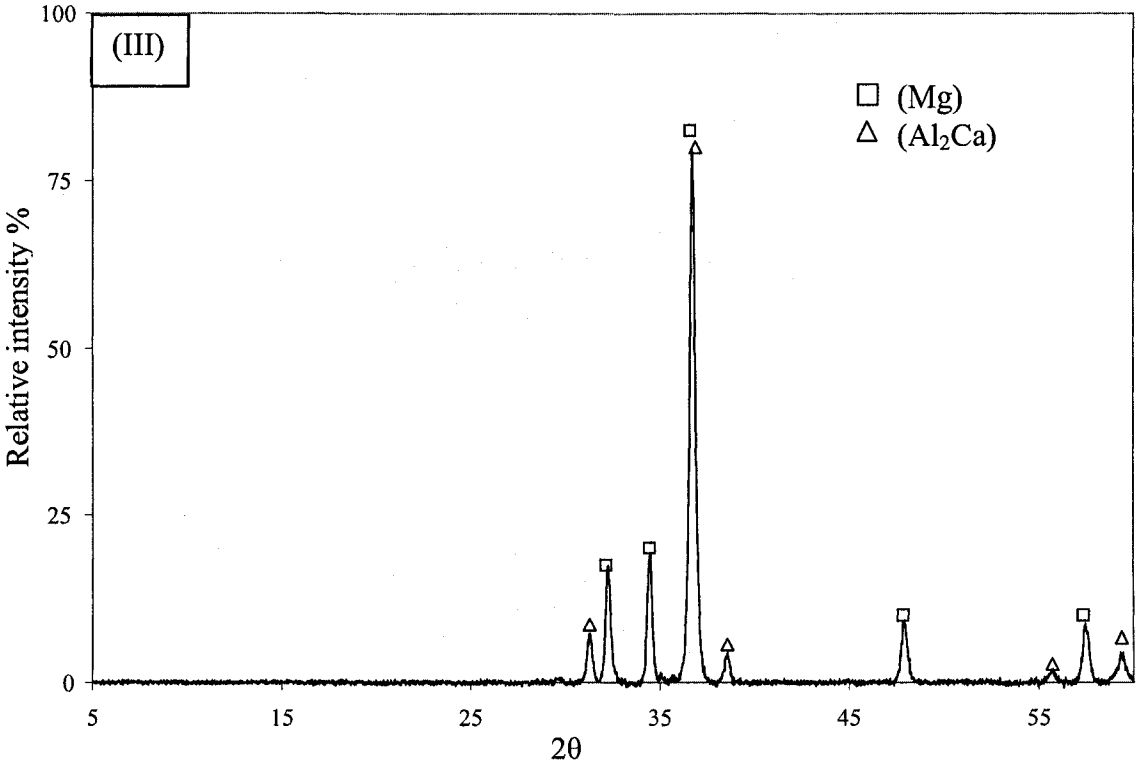

Region	Mg	Al	Ca	Phases
A	98.2±0.1	1.8±0.1	0.0±0.1	(Mg)
B	6.3±0.2	60.4±0.1	33.3±0.1	(Al_2Ca)

(IV)

Figure 7.27: *(I) Optical micrograph; (II) SEM image; (III) XRD pattern and (IV) EPMA analysis of composition 8 (72/15/13 wt.% Mg/Al/Ca).*

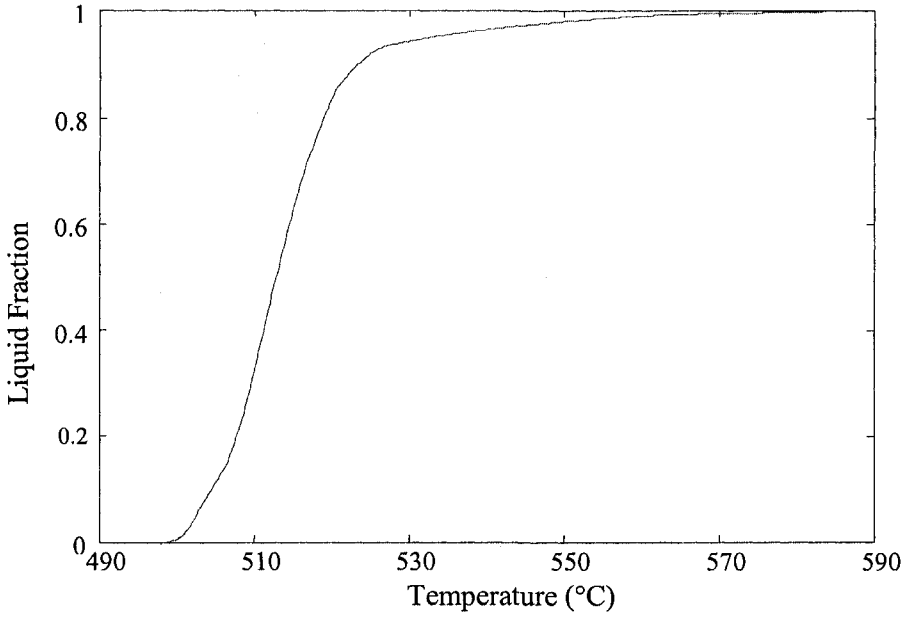

Figure 7.28: *Solidification curve deduced from DSC measurement of sample 8.*

Sample 9 is located in Mg+Mg_2Ca+C36 region as can be seen in Figure 7.1. The DSC spectra of this sample in Figure 7.29 show sharp and narrow peak at 511 and 535°C during heating and cooling, respectively. This is correlated with the ternary invariant transformation and very well supported in the microstructure seen in Figures 7.31(I), whereas, the weak signal corresponds to the liquidus that occurs at 744°C. Labeling the DSC signals on the vertical section in Figure 7.30 shows that the predicted solidus temperature agrees with the measurements, but the predicted liquidus point does not agree.

SEM image in Figure 7.31(I) shows large volume fraction of (Mg_2Ca) and dark area with small volume fraction representing (Mg). Moreover, lamellar structure surrounded with (Mg) and (Mg_2Ca) has been observed in this sample. XRD pattern of this sample identified three phases; (Mg), (Mg_2Ca) and C36 as shown in Figure 7.31(II). Due to the slow kinetics of formation of C36, it was not observed in the microstrucure of

this sample. According to EPMA analysis in Figure 7.31(III), (Mg_2Ca) dissolves 15.9±0.2 at.% Al and (Mg) dissolves 0.7±0.1 at.% Al.

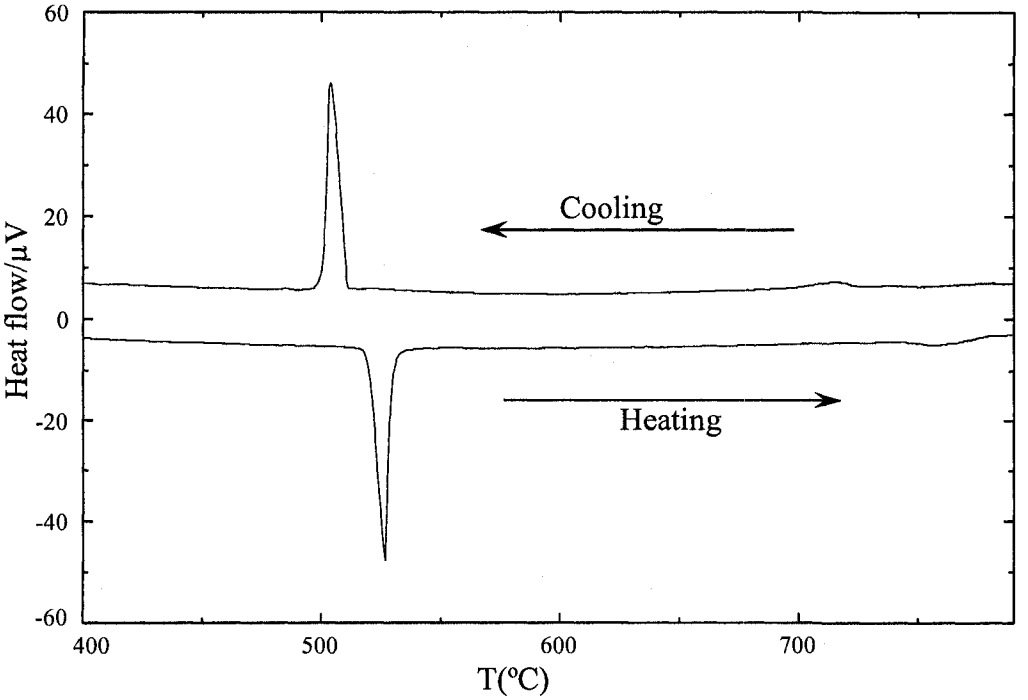

Figure 7.29: *DSC spectra of sample 9 (43.9/26.7/29.4 wt.% Mg/Al/Ca) during heating and cooling.*

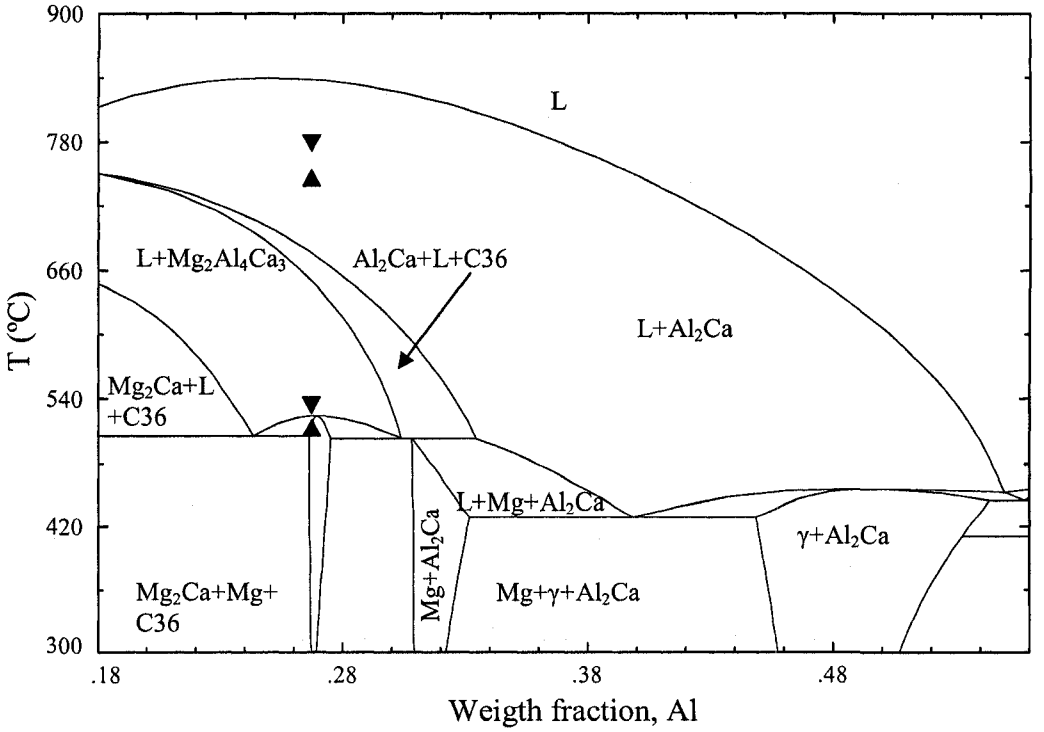

Figure 7.30: *Calculated vertical section at 43.9 wt.% Mg with DSC signals from heating and cooling curves of sample 9.*

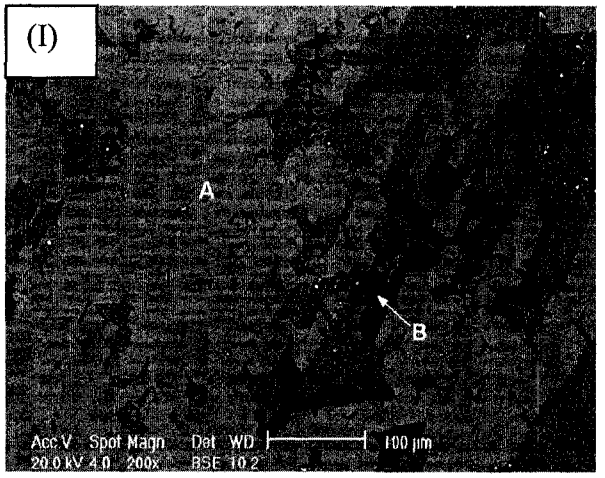

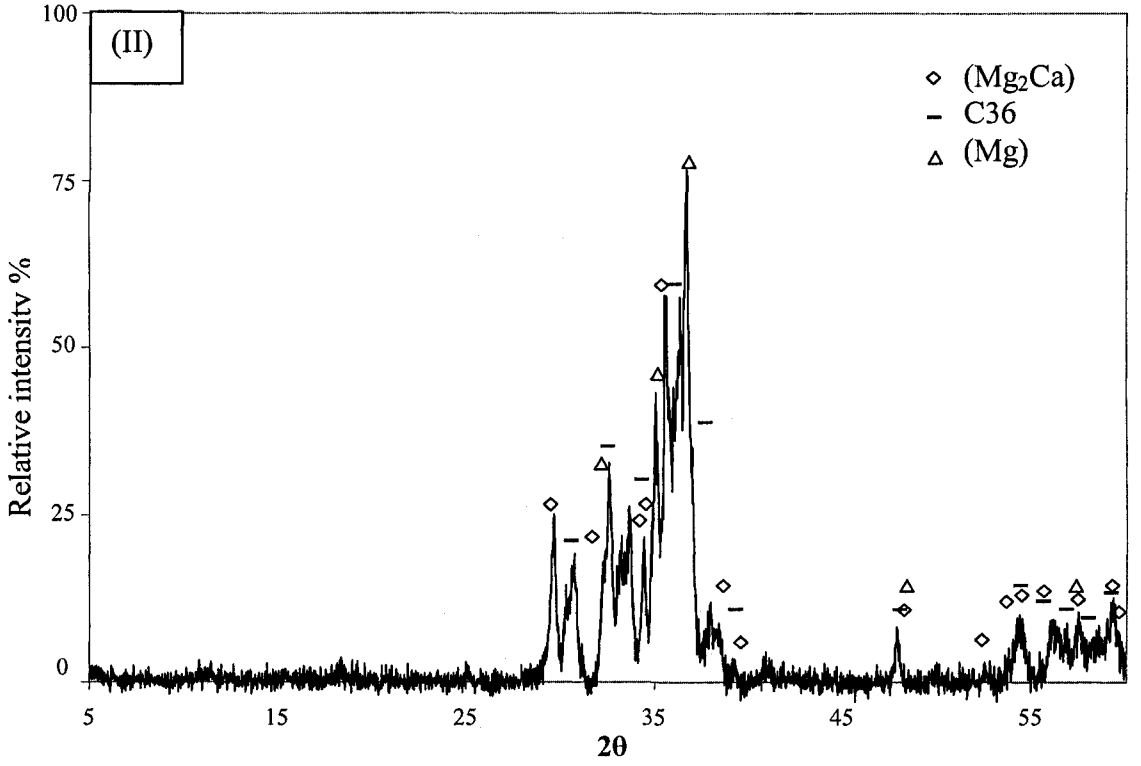

Region	Mg	Al	Ca	Phases
A	50.6±0.2	15.9±0.2	33.5±0.2	(Mg_2Ca)
B	99.2±0.1	0.7±0.1	0.1±0.1	(Mg)

(III)

Figure 7.31: *(I) SEM image; (II) XRD pattern and (III)EPMA analysis of composition 9 (43.9/26.7/29.4 wt.% Mg/Al/Ca).*

Sample 10 (21/39/40 wt.% Mg/Al/Ca), as can be seen in Figure 7.1, is located in Mg+Al_2Ca+C36 phase field. SEM image and EPMA analysis are shown in Figure 7.32. The SEM image in Figure 7.32(I) shows a large precipitates of (Al_2Ca) surrounded by lamellar structure. According to the EPMA analysis in Figure 7.32(II), (Al_2Ca) dissolves 7.2±0.3 at.% Mg at 300°C. Samples 10 is very brittle and oxidized; therefore, it was not possible to study it using DSC and XRD.

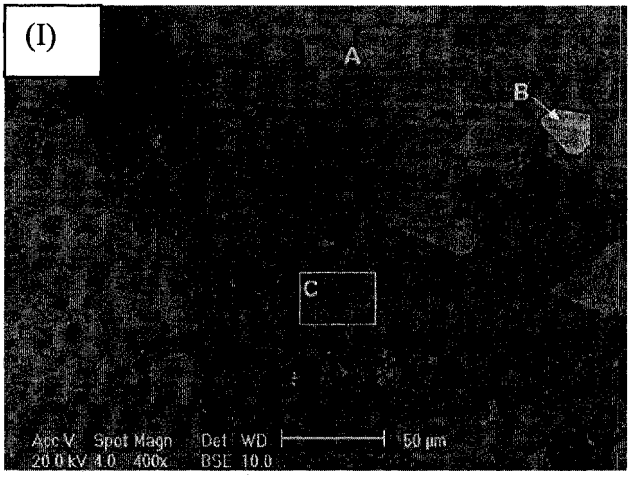

Region	Mg	Al	Ca	Phases
A	7.2±0.3	55.3±0.3	37.5±0.2	Al_2Ca
B	84.4±0.2	6.1±0.1	9.5±0.1	Two phases

(II)

Figure 7.32: *(I) SEM image and (II) EPMA analysis of composition 10 (21/39/40 wt.% Mg/Al/Ca).*

Sample 11 is located in the Mg_2Ca+Al_3Ca_8+C36 phase field as shown in Figure 7.1. SEM image in Figure 7.33(I) shows two distinct phases; C36 and (Mg_2Ca) which are located in regions K and L, respectively. These phases were verified by the XRD and EPMA analysis as can be seen in Figure 7.33(II) and (III). The chemical composition of the new ternary compound C36 is quite close to that reported by Amerioun *et al.* [188] and Suzuki *et al.* [147].

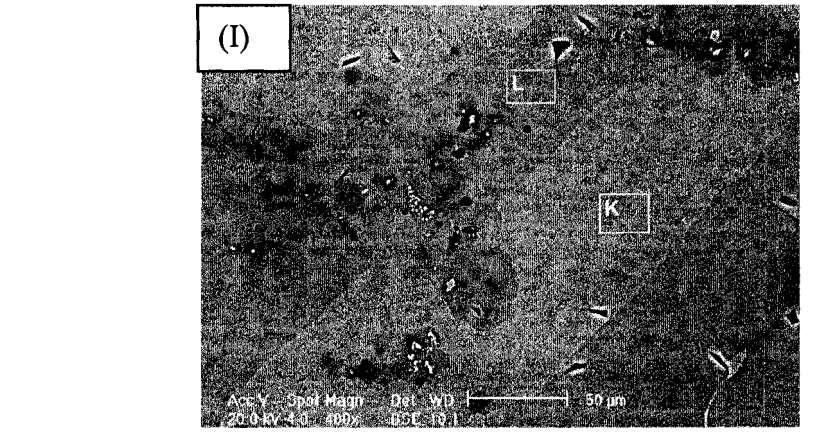

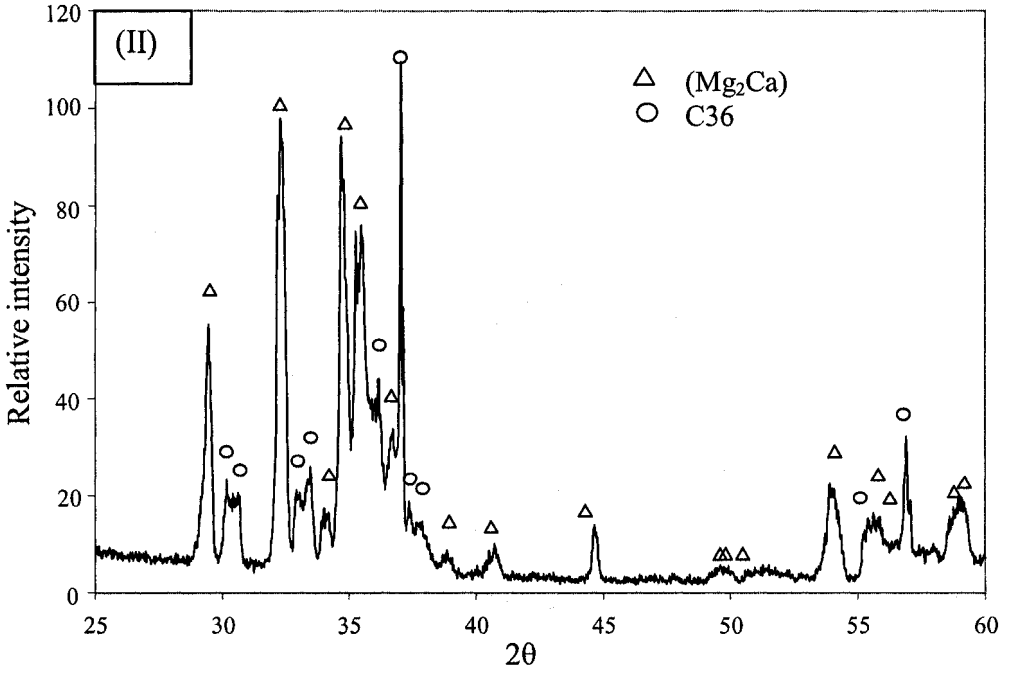

Region	Mg	Al	Ca	Phases
L	51.3±0.7	16.9±0.4	31.8±0.3	(Mg_2Ca)
K	21.3±1.3	45.2±1.3	33.5±0.1	C36

(III)

Figure 7.33: *(I) SEM image; (II) XRD pattern and (II) EPMA analysis of composition 11 (29/23/48 wt.% Mg/Al/Ca).*

To summarize, ternary solubilities of three binary intermetallic compounds in the Mg-Al-Ca system extended into the ternary system have been found and denoted as: (Al_2Ca), (Al_3Ca_8), and (Mg_2Ca) as can be seen in Table 7.1. In this work, the maximum solubility of Mg in Al_2Ca is found to be 8.6 at.%, compared to Gröbner's *et al.* [135]

results as 5.0 at.%. It was also observed that Mg_2Ca dissolved 22.3 at.% Al in accord with Gröbner's *et al.* [135] work who reported 22.0 at.% Al. The binary compound Al_3Ca_8 in the Al-Ca system dissolved 13.5 at.% Mg, compared to Gröbner's *et al.* [135] values as 10.0 at.% Mg.

Table 7.1: *Ternary solubility of the binary compounds in the ternary Mg-Al-Ca system.*

Phase	Solubility of the third element in the binary compounds, at.%		
	[135]	This work	Calculation
Al_2Ca	5.0 at.% Mg	8.6 at.% Mg	7.6
Al_3Ca_8	10.0 at.% Mg	13.5 at.% Mg	12.5
Mg_2Ca	22.0 at.% Al	22.3 at.% Al	15.0

CHAPTER VIII

Conclusions, Contributions and Suggestions for Future Work

8.1 Conclusions

Unlike conventional modeling, the liquids in binary sub-systems of the Mg-Al-Ca-Sr have been modeled using the modified quasichemical model in order to describe properly the influence of short-range ordering. Based on the experimental phase diagram and the thermodynamic properties in the literature, thermodynamic descriptions of the Al-Ca, Al-Sr, Mg-Al, Mg-Sr, Mg-Ca and Ca-Sr binary systems have been obtained. In addition, a thermodynamic database of the Mg-Al-Ca and Mg-Al-Sr ternary systems was constructed by incorporating the experimental findings in this work and the literature. In the Mg-Al-Sr system, ternary solid solubilities of six binary compounds extended into the ternary system; i.e. (Mg_2Sr), ($Mg_{38}Sr_9$), ($Mg_{23}Sr_6$), ($Mg_{17}Sr_2$), (Al_4Sr), and (Al_2Sr), and one ternary compound with stoichiometry $Mg_{58}Al_{38}Sr_4$ has been found. Three binary compounds; i.e. (Al_2Ca), (Al_3Ca_8), and (Mg_2Ca) in the Mg-Al-Ca ternary system dissolve the third component in the ternary system. A new ternary compound with chemical composition $Mg_2Al_4Ca_3$ has been reported. Based on the experimental data from this work, the location of the pertinent solid phases of the Mg-Al-Sr system and Mg-Al-Ca systems at 400 and 300°C, respectively, have been constructed.

The liquidus projection of the Mg-Al-Sr system is divided into fifteen primary crystallization fields: Al_4Sr, Al_2Sr, Al_3Sr_8, Al_7Sr_8, $Mg_{17}Sr_2$, $Mg_{23}Sr_6$, $Mg_{38}Sr_9$, Mg_2Sr, $Mg_{58}Al_{38}Sr_4$, Al, Mg, γ, β, Sr-fcc, and Sr-bcc. The model predicted five saddle points,

eight quasi-peritectics and five ternary eutectics. The calculated liquidus projection of the Mg-Al-Ca system is divided into thirteen primary crystallization fields: Al_4Ca, Al_2Ca, Al_3Ca_8, $Al_{14}Ca_{13}$, Mg_2Ca, Al, Mg, Al, γ, β, $Mg_2Al_4Ca_3$, Ca-bcc, and Ca-fcc. The model predicted four saddle points, four quasi-peritectics, one peritectic and five ternary eutectics.

For the Mg-Ca-Sr system, a comparison between the liquidus projection calculated using random solution model and the modified quasichemical model is presented. The random solution model agrees reasonably well with the experimental phase diagram, but the modified quasichemical model gives better agreement with the experimental thermodynamic data and the experimental phase diagram. Since experimental data on the mutual solubility between Mg_2Ca and Mg_2Sr could not be found in the literature, the Mg-Ca-Sr phase diagram is calculated and compared for the two cases of limited and complete solubility between these two compounds. In the Al-Ca-Sr system, a self-consistent thermodynamic database has been constructed using the modified quasichemical model. The model parameters of the Mg-Ca-Sr and Al-Ca-Sr systems are evaluated by incorporating all experimental data available in the literature.

Phase equilibria in the Mg-Al-Ca and Mg-Al-Sr systems have been studied using thermodynamic modeling coupled with experimental investigations such as thermal analysis using differential scanning calorimetry (DSC), microstructure characterizations using optical and scanning electron microscopy (SEM), and phase identification using XRD and electron probe micro-analyzer (EPMA).

The constructed thermodynamic dbase can be used to predict the effect of adding one of the promising alloying elements to a commercial Magnesium alloys.

8.2 Contributions

In this work thermodynamic modeling of the binary and ternary sub-systems of the Mg-Al-Ca-Sr quaternary system was constructed coupled with key experiments to resolve some issues in the literature and determine the solubility of the binary compounds in the ternary phase diagrams.

- In the current study, a self-consistent database for the Mg-Al-Ca-Sr system, one of the most promising Mg-based alloys for applications in automobile and aerospace industries have been constructed for the first time. Critical evaluations and optimizations of six binary systems namely; Mg-Al, Al-Ca, Mg-Ca, Al-Sr, Al-Ca and Ca-Sr and, four ternary systems: Mg-Al-Ca, Al-Ca-Sr, Mg-Al-Sr and Mg-Ca-Sr systems have been presented based on the experimental phase diagram and the thermodynamic properties which are available in the literature and from the current work.
- A new modeling technique, the modified quasichemical model, has been developed in order to treat the short range ordering in the liquid and permit the composition of maximum short-range ordering in a binary system to be freely chosen. This provides greater flexibility and ease fitting and better treatment of the configurational entropy which accounts for a non-random distribution of atoms.
- The maximum solid solubility of the binary compounds in the Mg-Al-Sr and Mg-Al-Ca systems has been calculated and verified using key experiments. Six binary compounds in the Mg-Al-Sr system extended into the ternary phase diagram and three binary compounds in the Mg-Al-Ca system dissolve the third element in the ternary system.

- Two ternary compounds in the Mg-Al-Sr and Mg-Al-Ca systems have been confirmed and included in the thermodynamic modeling.
- This is the first attempt to construct the ternary phase diagrams of the Mg-Ca-Sr and Al-Ca-Sr systems using the modified quasichemical model. Mg_2Ca and Mg_2Sr Laves phases in the Mg-Ca-Sr system are assumed to form one solid solution in the ternary phase diagram because of the similarity in the atomic size and crystal structure of Ca and Sr atoms.
- The present work has provided a thorough experimental study using thermal analysis and microstructure characterization coupled with thermodynamic calculations for the Mg-Al-Sr and Mg-Al-Ca systems. This provided better understanding of the phase equilibria in these systems.
- The heat transfer model was used to deduce the solidification curve from the DSC measurements.

8.3 Suggestions for Future Work

This study builds a foundation to study multi-component Mg-based alloys. It can be improved by further experimental studies to refine the thermodynamic modeling.

- Further experimental study is required to identify the crystal structure, the stability and homogeneity ranges of the ternary phases such as $Mg_2Al_4Ca_3$ and $Mg_{58}Al_{38}Sr_4$ using Orientation Imaging Microscopy (OIM) and Transmission Electron Microscopy (TEM) with specimen preparation using Focused Ion Beam (FIB).

- In preparing the ternary compounds, samples have to be heat treated for long time (one month at least because of slow kinetics of formation of these compounds).
- Further experimental study is required to identify the extended solubility of the binary compound $Al_{14}Ca_{13}$ in the Mg-Al-Ca system.
- In view of the fact that the atomic size and the crystal structure of Ca and Sr are similar, a possible ternary solubility of the third element in the Al-Ca and Al-Sr binary compounds exist in the Al-Ca-Sr system, and an investigation of the solubility between the Laves phases Mg_2Ca and Mg_2Sr in the Mg-Ca-Sr system is required.
- Experimental work on the Mg-Ca-Sr and Al-Ca-Sr systems is required.

REFERENCES

(1) D. Kramer, "Magnesium, its alloys and compounds," U.S. Geological Survey Open-File Report 01-341. Available on-line: http://pubs.usgs.gov/openfile/of01-341/.

(2) G.V. Raynor, "*The Physical Metallurgy of Magnesium and its Alloys*," Pregamon Press, Oxford, UK, 441, 1959.

(3) I.P. Moreno, T.K. Nandy, J.W. Jones, J.E Allison and T. M. Pollock, "Microstructure and Creep Behavior of a Die Cast Magnesium-rare Earth Alloy," Magnesium Technology 2002, *Proceedings of the Symposium held during the TMS,* Seattle, WA, United States, 111-116, 2002.

(4) R. Ninomiya, T. Ojiro and K. Kubota, "Improved Heat-Resistance of Mg-Al Alloys By the Ca Addition," *Acta Metallurgica Materialia*, 43(2), 669-674, 1995.

(5) Z. Zhang, A. Couture, "An Investigation of the Properties of Mg-Al-Zn Alloys," *Scripta Materialia*, 39(1), 45-53, 1998.

(6) C. Blawert, N. Hort, U.K. Kainer, "Automotive Applications of Magnesium and its Alloys," *Transactions of the Indian Institute of Metals*, 57(4), 397-408, 2004.

(7) A.A. Luo, M.P. Balogh and B.R. Powell, "Tensile Creep and Microstructure of Magnesium-Aluminum-Calcium Based Alloys for Powertrain Applications: Part 2 of 2," Society of Automotive Engineers, (*Light Metal Applications for the Automotive Industry: Aluminum and Magnesium*), [Special Publication] SP , 37-45, 2001

(8) K. Maruyama, M. Suzuki and H. Sato, "Creep Strength of Magnesium-based Alloys," *Metallurgical and Material Transaction-A*, 33(3), 875-882, 2002.

(9) W. Blum, P. Zhang, B. Watzinger, B. Grossmann, H. Lipowski and H. Haldenwanger, "Creep Resistance of Die-cast Mg-Al Alloys," *Magnesium alloys 2000*, 141-150, 2000.

(10) W. Blum, P. Zhang, B. Watzinger, B. Grossmann, H. Lipowski and H. Haldenwanger, "Comparative Study of Creep of Die-cast Mg-alloys AZ91, AS21, AS41, AM60, and AE42," *Material Science and Engineering-A*, 319, 735-740, 2001.

(11) B.L. Mordike, "Creep Resistance of Magnesium Alloys," *Material Science and Engineering-A*, 324(1-2), 103-112, 2002.

(12) T.J. Ruden, "Structural Design Trends for Magnesium Die Casting," *On Production, Refining, Recrystallization and Fabrication of Light Metals, Proceedings of the International Symposium*, Pergamon, NY, 341-347, 1990.

(13) W.E. Mercer, "Magnesium Die Cast Alloys for Elevated Temperature Applications," *SAE Warrendale*, PA, USA, 1990.

(14) T.G. Basner, M. Evans and D.J. Sakkinen, "Magnesium Casting Alloys," *SAE Technology* 930419, 1993.

(15) F. Hollrigl-Rosta, E. Just, J. Kohler and H.J. Melzer, "Magnesium in Volkswagen," *Light Metal Age,* 78(7-8), 22-23, 1980.

(16) E. Baril, P. Labelle and M.O. Pekguleryuz, "Elevated Temperature Mg-Al-Sr: Creep Resistance, Mechanical Properties, and Microstructure," Noranda, Montreal, Ca, *Journal of Material Science*, 55(11), 34-39, 2003.

(17) X.Z. Wang, "Experimental Investigation of the Mg-Al-Ca Ternary Phase Diagram," Concordia University, Montreal, Canada, *Masters Thesis*, 2005.

(18) F. Sommer, "Association Model for the Description of Thermodynamic Functions of Liquid Alloys II. Numerical Treatment and results," *Zeitschrift fuer Metallkunde*, 73(2), 77-86, 1982.

(19) P.P. Mishra, M. Milanarun, N. Jha, A.K. Mishra, "Thermodynamic Properties of Liquid Glass-Forming Ca-Mg Alloys," *Journal of Alloys and Compounds*, 340(1-2), 108-113, 2002.

(20) D. You, H.S. Schnyders, J.B. Van Zytveld, "Chemical Short-Range Order and the Meyer-Neldel Rule for Liquid Alloys: AlCa and GaAlCa," *Journal of Physics: Condensed Matter*, 9(7), 1407-1415, 1997.

(21) A.D. Pelton and P. Chartrand, "The Modified Quasi - Chemical Model : Part II. Multicomponent Solutions," *Metallurgical and Materials Transactions A: Physical Metallurgy and Materials Science,* 32A(6), 1355-1360, 2001.

(22) A.D. Pelton, S.A. Degterov, G. Eriksson, C. Robelin and Y. Dessureault, "The Modified Quasi-Chemical Model I-Binary Solutions," *Metallurgical and Materials Transactions B: Process Metallurgy and Materials Processing Science* 31B(4), 651-659, 2000.

(23) B.P. Burylev, A.V. Vakhobov and T.D. Dzhuraev, "Thermodynamic Activities of the Components in Aluminium-Barium and Aluminium Strnontium Alloys," *Russian Journal of Physics and Chemistry*, (48), 809-811, 1974.

(24) A.V. Vakhobov, T.T. Dzhuraev and B.N. Vigdorovich, "The Vapor Pressures of Aluminium-Strontium Alloys," *Russian Journal of Physics and Chemistry*, (48), 1306-1308, 1974.

(25) A.V. Vakhobov, K.K. Eshonov and T.D. Dzhuraev, "The Al-Sr-Nd Diagram," *Russian Metallurgy*, (4), 167-172, 1979 (English Translation).

(26) B. Closset, H. Dugas, M. Pekguleryuz and J.E. Gruzleski, "The Aluminum-Strontium Phase Diagram," *Metallurgical Transaction-A,* (17), 1250-1253, 1986.

(27) C. Wolverton, X.Y. Yan, R. Vijayaraghavan and V. Ozolins, "Incorporating First-Principles Energetics in Computational Thermodynamics Approaches," *Acta Material,* (50), 2187-2197, 2002.

(28) B.Q. Huang and J.D. Corbett, "Two New Binary Calcium-Aluminum Compounds: $Ca_{13}Al_{14}$, with a Novel Two-Dimensional Aluminum Network, and Ca_8Al_3, an Fe_3-Al Type Analogue," *Inorganic Chemistry*, (37), 5827-5833, 1998.

(29) D. Kevorkov and R. Schmid-Fetzer, "The Al-Ca system, part 1; Experimental Investigation of Phase Equilibria and Crystal Structures," *Zeitschrift fur Metallkunde*, (92), 946-952, 2001.

(30) G. Bruzzone and F. Merlo, "The Strontium-Aluminum and Barium-Aluminum Systems," *Journal of Less-Common Metals*, (39), 1-6, 1979.

(31) E. Sato, N. Kono, I. Sato and H. Watanbe, "Study on the Phase Diagram of Al-Si-Sr Ternary Alloy System," *Japanese Institute of Light Metal*, (35), 71-78, 1985.

(32) M.D. Hanna and A. Merlo, "Modification of Al-Si Microstructure-The Al-Si-Sr Phase Diagram from 0-20 wt.%Sr and 0-5.0 wt.% Sr," *Materials Research Society Symposium Proceedings, 19(Alloy Phase Diagram),* 411-416, 1983.

(33) C.B. Alcock and V.P. Itkin, "The Al-Sr (aluminum-strontium) System," *Bulletin of Alloy Phase Diagrams*, 10(6), 624-630, 1989.

(34) P. Chartrand and A.D. Pelton, "Critical Evaluation and Optimization of the Thermodynamic Properties and Phase Diagram of the Al-Mg, Al-Sr, Mg-Sr, and Al-Mg-Sr System," *Journal of phase equilibria,* (15), 591-605, 1994.

(35) Y. Zhong, C. Wolverton, Y.A. Chang and Z.K. Liu, "A Combined CALPHAD/first-Principles Remodeling of the Thermodynamics of Al-Sr: Unsuspected Ground State Energies by "rounding up the (un)usual suspects," *Acta Material,* (52), 2739-2754, 2004.

(36) C. Wang, Z. Jin and Y. Du, "Thermodynamic Modeling of the Al-Sr System," *Journal of Alloys and Compounds*, (358), 288-293, 2003.

(37) F. Sommer, J.J. Lee and B. Predel, "Thermodynamic Investigation of Liquid Al-Ca, Al-Sr, Mg-Ni and Ca-Ni Alloys," *Zeitschrift fur Metallkunde*, (74), 100-104, 1983.

(38) Y.O. Esin, V.V. Litovski, S.E. Demin and M.S. Petrushevski, "Enthalpies of Formation of Aluminum-Strontium and Barium-Silicon Melts," *Russian Journal of Physics and Chemistry*, (59), 446, 1985.

(39) S. Srikanth and K.T. Jacob, "Thermodynamic of Aluminum-Strontium Alloys," *Zeitschrift fur Metallkunde*, (82), 675-683, 1991.

(40) L. Donski, "Alloys of Ca with Zn, Al, Ti, Pb, Sn, Bi, Sb and Cu," *Zeitschrift Anorganische und Allgemeine Chemie*, (57), 201-205, 1908.

(41) K. Matsuyama, "On the Equilibrium Diagram of the Al-Ca System," Sci. Reports Tohoku University, (17), 783-789, 1928.

(42) H. Nowotny, E. Wormnes and E. Mohrnheim, "Investigation on the Al-Ca, Mg-Ca and Mg-Zr Systems," *Zeitschrift fuer Metallkunde*, (32), 39-42, 1940.

(43) E.D. Trubnyakova, N.A. Alekseeva, Yu.B. Lyskova, A.V. Vakhobov and I.N. Ganiev, "The Influence of Pr on Solubility of the Alkaline-Earth Metals in Al," *Dokl. Akad. Nauk. Tadzh. SSR*, (22), 672-674, 1979.

(44) G. Falkenhagen and W. Hofmann, "The Effect of High Speed Cooling on the Crystallization and on the Structure of Binary Alloys," *Zeitschrift fuer Metallkunde*, (43), 69-81, 1952.

(45) J.D. Edwards and C.S. Taylor, "Electrical Resistivity of Al-Ca Alloys," *Transaction of American Electrochemistry Society*, (50), 391-397, 1926.

(46) J.C. Jaquet and H. Warlimont, "Room Temperature Properties of Aluminum Alloy with a Microduplex Structure," *Zeitschrift fuer Metallkunde*, (72), 13-20, 1981.

(47) M. Notin, J.C. Gachon and J. Hertz, "Enthalpy of Formation of Al_4Ca and Al_2Ca and of the Liquid Alloys (Aluminum+Calcium)," *Journal of Chemical Thermodynamcis*, 14(5), 425-434, 1982.

(48) M. Notin, J.C. Gachon and J. Hertz, "Thermodynamic Data for Calcium-based Alloys from a New Galvanic Method," *CALPHAD*, 6(1), 49-56, 1982.

(49) E. Velesckis, "Application of Hydrogen Titration Method to a Thermodynamic Investigation of Solid Al-Ca Alloys," *Journal of Less-Common Metals*, (80), 241-255, 1981.

(50) P.V. Kocherov, Yu.M. Gertman and P.V. Geld, "Heats of Formation of Al-Ca Alloys," *Zeitschrift fur Anorganic Chemistry*, (4), 1106-1112, 1959.

(51) S.K. Preto, L.E. Ross, A.E. Martin and M.F. Roche, "Calcium/Iron Sulfide Secondary Cells," *Proceedings Symposium on Electrode Materials and Process for Energy Conversion and Storage*, 77(6), 241-255, 1977.

(52) D. Kevorkov, R. Schmid-Fetzer, A. Pisch, F. Hodaj and C. Colinet, "The Al-Ca System, Part 2: Calorimetric Measurements and Thermodynamic Assessment," *Zeitschrift fur Metallkunde*, (92), 953-958, 2001.

(53) K.T. Jacob, S. Srikanth and Y. Waseda, "Activities, Concentration Fluctuations and Complexing in Liquid Ca-Al Alloys," *Transactions of the Japan Institute of Metals,* (29), 50-59, 1988.

(54) E. Schürmann, C.P. Fünders and H. Litterscheidt, "Vapor Pressure of Ca above Ca- Si, Ca-Al and Ca-Al-Si Alloys," *Arch. Eisenhuttenews*, (46), 473-476, 1975.

(55) K. Ozturk, L.Q. Chen, Z.K. Liu, "Thermodynamic Assessment of the Al-Ca Binary System Using Random Solution and Associate Models," *Journal of Alloys and Compounds*, 340(1-2), 199-206, 2002.

(56) N. Baar, "On the Alloys of Molybdenum with Nickel, Manganese with Thallium, and Calcium with Magneisum, Thallium, Lead, Copper, and Silver," *Z. Anorg. Allg. Chem.*, 70, 362-366, 1911. [From British Library www.bl.uk, "Ca-Mg (Calcium-Magnesium)", Landolt-Bornstein Series IV/5c, pp. 22-25].

(57) M.W. Chase, "Heat of Transition of the Elements," *Bulletin of Alloy Phase Diagrams*, 4(1), 123-124, 1983.

(58) R. Paris, "Contribution on the Ternary Alloys," *Publ. Sci et Tech Ministére Air(France)*, 45, 39-41, 1934.

(59) J.L. Haughton, "Alloys of Magnesium. Part 6–The Construction of the Magnesium-Rich Alloys of Magnesium and Calcium," *Journal of Institute of Metal*, 61, 241-246, 1937.

(60) H. Vosskühler, "The Phase Diagram of Magnesium-Rich Mg-Ca Alloys," *Zeitschrift fur Metallkdune,* 29, 236-237, 1937.

(61) W. Klemm, F. Dinkelacker, "On the Behavior of Magnesium with Calcium, Strontium, and Barium," *Zeitschrift fur Anorganic Chemistry*, 255, 2-12, 1947.

(62) A.A. Nayeb-Hashemi, J.B. Clark, "The Ca-Mg (Calcium-Magnesium) System," *Bulletin of Alloy Phase Diagrams*, 8, 58-65, 1987.

(63) R. Agarwal, J. Lee, H. Lukas and F. Sommer, "Calorimetric Measurements and Thermodynamic Optimization of the Ca-Mg System," *Zeitschrift fur Metallkunde*, 86(2), 103-108, 1995.

(64) F. Sommer, B. Predel and D. Assmann, "Thermodynamic Investigation of Liquid Alloys in the Systems Mg-Ca, Mg-Sr, and Mg-Ba," *Zeitschrift fur Metallkunde*, 68(5), 347-349, 1977.

(65) E.C. Burke, "Solid Solubility of Calcium in Magnesium," *Journal of Metals, Transaction AIME*, 203, 285-286, 1955.

(66) W. Bulian and E. Fahrenhorst, "Solubility of Calcium in Magnesium," *Metallforschung*, 1, 70, 1946.

(67) W. Biltz and G. Hohorst, "Contributions to the Systematic Study of Affinity. XV. the Heats of Formation of the Compounds of Metallic Magnesium with Metallic Zinc, Cadmium, Aluminium and Calcium," *Zeitschrift fur Anorganische und Allgemeine Chemie*, 121(1), 1-24, 1922.

(68) J.F. Smith and R.L. Smythe, "Vapor Pressure Measurements over Calcium, Magnesium, and their Alloy and the Thermodynamics of Formation of $CaMg_2$," *Acta Metallurgica et Materialia*, 7, 261-267, 1959.

(69) P. Chiotti, R.W. Curtis and P.F. Woerner, "Metal Hydride Reaction, II. Reaction of Hydrogen with $CaMg_2$ and $CaCu_5$ and Thermodynamic Properties of the Compounds," *Journal of Less-Common Metals*, 7, 120-126, 1964.

(70) J.E. Davison and J.F. Smith, "Enthalpy of Formation of $CaMg_2$," *Transactions of the Metallurgical Society of* AIME, 242(10), 2045-2049, 1968.

(71) G.J. Gartner, "Application of an Adiabatic Calorimeter to the Determination of the Heats of Fusion and Heats of Formation of Several Metallic Compounds," Thesis, Iowa State University, Ames, Iowa, 1965.

(72) B.P. Burylev, "Thermodynamic Properties of Calcium Based Alloys," Termodin Termokhin Konstanty K.V. Astakhov, Ed., Izd. Nauka, Moscow, USSR, 32-39, 1970.

(73) R.C. King and O.J. Kleppa, "A Thermodynamic Study of Some Selected Laves Phases," *Acta Metallurgica et Materialia*, 12, 87-97, 1964.

(74) V.P. Mashovets and L.V. Puchkov, "Vapour Pressure over Molten Alloys in the System Mg-Ca," *Zhurnal Prikladnoi Khimii*, 38(5), 1009-1014, 1965.

(75) F. Sommer, "Thermodynamic Activities of Liquid Alloys in the System Ca-Mg Using a Modified Ruff Method," *Zeitschrift fur Metallkunde,* 70(8), 545-547, 1979.

(76) A.A. Nayeb-Hashemi and J.B. Clark, "The Mg-Sr (Magnesium Strontium) System," *Bulletin of Alloy Phase Diagrams*, 7(2), 149-155, 1986.

(77) H. Vosskühler, "The Structure of the Magnesium-Rich Alloys of Magnesium and Strontium," *Metallwirtschaft*, 18, 377-378, 1939.

(78) J.W. Brown, "The Strontium-Magnesium Phase System," *Ph.D. Thesis*, Syracuse University, (NY), 1973.

(79) J.P. Ray, "The Strontium-Magnesium Equilibrium Diagram," *Ph.D. Thesis*, Syracuse University, (NY), 1947.

(80) F. Sommer, "Determination of Thermodynamic Activities of Liquid Alloys in the Systems Mg-Sr and Ba-Mg," *Zeitschrift fur Metallkunde*, 71(7), 434-437, 1980.

(81) J.G. Schottmiller, A.J. King and F.A. Kanda, "The Calcium-Strontium Metal Phase System," *Journal of Physical Chemistry,* 62, 1446-1449, 1958.

(82) R.P. Elliott, "Constitution of Binary Alloys," first supplement, New York: McGraw-Hill Book Compound, 1965.

(83) J.F. Smith, O.N. Carlson and R.W. Vest, "Allotropic Modification of Calcium," *Journal of Electrochemistry Society*, 103, 409-413, 1956.

(84) W. Klemm and G. Mika, "Interactions of the Alkaline Earth Metals," *Zeitschrift fur Anorganische Allgemeine Chemie*, 248, 155-166, 1941.

(85) D.T. Peterson and V.G. Fattore, "Calcium-Calcium Hydride Phase System," *Journal of Physical Chemistry*, 65, 2062-2064, 1961.

(86) A.J. King, "X-Ray Study of the Calcium-Strontium Alloy Series," *Journal of American Chemistry Society*, 64, 1226-1227, 1942.

(87) C.B. Alcock, V.P. Itkin, "The Ca-Sr (Calcium-Strontium) System," *Bulletin of Alloy Phase Diagrams*, 7(5), 455-457, 1986.

(88) B. Predel and F. Sommer, "Thermodynamic Investigations of the Systems Calcium-Strontium, Calcium-Barium, and Strontium-Barium," *Physical of Condensed Matter*, 17(4), 249-265, 1974.

(89) J.L. Murray, "The Al-Mg (Aluminum-Magnesium) System," *Bulletin of Alloy Phase Diagrams*, 3(1), 60-74, 1982.

(90) M. Kawakami, "On the Equilibrium Diagram of the Aluminum-Magnesium System," Sci. Rep. Tohoku Univ., 727-747, 1936.

(91) G. Siebel and H. Vosskuehler, "Determination of the Solubility of Magnesium in Aluminum," *Zeitschrift fur Metallkdune*, 31(12), 359-362, 1939.

(92) N.S. Kurnakov and V.I. Micheeva, "On the properties of the Solid Solutions of Aluminum and Magnesium in the Al-Mg system," *Izv. Sekt. Fiz-Khim. Anal.*, 13, 201-208, 1940.

(93) N.S. Kurnakov and V.I. Micheeva, "Transformation in the Middle Portion of the System Al-Mg," *Izv. Sekt. Fiz-Khim. Anal.*, 13, 209-224, 1940.

(94) E. Butchers and W. Hume-Rothery, "On the Constitution of Aluminum-Magnesium-Zinc Alloys: The Solidus," *Journal of Institute of Metals*, 71, 291-311, 1945.

(95) W. Stiller and H. Hoffmeister, "Determination of Liquid-Solid Phase Equilibria of Aluminum-Magnesium-Zinc Alloy," *Zeitschrift fur Metallkdune*, 70(12), 167-172, 1979.

(96) E. Shcrmann and H.J. Voss, "Melting Equilibria of the Binary System of Magnesium-Aluminum," *Giesereiforschung*, 33, 43-46, 1981.

(97) N.C. Goel, Cahoon J.R., Mikkelsen, "An Experimental Technique for the Rapid Determination of Binary Phase Diagram: the Al-Mg System," *Metallurgical Transactions A.*, 20(A), 197-203, 1998.

(98) E. Schürmann and A. Fischer, "Melting Equilibria in the Ternary System of Aluminum-Magnesium-Silicon: I. Binary System of Aluminum-Magnesium; II. Binary System of Magnesium-Silicon," *Giessereiforschung*, 29(3), 107-113, 1977.

(99) E. Schürmann and I.K. Geisler, "Phase Equilibriums in the Solid Condition of the Aluminum- rsp. The Magnesium-rich Corner of the Ternary System of Aluminum-Lithium-Magnesium. Part 4. Phase Equilibriums in the Solid Condition of the Ternary System of Aluminium-Lithium-Magnesium," *Giessereiforschung*, 32(4), 167-170, 1980.

(100) P. Liang, H.L. Su, P. Donnadieu, M. Harmelin, A. Quivy, "Experimental Investigation and Thermodynamic Calculation of the Central Part of the Mg-Al Phase Diagram", *Z. Metallkdune*, 89(8), 536-40, 1998.

(101) N. Saunders, "A Review and Thermodynamic Assessment of the Al-Mg and Mg-Li Systems," *CALPHAD*, 14(1), 61-70, 1990.

(102) T. Czeppe, W. Zakulski, E. Bielanska, "Study of the Thermal Stability of Phases in the Mg-Al System," *Journal of phase equilibria*, 24(3), 294-254, 2003.

(103) Y. Zuo, Y.A. Chang, "Thermodynamic Calculation of the Al-Mg Phase Diagram", *CALPHAD,* 17(2), 161-174, 1993.

(104) K. Ozturk, A. Luo, "Phase Identification and Microanalysis in the Mg-Al-Ca Alloy System," *The Minerals and Materials Society (TMS)*, 195-200, 2003.

(105) G.R. Belton and Y.K. Rao, "A Galvanic Cell Study of Activities in Mg-Al Liquid Alloys," *Transactions of the American Institute of Mining, Metallurgical and Petroleum Engineers*, 245, 2189-2193, 1969.

(106) G.I. Batalin, V.E. Soloskij and T.B. Shimanskaja, "Enthalpies of Mixing Liquid Alloys of Aluminum with Magnesium and Antimony," *Ukrainskii Khimicheskii Zhurnal*, 37(4), 397, 1971.

(107) Y.J. Bhatt and S.P. Garg, "Thermodynamic Study of Liquid Aluminum-Magnesium Alloys by Vapor Pressure Measurements," *Metallurgical Transactions B: Process Metallurgy*, 7B(2), 271-275, 1976.

(108) J.M. Juneja, K.P. Abraham and G.N. Iyengar, "Thermodynamic Study of Liquid Magnesium-Aluminium Alloys by Vapour Pressure Measurement Using the Boiling Point Method," *Scripta Metallurgica*, 20(2), 177-180, 1986.

(109) B.L. Tiwari, "Thermodynamic Properties of Liquid Al-Mg Alloys Measured by the emf Method," *Metallurgical Transactions A*, 18, 1645-1651, 1987.

(110) R. Agarwal and F. Sommer, "Calorimetric Measurements of Liquid Al-Mg Alloys," *Zeitschrift fur Metallkdune*, 82, 118-120, 1991.

(111) V.N. Eremenko and G.M. Lukashenko, "Thermodynamic Properties of Liquid Solutions in the Magnesium-Aluminum System," *Ukrainskii Khimicheskii Zhurnal*, 28, 462-466, 1962.

(112) A. Schneider and E.K. Stoll, "Metal Vapour Pressure. I. Vapor Pressure of Magnesium over Aluminum-Magnesium Alloys," *Zeitschrift fur Elektrochemie und Angewandte Physikalische Chemie*, 47, 519, 1941.

(113) M.M. Tsyplakova and Kh.L. Strelets, "Thermodynamic Properties of a Magnesium-Aluminium System Studied by an emf Method," *Zhurnal Prikladnoi Khimii USSR.*, 42(11), 2498-2503, 1969.

(114) M.Y. Vyazner, A.G. Morachevskii and A.Yu. Taits, "Thermodynamic Properties of Magnesium-Aluminium System Molten Alloys," *Zhurnal Prikladnoi Khimii*, 44, 722-726, 1971.

(115) R. Gradinger and P. Stolfig, "Magnesium Wrought Alloys for Automotive Applications," Magnesium Technology 2003, Proceedings of the Symposium held during the Annual Meeting 2003 TMS, 231-236, 2003.

(116) S. Das, JOM 55 (11) (2003), p. 22-26.

(117) M. Pekguleryuz, E. Baril, P. Labelle and D. Argo, "Creep Resistant Mg-Al-Sr Alloys," *Journal of Advance Materials*, 35(3), 32-38, 2003.

(118) E. Baril, P. Labelle and A. Fischerworring-Bunk, "AJ (Mg-Al-Sr) Alloy System used for New Engine Block," Society of Automotive Engineers, SAE World Congress, 01-0659, SP. 1845, 97-106, 2004.

(119) A. Prince and N. Nikitina, "Aluminum-Magnesium-Strontium, Ternary Alloys," *A Comprehensive Compendium of Elevated Constitutional Date and Phase Diagram*, (16), 413-425, 1988.

(120) M.M. Makhmudov, A.A. Vakhobov, T.D. Dzhuraev and I.N. Ganiev, "The Combined Solubility of the Components in the Mg-rich and Al-rich Regions of the Mg-Al-Sr System," *Dokl. Akad. Nauk Tadzh.* SSR, (23), 25-28, 1980.

(121) M.M. Makhmudov, A.A. Vakhobov and T.D. Dzhuraev, "Liquidus Surface of the Al and Mg-Phases of the Mg-Al-Sr Diagram," *Dokl. Akad. Nauk Tadzh.* SSR, (24), 435-438, 1981.

(122) M.M. Makhmudov, A.A. Vakhobov and T.D. Dzhuraev, "Examination of the Quasibinary Sections of the Mg-Al-Sr System," *Izvestiys Akademii Nauk* SSSR, (6), 122-124, 1982 (English Translation).

(123) M.M. Makhmudov, A.A. Vakhobov and T.D. Dzhuraev, "Determination of the Liquidus Surfaces in the Sr-Mg_2Sr-Al_4Sr System," *Izvestiys Akademii Nauk* SSSR, (6), 41-143, 1982 (English Translation).

(124) B. Jing, S. Yangshan, X. Shan, X. Feng and Z. Tianbai, *Material Science and Engineering A.*, 412(1-2), 181-188, 2006.

(125) F. Czerwinski and A. Zielinska-Lipiec, "The Microstructure Evolution During Semisolid Molding of a Creep-Resistant Mg-5Al-2Sr Alloys," *Acta Materialia*, 53(12), 3433-3444, 2005.

(126) K. Ozturk, "Investigation in Mg-Al-Ca-Sr System by Computational Thermodynamics Approach coupled with First-Principles Energetics and Experiments," *Ph.D. Thesis*, The Pennsylvania State University, 2004.

(127) A. Janz, J. Gröbner, D. Mirkovic, M. Medraj, J. Zhu, Y.A. Chang, R. Schmid-Fetzer, "Experimental Study and Thermodynamic Calculation of Al-Mg-Sr Phase Equilibria," *Intermetallics*, 15(4), 506-519, 2007.

(128) M.A. Parvez, E. Essadiqi and M. Medraj, "Thermal Analytical Investigations of Ternary Mg-Al-Sr System by DSC," *Proc. CSME Forum*, 829-838, 2004 (Canada).

(129) M.A. Parvez, X. Wang, E. Essadiqi and M. Medraj, "Experimental investigation of the Equilibria in Mg-Al-(Ca,Sr) Systems," *Proceedings of Minerals, Metals and Materials Society* (TMS), 179-184, 2005.

(130) M.A. Parvez, M. Medraj, E. Essadiqi, A. Muntasar and G. Dénès, "Experimental Study of the Ternary Magnesium-Aluminum-Strontium System," *Journal of Alloys Compounds*, 402 (1-2), 170-185, 2005.

(131) M. Medraj, M.A. Parvez, E. Essadiqi and J. Li, "New Phases in the Mg-Al-Sr System", *Journal of Materials Science Forum*, 539-543, 1620-1625, 2006.

(132) M. Aljarrah, M.A. Parvez, E. Essadiqi, J. Li and M. Medraj, "Microstructural Characterization of Mg-Al-Sr Alloys", *Journal of Science and Technology of Advanced Materials,* 8(4), 237-248, 2007.

(133) F. Pan, M. Yang and Y. Ma, "Development of New Types of Magnesium Alloys Containing Sr or RE Elements," *Material Science*, 561-565, 191-197, 2007.

(134) M. Yang, F. Pan, J. Zhang and J. Zhang, "An Analysis of the Development and Applications of Current and New Mg-Al Based Elevated Temperature Magnesium Alloys," *Material Science*, 488-489, 923-926, 2007.

(135) J. Gröbner, D. Kevorkov, I. Chumak, R. Schmid-Fetzer, "Experimental Investigation and Thermodynamic Calculation of Ternary Al-Ca-Mg Phase Equilibria," *Zeitschrift fuer Metallkunde*, 94(9), 976-982, 2003.

(136) O. Beffort, and C. Hausmann, "The Influence of Ca-Additions on the Mechanical Properties of T300-C-fibre/Mg (Al) Metal Matrix Composites," *Magnesium Alloys and their Applications*, edit. K.U. Kainer, 215-220, 2000.

(137) M.O. Pekguleryuz, and E. Baril, "Creep Resistant Magnesium Die-Casting Alloys Based on Alkaline Earth Elements," *Materials Transactions*, 42(7), 1258-1267, 2001.

(138) A.A. Luo, M.P. Balogh, B.R. Powell, "Creep and Microstructure of Magnesium-Aluminum-Calcium Based Alloy," *Metallurgical and Materials Transactions A*, 33(3), 567-574, 2002.

(139) M.O. Pekguleryuz and J. Renaud, "Creep Resistance in Mg-Al-Ca Casting Alloys," *Magnesium Technology 2000*, US, 279-84, 2000.

(140) J.A. Catterall and R.J. Pleasance, "Constitution of Magnesium-Rich Magnesium-Aluminum-Calcium Alloys," *Journal of Institute of Metals*, 1817, 189-192, 1957.

(141) K. Ozturk, Yu. Zhong and Z.K. Liu, "Computational Thermodynamics and Experimental Investiagation of Mg-Al-Ca Alloys," Magnesium Technology 2003, TMS, *The Minerals, Metals and Material Society*, US, 113-117, 2003.

(142) V.G. Tkachenko, V.G. Khoruzhaya, K.A. Meleshevich, M.V. Karpets and V.V. Frizel, "Phase Equilibria in Mg-Al-Ca System," *Powder Metallurgy and Metal Ceramics*, 42(5-6), 268-273, 2003.

(143) K. Ozturk, Y. Zhong, A.A. Luo and Z.K. Liu, "Creep Resistance Mg-Al-Ca Alloys: Computational Thermodynamics and Experimental Investigation," *Research summary*, High Temperature Magnesium, 55(11), 40-45, 2003.

(144) A. Zuzuki, N.D. Saddock, J.W. Jones and T.M. Pollock, "Structure and Transition of Eutectic (Mg, $Al)_2Ca$ Laves Phase in a Die-cast Mg-Al-Ca Base Alloy", *Scripta Material*, 51(10), 1005-1010, 2004.

(145) F. Islam and M. Medraj, "Thermodynamic Evaluation and Optimization of the Mg-Al-Ca System," *Journal of Canadian Metallurgical Quarterly*, 44(4), 523-535, 2005.

(146) M. Aljarrah, M. Medraj, X. Wang, E. Essadiqi, G. Dénès, and A. Muntasar, "Experimental Investigation of the Mg-Al-Ca System," *Journal of Alloys and Compounds*, 438(1-2), 131-141, 2007.

(147) A. Zuzuki, N.D. Saddock, J.W. Jones and T.M. Pollock, " Phase Equilibria in the Mg-Al-Ca System at 773 and 673K," *Metallurgical and Materials Transactions A*, 37(A), 975-983, 2006

(148) Y. Zhong, J.O. Sofo, A.A. Luo and Zi Kui Liu, "Thermodynamic modeling of the Mg-Sr and Mg-Ca-Sr systems," *Journal of Alloys and Compounds*, 421(1-2), 172-178, 2006.

(149) M.A. Parvez, "Experimental Investigation of the Ternary Mg-Al-Sr System," Concordia University, Montreal, Canada, *Masters Thesis*, 2005.

(150) G.W. Hohne, W. Hemminger and H.J. Flammershiem, "Differential Scanning Calorimetry: an introduction for practitioners," Springer-Verlag Berlin Heidelberg, 1996.

(151) W. Hemminger and H. Cammenga, "Methoden der Thermischen Analyse," Springer-Verlag Berlin Heidelberg, 1989.

(152) S.W. Chen and C.C. Huang, "Solidification Curves of Al-Cu, Al-Mg and Al-Cu-Mg Alloys," *Acta Material*, 44(5), 1955-1965, 1996.

(153) A.P. Gray, "*Analytical Calorimetry," (Ed.: R. S. Porter and J. F. Johnson)*, 209-218, 1968.

(154) P. Villars, Pearson's Handbook, "Crystallographic data for Intermetallic Phases," 1997.

(155) W. Klemm and F. Dinkelocker, "Alloys of Magnesium with Calcium Strontium and Barium, *Zeitschrift fur Anorganic. Chemistry*, 255, 2-12, 1947.

(156) M. Aljarrah, U. Aghaulor and M. Medraj, "Thermodynamic assessment of the Mg-Zn-Sr system", *Intermetallics*, 15(2), 93-97, 2007.

(157) A. Suzuki, N.D. Saddock, J.W. Jones, and T.M. Pollock, "Solidification Paths and Eutectic Intermetallic Phases in Mg-Al-Ca Ternary Alloys," *Acta Materillia*, 53(9), 2823-2834, 2005.

(158) Y. Zhong, J. Liu, R.A. Witt, Y.H. Sohn and Z. Kui Liu, "Al_2(Mg,Ca) Phases in Mg-Al-Ca Ternary System: First-Principle and Experimental Identification," *Scripta Materilia*, 55(6), 573-576, 2006.

(159) H. Cao, C. Zhang, J. Zhu, G. Cao, S. Kou, R. Schmid-Fetzer and Y.A. Chang, "A Computational/Directional Solidification Method to Establish Saddle Points on the Mg-Al-Ca Liquidus," Scripta Materilia, 58(5), 397-400, 2008.

(160) A.T. Dinsdale, "SGTE Data for Pure Elements", *CALPHAD,* 15(4), 317-425, 1991.

(161) F. Sommer, "Association Model for the Description of Thermodynamic Functions of Liquid Alloys II. Numerical Treatment and results," *Zeitschrift fuer Metallkunde*, 73(2), 77-86, 1982.

(162) P.P. Mishra, M. Milanarun, N. Jha, A.K. Mishra, "Thermodynamic properties of liquid glass-forming Ca-Mg alloys," *Journal of Alloys and Compounds*, 340(1-2), 108-113, 2002.

(163) D. You, H.S. Schnyders, J.B. Van Zytveld, "Chemical short-range order and the Meyer-Neldel rule for liquid alloys: AlCa and GaAlCa," *Journal of Physics: Condensed Matter*, 9(7), 1407-1415, 1997.

(164) M. Blander and J. Braunstein, "Quasilattice Model of Molten Reciprocal Salt Systems," Annals of the New York Academy of Sciences, 79, 838-852, 1960.

(165) R.H. Fowler and E.A. Guggenhim, "Statistical Thermodynamic," Cambridge University Press, Cambridge, UK, 1939, 350-366.

(166) C.W. Bale, P. Chartrand, S.A. Degterov, G. Eriksson, K. Hack, R. Ben Mahfoud, J. Melançon, A.D. Pelton and S. Petersen, "FactSage Thermochemical Software and Databases," *CALPHAD*, 26 (2), 189–228, 2002.

(167) D. Hanson and M.L. Gayler, "The Constitution of the Alloys of Aluminum and Magnesium," *Journal of Institute of Metals*, 24, 201-232, 1920.

(168) W. Hume-Rothery and G.V. Raynor, "The Constitution of the Mgnesium-Rich Alloys in the Systems Aluminum-Magnesium, Gallium-Magnesium, Indium-Magnesium, and Thallium-Magnesium," *J. Institute of Metals*, 63, 201-226, 1938.

(169) K.A. Bol'shakov, P.I. Fedorov and E.I. Smarina, "β Phase of the Aluminum-Magnesium System," *Zeitschrift fuer Neorganicheskoi Khimii*, 8(6), 1412-1418, 1963.

(170) S. Samson, "The Crystal Structure of the Phase β-Mg_2Al_3," *Acta Crystalline*, 19, 401-413, 1965.

(171) H.M. Tensi, R. Schmid and H. Borchers, "Investigations of the Crystallization During Zone Melting of Rods of Binary Aluminum Alloys with Variable Melting Volume and Different Velocities of the Liquid Zone," *Zeitschrift fuer Metallkde*, 63(1), 22-28, 1972.

(172) E.S. Makarkov, "Crystal Structure of the Gamma Phase of the Systems Al-Mg and Tl-Bi," *Dokl. Akad. Nauk SSSR*, 74(5), 935-938, 1950.

(173) E. Butchers, G.V. Raynor and W. Hume-Rothery, "The Constitution of Magnesium-Manganese-Zinc-Aluminum Alloys in the Range 0-5 per cent Magnesium; 0-2 per cent Manganese; 0-8 per cent Zinc: I. The Liquidus," *Journal of Institute of Metals*, 69, 209-228, 1943.

(174) W.L. Fink and L.A. Willey, "Equilibrium Relations in Alloys of High Purity," *Trans. AIME*, 124, 85-86, 1937.

(175) E. Schmid, G. Siebel, "Mixed-Crystal Formation with Single and Polycrystalline Materials," *Zeitschrift fuer Physik*, 85, 37-41, 1933.

(176) B. Predel and K. Hulse, "Metastable Phases in the Aluminum-Magnesium System," *Zeitschrift fuer Metallkunde*, 69(11), 690-696, 1978.

(177) M.I. Zackarowa and W.K. Tschikin, "Kinetics of the Decomposition of Al-Mg Solutions," *Zeitschrift fuer Physik*, 95, 769-774, 1935.

(178) J.L. Haughton and R.J. Payne, "Alloys of Magnesium: Part III-Constitution of the Magnesium-Rich Alloys Containing Aluminum and Cadmium," *Journal of Institute of Metals*, 57, 287-298, 1935.

(179) P. Saldau and M. Zamotorin, "The Solubility of Aluminum in Magnesium in the Solid State of Different Temperatures," *Journal of Institute of Metals*, 48, 221-226, 1932.

(180) W. Bungardt and F. Bollenrath, "On the Diffusion of Magnesium in Aluminum," *Zeitschrift fuer Metallkunde*, 11, 377-383, 1938.

(181) E.H. Dix and F. Keller, "Equilibrium Relations in Aluminum-Magnesium Alloys," *Zeitschrift fuer Metallkunde*, 21(6), 205-206, 1929.

(182) V.N. Eremenko and G.M. Lukashenko,"Thermodynamic Properties of Liquid Solutions in the Magnesium-Aluminum System," *Ukrainskii Khimicheskii Zhurnal*, 28, 462-466, 1962.

(183) E.E. Lukashenko and A.M. Pogodayev,"Thermodynamics of Magnesium-Aluminum Molten Alloys, " *Izvestiya Akademii Nauk SSSR, Metally*, 5, 91-96, 1971.

(184) V.P. Kazimov and G.I. Batalin,"Calculation of Thermodynamic Properties of Al-Mg Melts by the Pseudopotential Method," *Ukrainskii Khimicheskii Zhurnal*, 49(8), 887-888, 1983.

(185) Z. Moser, W. Zakulski, K. Rzyman, W. Gasior and Z. Panek,"New Thermodynamic Data for Liquid Aluminum-Magnesium-Alloys from emf Vapor Pressures, and Calorimetric Studies, " *Journal of Phase Equilibria*, 19(1), 38-47, 1998.

(186) W. Kraus and G. Nolze, "PowderCell for Windows," Federal Institute for Material, Research and Testing Berlin, 1999, Version 2.3.

(187) F. Kohler, "Estimation of the Thermodynamic Data for a Ternary System from the Corresponding Binary Systems," *Monatshefte fuer Chemie*, 91, 738-740, 1960.

(188) S. Amerioun, S.I. Simak, and U. Haeussermann, "Laves-phase structural changes in the system CaAl2-xMgx," *Inorganic Chemistry*, 42(5), 1467-1474, 2003.

(189) G.W. Toop, Trans. AIME 233 (1965) 850-854.

(190) D. Porter and K. Easterling, "Phase Transformations in Metals and Alloys," UK, T.J. Press Ltd., Padstow, Cornwall, 1991.

(191) M. Aljarrah and M. Medraj, "Thermodynamic Assessment of the Phase Equilibria in the Al-Ca-Sr System using the Modified Quasichemical Model," *Journal of Chemical Thermodynamics*. (In press 2007).

(192) M. Aljarrah and M. Medraj, "Thermodynamic Modeling of the Mg-Ca, Mg-Sr Ca-Sr and Mg-Ca-Sr Systems using the Modified Quasichemical Model," *CALPHAD*. (In press 2007).

(193) W.J. Boettinger, U.R. Kattner and J.H. Perepexko, "DTA and Heat-Flux DSC Measurements of Alloy Melting and Freezing," Special Publication 960-15, November 2006.

(194) A. Hammami, and A.K. Mehrotra, "Non-isothermal crystallization kinetics of binary mixtures of *n*-alkanes: ideal eutectic and isomorphous systems," *Fuel* 75(4): 500, 1992.

Appendix

A-1 Crystallographic Data of Al_2Sr

Table A-1: *Crystal Structure data of Al_2Sr.*

Structure	Rhombic		
Spacegroup	Cu_2Ce		
Spacegroup number	227		
Lattice parameter (Å)	a	b	c
	8.325(5)	8.325(5)	8.325(5)
Angles	α	β	γ
	90.00	90.00	120.00
Atoms in unit cell	24		

Table A-2: *Atoms positions in the unit cell of Al_2Sr [154].*

Atom	Wyckoff position	x	y	z
Sr	8a	0	0	0
Al	16d	0.625	0.625	0.625

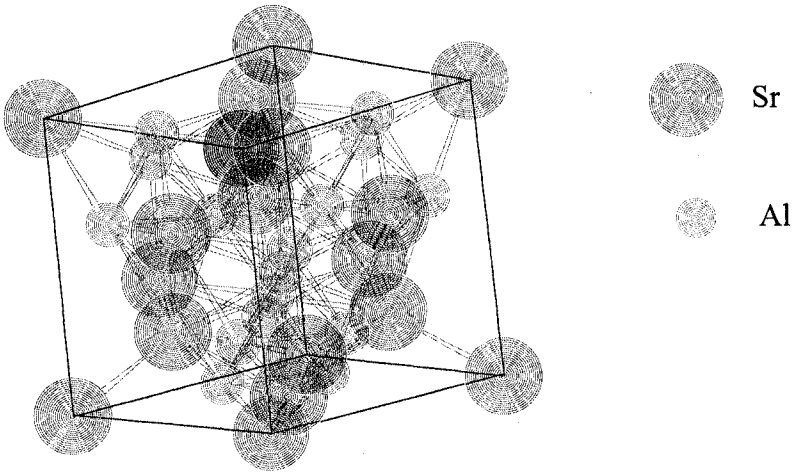

Figure A-1: *Al_2Sr unit cell.*

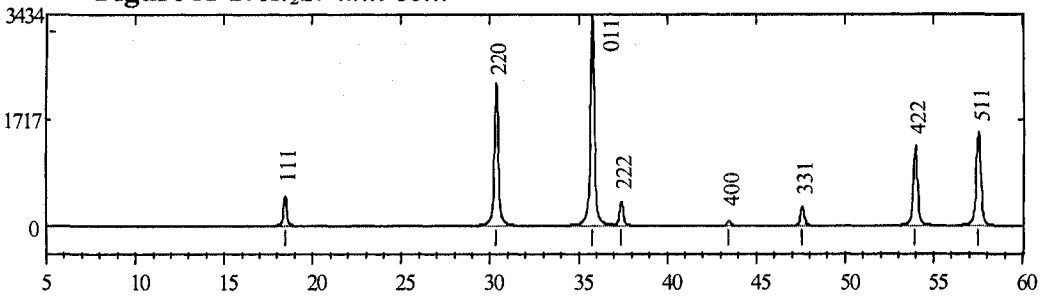

Figure A-2: *Calculated XRD diffraction pattern for Al_2Sr.*

A-2 Crystallographic Data of Al_4Sr

Table A-3: *Crystal Structure data of Al_4Sr.*

Structure	Tetragonal		
Structure type	Al_4Ba		
Spacegroup number	139		
Lattice parameter (Å)	a	b	c
	4.459	4.459	11.07
Angles	α	β	γ
	90.00	90.00	90
Atoms in unit cell	19		

Table A-4: *Atoms positions in the unit cell of Al_4Sr [156].*

Atom	Wyckoff position	x	y	z
Al	4e	0	0	0.3800
Sr	2a	0	0	0

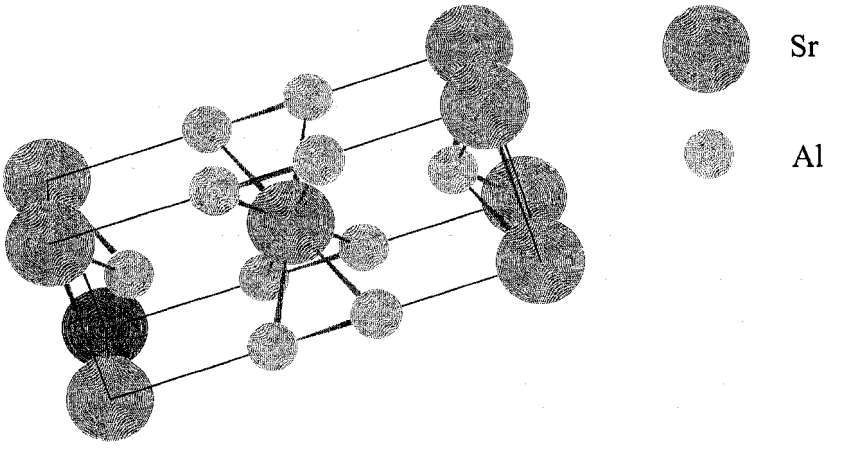

Figure A-3: *Al_4Sr unit cell.*

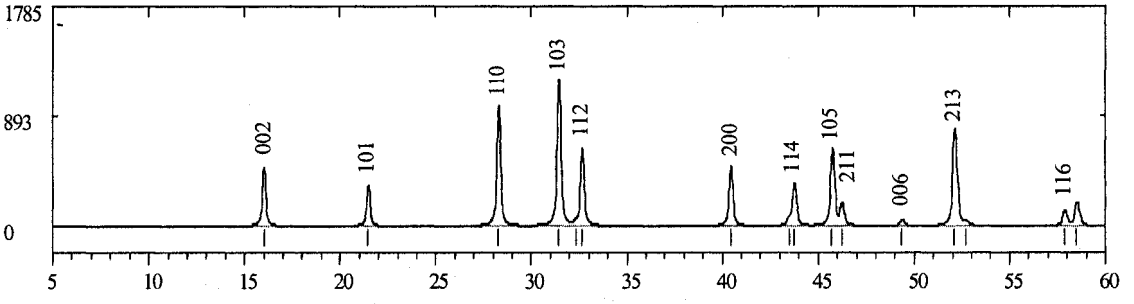

***Figure A-4**: Calculated XRD diffraction pattern for Al_4Sr.*

A-3 Crystallographic Data of Mg_2Sr

Table A-5: *Crystal Structure data of Mg_2Sr [156].*

Structure	Hexagonal		
Structure type	Mg_2Zn		
Spacegroup number	194		
Lattice parameter (Å)	a	b	c
	6.426	6.426	10.473
Angles	α	β	γ
	90	90	120
Atoms in unit cell	21		

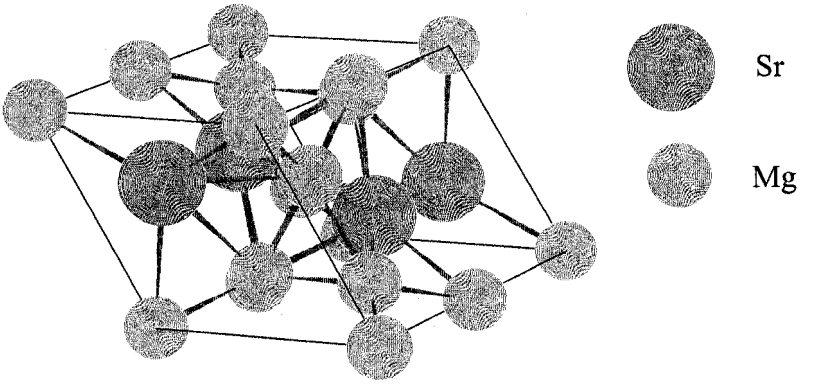

Figure A-5: *Mg_2Sr unit cell.*

A-4 Crystallographic Data of $Mg_{17}Sr_2$

Table A-6: *Crystal Structure data of $Mg_{17}Sr_2$.*

Structure	Hexagonal		
Structure type	$Ni_{17}Ti_2$		
Spacegroup number	194		
Lattice parameter (Å)	a	B	c
	10.535	10.535	10.356
Angles	α	β	γ
	90	90	120
Atoms in unit cell	42		

Table A-7: *Atoms positions in the unit cell of $Mg_{17}Sr_2$ [156].*

Atom	Wyckoff position	x	y	z
Sr1	2b	0	0	0.25
Sr2	2d	0.3333	0.6667	0.75
Mg1	4f	0.3333	0.6667	0.1041
Mg2	6g	0.5	0	0
Mg3	12j	0.3283	0.9627	0.25
Mg4	12k	0.1652	0.3305	0.9805

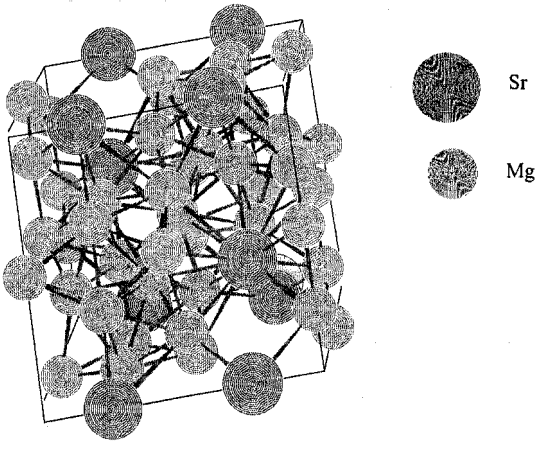

Figure A-6: *$Mg_{17}Sr_2$ unit cell.*

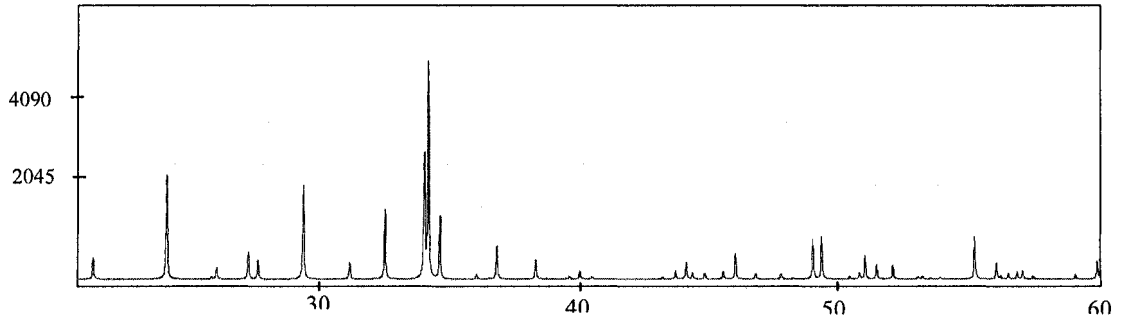

Figure A-7: *Calculated XRD diffraction pattern for $Mg_{17}Sr_2$.*

A-5 Crystallographic Data of $Mg_{38}Sr_9$

Table A-8: *Crystal Structure data of $Mg_{38}Sr_9$.*

Structure	Hexagonal		
Structure type	$Mg_{38}Sr_9$		
Spacegroup number	194		
Lattice parameter (Å)	a	b	c
	10.5	10.5	28.251
Angles	α	β	γ
	90	90	120

Table A-9: *Atoms positions in the unit cell of $Mg_{38}Sr_9$ [156].*

Atom	Wyckoff position	x	y	z
Mg1	4e	0	0	0.1575
Mg2	4f	0.3333	0.6667	0.0378
Mg3	4f	0.3333	0.6667	0.1426
Mg4	4f	0.3333	0.6667	0.6465
Mg5	6g	0.5	0	0
Mg6	12j	0.9611	0.8022	0.25
Mg7	6h	0.5312	0.0624	0.25
Sr1	12k	0.2337	0.4674	0.5547
Mg8	12k	0.5037	0.0074	0.617
Mg9	12k	0.1674	0.3348	0.6533
Mg10	12k	0.1743	0.3486	0.1898
Sr2	12k	0.1362	0.2724	0.0621

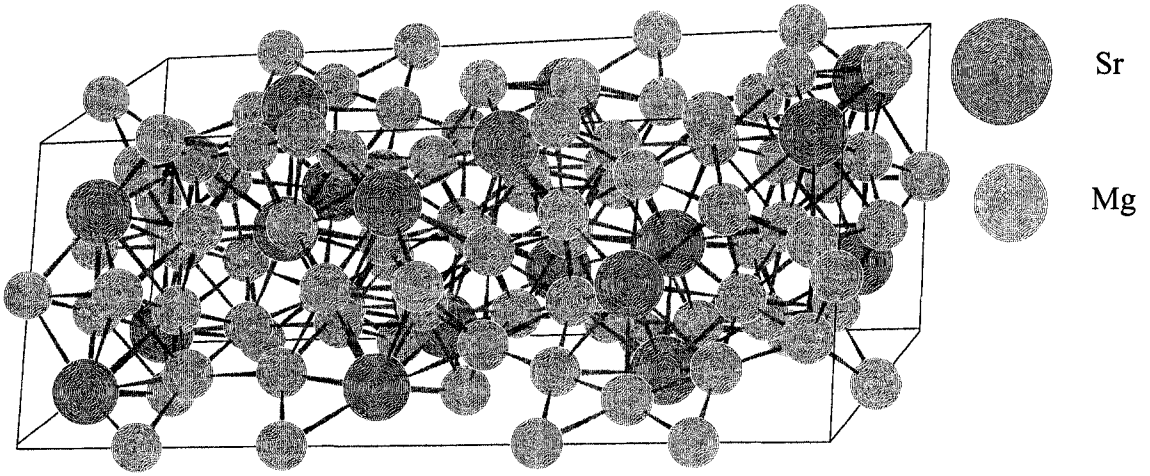

Figure A-8: *$Mg_{38}Sr_9$ unit cell.*

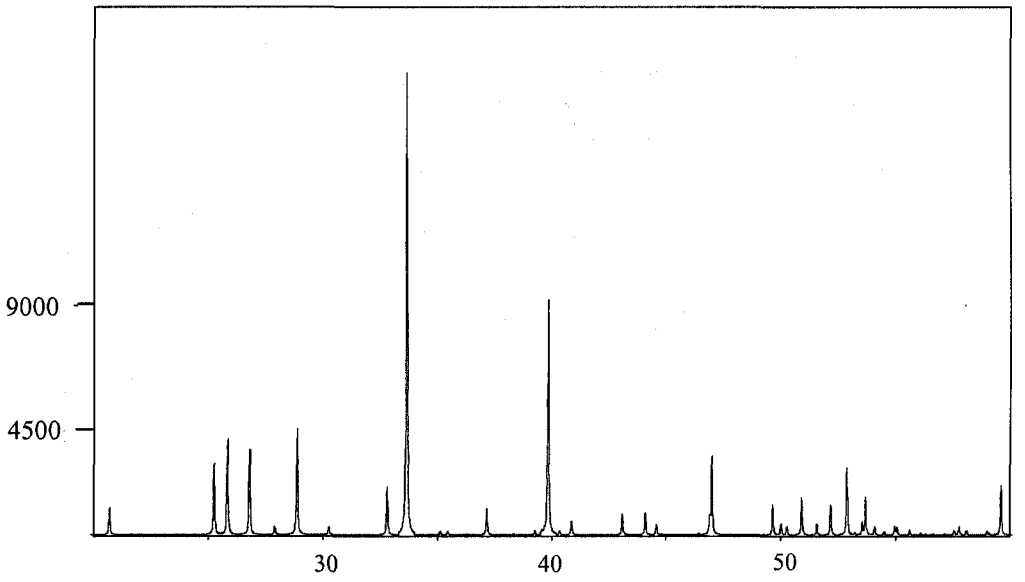

Figure A-9: *Calculated XRD diffraction pattern for $Mg_{38}Sr_9$.*

A-6 Crystallographic Data of $Mg_{23}Sr_6$

Table A-10: *Crystal Structure data of $Mg_{23}Sr_6$.*

Structure	Cubic		
Structure type	$Mn_{23}Th_6$		
Spacegroup number	225		
Lattice parameter (Å)	a	b	c
	14.9141	14.9141	14.9141
Angles	α	β	γ
	90	90	90

Table A-11: *Atoms positions in the unit cell of $Mg_{23}Sr_6$ [156].*

Atom	Wyckoff position	x	y	z
Mg1	4b	0.5	0.5	0.5
Mg2	24d	0	0	0
Sr	24e	0.2041	0.2041	0.2041
Mg3	32f	0.3741	0.3741	0.3741
Mg4	32f	0.1774	0.1774	0.1774

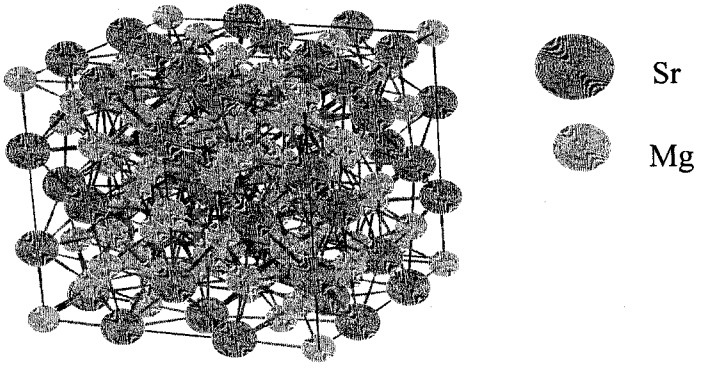

Figure A-10: *$Mg_{23}Sr_6$ unit*

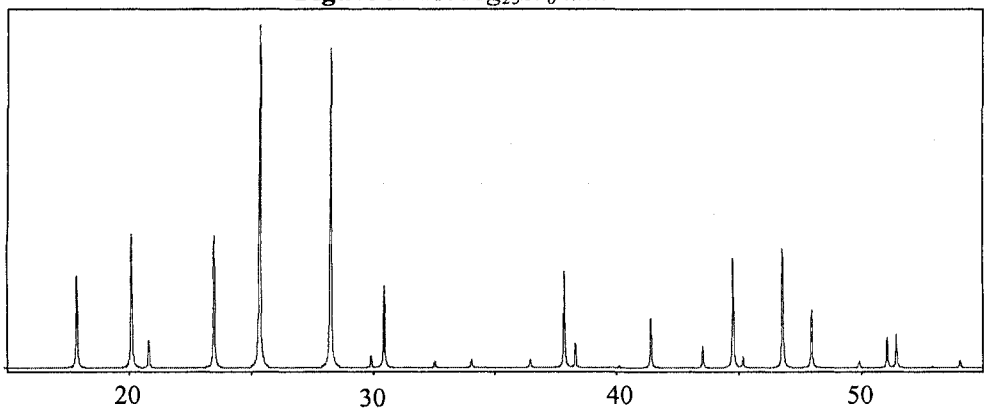

Figure A-11: *Calculated XRD diffraction pattern for $Mg_{23}Sr_6$.*

A-7 Crystallographic Data of Al_2Ca

Table A-12: *The crystal structure data of Al_2Ca*

Structure	Cubic		
Structure type	Cu_2Mg		
Space number	227		
Lattice parameter (Å)	a	b	c
	8.04	8.04	8.04
Angles	α	β	γ
	90°	90°	90°

Table A-13: *Atoms positions in the unit cell of Al_2Ca [156].*

Atom	Wyckoff position	x	y	z
Ca	8a	0	0	0
Al	16d	5/8	5/8	5/8

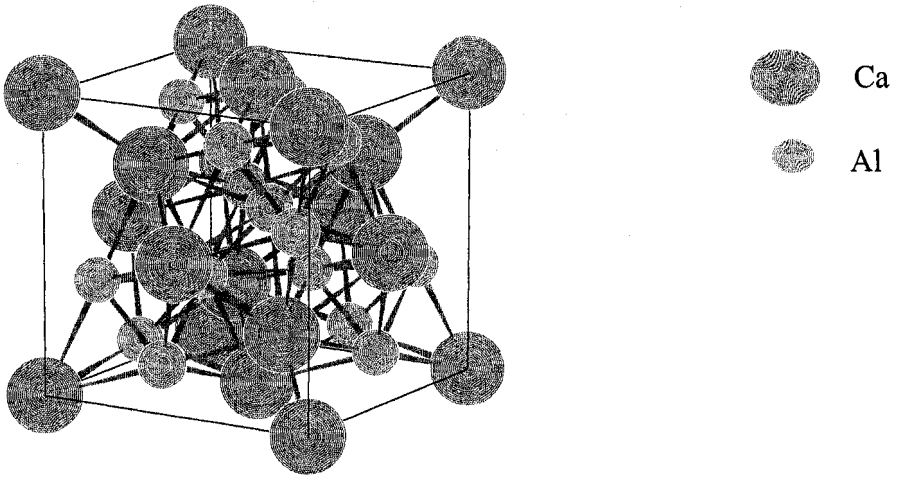

Figure A-12: Al_2Ca unit cell.

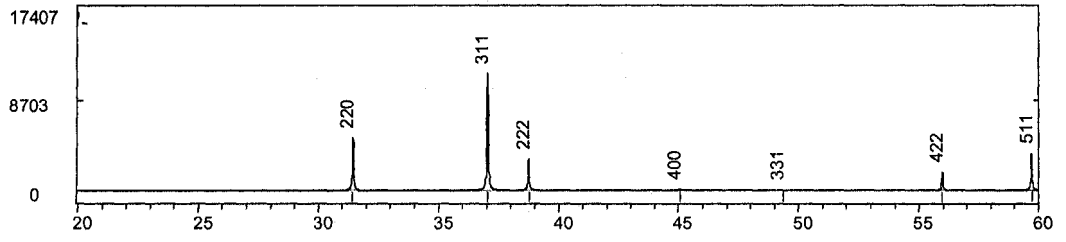

Figure A-13: *Calculated XRD diffraction pattern for Al_2Ca.*

A-8 Crystallographic Data of Al_4Ca

Table A-14: *The crystal structure data of Al_4Ca.*

Structure	Tetragonal		
Structure type	Al_4Ba		
Space number	139		
Lattice parameter (Å)	a	b	c
	4.353	4.353	10.7
Angles	α	β	γ
	90°	90°	90°

Table A-15: *Atoms positions in the unit cell of Al_4Ca [156].*

Atom	Wyckoff position	x	y	z
Ca	2a	0	0	0
Al1	4e	0	0	0.38000

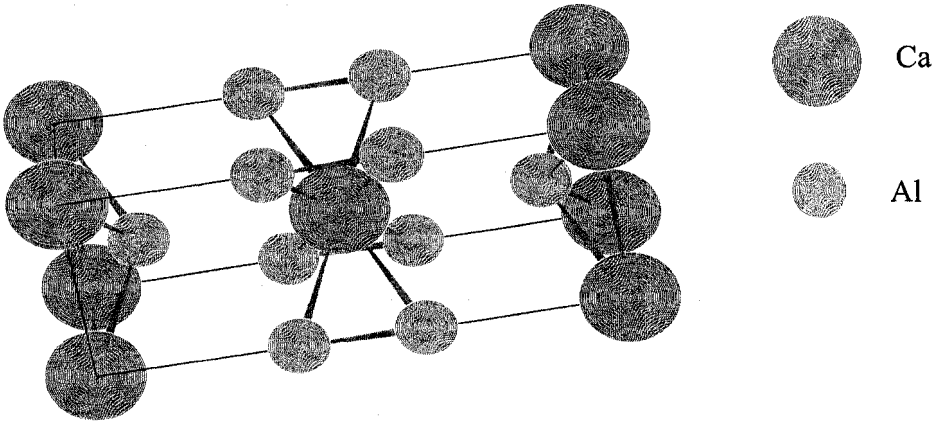

Figure A-14: *Al_4Ca unit cell.*

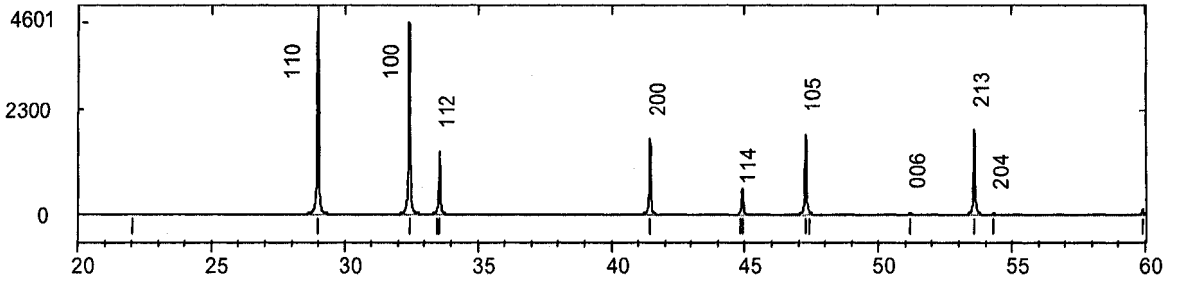

Figure A-15: *Calculated XRD diffraction pattern for Al_4Ca.*

A-9 Crystallographic Data of Al_3Ca_8

Table A-16: *The crystal structure data of Al_3Ca_8.*

Structure	Triclinic		
Structure type	Ca_8In_3		
Space number	2		
Lattice parameter (Å)	a	b	c
	9.495	9.5922	9.6704
Angles	α	β	γ
	99.057°	101.152°	119.613°

Table A-17: *Atoms positions in the unit cell of Al_3Ca_8 [156].*

Atom	Wyckoff position	x	y	z
Al1	1a	0	0	0
Al2	1h	1/2	1/2	1/2
Al3	2i	0.679(5)	0.348(5)	0.037(4)
Al4	2i	0.828(5)	.163(5)	.490(4)
Ca1	2i	.027(3)	.434(4)	.315(3)
Ca2	2i	.058(3)	.701(4)	.108(4)
Ca3	2i	.120(3)	.108(4)	.341(3)
Ca4	2i	.262(3)	.342(3)	.695(3)
Ca5	2i	.688(4)	-0.003(4)	.121(3)
Ca6	2i	.342(3)	.369(5)	.116(3)
Ca7	2i	.532(3)	.211(4)	.654(3)
Ca8	2i	.557(3)	.211(3)	.344(3)

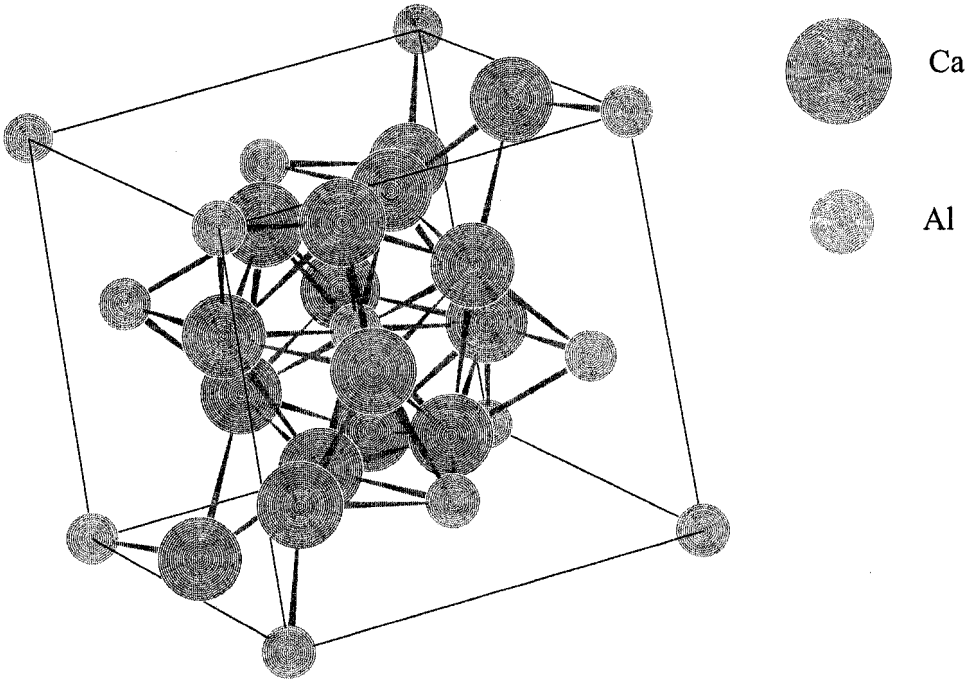

Figure A-16: *Al_3Ca_8 unit cell.*

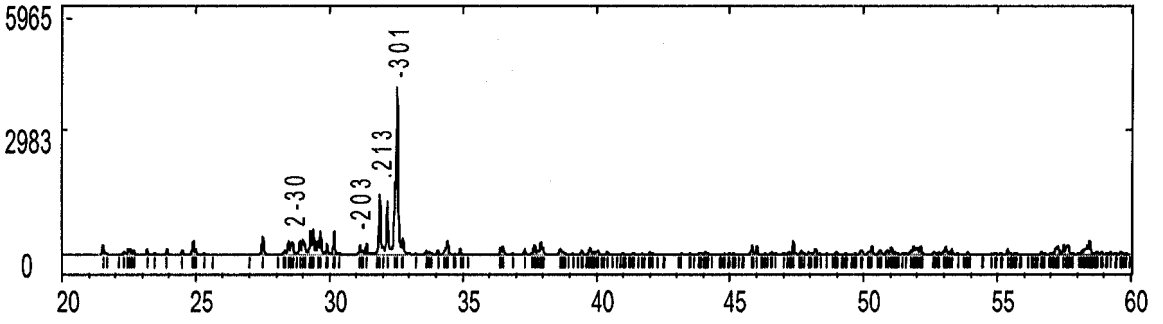

Figure A-17: *Calculated XRD diffraction pattern for Al_3Ca_8.*

A-10 Crystallographic Data of $Al_{14}Ca_{13}$

Table A-18: *The crystal structure data of $Al_{14}Ca_{13}$.*

Structure	Monoclinic		
Structure type	$Al_{14}Ca_{13}$		
Space number	12		
Lattice parameter (Å)	a	b	c
	15.551	9.873	9.726
Angles	α	β	γ
	90°	90°	90°

Table A-19: *Atoms positions in the unit cell of $Al_{14}Ca_{13}$ [156]*

Atom	x	y	z
Ca1	0.14628(7)	0.2027(1)	0.3659(1)
Ca2	0.36159(7)	0.2819(1)	0.2275(1)
Ca3	0.1969(1)	0	0.0851(2)
Ca4	0.5036(1)	0	0.2024(2)
Ca5	0	0	0.5
Al1	0.1581(1)	0.3653(2)	0.0827(2)
Al2	0.0013(2)	0	0.1578(3)
Al3	0.2586(2)	0	0.6548(3)
Al4	0.3398(2)	0	0.4311(3)
Al5	0	0.3542(2)	0.5
Al6	0	0.2249(2)	0

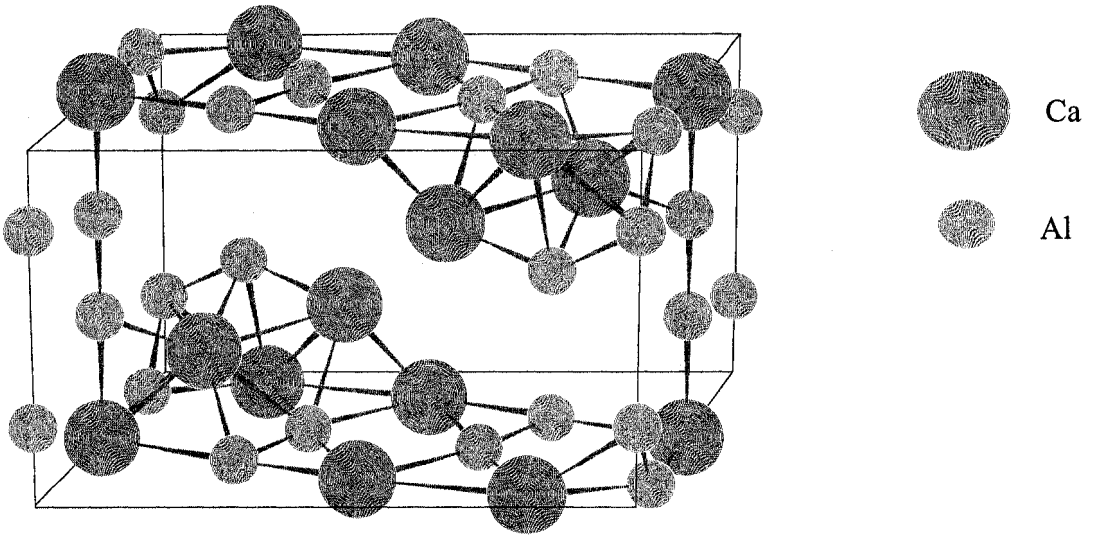

Figure A-18: *$Al_{14}Ca_{13}$ unit cell.*

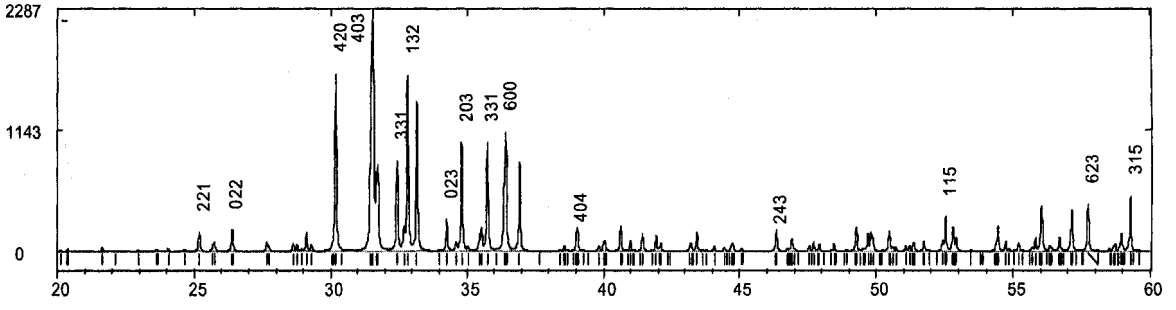

Figure A-19: *Calculated XRD diffraction pattern for $Al_{14}Ca_{13}$*

A-11 Crystallographic Data of γ

Table A-20: *Crystal Structure data of γ.*

Structure	Cubic		
Spacegroup number	217		
Lattice parameter (Å)	a	b	c
	10.55(3)	10.55(3)	10.55(3)
Angles	α	β	γ
	90°	90°	120°
Atoms in unit cell	58		

Table A-21: *Atoms positions in the unit cell of γ [156]*

Atom	Wyckoff position	x	y	z
Mg1	2a	0	0	0
Mg2	8c	0.3240	0.3240	0.3240
Mg3	24g	0.3582	0.3582	0.0393
Al	24g	0.0954	0.0954	0.2725

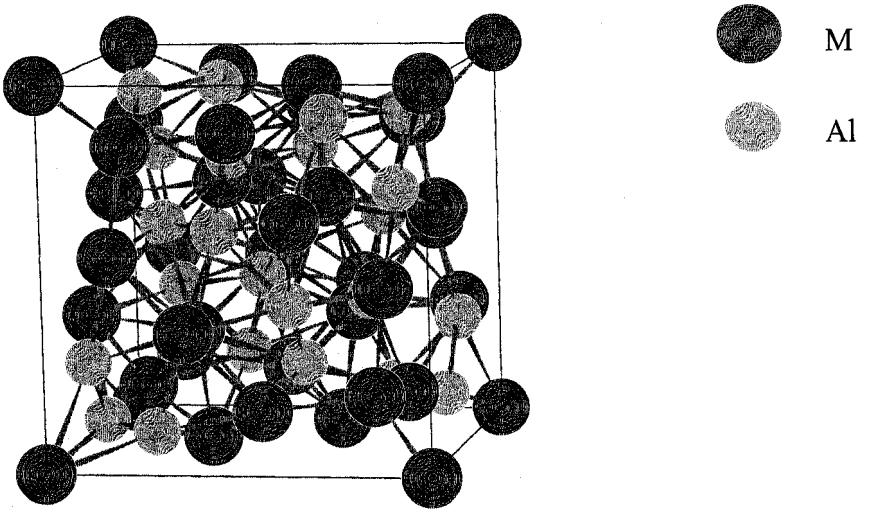

Figure A-20: *γ unit cell.*

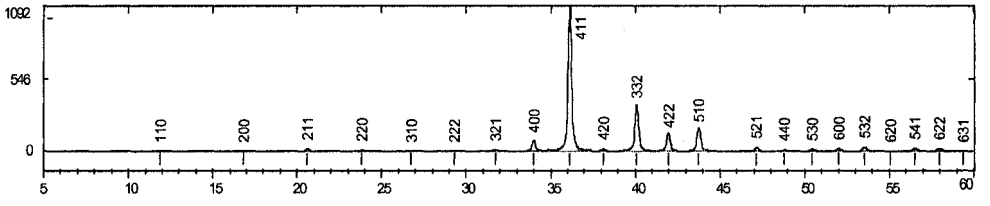

Figure A-21: *Calculated XRD diffraction pattern for γ.*

A-12 Crystallographic Data of β

Table A-22: *Crystal Structure data of β.*

Structure	Cubic		
Structure type	β		
Spacegroup number	227		
Lattice parameter (Å)	a	b	c
	28.239	28.239	28.239
Angles	α	β	γ
	90°	90°	90°
Atoms in unit cell	58		

Table A-23: *Atoms positions in the unit cell of β [156]*

Atom	Wyckoff position	x	y	z
M	4a	0	0	0

M = Al, Mg

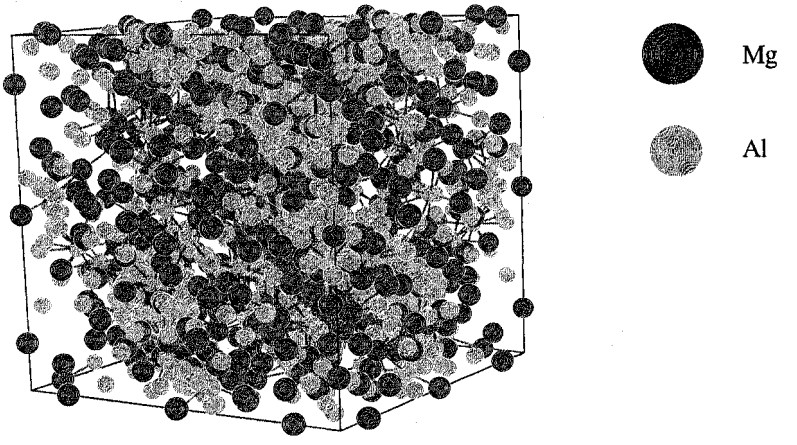

Figure A-22: *β unit cell.*

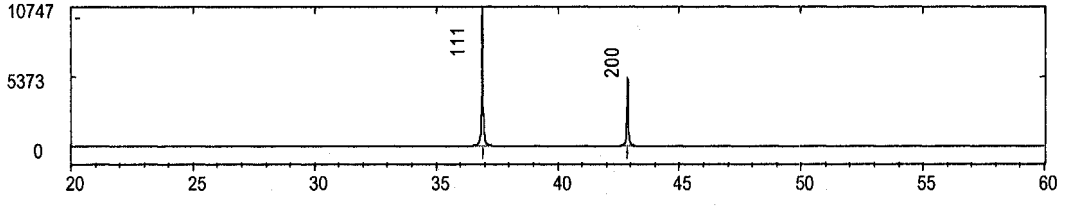

Figure A-23: *Calculated XRD diffraction pattern for β.*

A-13 Crystallographic Data of Mg_2Ca

Table A-24: *Crystal Structure data of Mg_2Ca.*

Structure	Cubic		
Spacegroup number	217		
Lattice parameter (Å)	a	b	c
	10.55(3)	10.55(3)	10.55(3)
Angles	α	β	γ
	90°	90°	120°
Atoms in unit cell	58		

Table A-25: *Atoms Positions in the Unit Cell of Mg_2Ca [156].*

Atom	Wyckoff position	x	y	z
Mg1	2a	0	0	0
Ca	4f	1/3	2/3	0.062
Mg2	6h	0.830	0.660	1/4

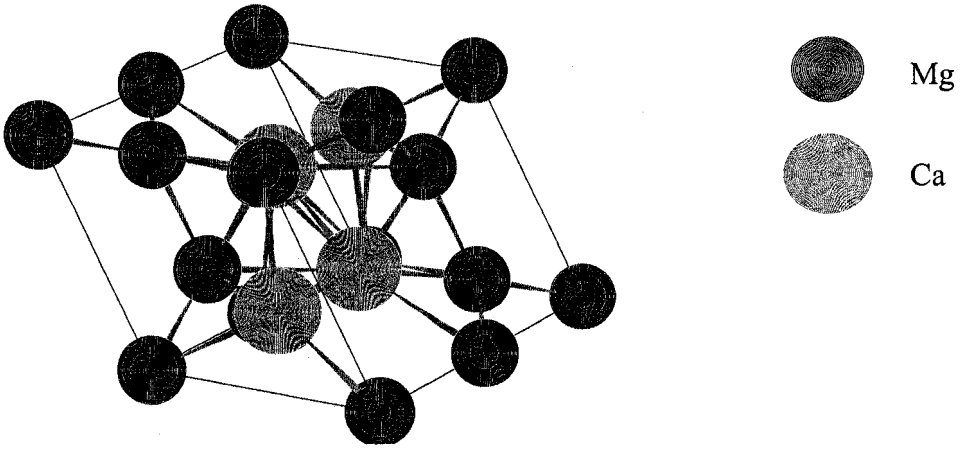

Figure A-24: *Mg_2Ca unit cell.*

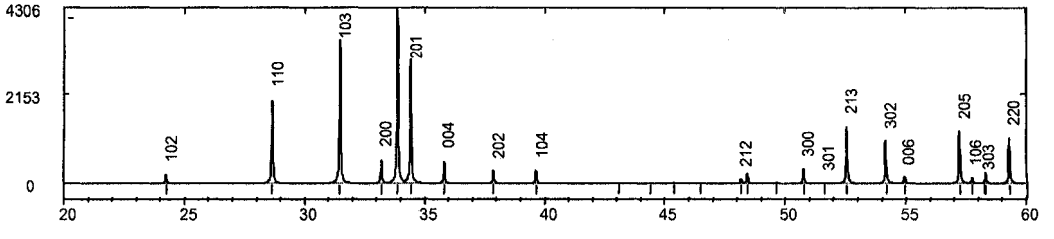

Figure A-25: *Calculated XRD diffraction pattern for Mg_2Ca*